THE INFLUENCE OF ABRASIVE SURFACE TOPOGRAPHY ON THE BASIC MECHANICS OF THE METAL GRINDING PROCESS

A Thesis submitted to the University of Leeds
for the Degree of Doctor of Philosophy

by

D. Graham, B.Sc. (Hons.)

Department of Mechanical Engineering
The University of Leeds

November 1970

ABSTRACT

The successful prediction of abrasive wheel behaviour should greatly simplify the complex problem of wheel selection. This investigation examines the influence of abrasive surface topography on the actual mechanics of the metal removal process.

The characterisation of abrasive surfaces using statistical properties of the cutting profile is discussed.

A study is undertaken which examines the influence of abrasive grit geometry on the mode of metal deformation. In these tests, every consideration is given to reproducing conditions realistic of a practical grinding operation.

A simplified plunge grinding operation is then considered to determine the influence of various process parameters on the mechanics of metal removal.

Finally, a computer simulation of the above grinding operation, using Monte Carlo simulation techniques, is presented.

CONTENTS

CONTENTS (continued)

CONTENTS (continued)

CHAPTER I

INTRODUCTION

1.1 GENERAL

Despite the many recent developments in the field of metal working which have led to both the improvement of existing methods and to the introduction of a variety of new techniques, the grinding process still remains one of the most important and widely used operations for the precision finishing of components.

Over the last ten years, the amount of research into this unique metal removal operation has increased substantially, but even today, the vast amount of grinding undertaken in industry is still conducted according to numerous rules of thumb based on past experiences. This situation is clearly unsatisfactory when one considers the expanding needs of modern technology. For example, new expensive alloys which often possess poor machinability are continually being introduced to perform highly specialised functions. The demand for better surface textures and geometrical accuracy has also steadily increased as engineers strive to meet modern design requirements. In addition, as a result of the developments in ceramic research, considerable progress has been made in the manufacture of new and improved abrasive materials. Consequently, experience alone is of little value in realising the full potential of the wide range of synthetic abrasives now available.

Looking further ahead, the optimisation and control of complete manufacturing systems is slowly becoming a reality. In the limit, the effectiveness of such a programme will depend upon the degree of success with which each individual element of the process can be accurately described in mathematical terms. A complete understanding of the basic mechanics of the metal grinding process is therefore a clear necessity.

1.2 METAL GRINDING PRACTICE

Although metal grinding can be accomplished by using either abrasive wheels or belts, and can be utilised in the removal of large or small quantities of material, the following remarks are concerned primarily with the implementation of the process as a precision finishing operation using abrasive wheels.

In practice, the principal problem is the selection of an abrasive wheel which will contend satisfactorily with the operating conditions and material to be processed. Several important factors influence this selection, which is generally a compromise between satisfactory operation and economic production.

Quite apart from the difficulties in achieving the desired geometrical accuracy and surface texture, there are complications which arise from the inevitable deterioration of the wheel cutting surface during operation, and the metallurgical damage which is often inflicted upon the workpiece surface. This deterioration can in some cases be so severe as to result in the gross breakdown of the wheel surface. This behaviour is generally referred to as a "soft" action. Alternatively, the wheel surface may "glaze" and in this case the behaviour is described as "hard". In general, an attempt is made to select wheels which operate between these two extremes, periodic regeneration of the abrasive surface being accomplished by the "dressing operation" in which a diamond tool is traversed across the rotating wheel surface. Worn grains and trapped particles of metal are torn out from the surface thus presenting a new cutting surface capable of further work.

The metallurgical damage to the outermost layers of the workpiece, resulting from severe plastic deformation and thermal effects, can have a considerable influence on the mechanical properties of the material.

High induced residual stresses may also cause cracking in the surface layers resulting in an unacceptable product. These undesirable effects can often be diminished by careful application of coolants and lubricants to the grinding region, together with bulk cooling of the workpiece.

In conclusion, it can be said that metal grinding practice has tended to develop more as an art rather than a science, and this trend will continue until a better understanding of the process mechanics can be obtained.

1.3 PROJECT OBJECTIVES

From the point of view of the research worker, the grinding operation presents a metal removal process of inherent complexity, possessing several salient features which clearly distinguish it from the more conventional machining operations such as milling, drilling, turning, etc:-

(1) The cutting speed is much higher and is usually about 6,000 ft/min, but can be as high as 12,000 ft/min.

(2) The profile of the abrasive surface topography is virtually random, which is in sharp contrast to the above mentioned machining processes where, for research purposes, the shape of the cutting tool is relatively easy to define and control.

(3) Because of the fundamental geometry associated with the interaction of individual abrasive grits and workpiece, the resultant groove geometries tend to be characterised by high width to depth ratios. This in turn gives rise to a complex combination of rubbing, plastic displacement, and microcutting phenomena within the grinding zone.

(4) The scale of deformation is very small. As a consequence, the various grain-workpiece interactions tend to occur on a scale where the shear strength of the material varies according to the "size effect". Also, experimental evaluation of basic parameters is somewhat complicated because of the relatively small magnitude of the forces and distances involved.

This project, which in the long term is concerned with the scientific application of grinding machines and abrasives, investigates the influence of abrasive surface topography on the basic mechanics of the metal grinding process. Much of the work is necessarily devoted to the development of experimental techniques and their application to situations which are realistic of those encountered in actual grinding practice. There are five main objectives which are stated below:-

1. To present a comprehensive survey of both metal grinding research and work in other closely related fields.

2. To examine one of the most fundamental problems in grinding research, viz. the successful quantitative description of abrasive surfaces. Abrasive surface topography will in general be the resultant of the basic wheel structure and the superimposed effects of the previously mentioned dressing conditions. This section examines the effect of dressing conditions upon the basic statistical properties of the wheel profile, i.e. the mean, standard deviation and skewness of the height distribution, and the autocorrelation function and power spectrum.

3. To study the nature of metal removal in grinding. This is facilitated by using tools of known geometry to simulate the

action of abrasive grits. The high speed interaction of a single tool with a stationary workpiece has been investigated with the emphasis on reproducing conditions which are realistic of the grinding process, e.g., impact speed and duration, minute scale of deformation, and workpiece material. The influence of tool profile and cutting velocity upon the energy consumed and the mode of metal removal is a major consideration.

4. To investigate a simplified grinding operation, viz., the plunge grinding of strip under constant load. The effects of dressing conditions and the application of various coolants are considered, and the results are interpreted in the light of the findings of the previous two sections. The possible use of the measurement techniques developed in Chapter III to study the influence of different wear processes upon the overall abrasive topography is also discussed.

5. To develop a computer simulation of the grinding operation encountered in Chapter V. This is essentially a simplified mathematical model which incorporates a random number generator to produce profiles having discrete height distributions in keeping with the experimental findings of Chapter III. By making assumptions regarding the spacing and shape of asperities etc., the resultant groove geometry, mode of metal removal and specific cutting energy are predicted. Comparisons are then made with the experimental results of Chapter V.

CHAPTER II

LITERATURE REVIEW

2.1 THE CHARACTERISATION OF ABRASIVE SURFACES

2.1.1 SURFACE TEXTURE MEASUREMENTS IN GENERAL

Before considering the papers which deal specifically with the fairly recent problems of abrasive surface characterisation (see Section 2.1.2), it is necessary to review briefly the methods and literature concerned with the more general field of surface texture measurement.

Standard techniques for both qualitative and quantitative descriptions of surfaces are well established, and include among others, profilometry, interferometry, and electron microscopy. However, since one of the primary objectives of this project is to present a quantitative description of abrasive surfaces, only methods concerned with the numerical assessment of surface properties are considered.

In general, the analysis is carried out on a two dimensional profile which is assumed to be representative of the entire surface. Although this profile can be obtained by a variety of different methods, it is usual to use a stylus tracing instrument. A diamond stylus is traversed across the surface to be measured, and an electrical output directly proportional to displacement is obtained. The main disadvantage of such a method arises from the unavoidable distortion of the surface profile caused by the finite dimensions of the stylus. However, since the signal is already in a form suitable for electronic analysis, and interpretation is relatively easy, the technique is likely to continue unsurpassed as a convenient method of obtaining surface profile measurements.

The different approaches to quantitative description of surfaces can be considered in terms of the mathematical properties of the surface profile:-

(1) Simple numerical properties, e.g., C.L.A., R.M.S., and H_{max} values (for definitions see (2)). These well known expressions have long been important considerations in defining the microtopography of surfaces. However, the inadequacy of such parameters unless accompanied by a detailed description of the manufacturing process has already been pointed out by many workers (more recently Greenwood[1]). No indication is given as to how the surface might behave in a realistic engineering application, e.g., wear characteristics, etc. In addition, the parameters do not facilitate such calculations as the initial approach of two bodies, the probability of plastic deformation, or the elastic recovery after unloading, etc.

(2) The statistical height distribution. The distribution of asperity heights has been found to give a meaningful picture of the surface topography. The analysis can be confined to the distribution of asperity peaks, or extended to cover the overall height variation. Figs. 1a and 1b show a typical surface profile and the resultant height distribution. Williamson[2] analysed the distribution of heights for surfaces prepared by a variety of methods, and concluded that the peak and upper height distributions were nearly always Gaussian. Deviations were experienced, however, in the lower height regions.

Using the notation of Fig. 1, the following parameters can be determined from the height distribution:-

a) Mean height, $m_y = \int_{-\infty}^{\infty} y.\ f(y)\ dy$

b) Range of heights, $H_{max} = y_{max} - y_{min}$

c) The centre line average, C.L.A.

$$= \int_{-\infty}^{\infty} (y - m_y)^{\blacksquare}\ f(y)\ dy$$

d) The variance, σ^2

$$= \int_{-\infty}^{\infty} (y - m_y)^2\ f(y)\ dy$$

where σ = standard deviation or r.m.s. value

e) The Skewness, Sk

$$= \int_{-\infty}^{\infty} (y - m_y)^3\ f(y)\ dy$$

f) The Kurtosis, K.

$$K = \int_{-\infty}^{\infty} (y - m_y)^4\ f(y)\ dy$$

The effect of different degrees of skewness and kurtosis upon the basic height distribution is shown in Figs. 2a and 2b. Following an extensive investigation of a large number of surfaces, Peklenik[3] was unable in practice to establish a relationship between these two parameters and the C.L.A. or σ values.

(3) The bearing area curve, or in statistical terms, the cumulative height distribution. This was first suggested by Abbott and Firestone[4], and has since become a useful criterion of surface roughness[5,6]. The curve is derived from the profile as shown in Fig. 3. For each height considered,

Fig. 1 Profile Height Distribution

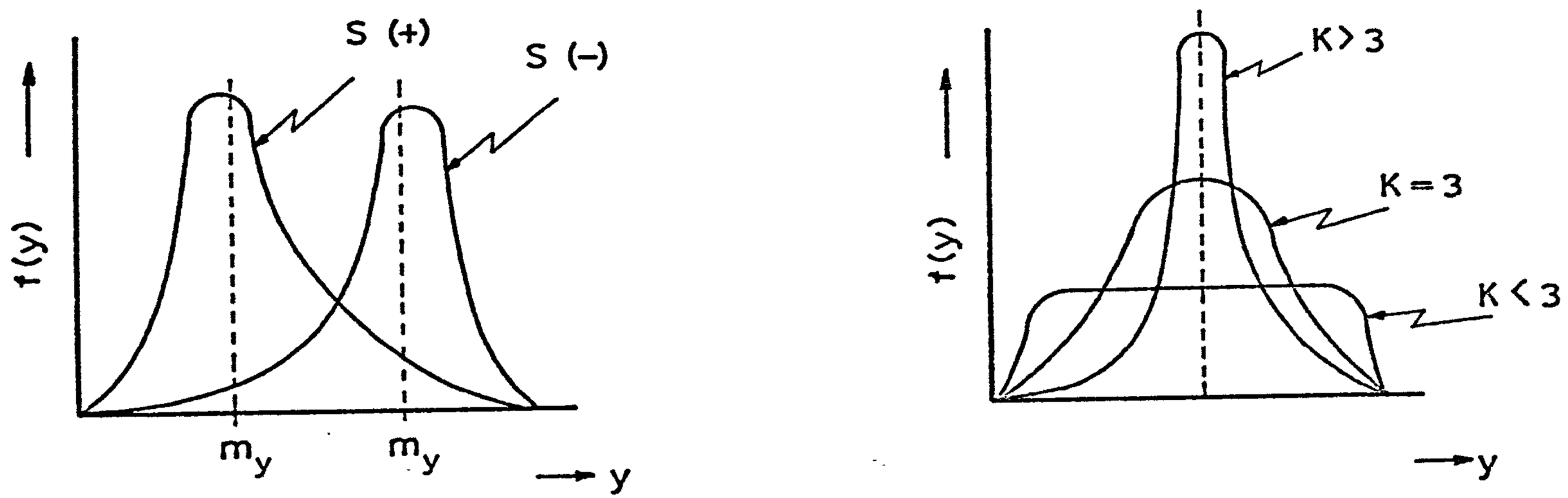

Fig. 2 Effect of Skewness and Kurtosis

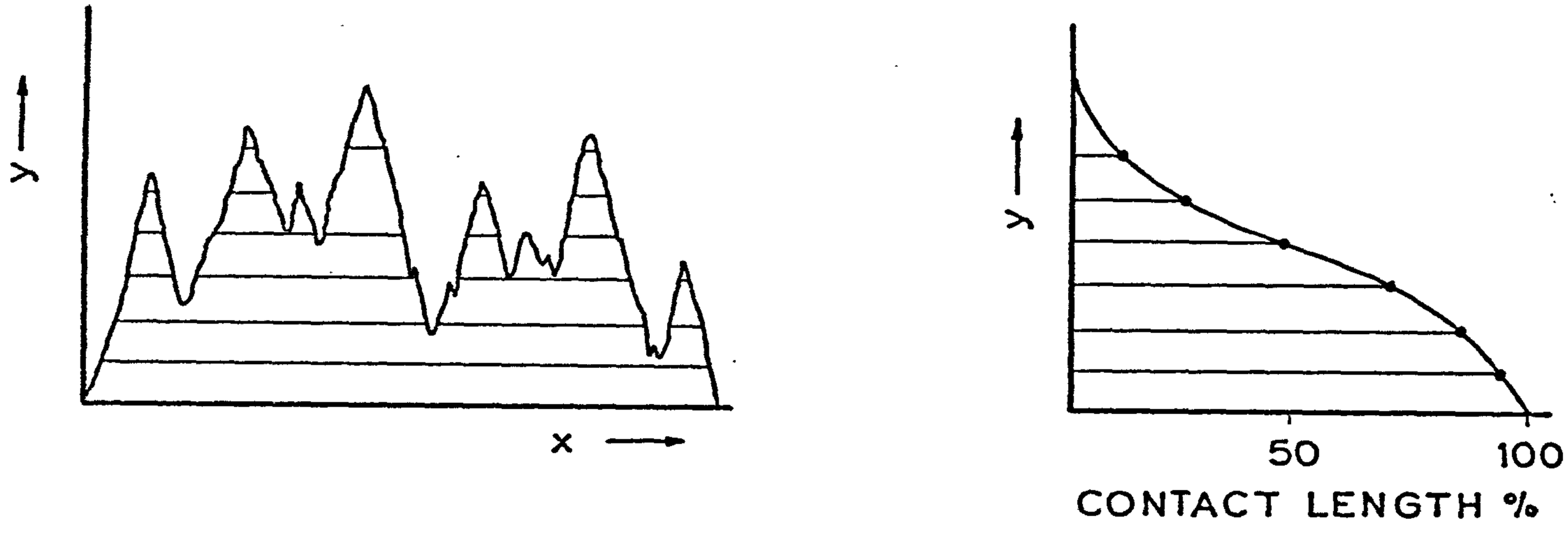

Fig. 3 Construction of Bearing Area Curve

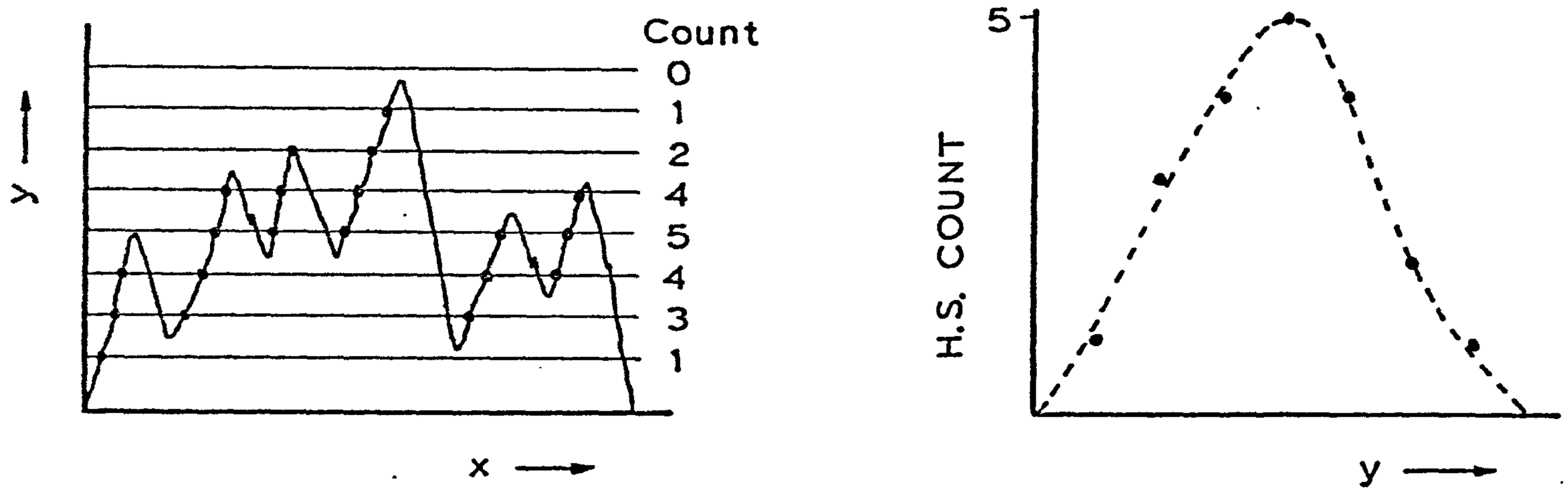

Fig. 4 Construction of H.S. Count (After Reason[5])

a line is drawn along the profile and the fraction of the surface above the line is measured. Essentially, it is a measure of the rate at which the surface "fills in", plotted against the level of penetration.

(4) Reason[5] has discussed the so called "high spot count" which exists in two forms. One counts the number of positive going intersections of the profile with a reference level (Fig. 4), while the other computes the number of times the tangent to the profile changes from positive to negative when rolling round those peaks considered to be significant. Reason discovered that when the flanks of a cut surface having an obvious traverse feed are serrated, the count at different levels fluctuated considerably, and at all levels was greater than that which would correspond with the traverse feed.

(5) Slope and curvature measurements. Wishing to relate frictional behaviour to the slope and curvature of surface profiles, Myers[7] arranged for the profile data to be fed into an analogue computer which calculated the mean slope and curvature. More recently, Kubo[8] has developed an instrument for measuring the slope distribution.

Peklenik[3] has stated that a "division between large and small scale surface deviations (the so called waviness and roughness) is desired because their effect on functional behaviour is different". He also points out that "the measuring techniques employed for their detection have been developed on basically different concepts". All surfaces contain periodic and random functions, and by introducing the techniques of random process analysis, Peklenik has distinguished[3,9,10,11]

between the periodic carrier profile and the superimposed random content which imparts real roughness to the surface. To this end, the auto-correlation function $R_{yy}(\lambda)$ is an important consideration:-

(6) The autocorrelation function $R_{yy}(\lambda)$. This is defined as

$$R_{yy}(\lambda) = \lim_{L \to \infty} \frac{1}{L} \int_{-L/2}^{L/2} (y_x - m_y)(y_{x+\lambda} - m_y)\, dx$$

where the notation is as shown in Fig. 5a. Fig. 5b gives a typical autocorrelation function. The function is essentially a measure of the extent to which the profile repeats itself with distance, and is thus capable of indicating directional properties along the line of the profile.

(7) The above analysis can be extended to 3-D by considering the cross-correlation function $R_{yz}(\lambda)$ where

$$R_{yz}(\lambda) = \lim_{L \to \infty} \frac{1}{L} \int_{-L/2}^{L/2} (y_x - m_y)(z_{x+\lambda} - m_z)\, dx$$

and z(x) are the height ordinates of an adjacent profile. In general, for surfaces having pronounced directional patterns (Fig.6), $R_{yy}(\lambda)$ and $R_{zz}(\lambda)$ have the same shape. R_{yz} resembles either R_{yy} or R_{zz} and the maximum value of $R_{yz}(\lambda)$ approaches unity as a function of b, the distance between successive profiles.

(8) The power spectrum, S_y. The information obtained from correlation measurements can also be presented in the frequency domain by considering the Fourier transform of the auto-correlation function, known as the power spectrum (Fig. 7). This is given as:-

$$S_y(w) = \frac{2}{\pi} \int_0^{\infty} R_{yy}(\lambda) \cos w\, d\lambda$$

where $w = 2\pi f$, f in cycles/unit length.

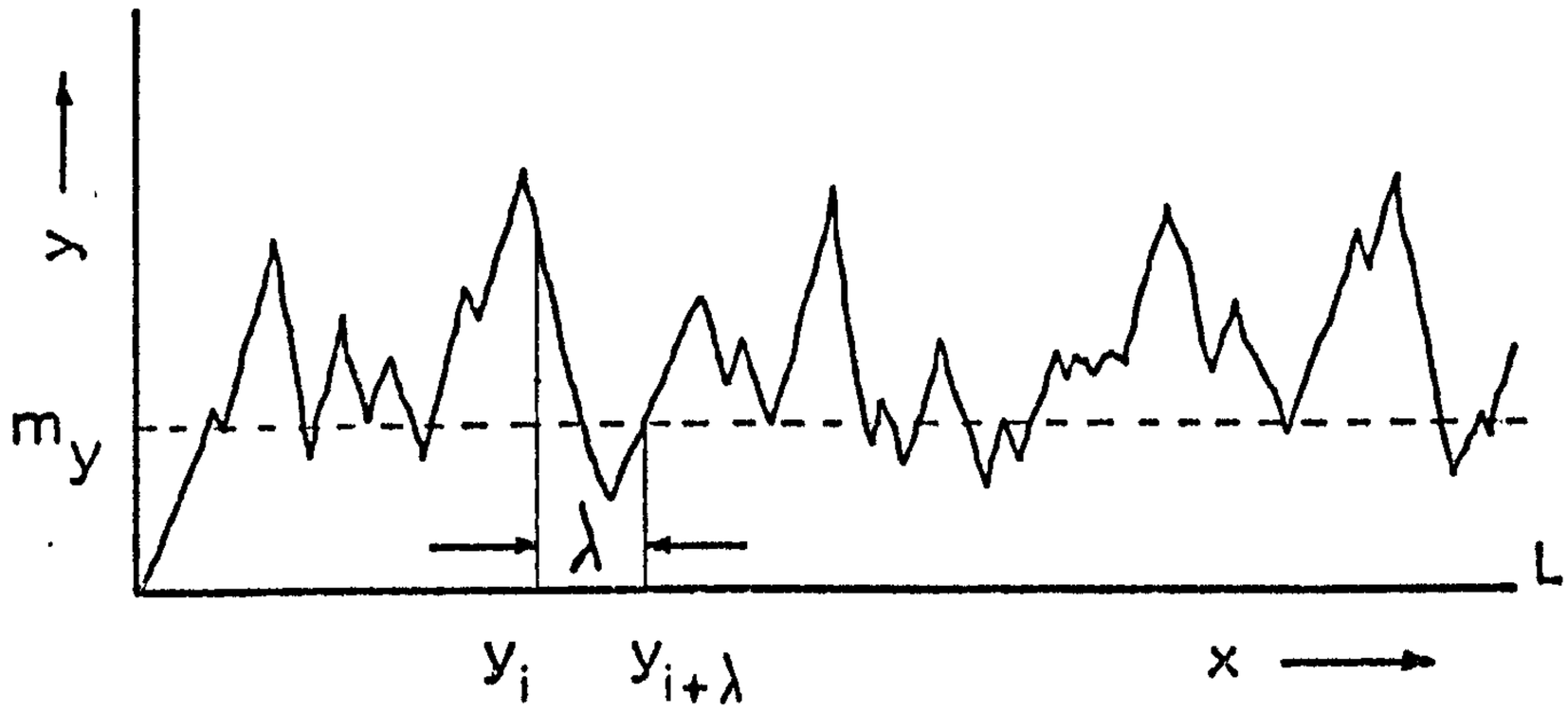

Fig. 5a Surface Profile

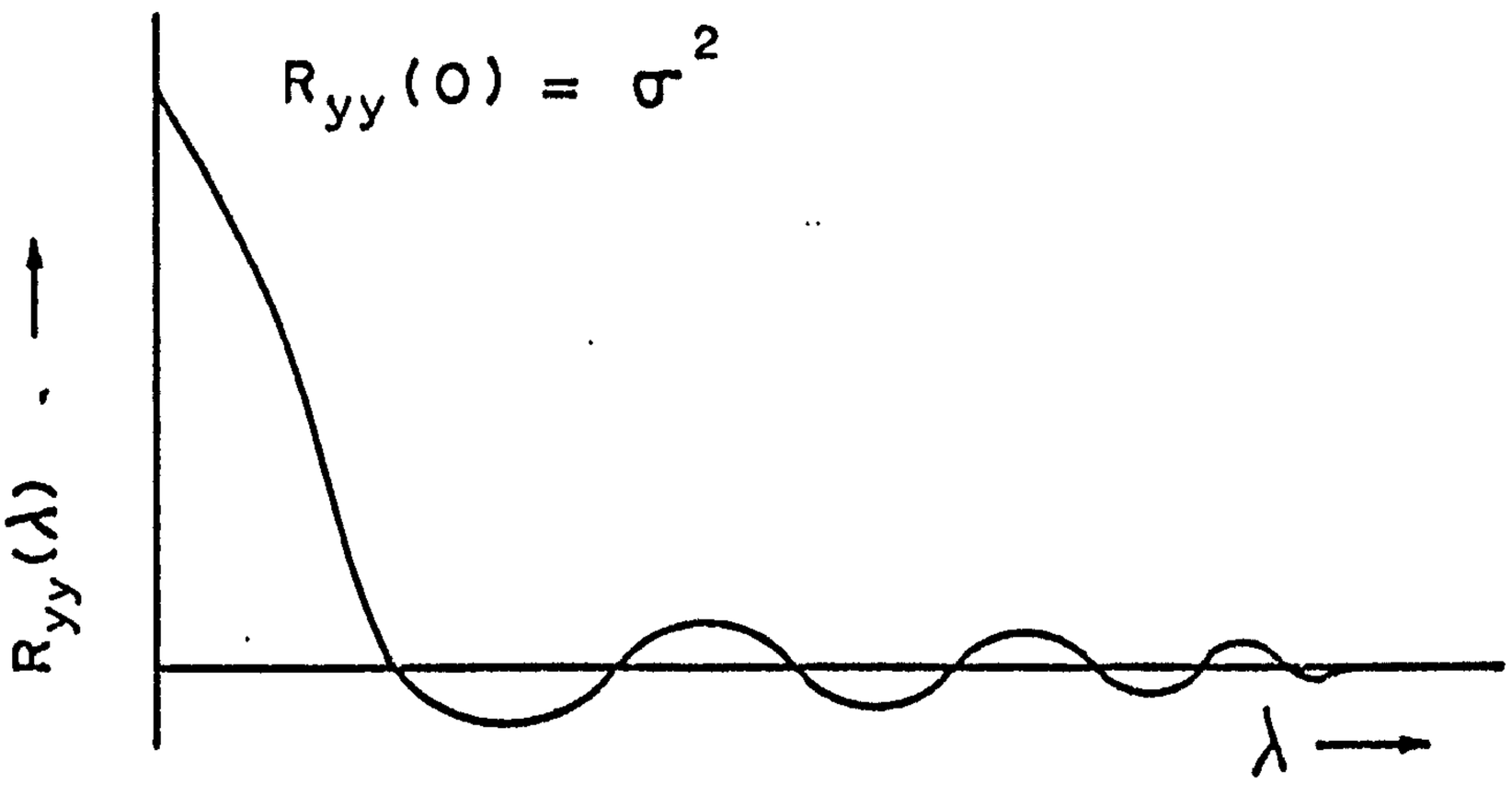

Fig. 5b Autocorrelation Function

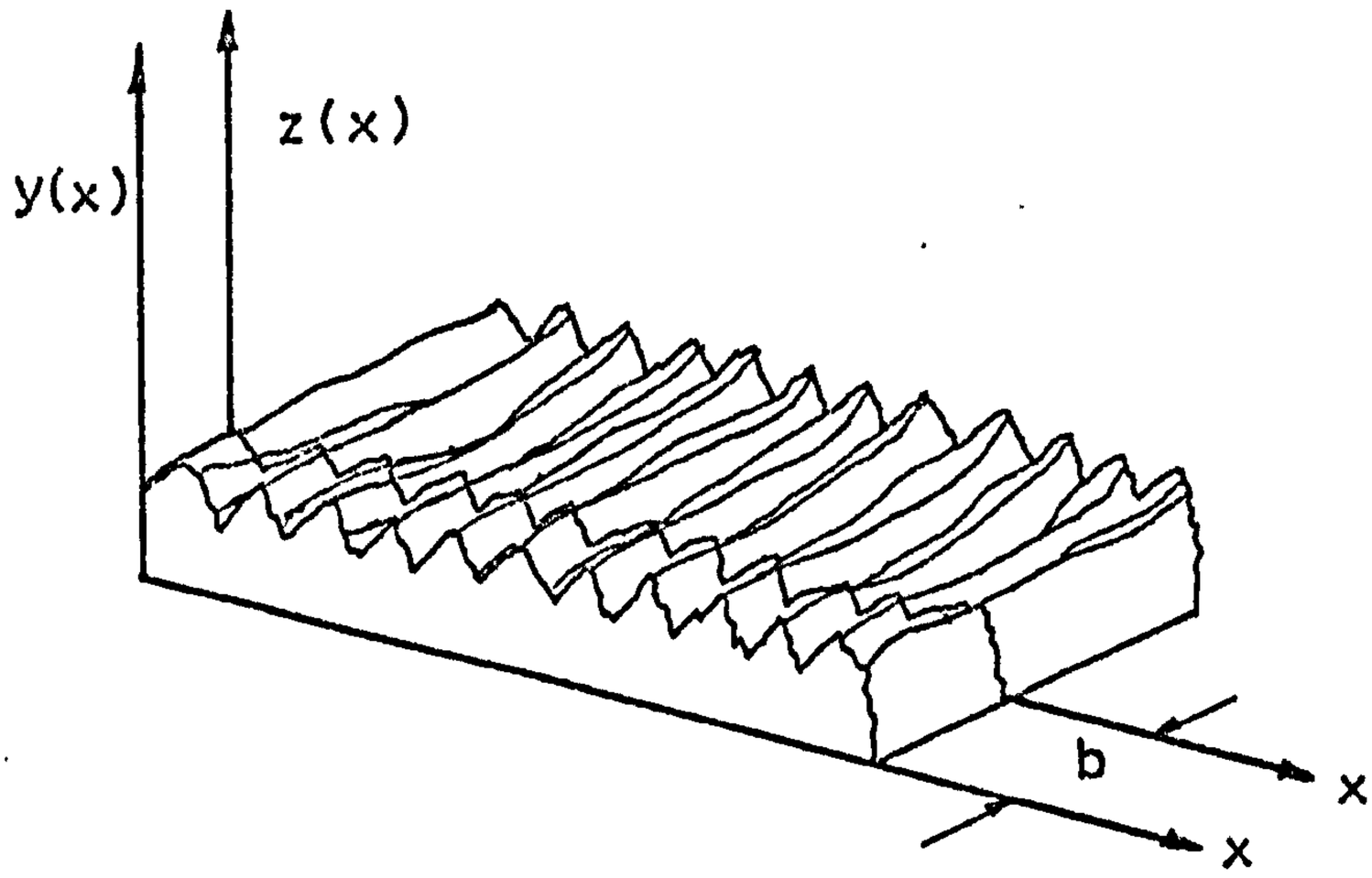

Fig. 6 Surface with Strong Directional Pattern

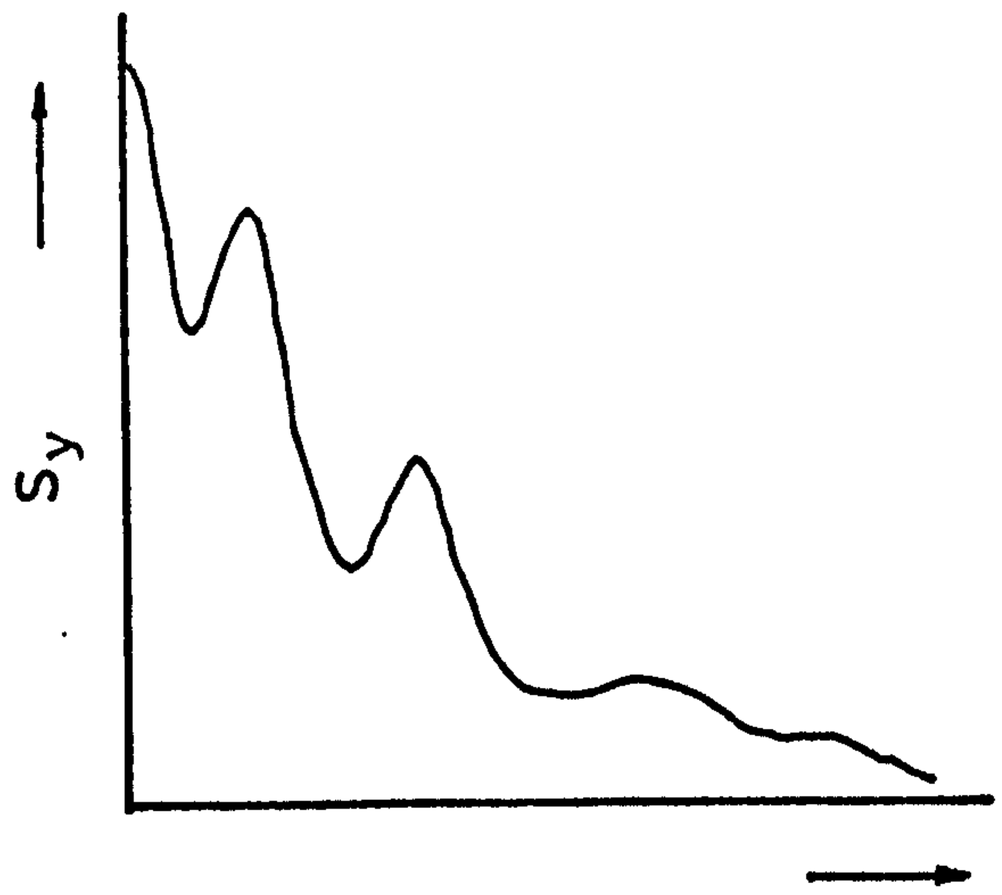

Fig. 7 Power Spectrum

In practice, the disadvantages of the application of random process analysis stem largely from the prohibitive cost of the sophisticated equipment and the large amount of digital information required. The latter is not always available with surfaces of limited size. In addition, it takes a great deal of skill and understanding to interpret the various correlation functions, and it is for this reason that the simple numerical values of C.L.A., R.M.S., etc., will always remain important surface texture parameters.

2.1.2 ABRASIVE SURFACE MEASUREMENTS

In addition to the problems encountered in general surface texture measurement, further complications arise when considering abrasive surfaces. For example, the range of amplitude variations within the surface is much larger. Also, since the wheel structure is porous, large voids and included cavities are to be found in the surface. As a result, in examining abrasive topography, several specialised techniques have been employed:-

(1) Rolling the wheels under various loads over soot covered glass[12]. In this early investigation, the soot was spread over the glass to a known thickness (usually 0.0001 in.). The impression left by the wheel was examined to give a measure of the abrasive asperity concentration.

(2) Taper sections of the workpiece. This method has been used fairly extensively to obtain a measurement of abrasive topography[12,13,14]. The main criticism of this technique is that the final workpiece texture is a result of the interaction of many individual abrasive cutting profiles, and hence the true shape of the profile may be obscured.

(3) Examination by projection of the impressions left by wheels when grinding thin strips of metal[15]. The same criticism as above can be levelled at this method. In addition, the profiles obtained by the last two methods are not in a suitable form for rapid analysis.

(4) Analysis of thermal impulses obtained when grinding micro-thermocouples. This method was used by Redko[16] to determine the number of active cutting asperities within the wheel surface.

(5) Optical techniques. Recently[17], research workers have used a photoelectric circuit, etc., to analyse beams of light reflected off the rotating wheel surface. The problem here is essentially one of interpretation, but it appears that an increase in the signal output correlated well with the development of wear flats on the wheel surface.

(6) Stylus scanning techniques. The relative merits of such methods have already been discussed in Section 2.1.1. When used in connection with abrasive surfaces, it must be remembered that because of the porous nature of the wheel structure, a continuous "touching" profile should not be possible. It can be assumed that where continuous profiles have been obtained[18], the depth of penetration is sufficiently great to make stylus distortion considerable.

Having considered the various methods for measuring abrasive profiles, attention can now be turned to their subsequent analysis.

Abrasive wheel surfaces can be classified in part according to the initial wheel specifications designated by the manufacturer.

A typical specification might be:- A23 - 46 - K5 - VBE. Reading from left to right, the designation refers to the type of abrasive, the grain size, the hardness grade and the wheel structure number, and finally the type of bond. The grain size determines to a large extent the size of the cutting asperities, whilst the structure number is a measure of porosity, influencing the asperity spacing. Early investigations[12,13,14,19,20,21] centred around determining such constants as the density and equivalent radius of active asperities, and the form factor (ratio of asperity width to depth) as a function of the above basic wheel specifications. More recently, Peklenik[18] has introduced a rigorous statistical analysis to the abrasive profile. After a comprehensive investigation of grinding wheel surfaces had shown the surface profiles to be both stationary and ergodic, he suggested that the following parameters give a complete description of the wheel cutting surface:-

a) The number of cutting profiles, n_z, which move perpendicular to the plane, E, normal to the grinding direction, Fig. 8.

b) Average height m_y and the autocorrelation function, R_{yy}.

c) Cross correlation function for elementary cutting profiles passing through the plane, E.

Empirical relationships were suggested between the number of cutting profiles, n_z and the wheel hardness and grain size. Typical autocorrelation functions are shown in Fig. 9. Since the grain depth of cut is an important parameter in grinding mechanics, the variation in R_{yy} and m_y with the profile level was also given. The depth of penetration appeared to have little effect on the function, R_{yy}.

McAdams[22] has introduced the power spectrum, S_y, to distinguish between two surfaces having the same height variation but different cutting properties because of the different frequency components

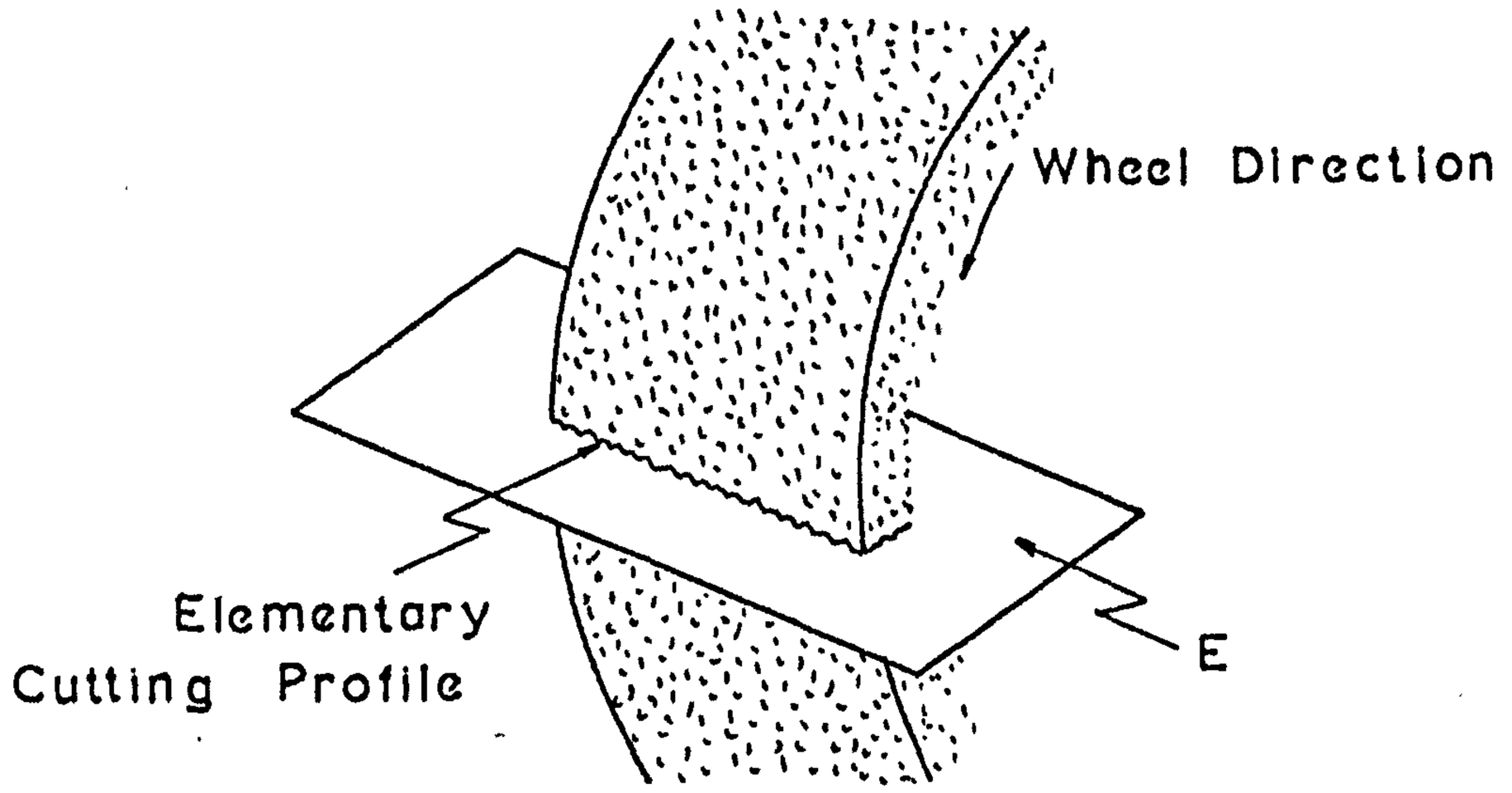

Fig. 8

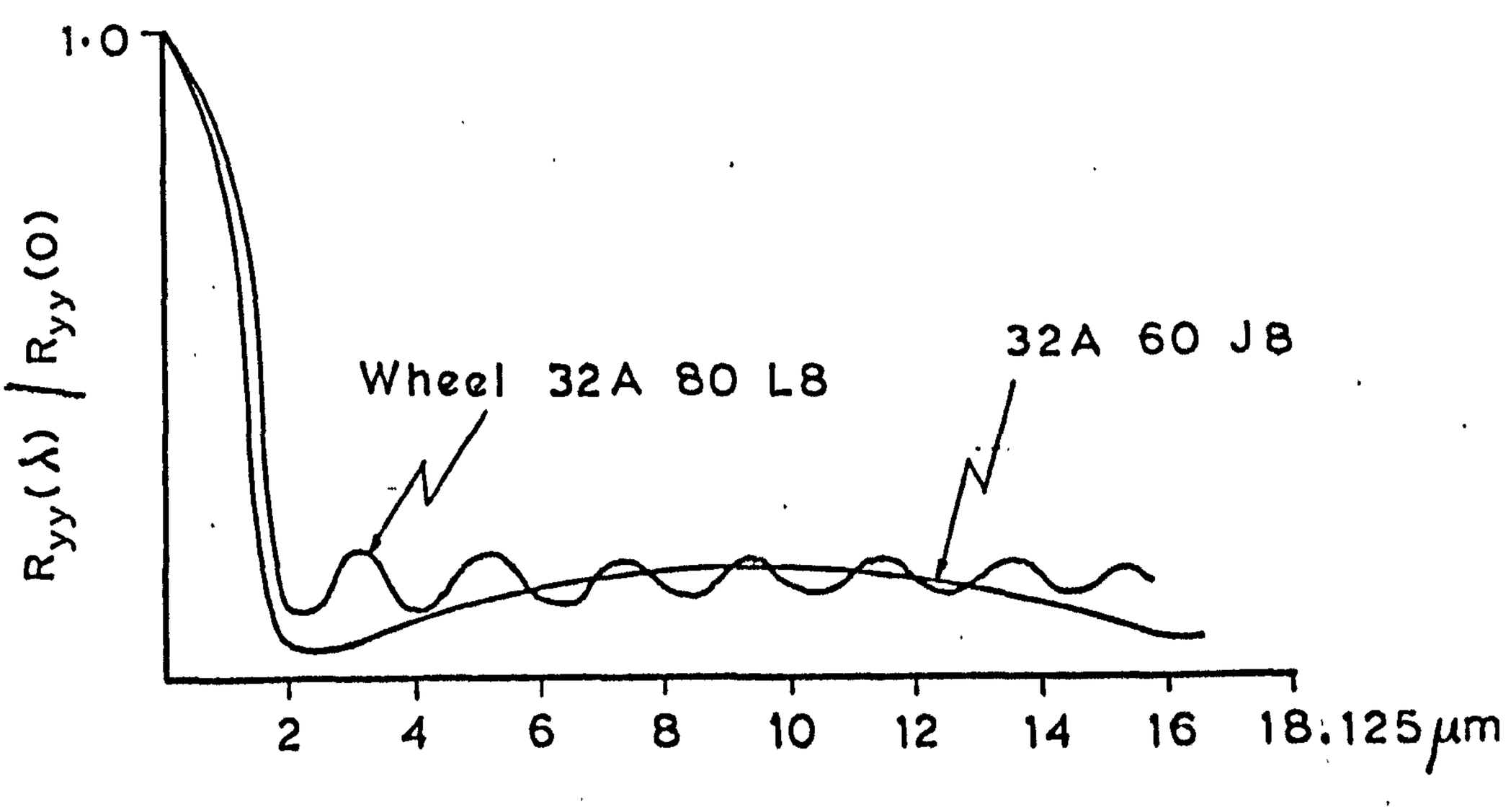

Fig. 9 Typical Autocorrelation Functions (After Peklenik[18])

constituting the surface. The cross correlation function is also discussed and a distinction made between positive, zero, and negative correlation by considering the decay characteristics of the function. He suggested that positively correlated profiles were those in which high points follow high points and low follow low. Zero correlation implied that successive rows of grits were randomly disposed so that the probability of a high following a high was just the same as that of a high following a low. Negative correlation implied that high points tended to follow low ones and vice versa, the profile thus "filling in" rapidly. From a performance point of view, the latter arrangement is highly desirable since the load per particle is equalised, wear reduced, and the surface texture of the ground component improved.

2.1.3 INFLUENCE OF DRESSING CONDITIONS ON ABRASIVE SURFACE PROPERTIES

There are basically two types of dressing procedure:-

(1) Diamond dressing, in which a single diamond or cluster is used to machine the wheel profile.

(2) Crush dressing. This process is usually associated with form grinding and requires a hardened steel roller to be fed radially into the wheel.

In this project, the first technique is adopted, since the method is more commonly used particularly in the precision grinding regime.

Looking through the literature, it appears that the work of Pahlitzsch[23,24] is very significant in that it is one of the few investigations which has attempted to relate dressing conditions to the resulting wheel roughness. The results were presented in the form of a 3-D graph, showing the effective wheel roughness as a function of the

dresser feed and depth of penetration, (Fig. 20). It was concluded that the effect of the diamond cross feed was far greater than that of depth, the influence of wheel speed being negligible.

Although many other investigators have considered the effects of dressing conditions, the objective has usually been to study the resultant radial wheel wear (see Section 2.3.3), the metal removal rate, and component surface texture, etc.[25] It is the author's opinion that a detailed investigation of the effects of dressing conditions upon the abrasive surface properties would constitute a useful contribution to grinding research.

2.2 STUDIES OF THE NATURE OF METAL REMOVAL IN GRINDING

2.2.1 SIGNIFICANCE OF WORK IN THE RELATED FIELDS OF FRICTION AND WEAR

Although metal grinding is usually considered within the context of metal cutting operations, it is essentially a high speed surface interaction problem. As a consequence, it displays many features common to the closely related field of friction and wear. Therefore, before considering the specific action of abrasive grits, it is worthwhile to examine the more general behaviour of two surfaces in sliding contact. The complex frictional bonds which occur have received a great deal of attention by numerous workers in both fundamental surface physics and associated subjects such as lubrication and wear.

The recent classification of the destruction of frictional bonds by Kragelskii[26] is of particular interest here. A spherical indentor was assumed to slide over a flat surface (Fig. 10), and it was suggested that five distinct types of event may occur:-

1. Elastic displacement
2. Plastic displacement
3. Microcutting
4. Trapping of surface films and subsequent destruction
5. Scuffing of surface films accompanied by tearing in depth

The first three were considered to arise during the mechanical interaction of asperities, and the last two as a consequence of molecular interactions.

In general, the action of a sliding indentor on a flat surface exhibits a number of distinct characteristics. The surface layers will become extensively deformed under the simultaneous action of normal and tangential loading, the resultant surface being either smooth as associated with elastic and plastic deformation, or jagged as a result of micro-cutting, scuffing and tearing in depth. A plastic wave will precede the indentor and extensive side swell may occur. When plastic deformation around the indentor is prevented, movement will either stop or material will pile up and eventually be sheared off. The high degree of strain in the surface layers may lead to complex chemical and mechanical changes influencing the resultant frictional behaviour. At very high speeds, metal surfaces will be subjected to extensive frictional heating which may result in thermal softening, or in extreme cases, bulk melting of the metal surface.

Following his initial classification of frictional bonds, Kragelskii examined the factors influencing the likely nature of an interaction. The h/R ratio was found to be an important criterion, where h = depth of penetration and R = radius of the contacting asperity. Another important consideration was the variation in shear strength with depth. From the point of view of grinding (see later), an important relationship

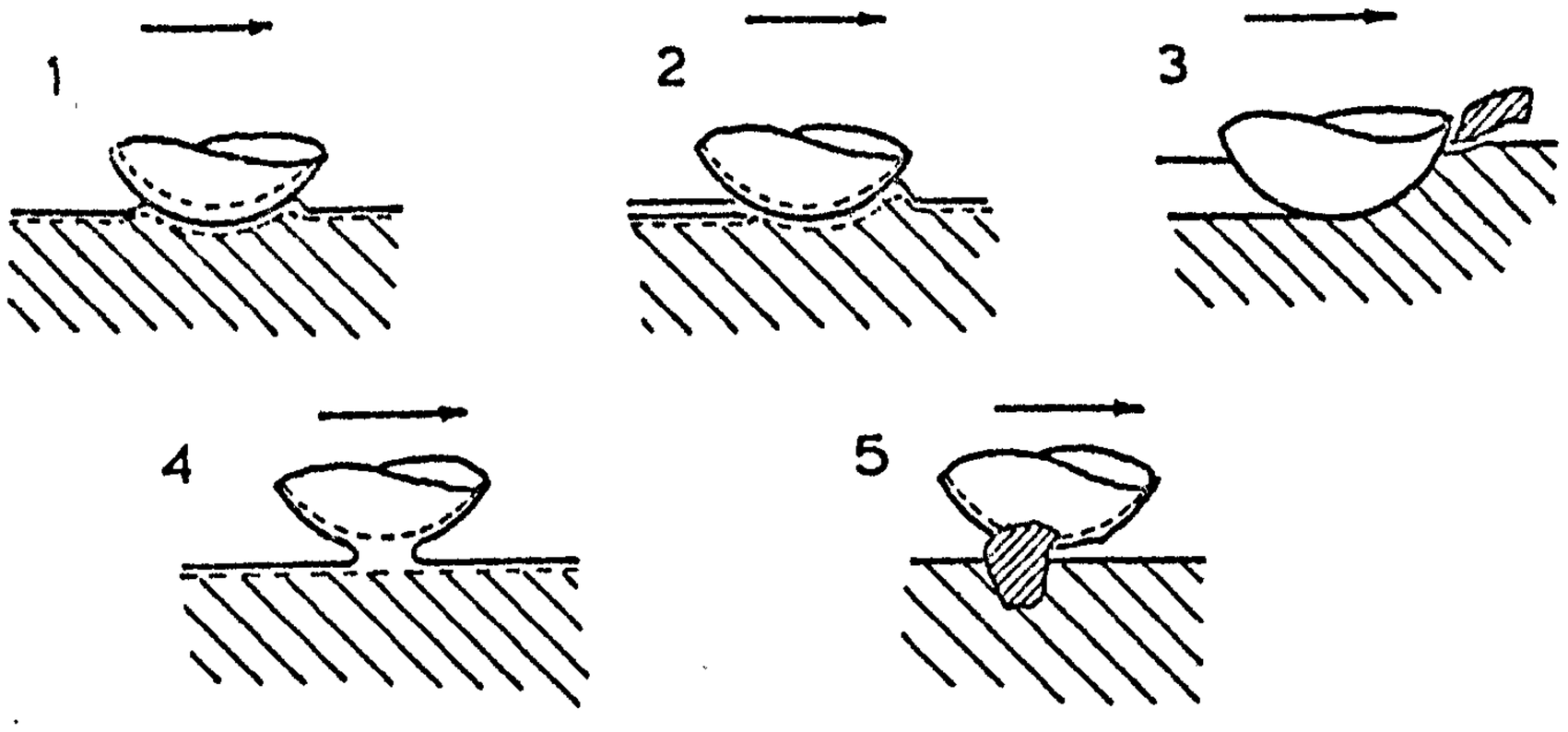

Fig. 10 Types of Surface Destruction
(After Kragelskii[26])

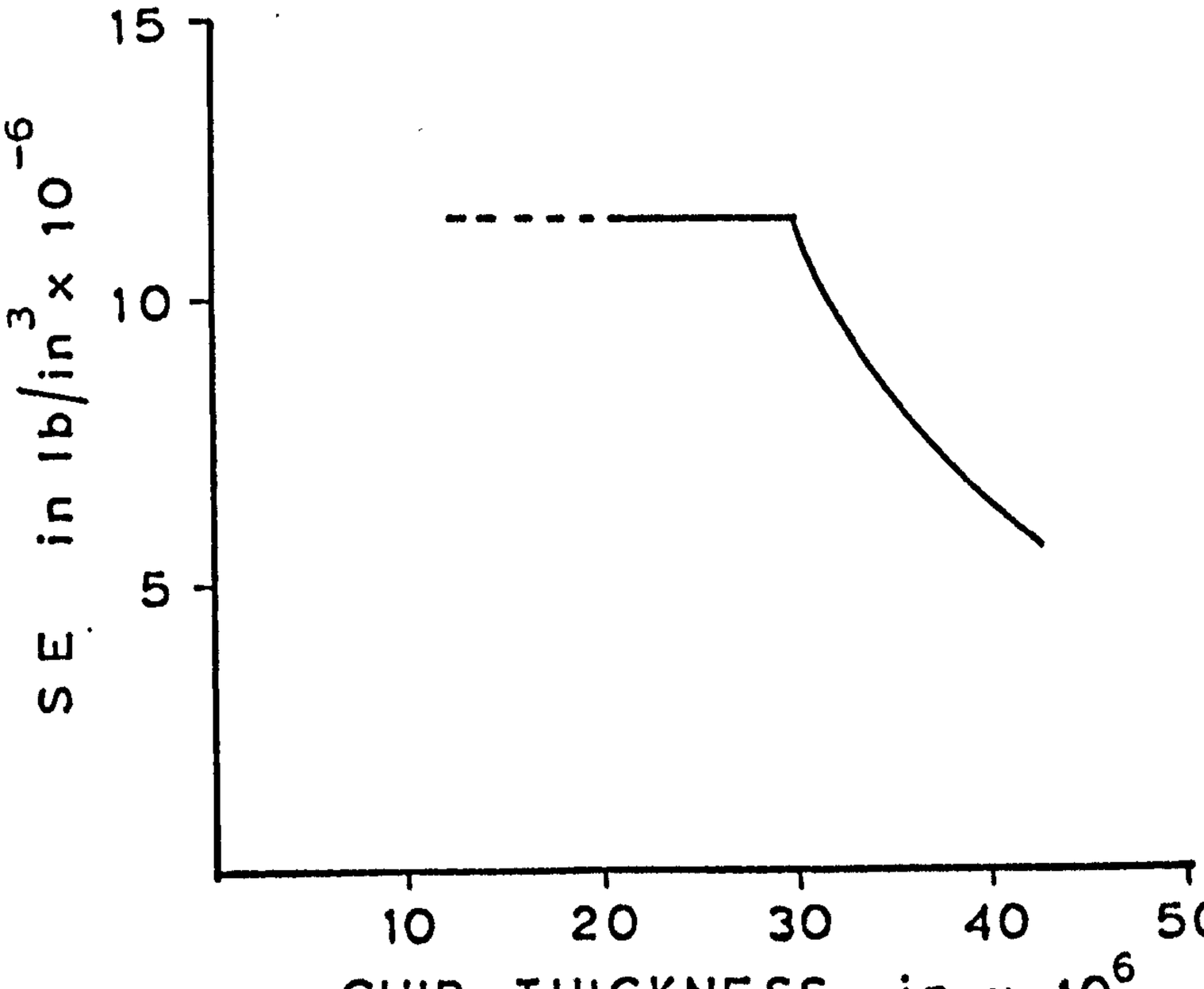

Fig. 11 Influence of the Size Effect
(After Backer et al[12])

was suggested for a critical depth of penetration, t_c, at which a transition from Type 2 to Type 3 destruction occurred. This critical depth was shown to increase with higher values of R and lower values of μ, the molecular coefficient of friction between the indentor and work.

Only a cursory examination of the grinding process is necessary to determine the relevance of the previous remarks to this mode of metal removal. Asperities of various shapes and sizes are seen to engage the workpiece surface, the actual grain depth of cut being generally less than 0.0002 in. The scratch left by any one grit will be characterised by a high width to depth ratio and it has been shown that considerable side swell may occur[27]. Since the cutting speed is generally upward of 5,000 ft/min , high instantaneous temperatures could develop giving rise to complex chemical and thermal softening phenomena. These will be accompanied by unpredictable strain rate and work hardening effects, the nett result being difficult to ascertain.

In fact, the metal surfaces will be subjected to all the types of damage specified by Kragelskii, although the ones of significance are the ploughing Type 2, the microcutting Type 3, and in some cases where the adhesive forces become excessive, the tearing in depth associated with Type 5. Class 3 destruction, which is generally undesirable in the normal contact of mating surfaces, may be considered the most efficient type of surface deformation from the point of view of metal removal in grinding. Types 1, 2 and 4 are inefficient since energy is wasted in in repeated deformations of the surface and in friction between the abrasive and metal, without any metal being removed. In addition, the resultant high temperatures produce excessive wheel wear rates. Type 5 wear, which may occur when the wheel is heavily "loaded" with metal particles, causes severe damage to the metal surface and must be avoided.

2.2.2 INVESTIGATIONS ON THE GRINDING PROCESS

The study of metal removal in grinding has been complicated by the extraordinary complexity of the abrasive surface geometry. In 1952 Backer et al[12], in order to simplify the geometry, utilised the micromilling process to simulate the type of metal removal encountered in grinding with particular regard to scale and speed. They discovered that the chip thickness is an important parameter in determining cutting behaviour, and observed a significant increase in specific energy, S.E., (the energy required to remove unit volume of material) with decreasing chip thickness - the so called "size effect" (Fig. 11). Subsequently[28] the S.E. was found to decrease with increasing cutting velocity, this being attributed to the reduction in friction at the chip-grain interface.

Armarego and Brown[29] expanded the work, again using the micro-milling technique and tools of known geometry. Theoretical and empirical relationships were presented for the variation in cutting force and S.E. with depth of cut. Their data on rectangular tools contradicted the size effect, the energy actually decreasing with a decrease in chip thickness.

Up to this point, microcutting was assumed to be the predominant mode of metal removal, little consideration being given to the rubbing and ploughing regimes. However, in 1962 Hahn[30] presented evidence to substantiate the presence of metal ploughing phenomena in the grinding operation. Whilst investigating a controlled force system he noticed a sharp change in the gradient of the normal force intensity curve when plotted against the wheel depth of cut, and attributed this to the transition from a mode of metal removal predominantly ploughing, to one of cutting (Fig. 12). In a later paper[31] he makes a distinction between two materials A and B, A being characteristic of easy to grind

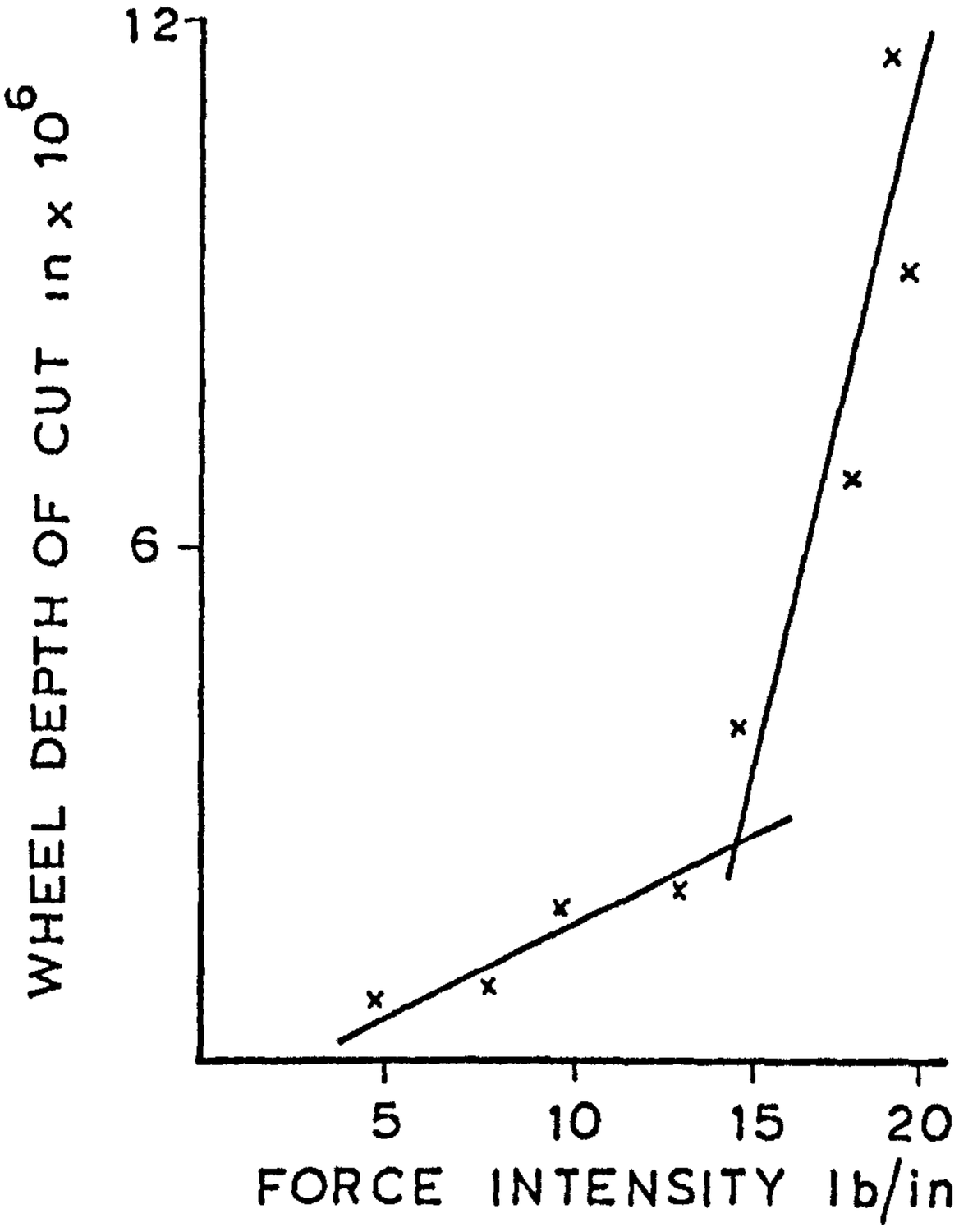

Fig. 12 Evidence of a Transition in the Mode of Metal Removal
(After Hahn[30])

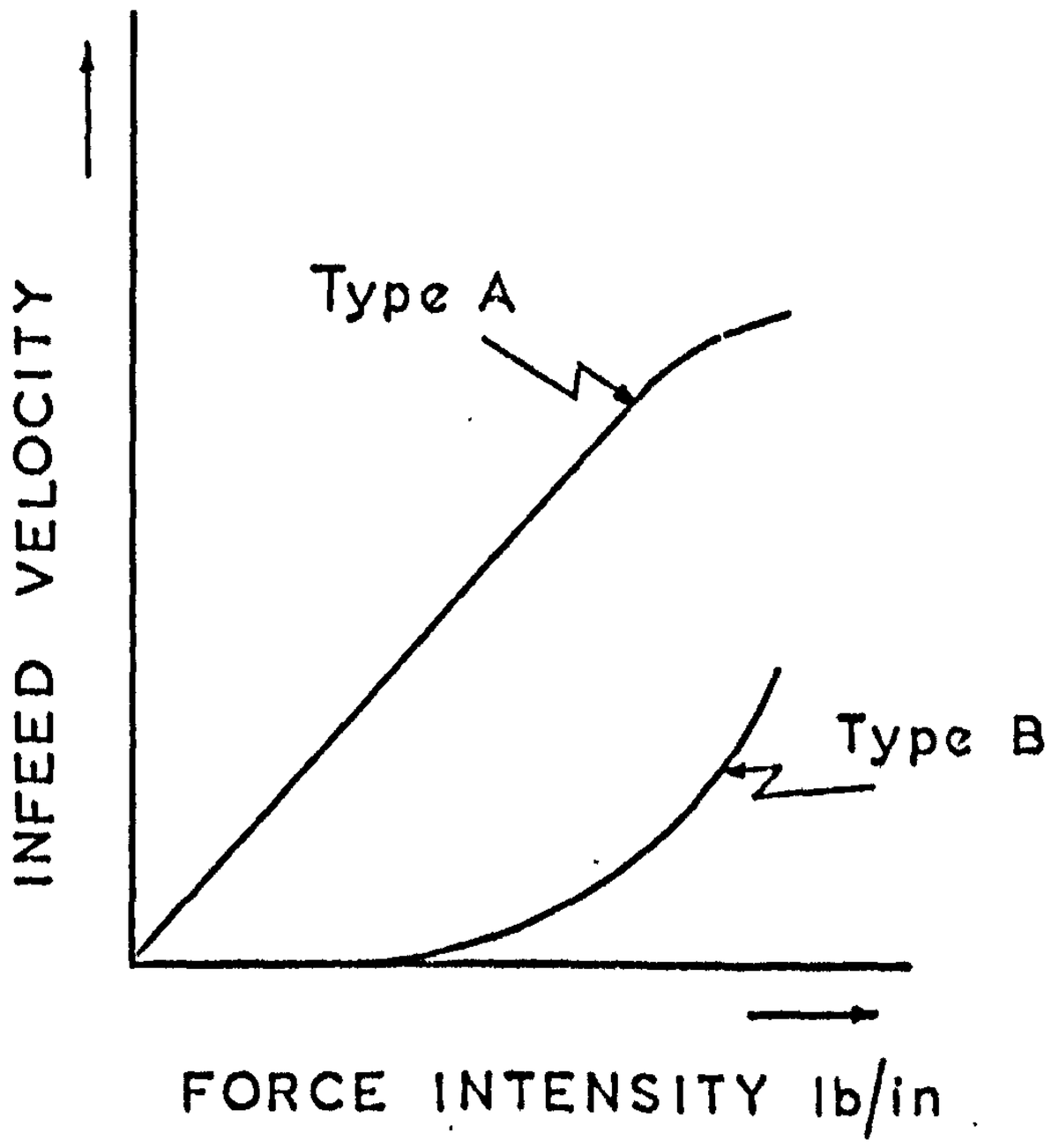

Fig. 13 The Grindability of Materials
(After Hahn[31])

metals, and B being representative of a group of materials having poor grindability. Fig. 13 shows the normal force intensity, F_N, plotted against the infeed velocity v_i. In the case of difficult to grind materials, v_i is not a linear function of F_N and there appears to be a threshold value of F_N which must be exceeded for metal removal to take place. He suggested that this is a consequence of the large amount of rubbing and ploughing associated with Type B materials. It was also postulated that the predominance of rubbing and ploughing phenomena associated with Type B materials was a consequence of the reluctance for fracture to occur within the "free plastic surface" preceding the grain (Fig. 14).

Having established the presence of rubbing and ploughing mechanisms in practical grinding operations, attention turned to a more detailed investigation of the factors influencing the mode of metal removal.

The significance of tool geometry as demonstrated by Kragelskii has already been discussed. About the same time, Sedriks et al[32] studied the action of loaded pyramidal tools when cutting lead at a speed of 1 in/min. The resulting groove cross-sectional area, A, was considered a function of the effective negative rake angle, α. As α became more positive, a rapid increase in A was observed at $\alpha = -30^{\circ}$ (Fig. 15). This was assumed to be the critical rake angle, α_c, at which the mode of metal removal changed from plastic deformation or ploughing to microcutting. The plastic deformation was analysed using Bowden and Tabor's[33] expression to determine the ploughing coefficient of friction, whereas the classic metal cutting analysis of Merchant[34] was applied to the microcutting regime. The analysis was also extended to include fully work hardened metals and alloys[35]. It was shown that the critical negative rake angle was determined primarily by the coefficient

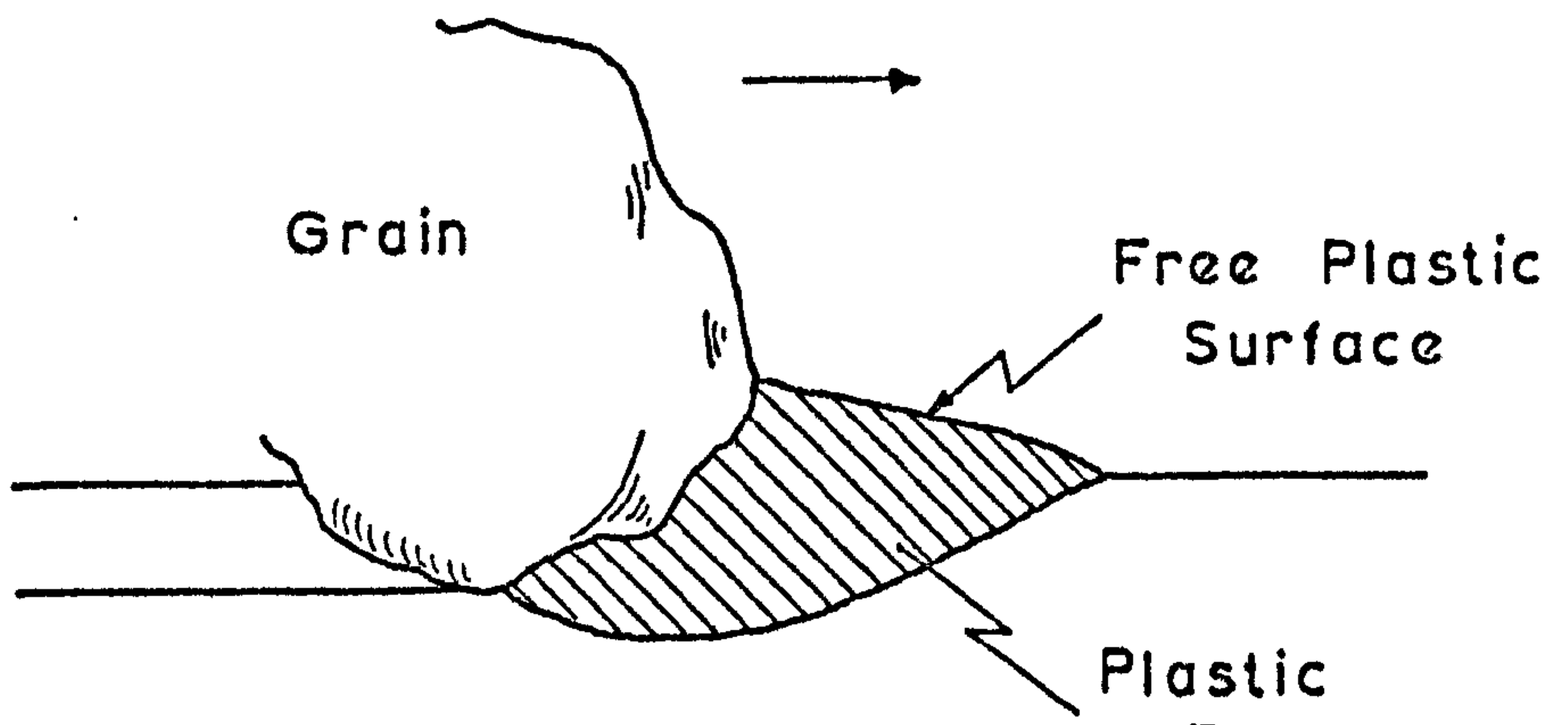

Fig. 14 Formation of a Free Plastic Surface (After Hahn[30])

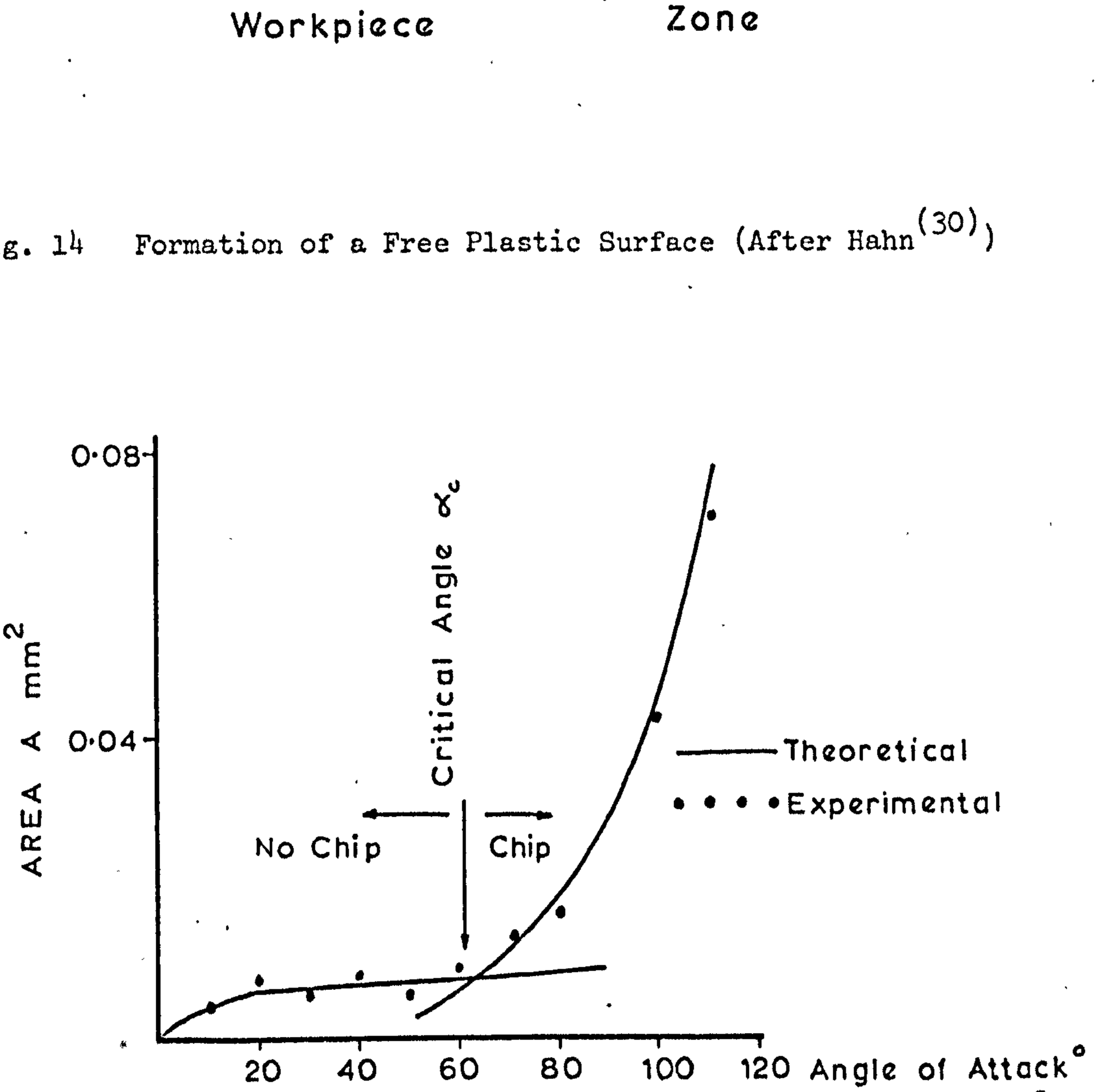

Fig. 15 Determination of the Critical Angle of Attack
(After Sedriks et al[32])

of friction between the contacting surfaces, whilst the initial increase in the force opposing the motion of an abrasive particle due to prior deformation of the workpiece was a consequence of an increase in hardness.

Rubenstein et al[36] investigated a micro-turning operation, and concluded that the method of metal grinding is no different in essence from other metal cutting techniques, and that any discrepancies can be attributed to the high negative rake angles inherent in the wheel structure. The critical rake angle was estimated to be in the region of -60° which is in considerable disagreement with the value obtained by Sedriks.

Rowe et al[37] have developed an elementary theory of metal displacement in grinding making the assumption that it is analagous to bulge formation in strip drawing. They predicted that metal can be removed in the form of continuous swarf or be displaced without actual removal. To this end, the geometry of the grit was considered to be a major factor. A qualitative explanation of the influence of friction and strain hardening was given, and the theory was supported by experimental evidence gained from large scale tests involving the cutting of plasticine with perspex tools.

By using specially prepared grinding wheels, Tanaka et al[38] have been able to study the influence of various abrasive wheel parameters upon the transition depth, t_c, under realistic grinding conditions. (Ideally t_c should be minimised in order to increase the percentage of abrasive asperities actively engaged in cutting.) The value of t_c was seen to increase with increasing wheel hardness and grit size, and to decrease with increasing velocity. Shonozaki et al[39] obtained estimates of the tangential cutting force, T, and the normal force, N, developed when cutting single grooves with a specially designed fly

cutter at speeds of up to 60 ft/min (Fig. 16). They concluded that the regions of rubbing, ploughing and microcutting were in evidence at subsequent sections along the groove, and that a rise in the N/T ratio signified an increase in the extent of the ploughing phenomenon.

Continuing this approach, Crisp et al[40] examined the forces developed when real abrasive grits cut single grooves in metal surfaces, at speeds more consistent with normal grinding practice (6,000 ft/min). They concluded that the high groove width to depth ratios obtained led to extensive rubbing and ploughing phenomena which resulted in high specific energies.

Despite the considerable amount of experimental work which has been undertaken into the mode of metal removal, there appears to be a considerable lack of information based on conditions realistic of the actual metal grinding process. Although the information gained from slow speed/large scale of deformation tests may make a substantial contribution to the understanding of metal grinding mechanics, the true validity of any conclusions drawn from such data is questionable, when one considers the vastly different conditions of a practical grinding operation.

2.3 FURTHER ASPECTS OF THE GRINDING PROCESS

2.3.1 FORCE AND ENERGY CONSIDERATIONS

The earliest papers to be published on the mechanics of metal grinding appear to have been published by Alden[41] and Guest[42]. Expressions were obtained for the maximum undeformed chip thickness, t. The maximum force per grain was then assumed to vary as t by Alden and as t^2 by Guest. Following further estimates of chip thickness by

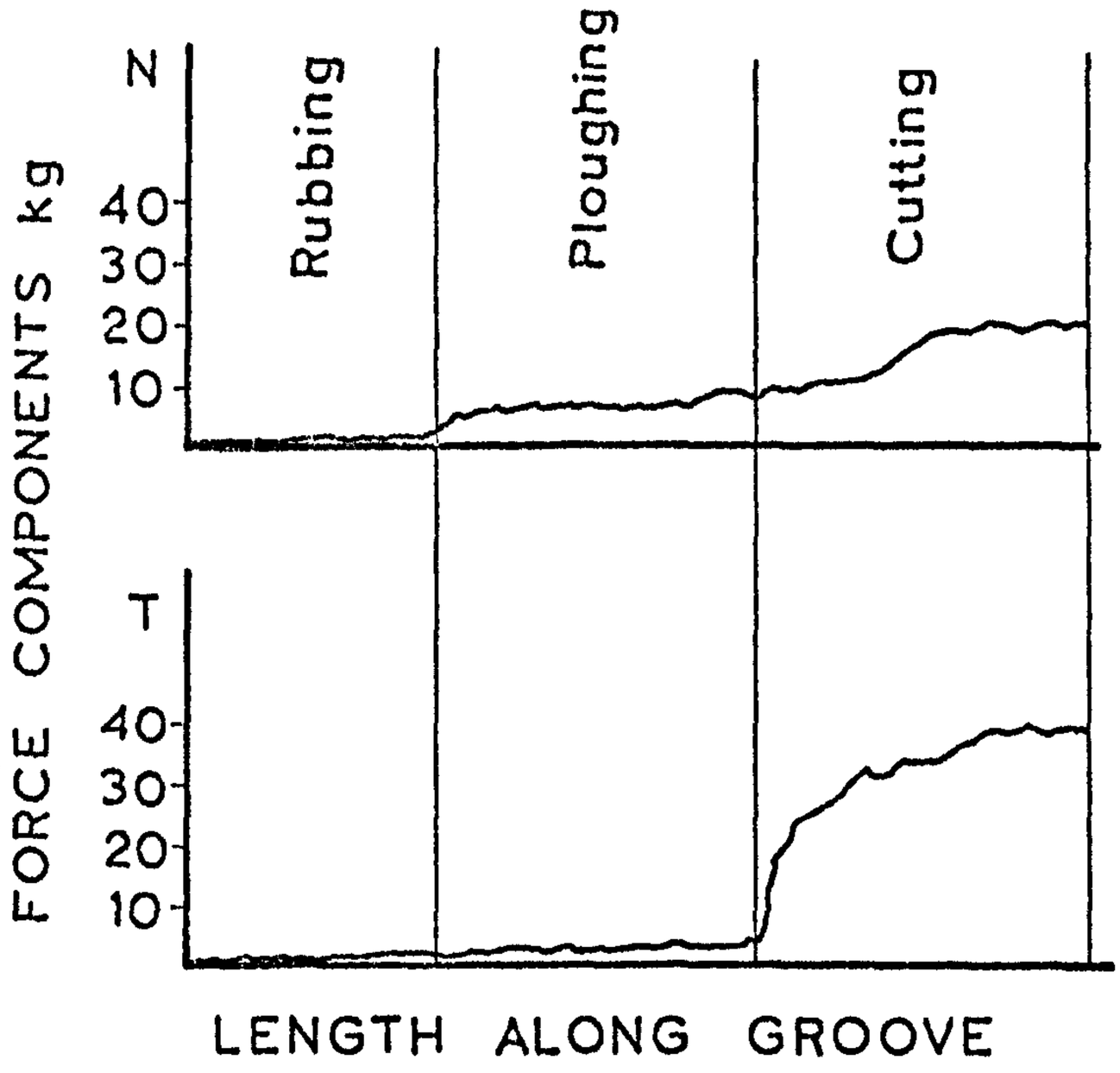

Fig. 16 Force Traces Associated with the Formation of Individual Grooves (After Shonozaki et al[39])

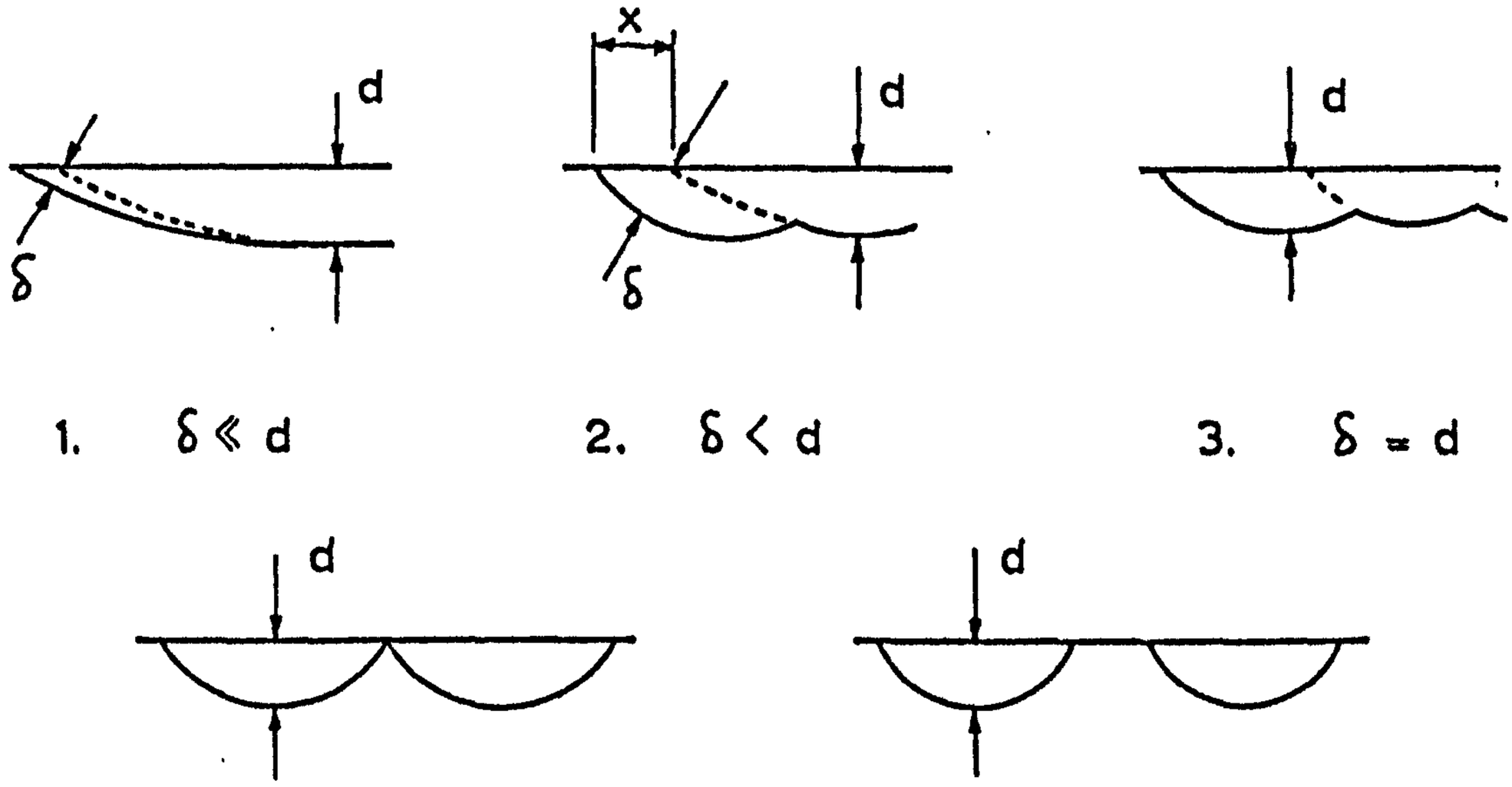

Fig. 17 Types of Groove Formation (After Reichenbach et al[45])

Hutchinson[43] and Heinz[44], Reichenbach et al[45] classified grinding chips into five distinct types depending on their thickness to length ratio (Fig. 17). The classifications covered all types of wheel grinding and it was found that the S.E. was strongly dependent upon chip type.

In 1952 Marshall and Shaw[46] developed the first dynamometer for measuring directly the tangential and normal forces during a simple surface grinding operation. They established the "coefficient of grinding" as the ratio of the tangential and normal forces and determined a value of approximately 0.5 for steel. They stressed the importance of S.E. as a criterion for interpreting grinding data and found the value to be about 10×10^6 lb f/in^2 for steel. An interesting comparison can be made with straightforward single point turning data, where the above results are approximately 2 and 0.5×10^6 lb f/in^2. The large discrepancy in energy is indicative of the overall inefficiency of the grinding process when compared with more conventional machining operations. The grinding force components and S.E. were observed to be independent of the material hardness, this being attributed to the size effect.

The previously reported (Section 2.2.2) work of Backer[12] and Armarego[29] is also of interest here. By considering the mean effective rake angle of the grinding process to be 0°, Backer determined the percentage energy due to shear. He further concluded that the percentage of total energy due to friction increased as the depth of cut decreased.

Grisbrook[47] also examined the forces developed in surface grinding and substantiated the values of S.E. and grinding ratio determined by Marshall and Shaw[46].

Kumagai et al[48] have investigated the role of the frictional force in grinding, with a view to ascertaining the relative merits of wheels treated with lubricants in various ways. The work is interesting in that it attempts to separate the cutting and sliding components of the tangential cutting force, T. Using a surface grinding operation and specimens of decreasing width, b, the relationship between the forces T and N, and b was determined (Fig. 18). A value for the coefficient of friction between wheel and workpiece, μ, was derived by extrapolating the results to $b = 0$ and defining $\mu = (T/N)_{b=0}$. The tangential force was assumed to consist of two components, the frictional force T_f and the cutting force T_c. By assuming $T_f = \mu N$, the magnitude of the work done in actually shearing the metal was determined (shaded area Fig. 18).

Story[49] has also succeeded in a similar isolation of the sliding components when grinding with coated abrasives. During the initial stages of grinding, the tangential component obtained experimentally was considered to be entirely due to cutting, the wheel being in a sharp condition. In the final stages of grinding when the wheel became worn, the tangential component was assumed to be entirely due to sliding. An expression was determined for the rate of stock removal which was claimed to be a good fit for much of the data gathered in constant force plunge grinding experiments.

Hahn[31] has developed a theory of metal removal for metals in the absence of extensive rubbing and ploughing. Based on the previously mentioned "metal removal parameter", he considers the theory of a system where all the active grits in the interference zone are condensed to give a continuous effective width of cut, the elasticity of the wheel - workpiece system being allowed for in calculating the depth of

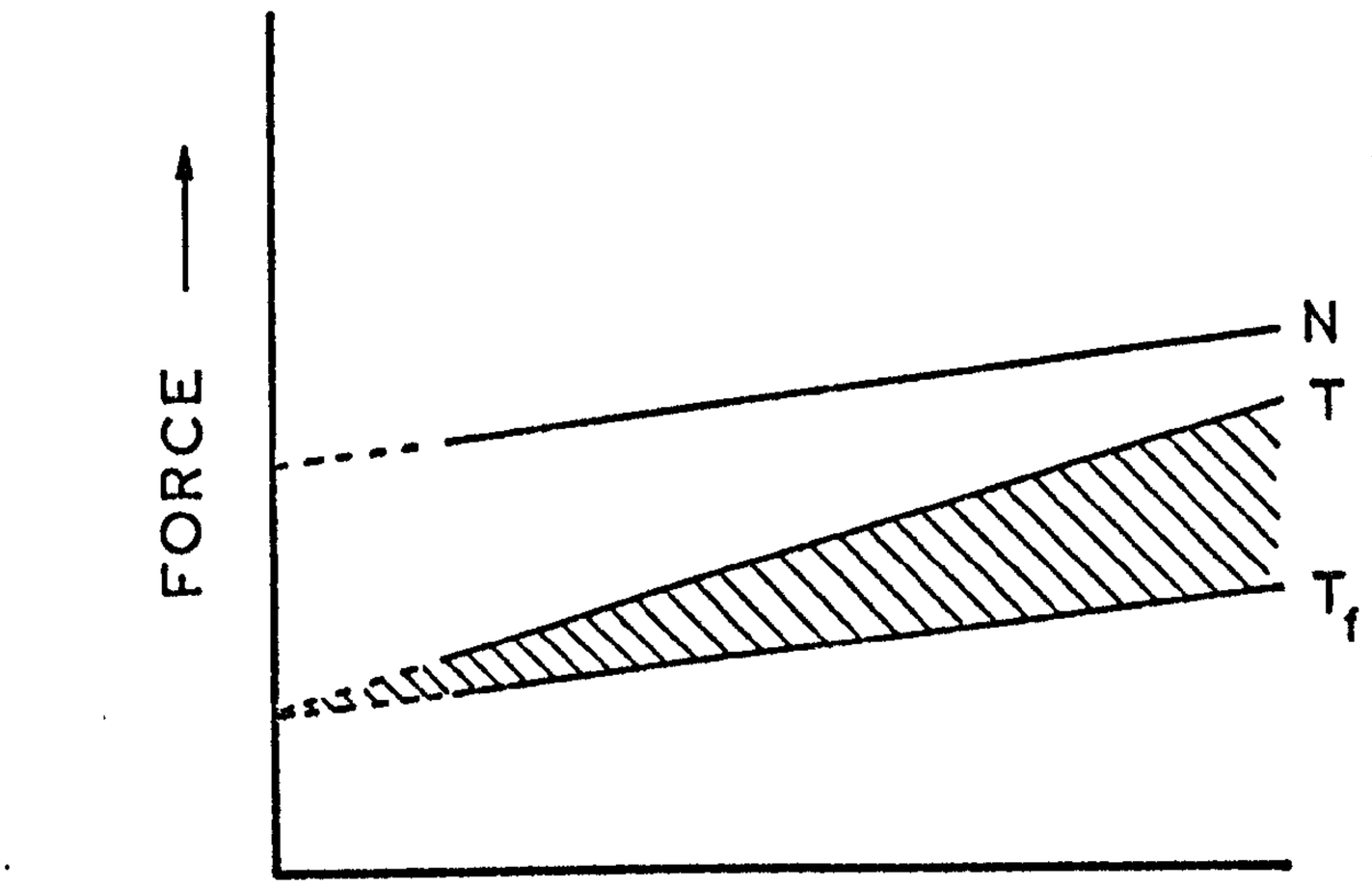

Fig. 18 Determination of the Frictional Force (After Kumagai et al[48])

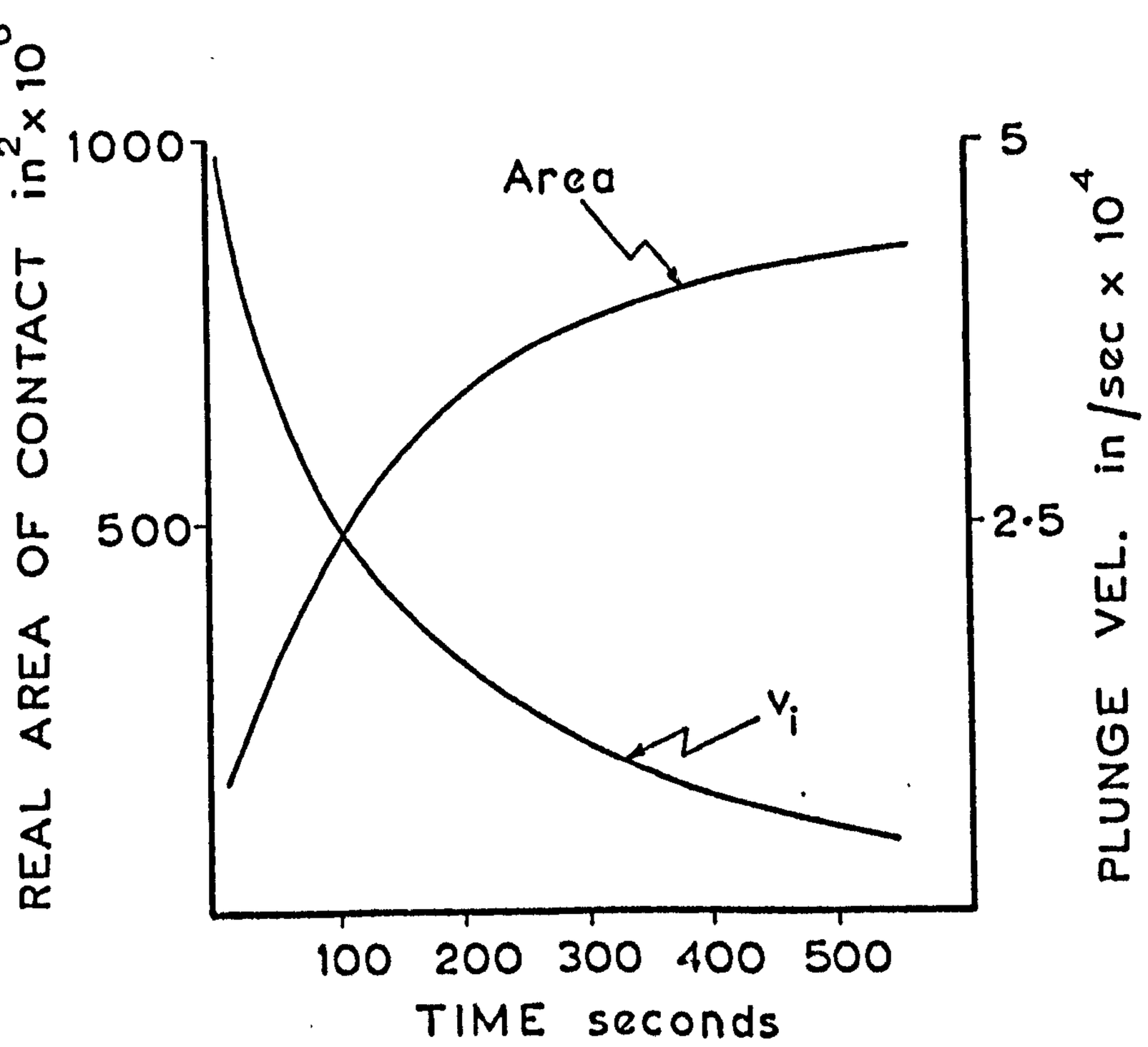

Fig. 19 The Effect of Abrasive Wear upon the Real Area of Contact and the Infeed Velocity (After Hahn[53])

cut. The results gave a simple empirical equation for the metal removal parameter (or an equivalent S.E.) which was in agreement with experimental observations.

2.3 2 ABRASIVE WEAR

Before continuing, it should be noted that throughout this report, the term "abrasive wear" refers to the deterioration of the abrasive material. This is pointed out to avoid any confusion with the terminology adopted in general wear studies, in which "abrasive wear" usually refers to the deterioration of the metal surface by abrasive processes.

In the past, three distinct types of abrasive wheel wear have been classified:-

1. Attritous wear
2. Partial fracture of grains
3. Complete dislocation of grains caused by bond failure.

The first type occurs as a result of continued mechanical interactions giving rise to wear by plastic flow[50], disintegration[51] and chemical solubility[52].

It is generally assumed that attritous wear increases the area of contact between the abrasive grit and workpiece[51,53] and results in a deterioration of the wheel's cutting ability. Detailed microscopic studies of the abrasive grain surface have been undertaken, particularly in Japan[54,55]. It appears that the surfaces of newly dressed grits have a very fine serrated structure. On grinding, the surfaces become relatively smooth and develop striation marks in the grinding direction.

The probability of the occurrence of the second or third type of wear depends to a large extent on the wheel hardness, and the relative strengths of the grain and bond. In hard grade wheels, the strength of the bond bridges may be high compared with that of the grain, and partial fracture is likely. On the other hand, with soft grade wheels having weak bonds, total dislocation of grains will be the probable mode of fracture.

Yoshikawa[56] et al have investigated the fracture of bond bridges in grinding wheels. An analysis was undertaken assuming the mechanism to be analogous to the fracture of brittle materials. They concluded that the wear rate could be expressed as a single exponential of the grinding velocity and a double exponential of the grinding force.

Hahn[53] has approached the problem of wheel wear in a different manner. In ref(30) he introduced the idea of a sub-surface thermally induced stress in a grit, caused by the heat conducted into the grit during its brief engagement with the workpiece. Thus as the wear flat on the grain gradually increases, the heat input to the grain surface rises, thereby increasing the sub-surface thermal stress until finally the grain fractures. In this way an equilibrium distribution of the grain population is reached (Fig.19). A further correlation was obtained between the rate of wheel wear and the length of the interference zone (the concept of an interference zone is discussed in ref(30) where it was shown that the heat input to the grain increased as the length of the zone increased). No correlation was observed between the rate of wheel wear and the average normal stress. This led Hahn to conclude that wheel wear can be satisfactorily explained by the thermal stress fracture mechanism and is not dependent on the fracture caused by the mechanical loading of grains. It seems more likely however, that fracture wear is a combination of mechanical and

thermal mechanisms, the former being predominant in soft wheels, the latter in hard wheels. It is also worth noting that providing the wear rate is not catastrophic, fracture wear may be desirable as it produces a wheel "self-sharpening" action as new cutting edges are continually regenerated.

2.3.3 THE INFLUENCE OF DRESSING CONDITIONS ON ABRASIVE WEAR

The influence of dressing conditions upon wheel wear was first considered by Pahlitzsch[23]. He presented an interesting graphical relationship between the dressing feed and depth, and the wheel roughness (Fig. 20). The two envelopes A and B represented the wheel roughness before and after grinding. The curve XY was deemed to describe a set of conditions for which the abrasive surface roughness did not change:- the so-called "optimum dressing conditions".

A similar set of conditions was specified by Makino[57] based on the variation of cutting point spacings during grinding. The number of large spacings was seen to increase when grinding with finely dressed wheels whereas an increase in the total of small spaces was observed for coarse dressing conditions. It was postulated that optimum dressing conditions would be attained when the cutting point spacing remained constant throughout the grinding operation.

Pattinson et al[15] have identified three distinct stages of abrasive wheel wear (Fig. 21):-

a) A primary region of rapid wear

b) A secondary region of more uniform and decreased wear

c) A tertiary region. This occurred only under certain conditions and caused an increase in the wear rate after the wheel had become glazed.

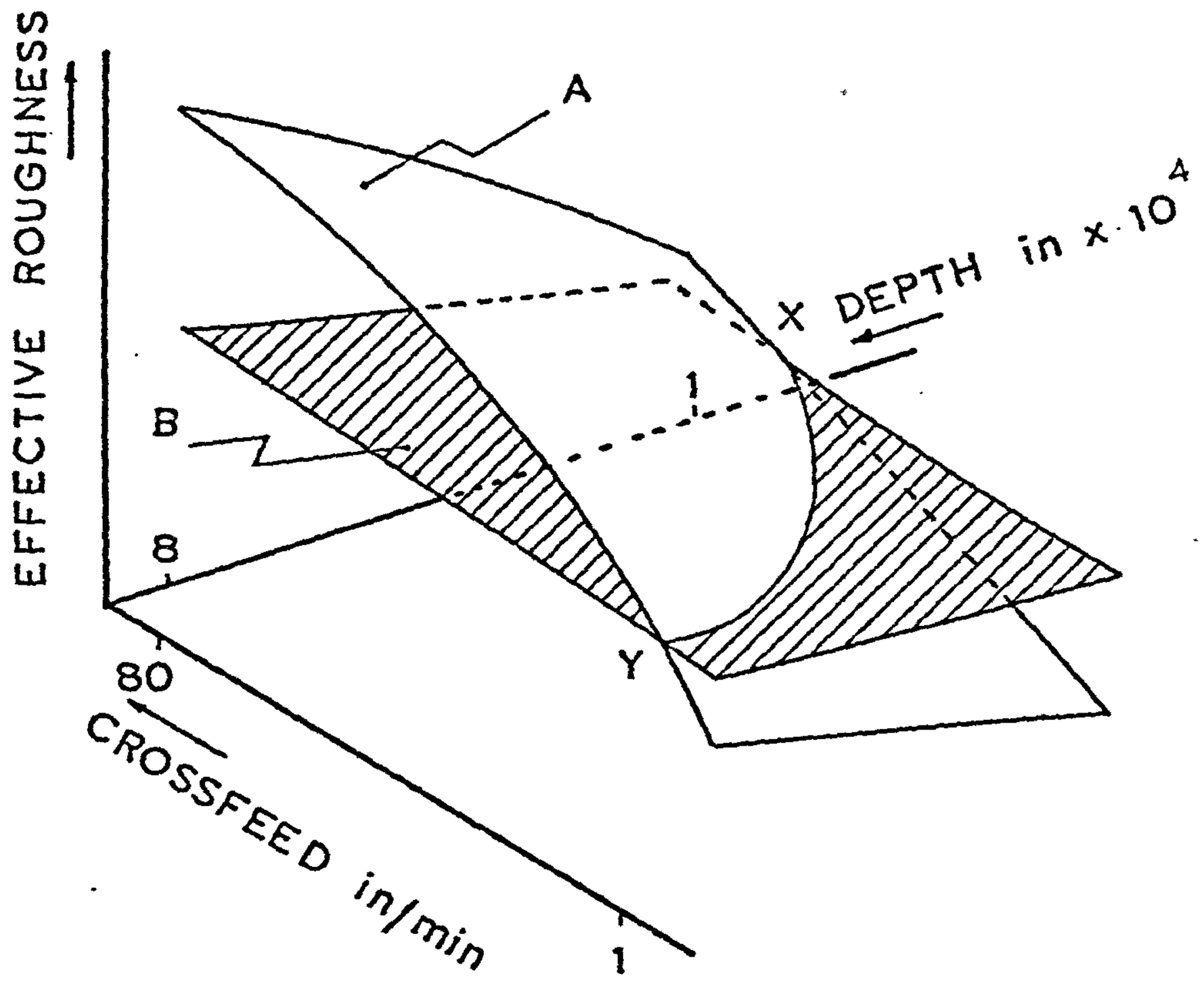

Fig. 20 Abrasive Surface Topography Measurements (After Pahlitzsch[23])

Coarse dressing produced a wheel surface having a relatively low density of active cutting edges and a large amount of primary wear. It was suggested that rough dressing resulted in severe damage to the wheel structure causing grains to fracture out readily during grinding - hence the large primary wear. The number of active cutting edges was observed to increase steadily with wear, the rate of increase being much higher for finely dressed wheels.

The above work is typical in that it does not include a detailed quantitative examination of the newly dressed surface profile. With a knowledge of even, say, the elementary statistical parameters associated with the asperity height distribution, the prediction and explanation of wheel behaviour would probably have been greatly simplified.

2.3.4 THE APPLICATION OF GRINDING FLUIDS

Harada et al[58] have used a constant load plunge grinding system to investigate the performance of various grinding fluids. They concluded that in wet grinding with water soluble type fluids, the grain flank wear is less than in dry grinding, giving increased efficiency. A wheel self-sharpening action was also evident resulting from the thermal fracture of grains accentuated by the alternate heating and quenching. When steel specimens were ground, the wear rate of SiC grains was higher than that of Al_2O_3 grains, indicating the presence of chemical effects.

Duwell et al[59,60] considered the grinding of mild steel, stainless steel, commercially pure titanium and aluminium, in air, the inert gas argon, under a water flood, and with a proprietary lubricant. In all cases, the substitution of argon for air in the grinding interface region resulted in a catastrophic increase in the energy consumed. A number of theories were proposed to explain the mechanism by which

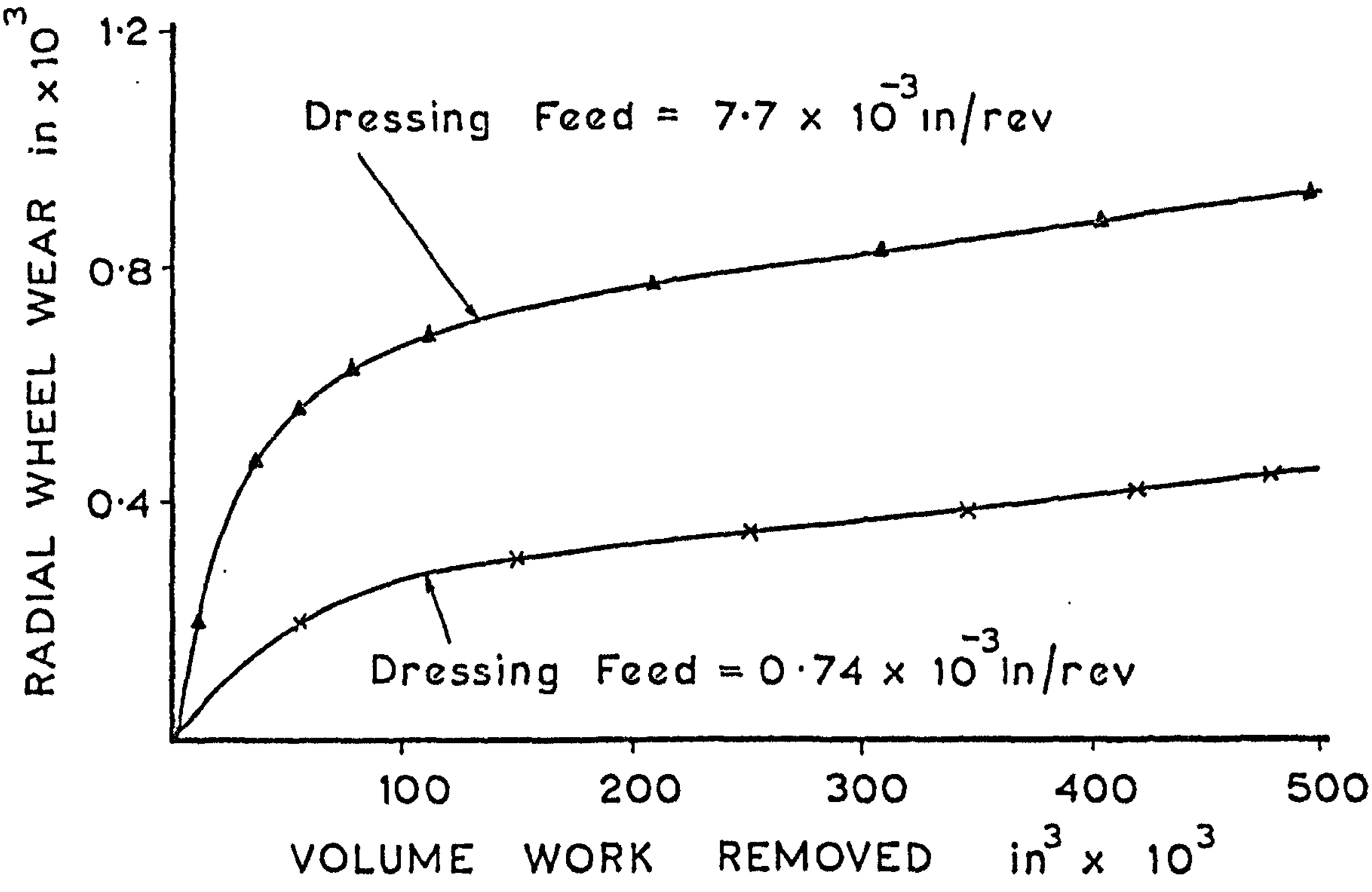

Fig. 21 Primary and Secondary Wear Regimes (After Pattinson et al[15])

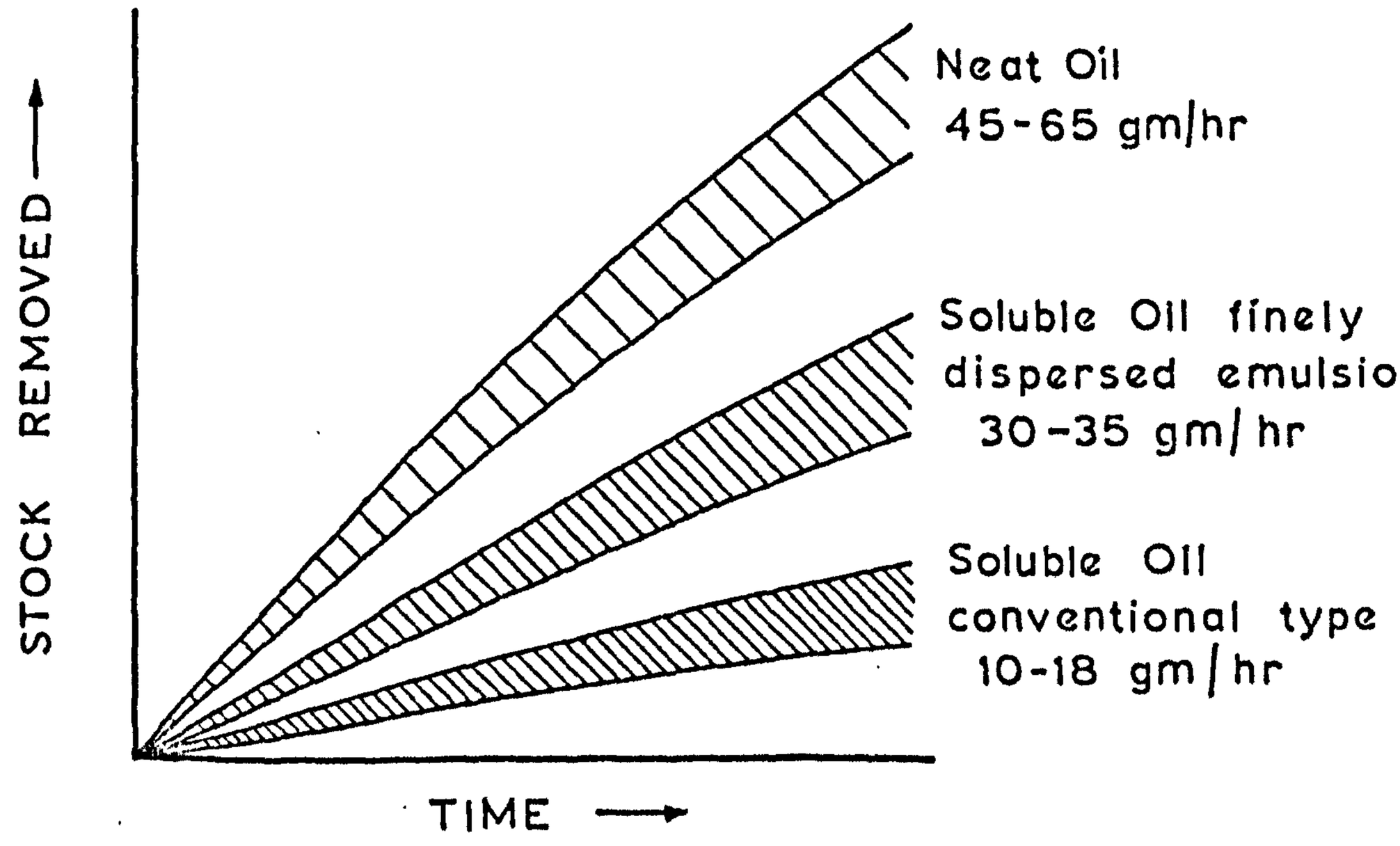

Fig. 22 Effect of Lub rication on the Metal Removal Rate
(After Chalkey[61])

reactive chemicals decrease the energy required for chip formation, and thereby diminish tool wear. These included a decrease in adhesion at the grain - workpiece boundary, the prevention of chip rewelding, and a decrease in metal strength caused by oxidation.

Chalkey[61] has studied the grinding of hard materials, e.g., carbides, using diamond impregnated wheels. A variety of cutting oils were employed and a substantial reduction in wheel wear resulting from increased lubrication at the grain - workpiece interface was noticed This is illustrated in Fig. 22 where the stock removal rate is seen to be higher for neat oils.

When using cutting fluids on an internal plunge grinding operation, Hahn[53] observed a considerable hydrodynamic effect. As the flow rate was increased, the radial stock removal rate was observed to decrease, and an appreciable reduction in the cutting force was also observed. By considering the passage of a worn abrasive flat through the grinding zone, he confirmed theoretically that a considerable load could be supported by hydrodynamic effects.

Furuichi et al[62] have shown that using emulsion type grinding fluids, the effect of emulsifier concentration on the rate of stock removal varied markedly with the wheel dressing conditions. For any one fluid, an optimum value of fluid concentration for maximum grindability was observed, the optimum being shifted to a higher value with increasing wheel roughness. This raises the important consideration that when evaluating the performance of cutting fluids using free infeed plunge grinding techniques, the wheel dressing conditions must be taken into account.

The main effects of applying cutting fluids can be summarised as follows:-

1) A substantial reduction in the wheel - workpiece interface

temperature. This results from two distinct mechanisms, viz., the conducting away of heat by the fluid and a lubrication effect causing a reduction in frictional heating. Wheel wear is depressed, surface finish is improved, the risk of metallurgical damage to the workpiece surface is minimised, and the reduction in thermal expansion facilitates the attainment of geometrical accuracy.

2) A chemical effect. The nascent surfaces and high temperatures present in the cutting zone offer favourable conditions for extraordinary chemical reactivity. The presence of cutting fluids will have a marked effect on both the type and speed of reactions, which in turn influences the resultant temperature, the frictional behaviour, and the rate of wear by chemical solubility.

3) A wheel self-sharpening action may be induced.

4) Continually washing the wheel surface ensures that debris is cleared away, and the wheel is kept "open" and "free-cutting".

Although not really the subject of this work, the many other factors involved in the selection of grinding fluids such as corrosion properties, susceptibility to bacterial contamination, chemical stability, disposal problems, and economic considerations are conveniently dealt with in articles similar to ref. (63).

CHAPTER III

ABRASIVE SURFACE TOPOGRAPHY MEASUREMENT

This chapter deals with a quantitative description of abrasive surfaces in terms of the basic statistical properties of the surface profile, e.g., mean, standard deviation, skewness of the height distribution, and the autocorrelation and power density functions. The practical aspects of obtaining such measurements and their eventual contribution to the understanding of abrasive wheel behaviour are major considerations.

It was shown in Section 2.1.3 that the effect of the dressing operation on abrasive wheel surface properties has largely been ignored. For this reason, considerable attention has been given to variations in dressing conditions.

3.1 APPARATUS

As already discussed (Section 2.1.1), despite its many shortcomings, the stylus tracing technique still presents a convenient method of obtaining surface profiles, and is thus adopted here. In the present work, however, a conventional instrument cannot be used. This is mainly because the large amplitude fluctuations and abrasive nature of the surfaces would undoubtedly damage the delicate stylus tracing mechanism. A special scanning device integral with the grinding machine was therefore constructed. This permitted scanning in both the axial and circumferential directions without removing the wheel from the machine. In addition, by suitably mounting the measuring head on the grinding machine table, complicated alignment problems were avoided. This also simplified the overall design of

the device, since it was possible to make use of the accurate machine infeed and crossfeed facilities.

3.1.1 THE GRINDING MACHINE

A standard Jones Shipman cylindrical grinder, Model 1310 was used. Two minor modifications were made to provide the required axial and circumferential scanning facilities for measurement purposes:-

a) Axial scanning

Here the abrasive wheel was held stationary and the measuring head traversed automatically across the wheel surface by way of the machine table. In order that the surface profile should not become distorted by the stylus resonance, the scanning speed was limited to 1 in/min. Although the automatic drive, which is hydraulically controlled, is capable of attaining a wide range of traverse speeds, it was found that at very low speeds (less than 5 in/min.) the movement became erratic. For this reason it was decided to utilise the purely mechanical manual drive which was available on the machine, in the following way:-

A fractional hp DC motor with suitable gear box and reverse switch was mounted adjacent to the grinding machine, and coupled to the manual drive by a simple pulley and belt system. Before operating, the table was traversed at full speed and maximum sweep using the hydraulic drive, to ensure adequate lubrication of the slideways. On engaging the alternative mechanical drive, a constant axial scanning speed of 1 in/min was then obtained.

b) Circumferential scanning

In this case, the measuring head was held stationary, and the wheel surface rotated across the front of the stylus. Assuming an average wheel diameter of 12 in., a rotational speed of 0.0265 rpm was necessary to achieve a surface speed of 1 in/min. This was accomplished by using a variable speed DC motor (0 - 250 rpm) in conjunction with a double worm reduction gear box of 10,000:1 speed ratio. The motor and gear box were mounted on a stand adjacent to the drive pulley located on the grinding wheel spindle. The main belt drive was disconnected and the slow speed attachment operated through a self-aligning coupling linked to the drive pulley. Again, after a suitable warm up period with the wheel rotating at full speed, satisfactory slow speed rotation was obtained.

The grinding machine complete with modifications is shown in Fig. 23.

3.1.2 THE MEASURING SYSTEM

The measuring head is shown in position on the grinding machine in Fig. 24a. The associated electronics are shown in Fig. 24b.

The displacement sensitive element is a Vibrometer TS/1230 inductive feeler. Essentially, this consists of an inductive movable core and forms a half-bridge circuit. The core is guided by two diaphragms and protrudes from the transducer casing in the form of a small threaded feeler to permit the mounting of different tips. In this case a diamond stylus taken from a standard Tomlinson profilometer was used. The transducer has a range of ± 0.025 in.

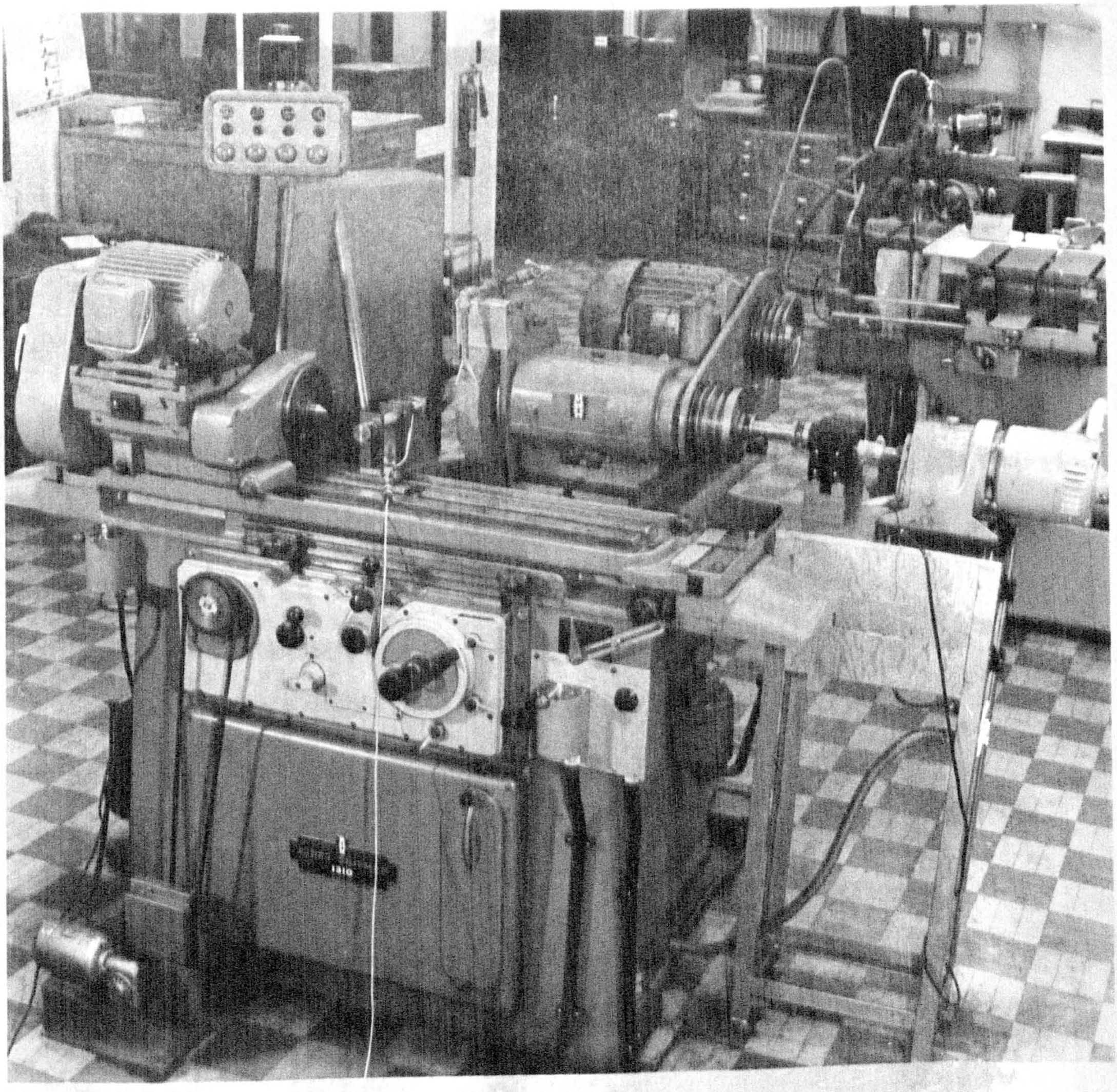

Fig. 23 Cylindrical Grinding Machine and Modifications

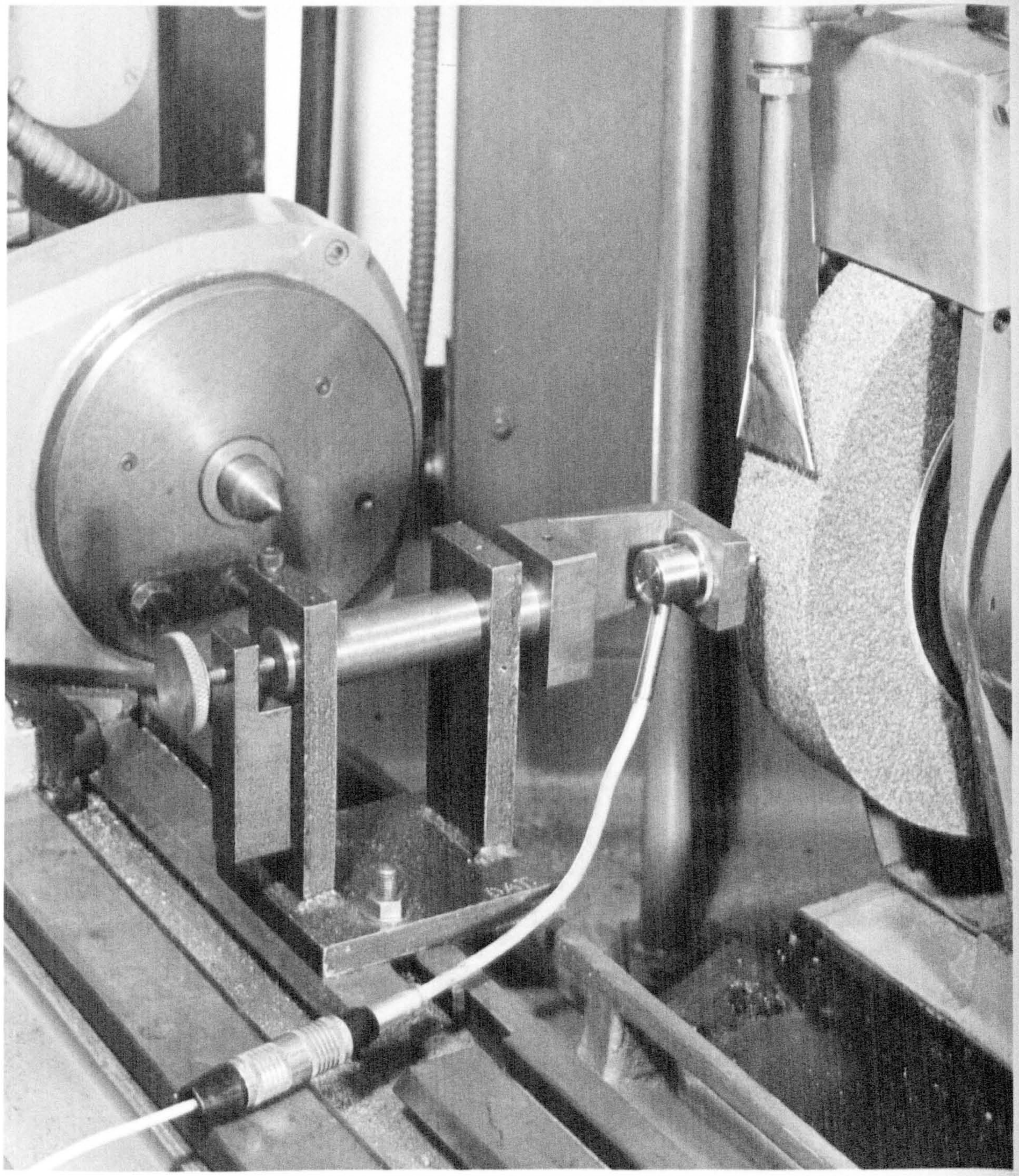

Fig. 24a The Measuring Head

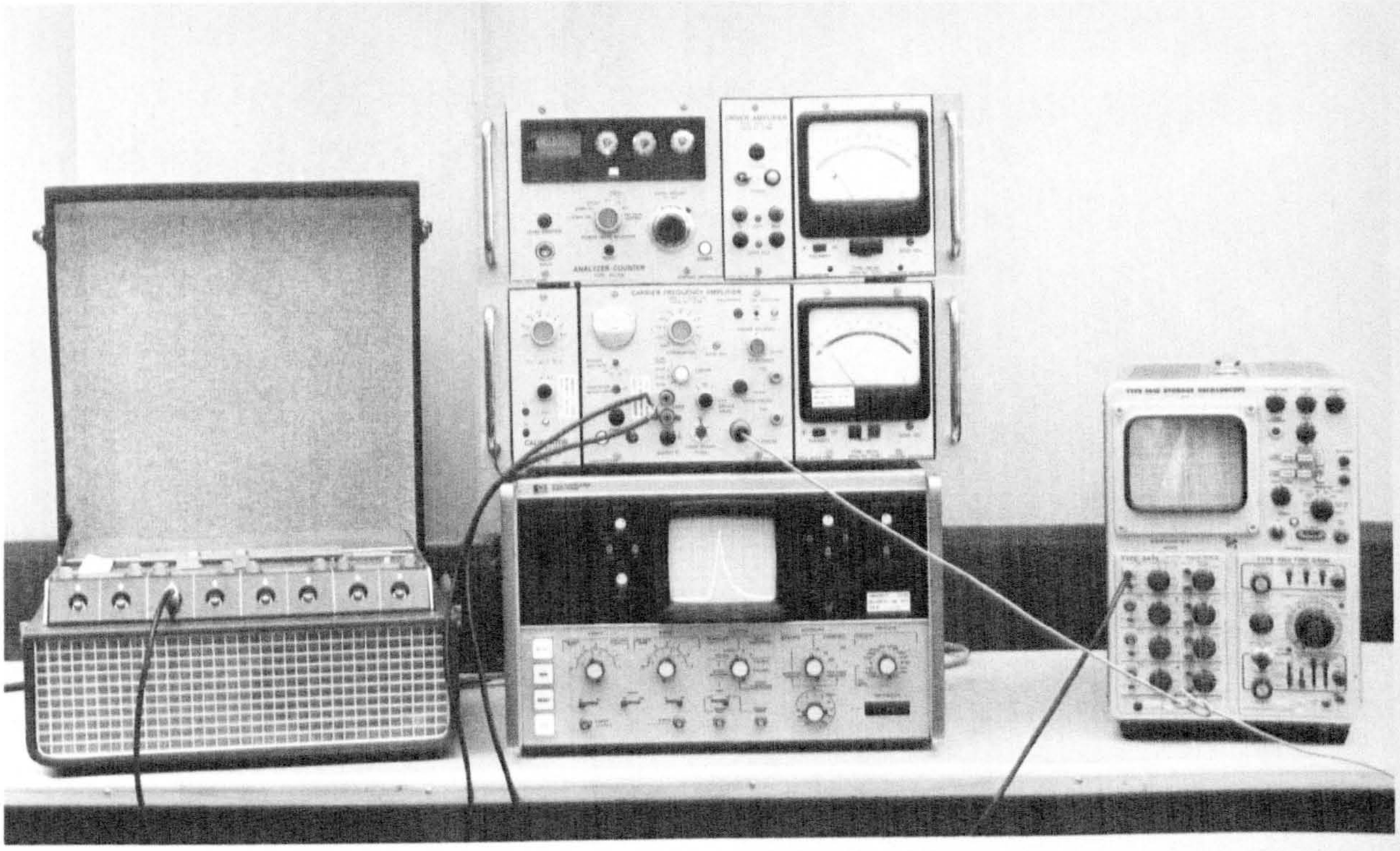

Fig. 24b Measurement Electronics

with a stated linearity of ± 1%, when used in conjunction with a Vibrometer fully transistorised precision carrier frequency amplifier Type 8 - CFA - 1/B.

In first examining the feasibility of the measuring system, the signal was recorded on UV paper. Although this was satisfactory for qualitative work and simple quantitative measurements, a detailed mathematical investigation of the surface profile could only be carried out using further electronic techniques. Two systems were used, both based on commercially available instruments:-

1. Analysis based on a high spot count of the surface profile.

   This system (Fig. 25, system 1) incorporates a single channel Vibrometer statistical distribution analyser Type AC - 1/A. Essentially, this counts the number of times the signal transcends a predetermined voltage level selected by the user. Before the next impulse arises and can be counted as an amplitude, the signal must drop 1 volt below the selected level. The instrument therefore yields a high spot count as suggested by Reason[5] (Section 2.1.1). An estimate of the count over the entire measurement range could be obtained ideally by using a ten channel version of the instrument and setting each channel to a different threshold voltage. In this case, however, only a single channel instrument was available and hence the signal had to be recorded and repeatedly played back through the analyser, set each time at a different threshold level. Since the operating range of the analyser is 0 - 10 volts and the maximum output voltage of the recorder is only one volt, a drive amplifier had to be incorporated into the

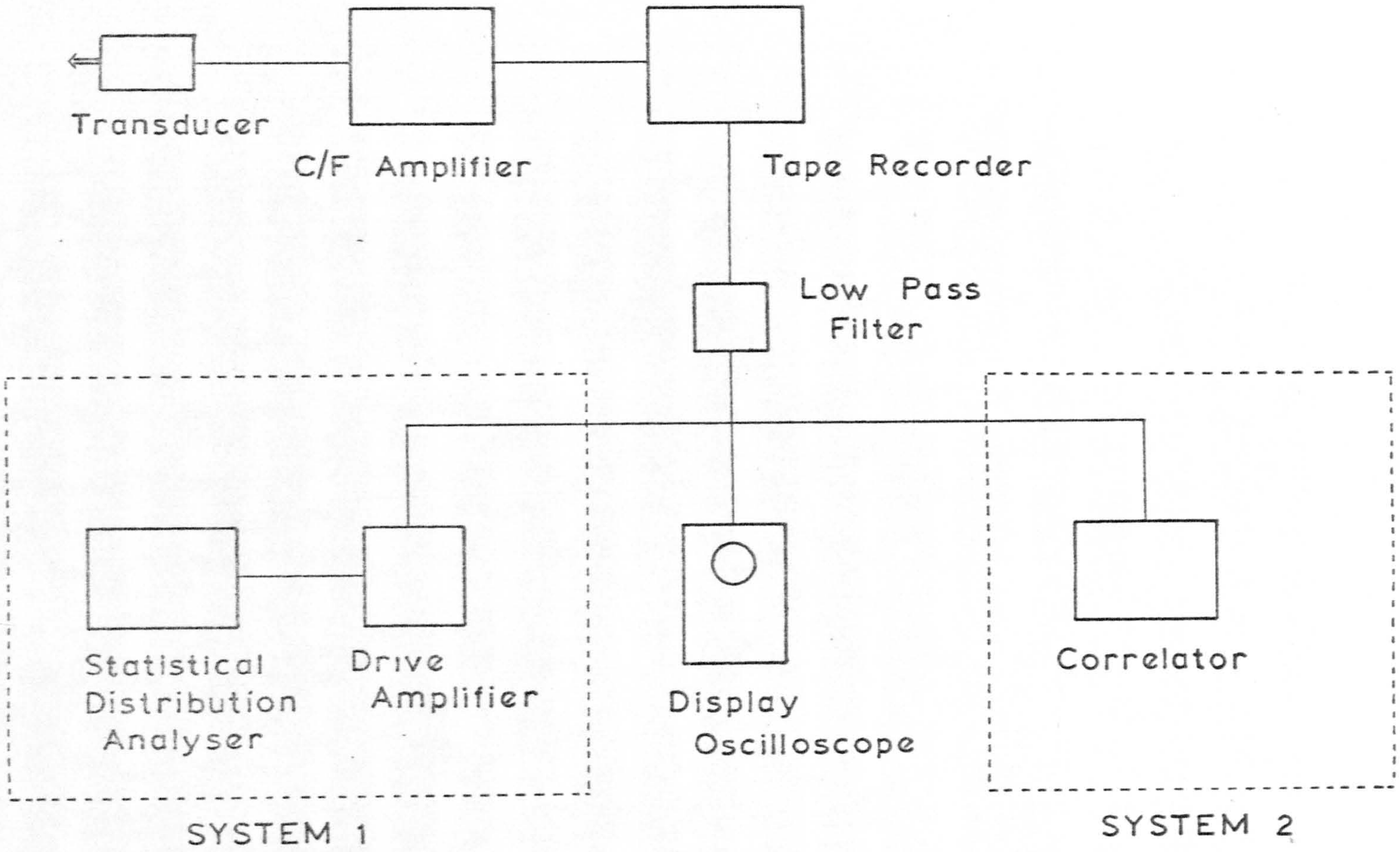

Fig. 25 Measuring Apparatus

circuit. This had the unfortunate effect of amplifying the tape noise level with the result that the high spot count readings became unreliable. This problem was eventually overcome by including a low pass filter (cut - off 10 c/s) assuming all tape noise to be of a higher frequency.

Although the system proved to be a considerable improvement on the time consuming visual analysis of UV traces, the method gave only limited information about the surfaces under consideration. Also, the time taken to obtain results still limited the range of experimental work.

2. A real time analysis using a correlator.

During the latter part of this project, a Hewlett Packard Model 3721 A Correlator became available, which permitted a much more rigorous and speedy analysis of the surface profiles. The instrument is an all digital, dc to 250 kHz signal analyser, which is capable of making the following measurements:-

a) Estimation of probability distributions (normal and cumulative)

b) Determination of autocorrelation functions

c) Determination of cross-correlation functions

d) Signal averaging (signal recovering, the process of recovering the wave shape of repetitive signals buried in noise).

In this project, only the first two modes of operation were used. The computed functions are displayed using 100 points on a built in cathode ray tube (CRT), and being essentially an "on line" instrument, statistical behaviour can be observed in real time. This constitutes one of the major

advantages of the instrument as sampling times, averaging time constants, etc., can be quickly adjusted to give the required information in its most acceptable form. When used in conjunction with the measuring transducer, the signal could be fed directly to the correlator since signals can be accepted in the range 40 mV to 4V rms. In most cases, however, a tape recorder was used (System 2 of Fig. 25) in order that a complete record of the experimental work could be made and analysed at a later stage.

3.1.3 WHEEL SPECIFICATIONS

Two wheels were used in the investigation:-

20A 80 - K5 - VBE

20A 46 - K5 - VBE

These are aluminium oxide wheels of equal hardness, structure number, and bond type. The only variable is the nominal grain size. The nominal diameters of abrasive grits based on the average of a large number of samples have been determined by Redko[14] and Baul[69]. For the 80 and 46 wheels, they are 0.0075 in. and 0.015 in. respectively.

3.2 EXPERIMENTAL PROCEDURE

3.2.1 THE DRESSING OPERATION

This was carried out using a single point diamond (cone angle 110°) mounted on the machine table according to standard practice. To ensure repeatability of surface properties with dressing conditions, the operation was standardised as follows:-

a) The wheel was initially dressed fine. This was accomplished by taking successive cuts of decreasing severity in order to eliminate the effects of the previous wheel history. In practice, it was found that coarse dressing conditions influenced the wheel structure to a depth considerably greater than the actual depth of penetration of the diamond.

b) The required dressing conditions were then selected and the operation repeated at least five times, the dressing depth being reset after each pass.

All dressing operations were undertaken in the presence of a cutting fluid (a 40:1 concentration of Shell Dromus D). This protected the diamond dresser and prevented abrasive fragments from becoming trapped in the wheel surface. For the majority of the work, four different dressing conditions were adopted:-

CONDITION	f in/min	d in x 10^4
A	1	1
B	30	3
C	50	5
D	80	8

This wide range of conditions was chosen so as to coincide with those used by Pahlitzsch[23]. In fact, the conditions represent a diagonal on the three dimensional graphical relationship suggested by this author (Fig. 20).

3.2.2 CALIBRATION OF THE MEASURING HEAD

The transducer was calibrated initially using a micrometer head to deflect the stylus a known distance, and observing the voltage output on a display oscilloscope. Subsequently, it was found that the

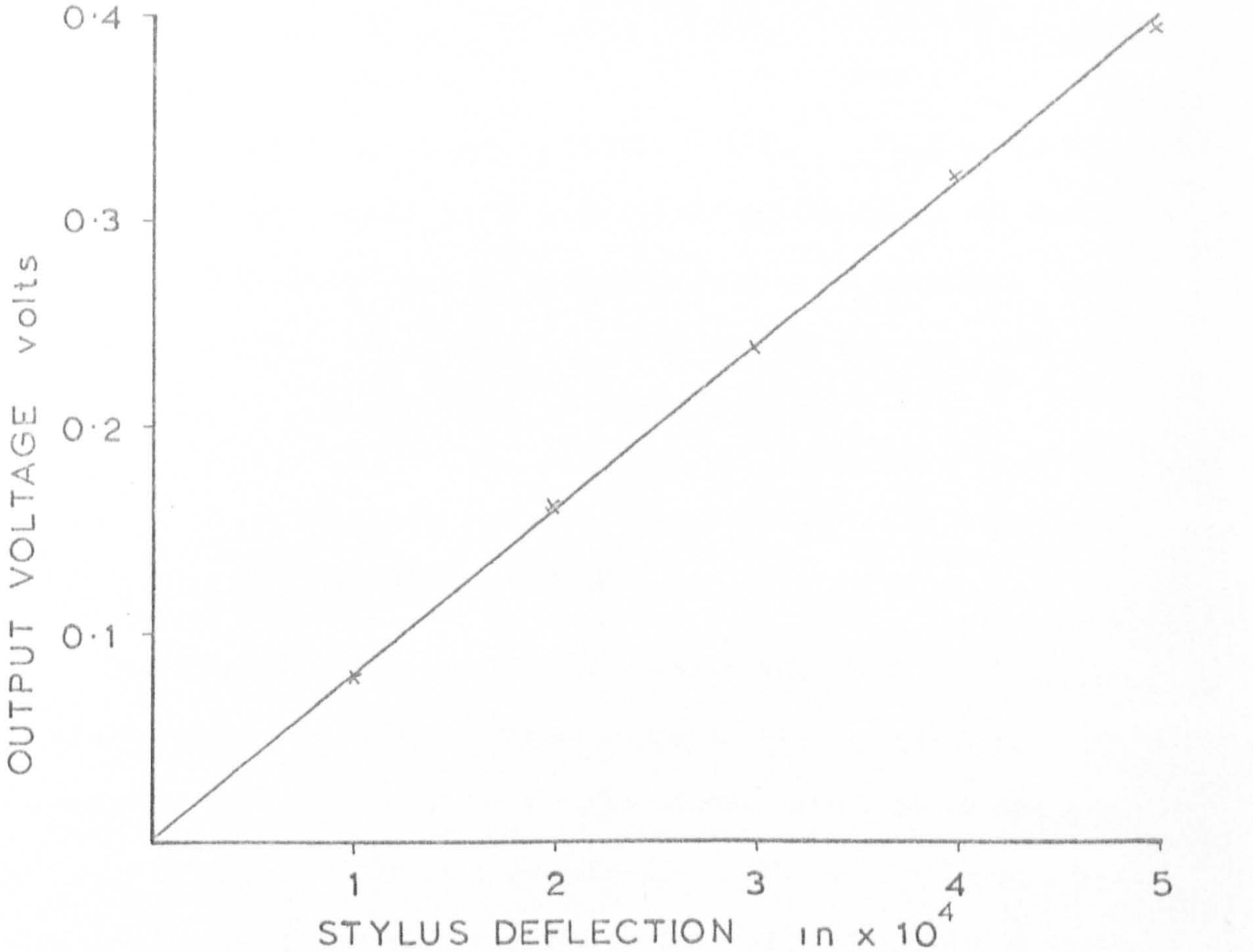

Fig. 26 Stylus Calibration

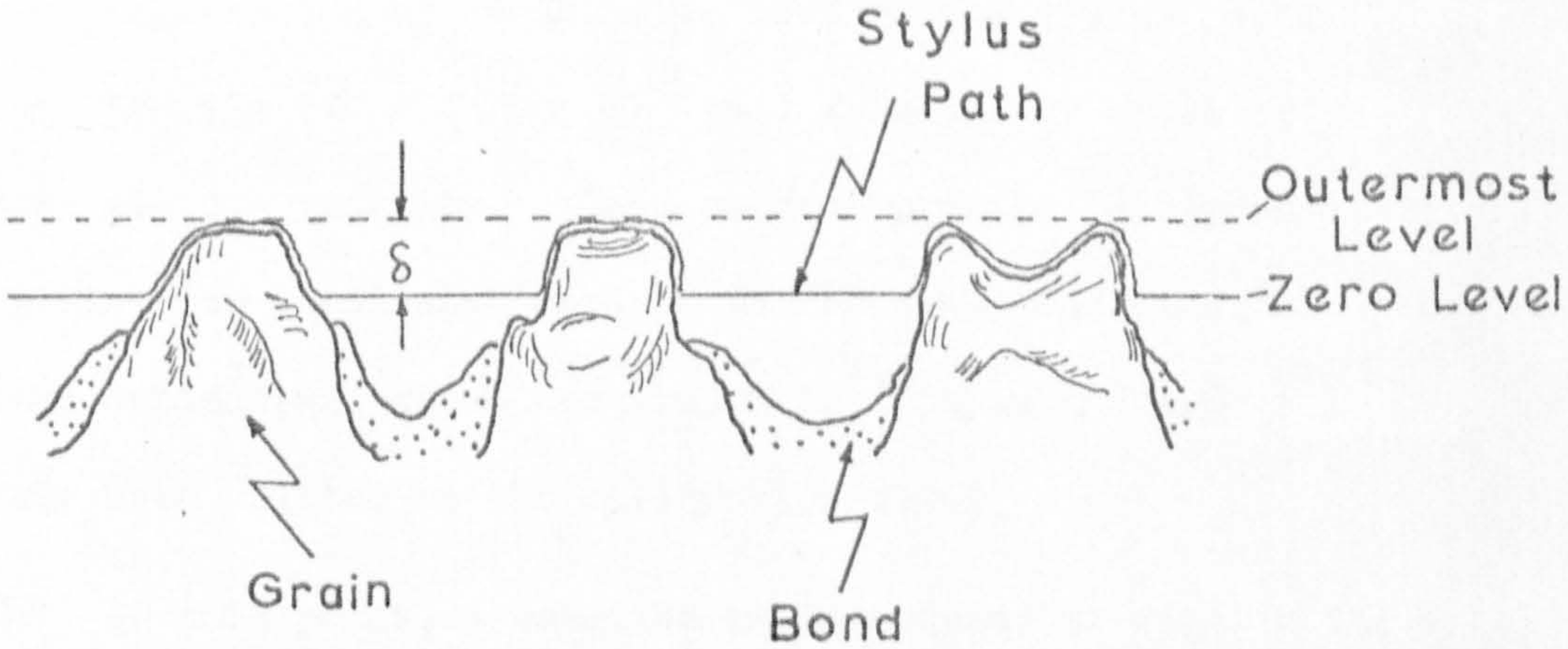

Fig. 27 Schematic Representation of Abrasive Profile and Stylus Path

transducer could be calibrated in situ by placing the stylus in contact with the wheelhead casing and feeding the latter forward in increments of 0.0001 in. using the accurate infeed facility. This permitted frequent and rapid checks to be made on the calibration, and enabled a wide range of sensitivities to be used depending on operating conditions. Fig. 26 shows a typical calibration graph for the maximum sensitivity setting, i.e., a scanning level, δ , of 0.0005 in.

3.2.3 THE PROFILE MEASUREMENT

Measurements of the surface were initially carried out in the circumferential direction. The scanning level, δ, and the desired sensitivity were first decided and the signal zeroed to ensure that the point of no stylus deflection coincided with the zero voltage level. The abrasive wheel was then rotated at the required speed and moved towards the stylus in increments of 0.0001 in., the resultant stylus deflection being monitored on the oscilloscope. This was continued until the desired value of δ had been attained. Fig. 27 gives a schematic representation of an abrasive surface and stylus path. Fig. 28 is an actual profile ($\delta = 0.5 \times 10^{-3}$ in.) recorded by means of the oscilloscope storage facility. This surface profile is representative of an 80 grain size wheel when dressed to the fine condition, A. The vertical and horizontal scales are 1.25×10^{-4} in/cm and 1.65×10^{-2} in/cm respectively when related to the calibration curve.

NOTE: At this point, a notation is introduced to signify the wheel grain size, the dressing condition and the scanning depth in thousandths of an inch. The conditions are simply listed in the order quoted, e.g., for the profile depicted in Fig. 28, the notation would be 80 A0.5.

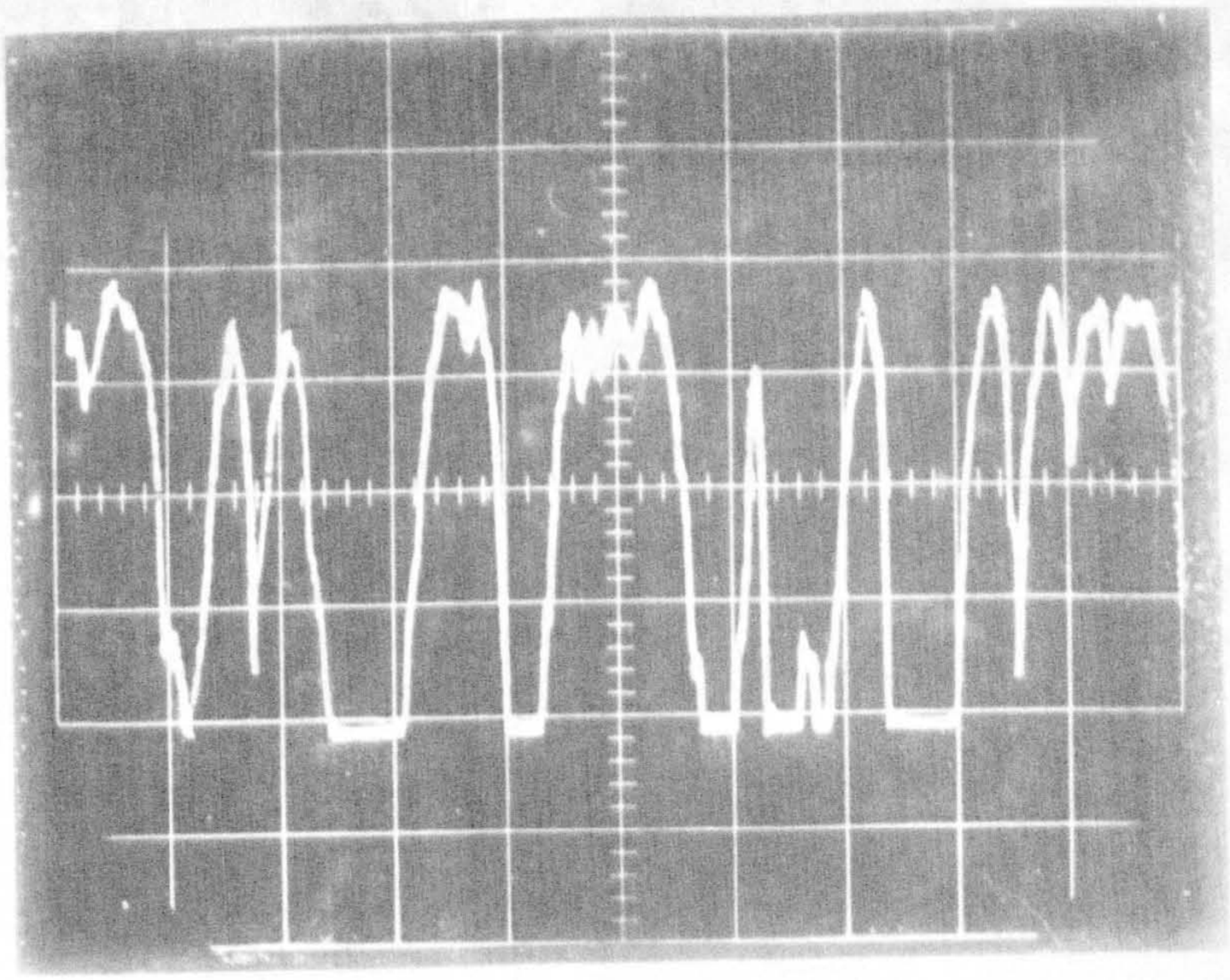

Fig. 28 Surface Profile of a Fine Dressed Wheel

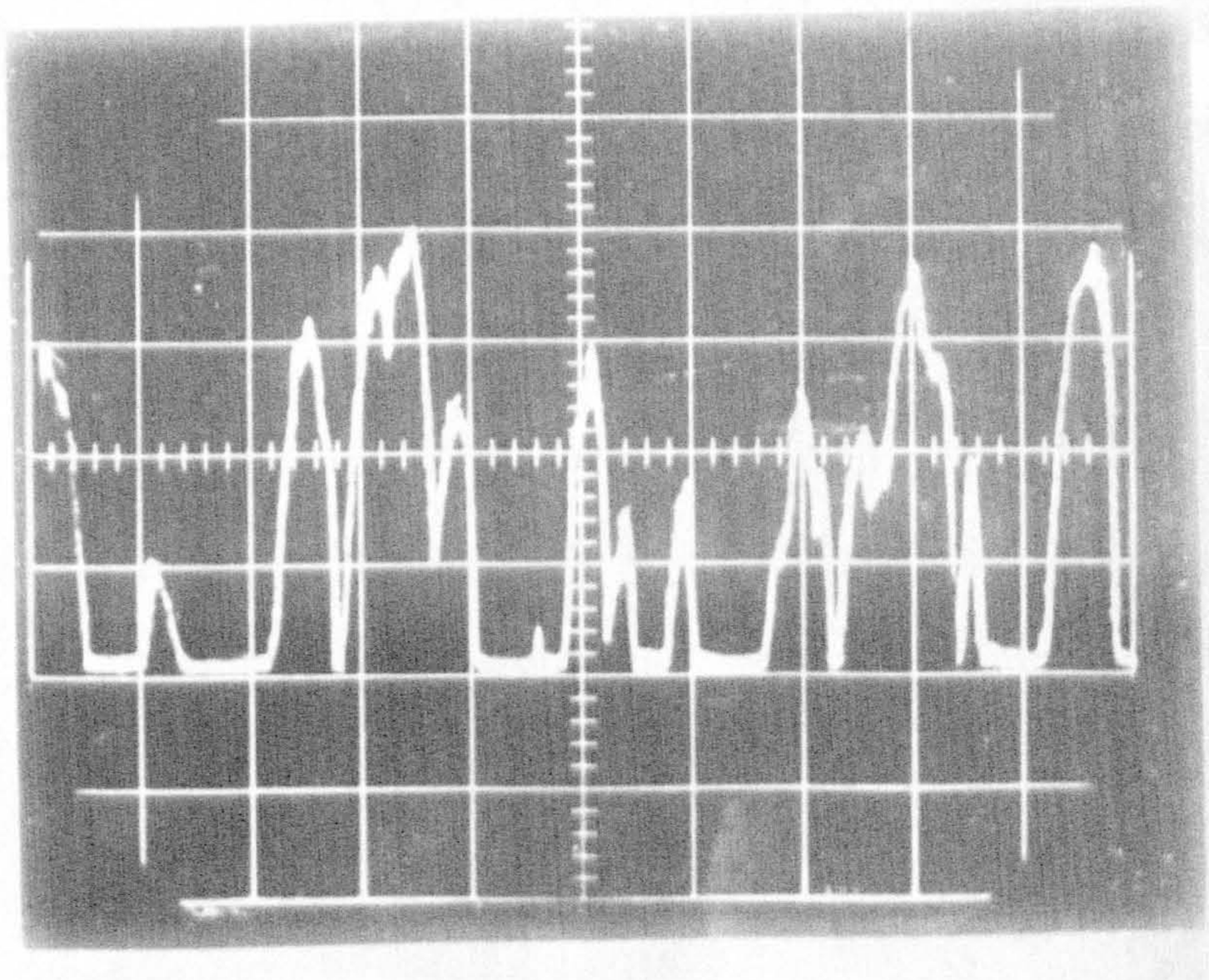

Fig. 29 Surface Profile of a Coarse Dressed Wheel

In practice, the desired value of δ was easily attained when experimenting with fine dressing conditions, since the highest asperity peaks all tended to fall at the same level (Fig. 28). However, as the dressing operations increased in severity, δ was more difficult to adjust because the outermost peaks tended to display a considerable variation in height (Fig. 29 - condition 80 B0.5).

Once the measuring head had been successfully positioned, an analysis of the profile can be carried out using either of the two previously discussed measuring systems. In the case of the high spot count, the use of the instrument was quite straightforward, the number of high spots at a given level being displayed on a digital read out. With the correlator, however, the measurement process is more involved, and considerable care has to be given to the many instrument settings.

In what follows, the experimental difficulties associated with probability and correlation measurements are discussed, reference being made to the implications of certain instrument settings where applicable. For a more fundamental description of the correlator, Appendix A should be first consulted. The Appendix also contains a brief discussion of the errors involved in computing the various statistical parameters.

1. PROBABILITY MEASUREMENTS

A diagrammatic representation of a typical abrasive wheel probability density function (pdf) is given in Fig. 30. The horizontal scale represents the height variation whilst the vertical scale is a measure of probability. The zero level, outermost level, and scanning depth, δ , as defined in Fig. 27 are indicated. The probability peak occurring at the zero level is mainly a consequence of the wheel porosity and the scanning depth.

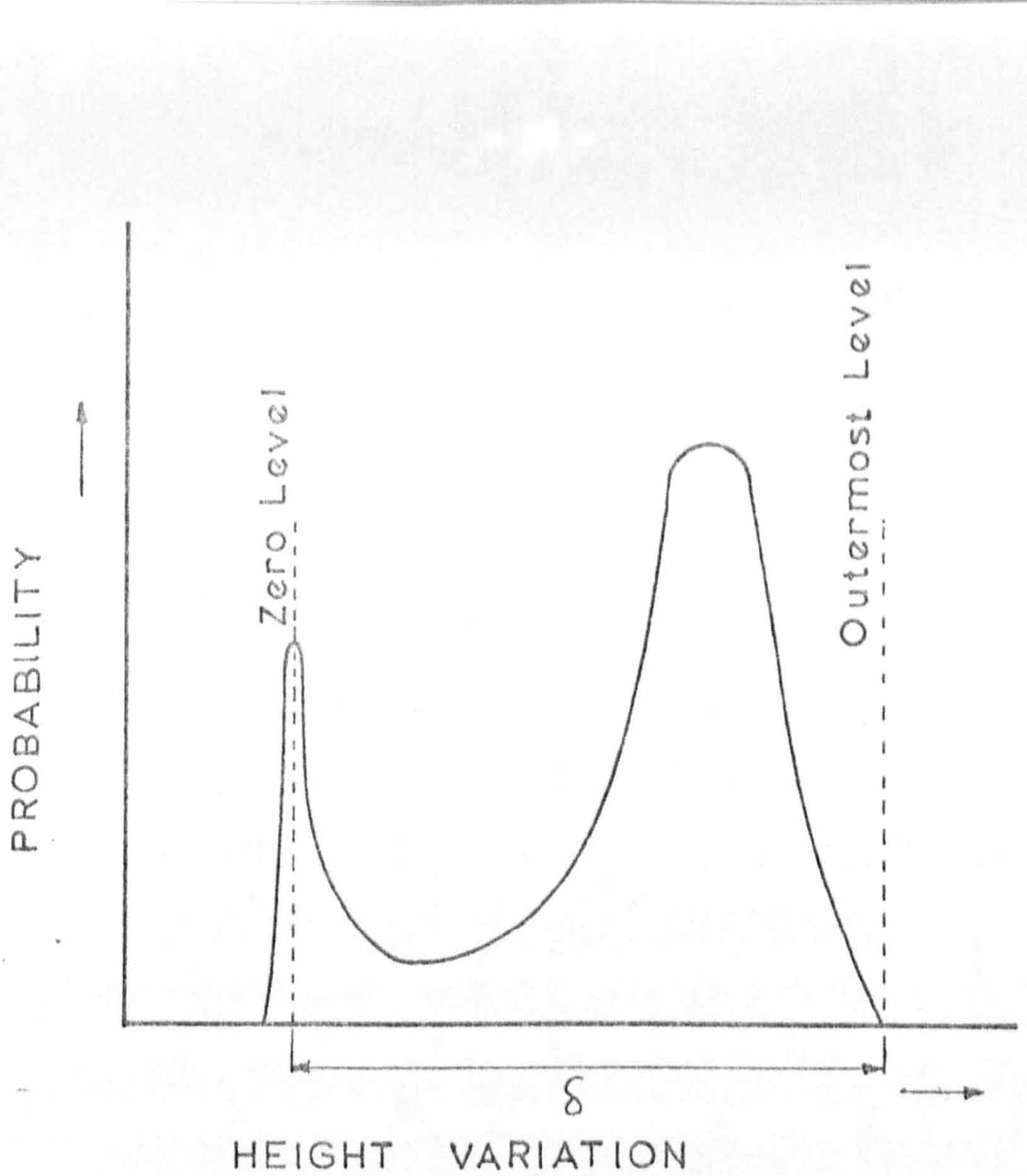

Fig. 30 A Typical pdf Measurement

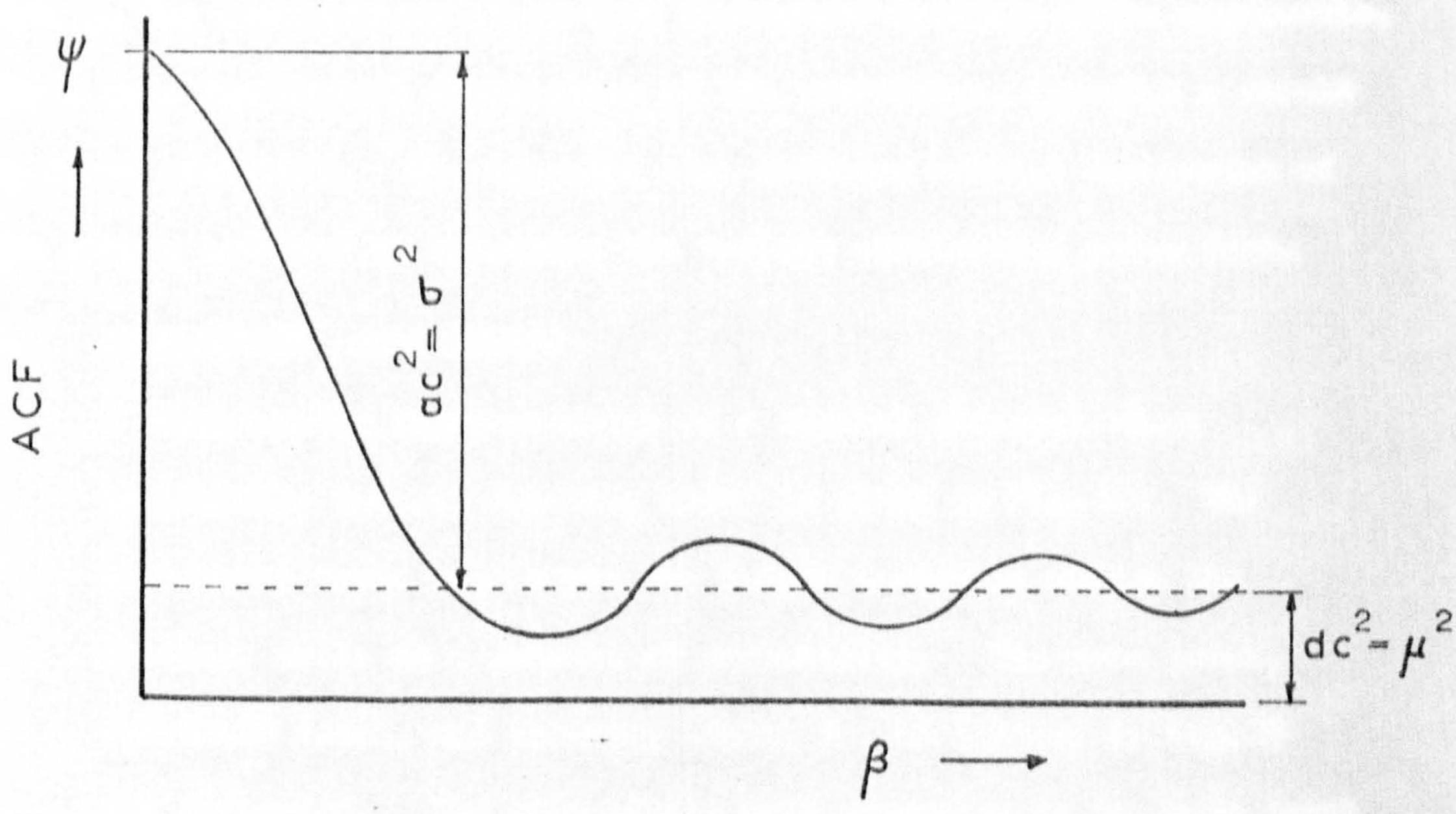

Fig. 31 A Typical Autocorrelation Function

All pdf measurements were carried out using the dc cut-off since the problem of display interpretation is simplified.

The voltage sensitivity was selected in conjunction with the transducer sensitivity to give 4 cm deflection, i.e., 40 points on CRT for all values of the stylus penetration, δ.

The sampling interval was set at 0.167×10^{-3} in. which corresponded to a correlator sampling time, Δt, setting of 10 millisecs., when related to the scanning speed. The minimum sampling lengths were 2 in. and 3 in. in the axial and circumferential directions respectively.

The profiles were first analysed using the summation mode of averaging. However, for profiles with a high zero probability, e.g., coarse dressed and small δ, this mode is not satisfactory. This is because the measurement process stops when the zero probability reaches full scale deflection, giving poor definition over the "positive" height range. In these cases, the exponential mode of averaging was utilised. Here, the measurement continues after full scale deflection (the spot returning to zero) and with a suitable averaging time constant ($= N\Delta t$), the pdf can be magnified over the positive height range for greater accuracy. The zero probability height is then meaningless, however, unless a record is kept of the number of times the spot cycles the screen.

2. CORRELATION AND SPECTRAL MEASUREMENTS

Consider the surface profile to consist of an ac and a dc component,

i.e., $y(x) = ac + dc.$

Then the autocorrelation function R_{yy} is given by

$$R_{yy}(\beta) = \frac{1}{L} \int_{L \to \infty}^{+L/2} y_x \cdot y_{x+\beta} \, dx \qquad \text{(Fig. 31)}$$

where y = height ordinate

x = subscript denoting position along the profile

β = correlation interval (= sampling interval)

and L = profile length

The mean squared value of the signal is given by

$$\psi_x^2 = ac^2 + dc^2 = R_{yy}(0)$$

The value of ac is a measure of the standard deviation, σ, whilst the dc level gives an estimate of the mean height, μ. Thus correlation measurements should yield an estimate of σ and μ. Further measurements can be taken from the autocorrelation function (ACF) which indicate the change in profile properties along the surface. One simple measurement is the distance at which two points on the surface can be considered independent events. This has arbitrarily been defined[9,70] as the value of β at which R_{yy} has declined to 10% of $R_{yy}(0)$.

A more rigorous analysis of the profile can be carried out by taking the Fourier transform of the ACF to give the power spectrum.

All correlation measurements were made in the circumferential direction using the summation mode of averaging.

The selection of the sampling interval, β, was an important consideration and needs further explanation. The problem is best approached by considering the profile in the frequency domain, i.e., in terms of its spectral analysis. The many theoretical and practical aspects of spectral analysis have been discussed by numerous authors, e.g., ref. 66, 67, 68. Briefly, the basic requirements for the practical determination of power spectra are:-

a) The sampling interval must be sufficiently small to permit an estimate of the spectrum to be made over the range of frequencies

which are of interest. If f_{max} is the maximum frequency, then the following condition must hold:-

$$\beta \leqslant \frac{1}{2f_{max}}$$

If the analysis is limited to the scale of an abrasive grit, an estimate of f_{max} can be obtained. For the 80 wheel, the nominal grain diameter was quoted as 0.0075 in. With a scanning speed of 1 in/min, the width of a peak as a function of time would be 450 millisecs, i.e., f_{max} = 2.2 c/s.

Hence $\Delta t \leqslant \frac{1}{4.4} \leqslant 220$ millisec

In practice a scanning interval of Δt = 100 millisec, i.e., β = 1.67×10^{-3} in. was used. This gave a measuring bandwidth of 5 c/s which was considered adequate since measurements of the profile using the storage scope revealed virtually no power above this frequency.

b) The power spectrum must be zero above $\frac{1}{2\Delta t}$. If this is not true, the problem of aliasing will arise, where frequency components above $\frac{1}{2\Delta t}$ in the initial signal will appear in the range $-\frac{1}{2\Delta t} < f < \frac{1}{2\Delta t}$. This is not a major problem in the present work since it has already been established that the power spectrum is zero above 5 c/s.

c) The bandwidth of the spectral window and the required number of autocorrelation points, m, for computation of the power spectrum must be determined. The technique of using spectral windows is extensively dealt with in ref. 68. Basically, the process is a smoothing operation on the power spectral estimate determined from the "raw" correlation measurements. The type of window adopted, the resolution bandwidth and the

value of m are further discussed in Appendix A2, since they have a direct influence on the estimation error. For the same reason, the selected value of the sample size, N, is also considered in the Appendix A2.

3.3 RESULTS AND DISCUSSION

Although a considerable amount of work was undertaken using the high spot count technique, because of its limitations compared with the correlator, this is reported only briefly. The majority of results discussed relate to the measurements obtained using the correlator, and are considered under the following headings:-

1. Probability measurements
2. Correlation and spectral measurements

3.3.1 PROBABILITY MEASUREMENTS

The influence of dressing conditions and grain size upon the pdf is shown in Fig. 32. The pdf's were obtained on the exponential averaging mode, and consequently the magnitude of the zero probability peak is of no special significance (as discussed in Section 3.2.3). For the fine dressing conditions, Fig. 32a and b, the distribution can be seen to have a marked negative skewness. As the severity of the dressing operation increases, the distribution becomes less skewed Fig. 32c and d. Indeed, with a very coarse dressing, the distribution tends to skew positively. This change in shape of the pdf gives a realistic indication of the change in the distribution of asperities with dressing conditions. For a fine condition, the peaks tend to terminate at the same level and the density of asperities in the outermost levels is high. With coarser conditions, there is a much

a)
Condition 80A0.5

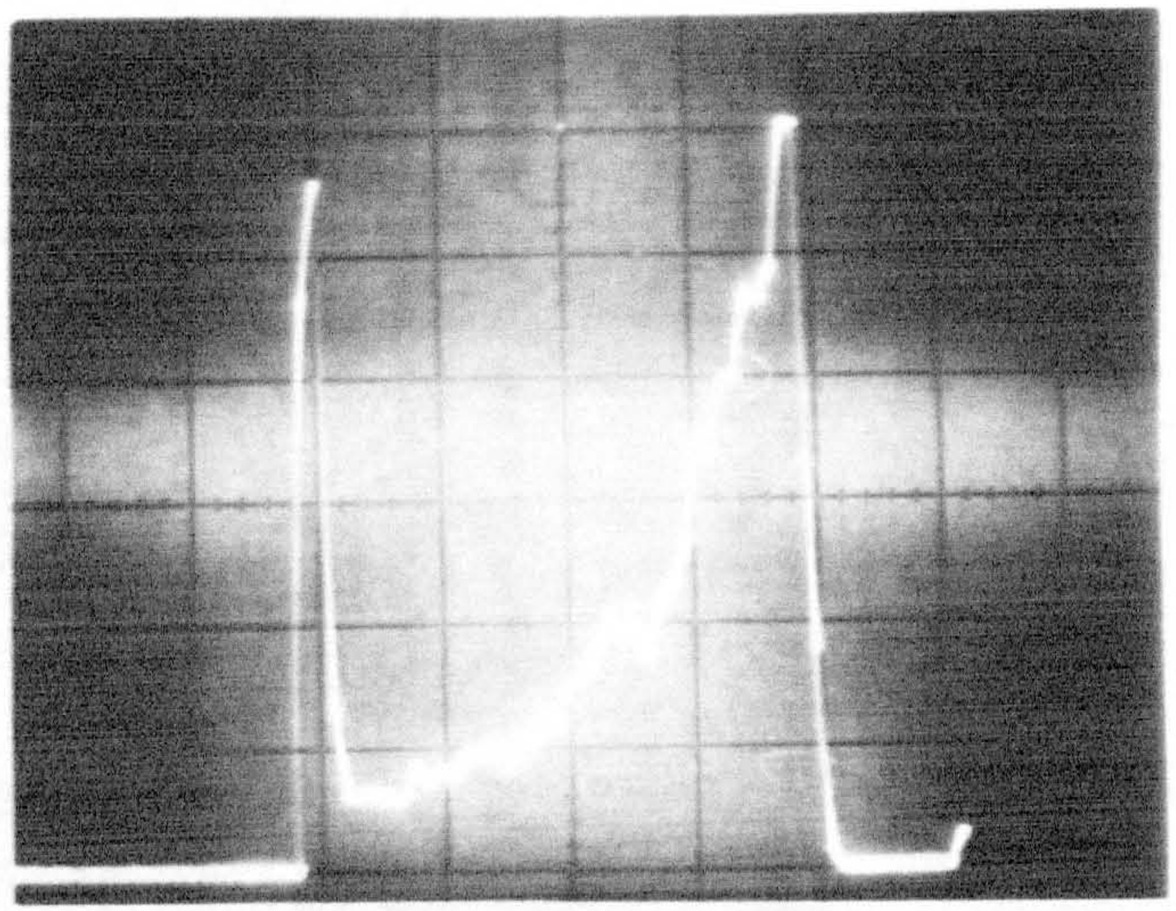

b)
Condition 46A0.5

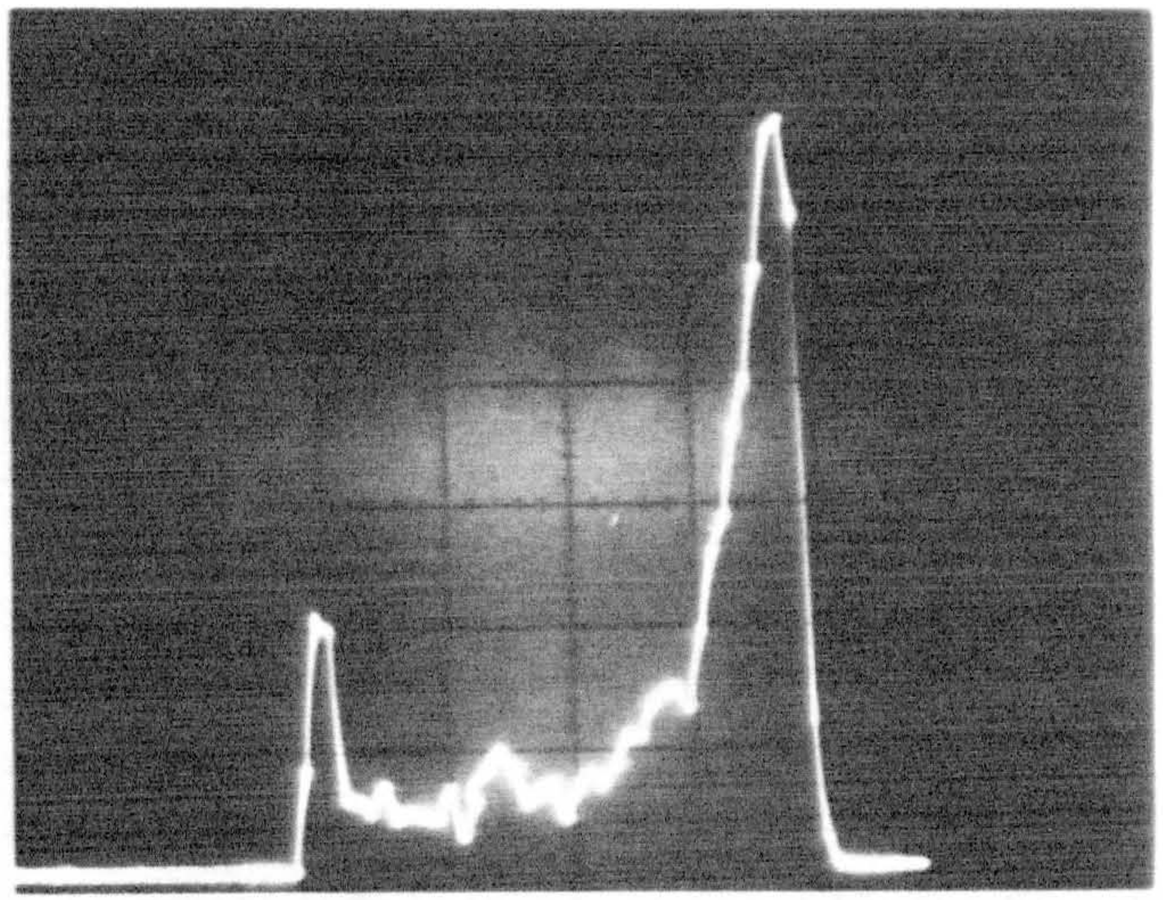

c)
Condition 80B0.5

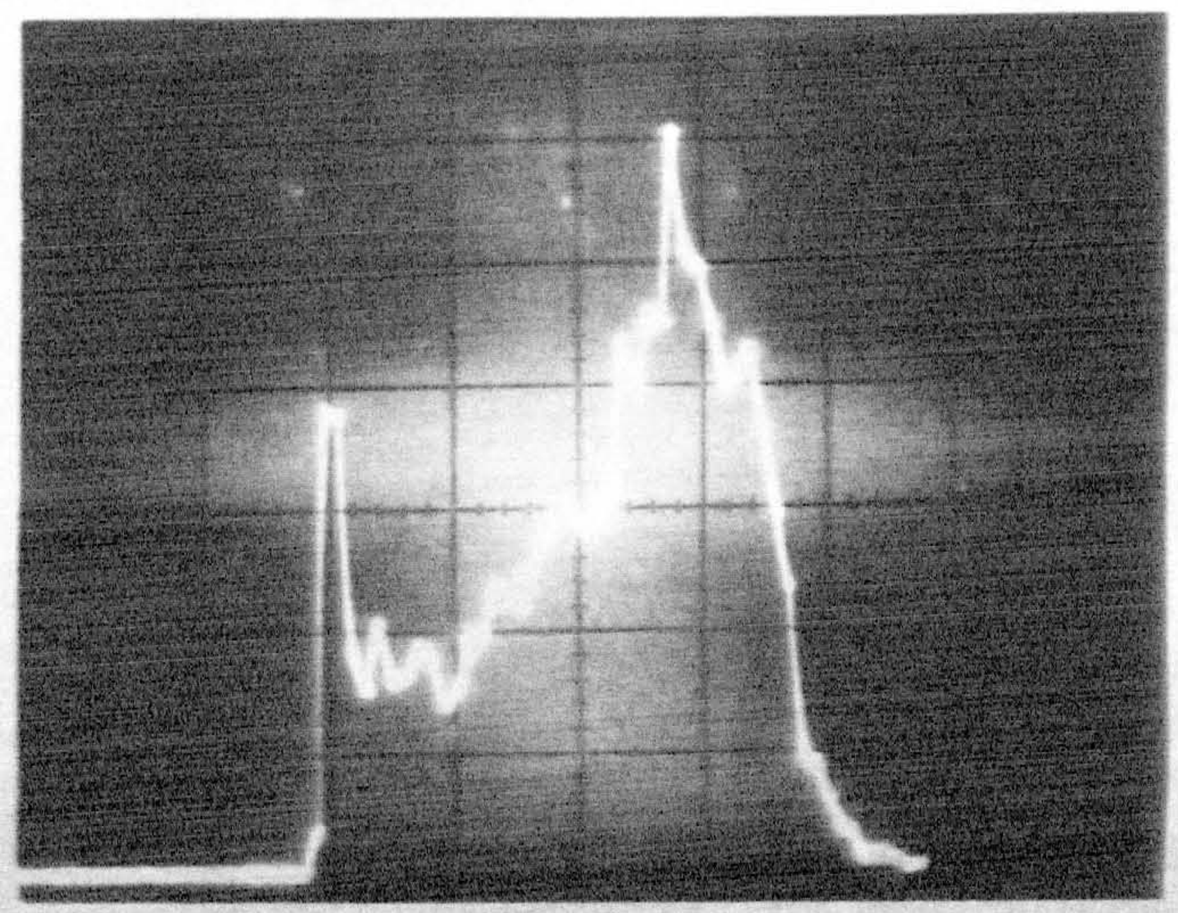

d)
Condition 46B0.5

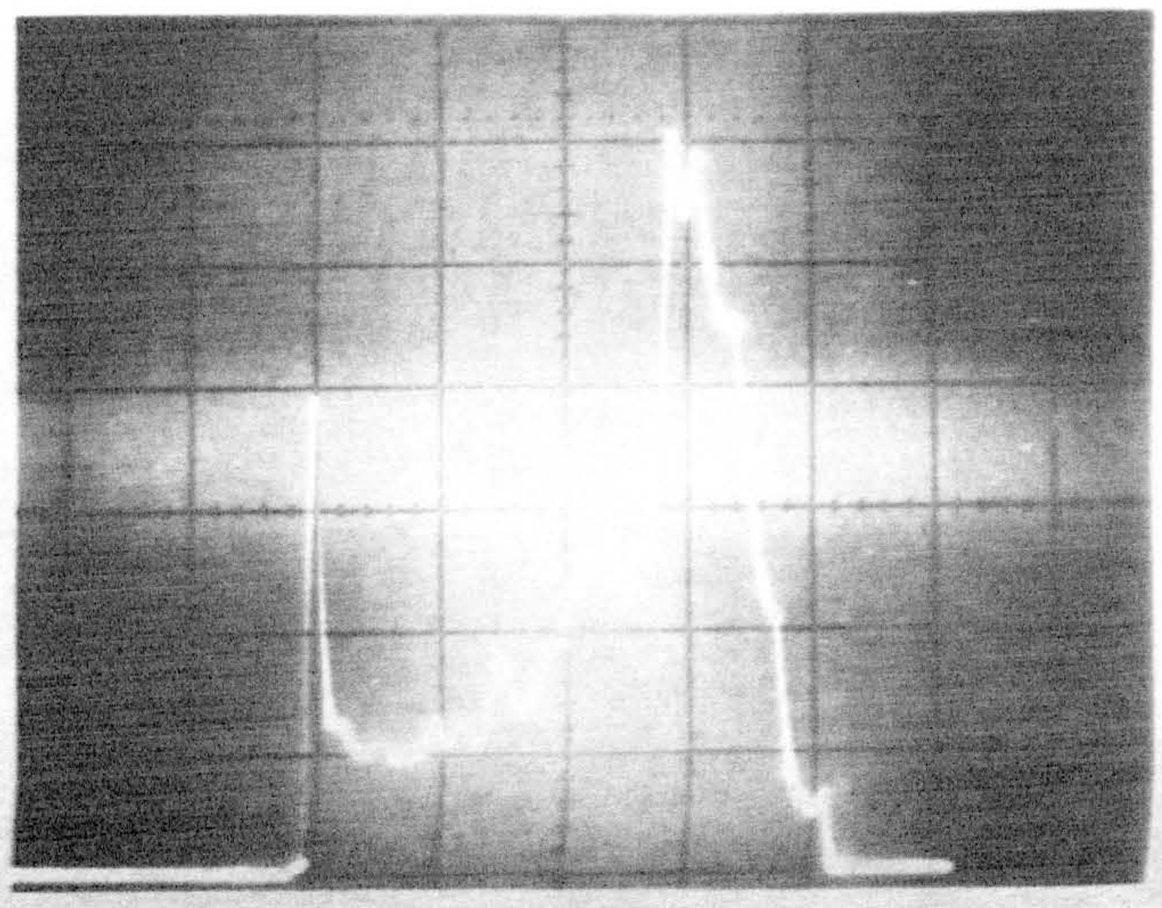

Fig. 32 Correlator Determination of Probability Density Functions

wider spread of amplitude components and the density of asperities in the outermost levels is correspondingly lower.

The influence of grain size upon the pdf is also evident from Fig. 32. The distribution is seen to exhibit increased negative skewness with an increase in nominal grain diameter. This is considered to be a direct consequence of the flatter nature of asperity peaks associated with the larger grain sizes.

A quantitative measurement of the changes in distribution can be made by considering the following parameters derived from a digital read out of the pdf's .

a) The percentage spacing, S.

If $k_1, k_2, \ldots k_n$ are the number of events occurring at the different height levels and k_o is the number of observations at the zero level, then for any value of S

$$S = \frac{k_o}{\sum_{i=o}^{m} k_i}$$

The parameter is a measure of the asperity spacing resulting from the initial wheel porosity and the superimposed dressing conditions. The value of S is shown as a function of δ for different dressing conditions and the two wheels under consideration in Fig. 33. For both wheels, there is an increase in spacing with an increase in the severity of the dressing operation. The effect of a reduction in grain size is to decrease the percentage spacing which is a direct consequence of the finer wheel structure. The difference between the two wheels, however, is much larger than anticipated since for wheels with equal porosity once could reasonably expect the value of S to be approximately constant for any value of δ/R. The

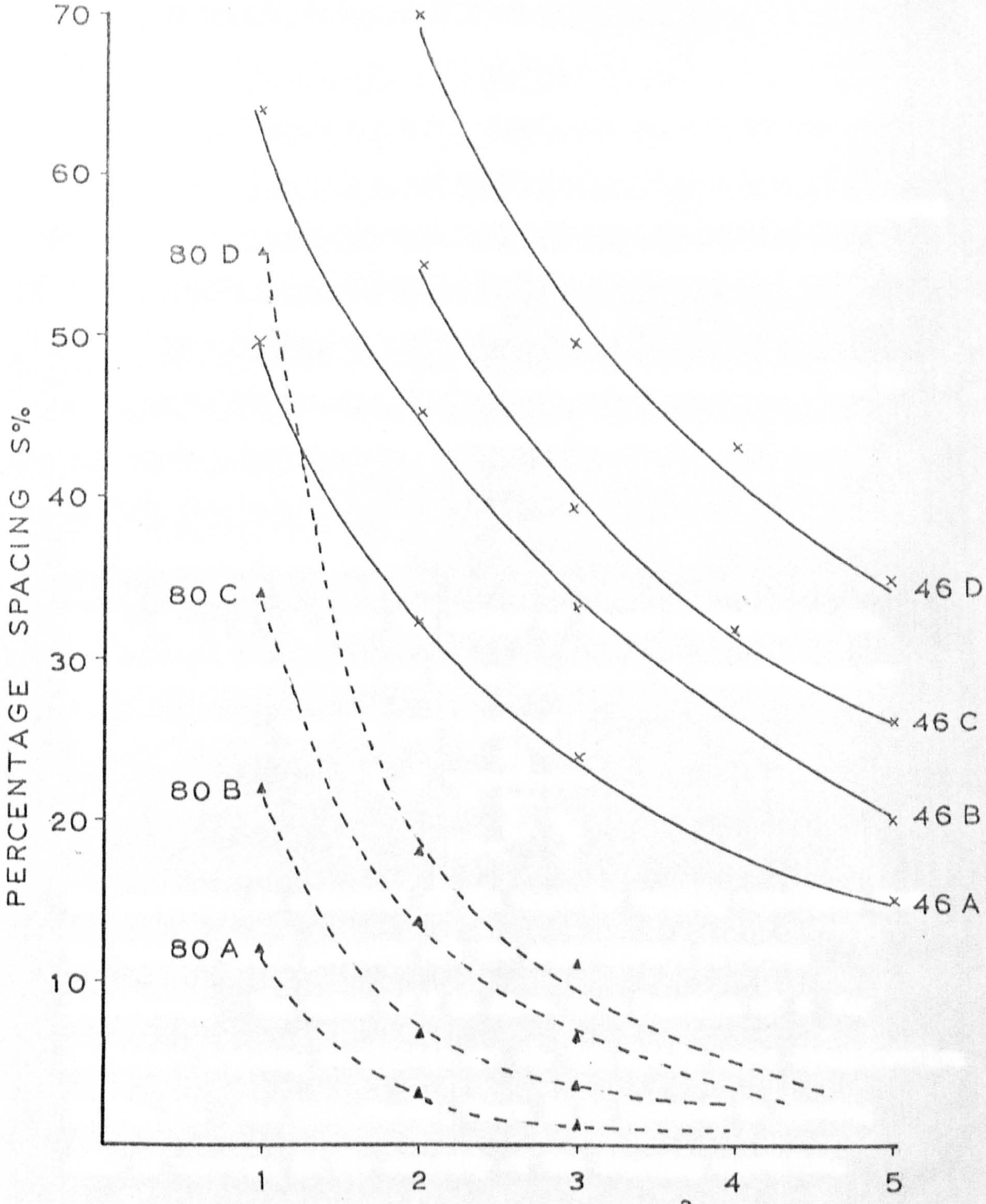

Fig. 33 Variation in Percentage Spacing, S

discrepancy can be attributed to stylus distortion which is greater in the case of finer wheel structures. This distortion is due mainly to the cone structure of the stylus tip which limits penetration into the cavities.

The value of S is also seen to decrease with δ , but again, the convergence of the 80 wheel curves is indicative of considerable distortion. The study of surface properties as a function of δ has important implications. During a standard grinding operation, the grain depth of cut is unlikely to exceed 0.0002 in. From this point of view, one could then argue that the range of interest lies between $0 < \delta < 0.0002$ in. However, the underlying structure is important for two reasons. Firstly, it has an important bearing on wheel wear. Secondly, the strength of the underlying structure will no doubt influence the elasticity of the grain mounting, which has already be shown to have an important effect on the grain-workpiece interaction[30].

b) The mean height, μ.

Fig. 34 shows the variation in μ with δ for different dressing conditions. The figures are average values of readings taken in the circumferential and axial directions and are concerned with the positive height distribution only, i.e., neglecting the zero ordinates. The value of μ is seen to increase with finer dressing conditions, indicative of an increase in the density of cutting asperities in the outermost levels. The mean also increases with δ , but it is unreliable to draw any conclusions for large values of δ where the effects of stylus distortion would be to exaggerate the true value of μ. It can be seen that for the fine conditions, μ tends to be greater than the median and for coarse conditions vice versa.

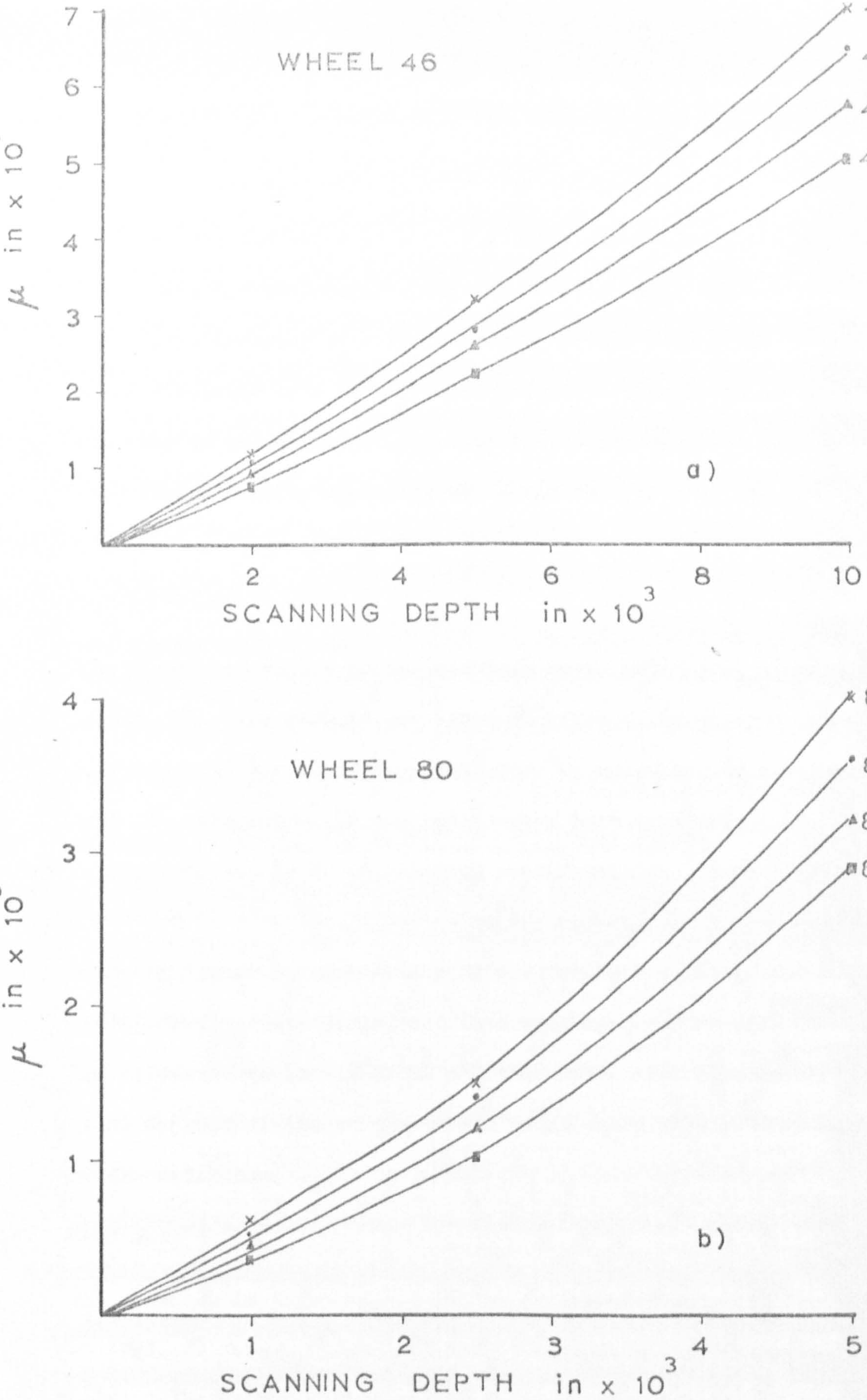

Fig. 34 Variation in Mean Height, μ

It is interesting to compare the effect of dressing conditions in the axial and circumferential directions, Fig. 35. In the fine dressing condition, the value of μ in the circumferential direction is less than the value of μ in the axial direction, the opposite being true for the coarse condition. This would suggest that changes in dressing conditions affect surface properties in the axial direction to a much greater extent. This is to be expected if the dressing operation is considered to be analogous to a simple turning operation where the tool removes its own profile.

c) Standard deviation, σ

The normalised values of the standard deviation, σ/μ, are shown in Fig. 37. The results are again averages of axial and circumferential readings. Also, the σ and μ values are derived from the entire profile and include the zero ordinates (for comparison with later correlation measurements). The standard deviation is seen to increase with an increase in the severity of dressing, which is again indicative of the wider range of amplitude fluctuations present in a roughly dressed surface. The measurements in the axial and circumferential directions (Fig. 36) support the conclusions already drawn from μ, the mean height estimates.

d) Skewness, Sk.

The skewness is shown as a function of dressing condition (based on feed, f) for $\delta = 1 \times 10^{-3}$ in. in Fig. 38 - positive heights only. The curves reiterate the previous observations on the change in distribution with dressing conditions and grain size.

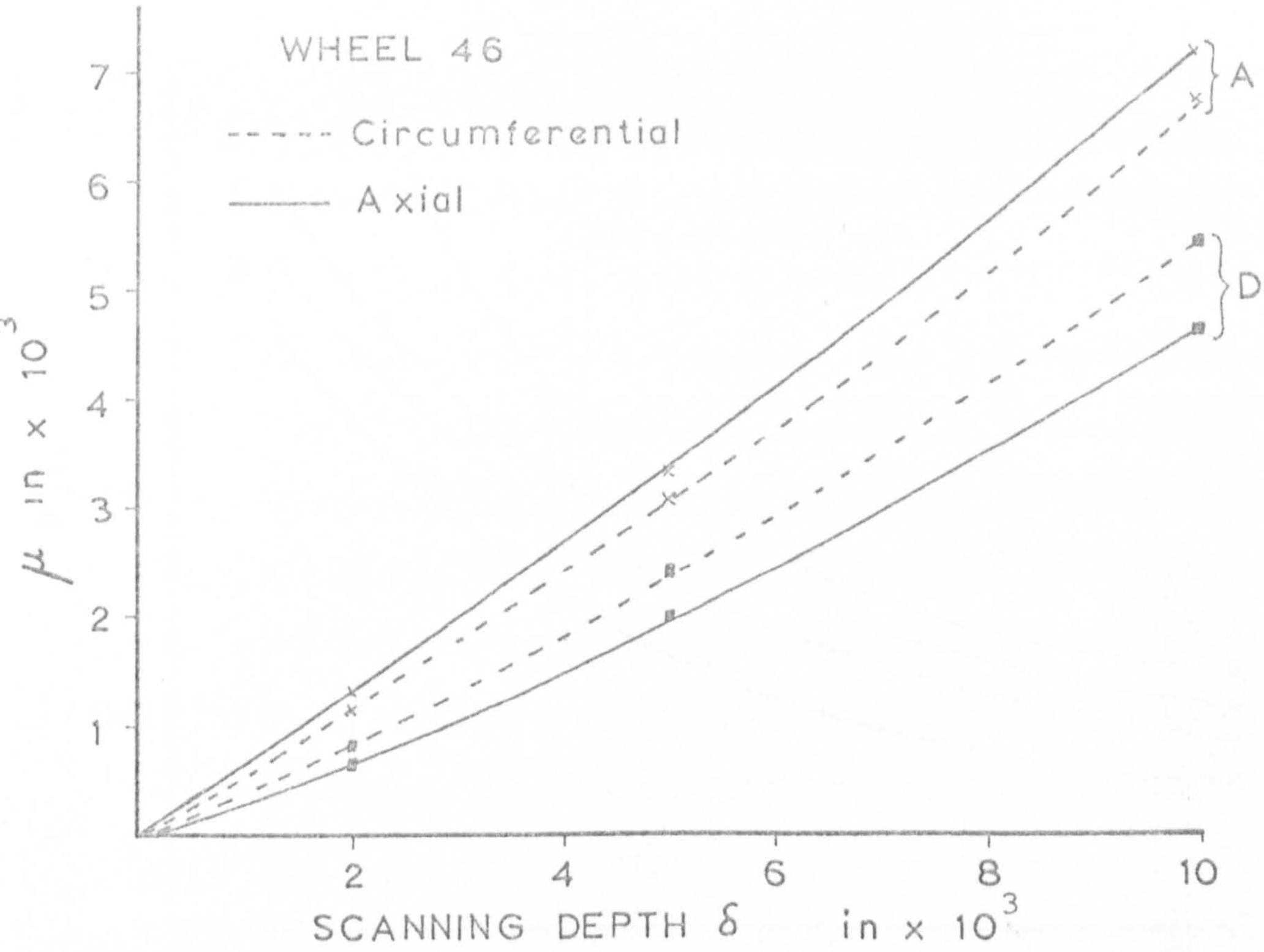

Fig. 35 Variation in Mean Height with Direction

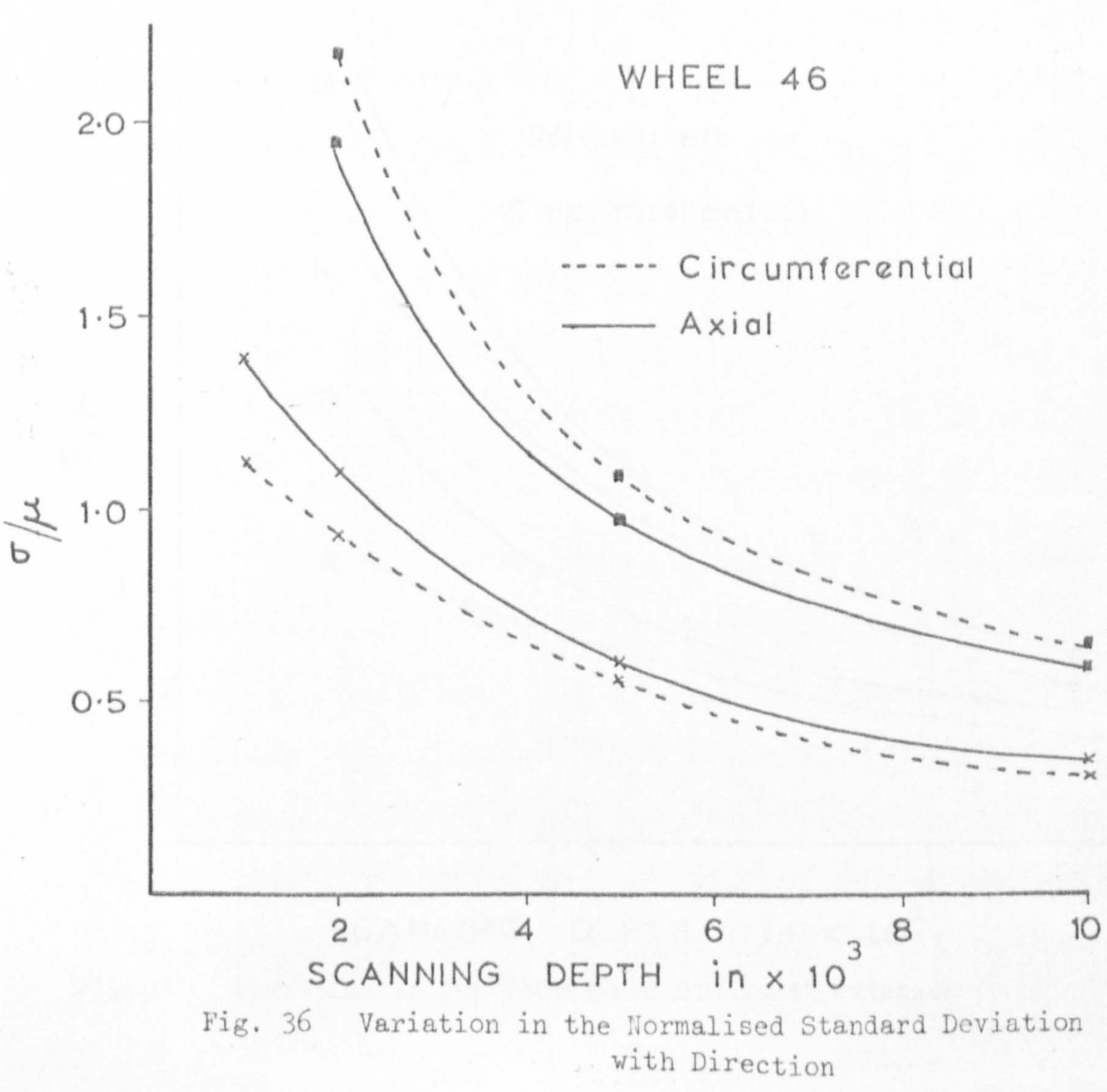

Fig. 36 Variation in the Normalised Standard Deviation with Direction

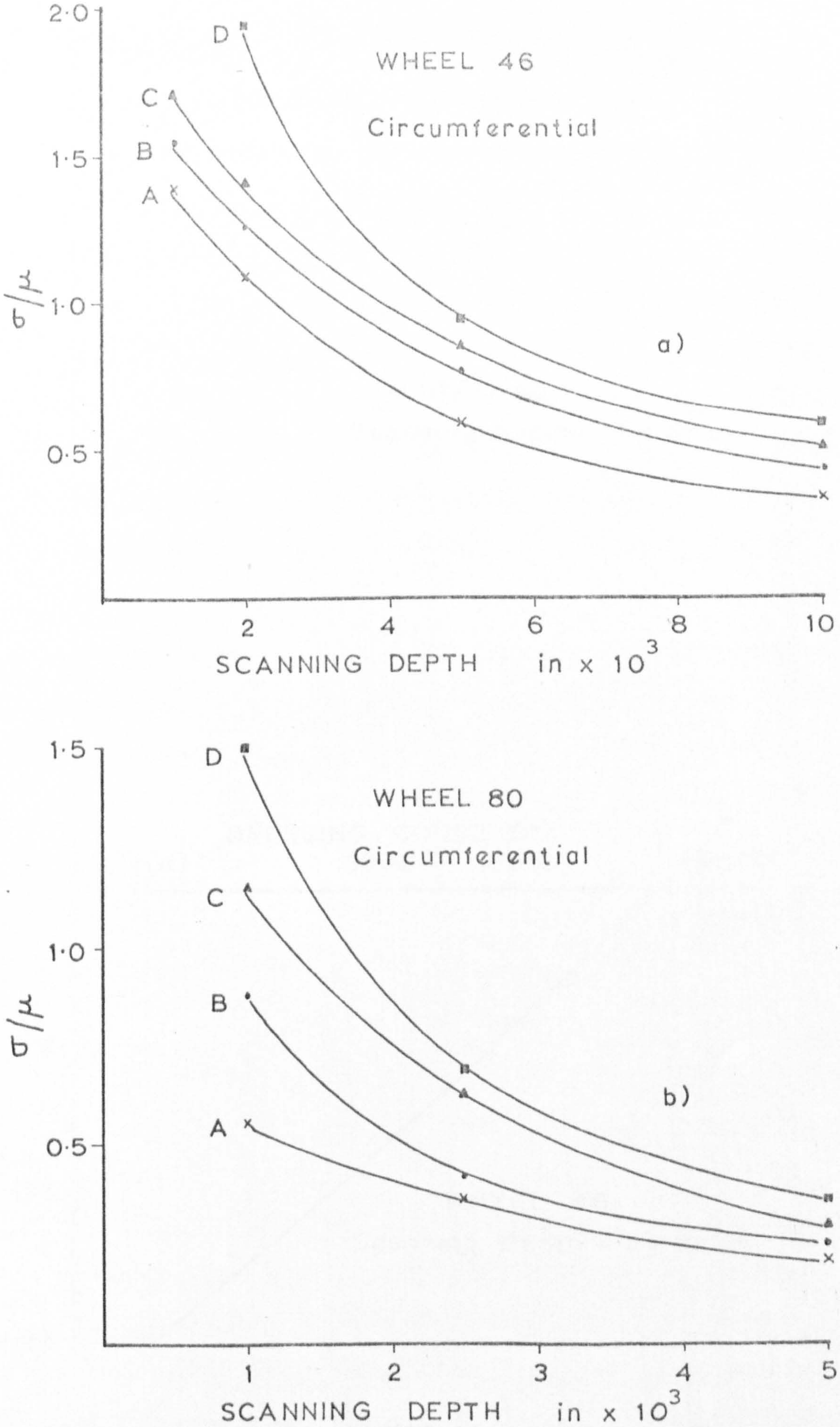

Fig. 37 Variation in the Normalised Standard Deviation

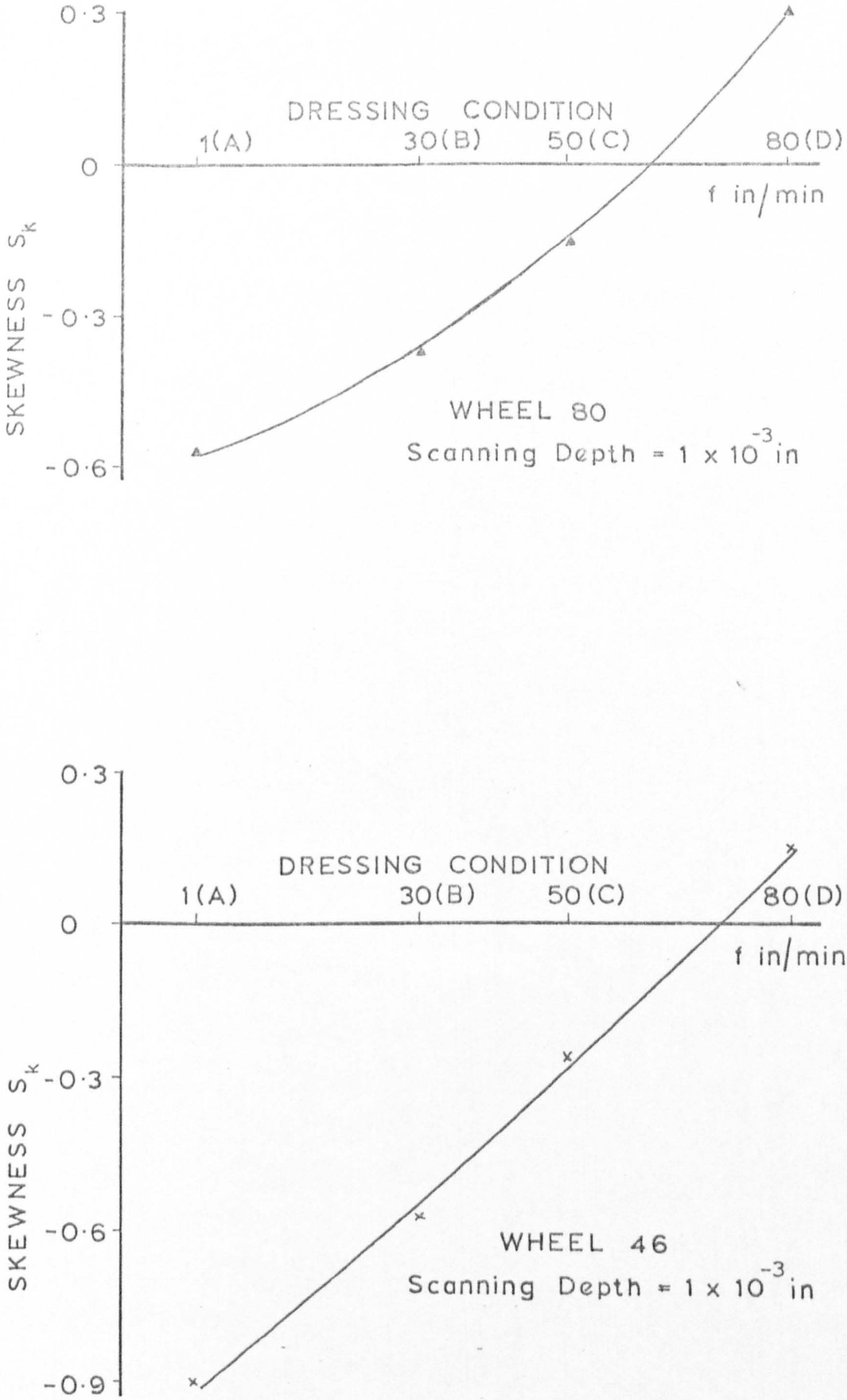

Fig. 38 Variation in Skewness

e) Bearing area curve.

The bearing area curve can be considered to correspond to the cumulative height distribution. Although the results below were obtained from the digitised read out of the pdf's, the correlator is capable of computing directly the integrated pdf (Fig. 39). The variation in bearing area curve wtih grain size and dressing conditions is shown in Fig. 40. The values of the percentage spacing are also included to give a more realistic picture of the wheel surface. In ref. 5 the idea of a "consolidated asperity" is introduced, where the bearing area curve is joined with its mirror image and then repeated along the profile length to simulate the measured surface. Viewed in this light, the increase in asperity spacing with dressing conditions, and the finer nature of the 80 wheel is evident from Fig. 40. Also of interest is the actual shape of the consolidated asperity. For rough conditions, the peak tends to be narrow when compared with the finer dressing conditions. This would suggest in practice a rapid initial wear rate of coarsely dressed wheels. This was demonstrated by Pattinson et al[15] (Fig. 21, Section 2.3.3). They suggested the rapid primary wear rate associated with coarse dressing was caused by severe damage to the underlying wheel structure. From the bearing area measurements, however, it is to be expected that the initial wear rate will be rapid, regardless of the stability of the underlying structure. As the depth below the surface increases, the gradient of the curves is approximately the same, suggesting that the wear rates of differently dressed wheels will eventually settle down to a constant value (neglecting the changing wheel structure during grinding). This is in fact found to be the case[15] as wear rates in the secondary regime level out to approximately the same value (Fig. 21).

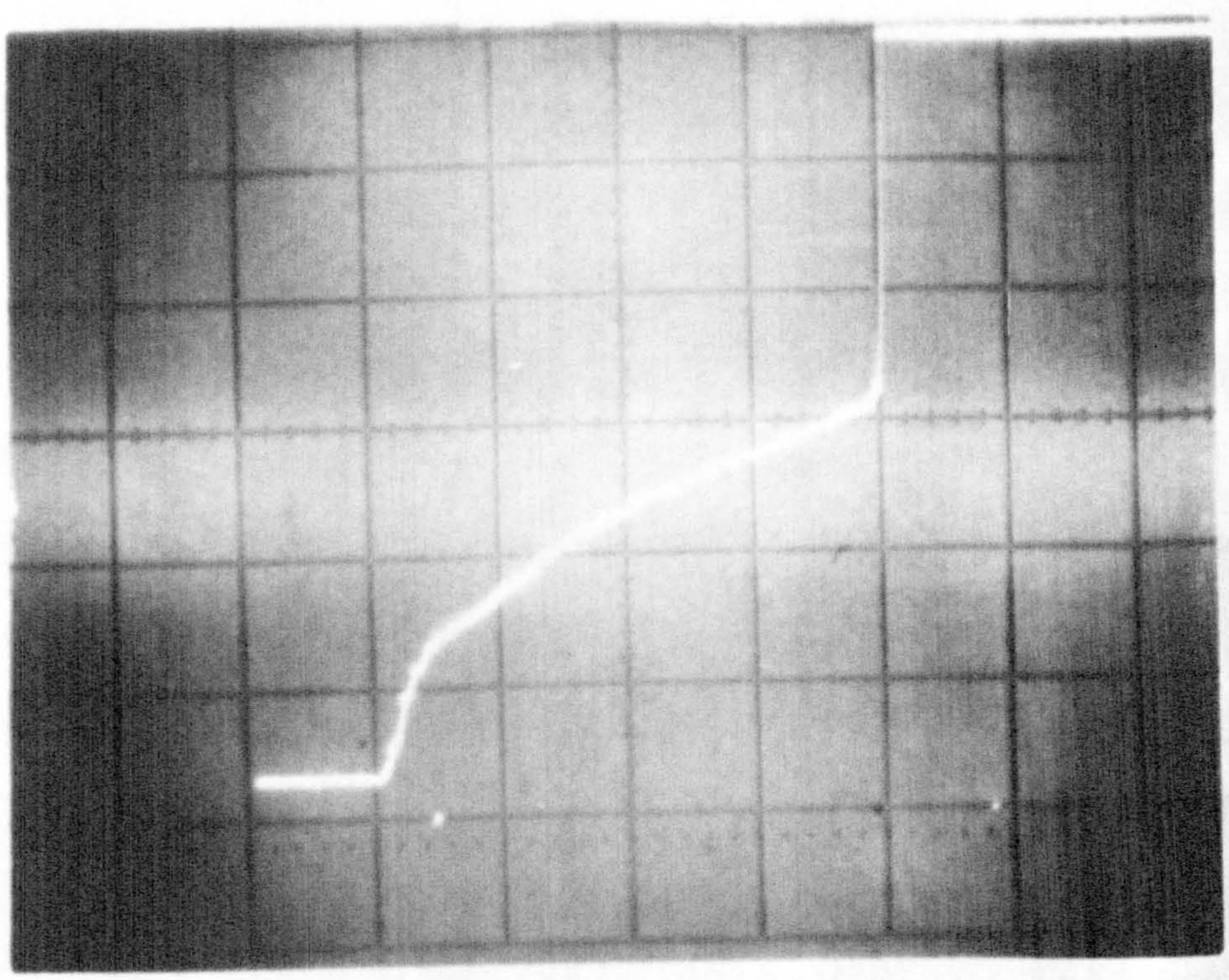

Fig. 39 Correlator Determination of the Integrated pdf

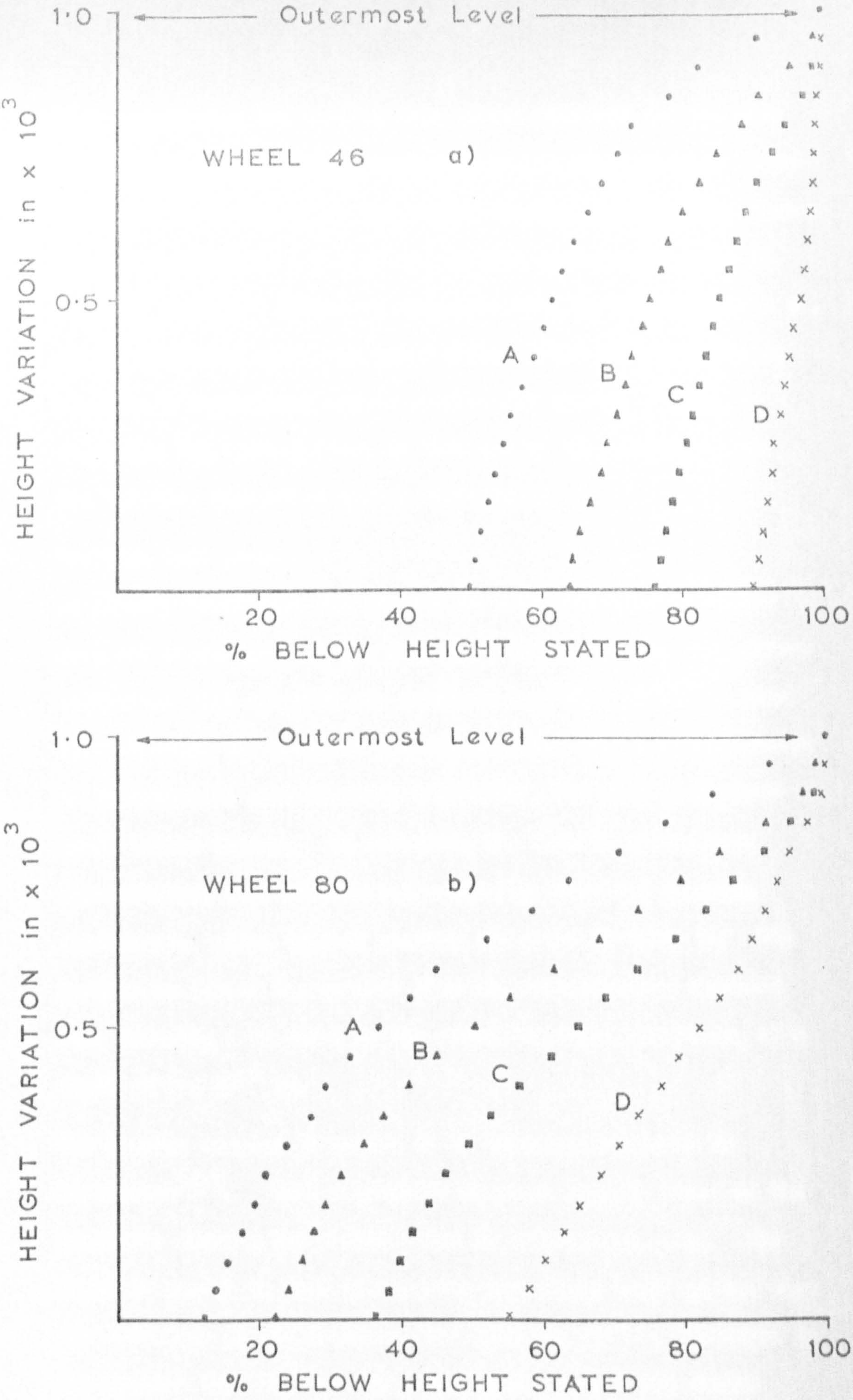

Fig. 40 Cumulative Height Distribution Curves

When considering the bearing area curves obtained for the same surface, but for different values of δ, it would seem reasonable to expect agreement where the curves overlap, provided the distortion is negligible. The result of this exercise is shown in Figs. 41 and 42. It can be seen that this is true for small δ, coarse dressing, and large grain size. For other conditions, however, a discrepancy exists between the curves. Thus, by comparing the bearing areas in this way it is possible to see the relative effects of stylus distortion.

f) The high spot count.

As already mentioned, the results of this measuring technique were not encouraging. The high spot counts for the two extreme conditions 46A5 and 46D5 are shown in Fig. 43. It can be seen that although the previous pdf measurements show a marked change in distribution with dressing conditions, the high spot count shows little change. In addition, the results showed poor repeatability when considering nominally identical dressing conditions. Some typical results are given in Table I. The parameters listed are derived from the distributions obtained when scanning a 46 wheel in the circumferential direction, at a depth of 5×10^{-3} in.

The results enabled 3D graphs to be drawn as suggested by Pahliztsch[23]. Such a graph is shown in Fig. 44 based on the parameter showing the widest range in values, i.e., Sk. The graph is useful in that it supports the widely held opinion that the influence of the dressing feed upon the surface structure is far greater than that of the dressing depth over the ranges considered.

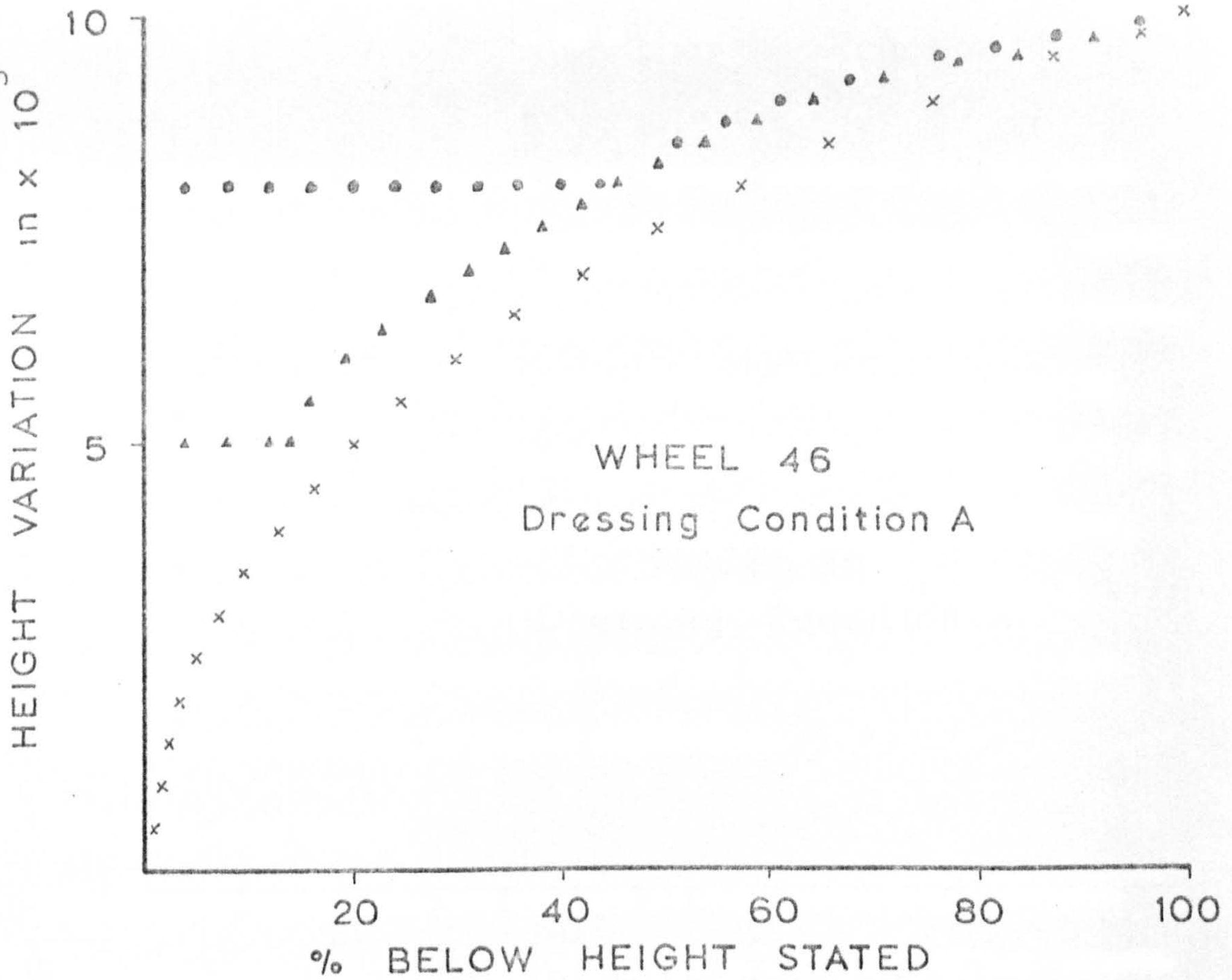

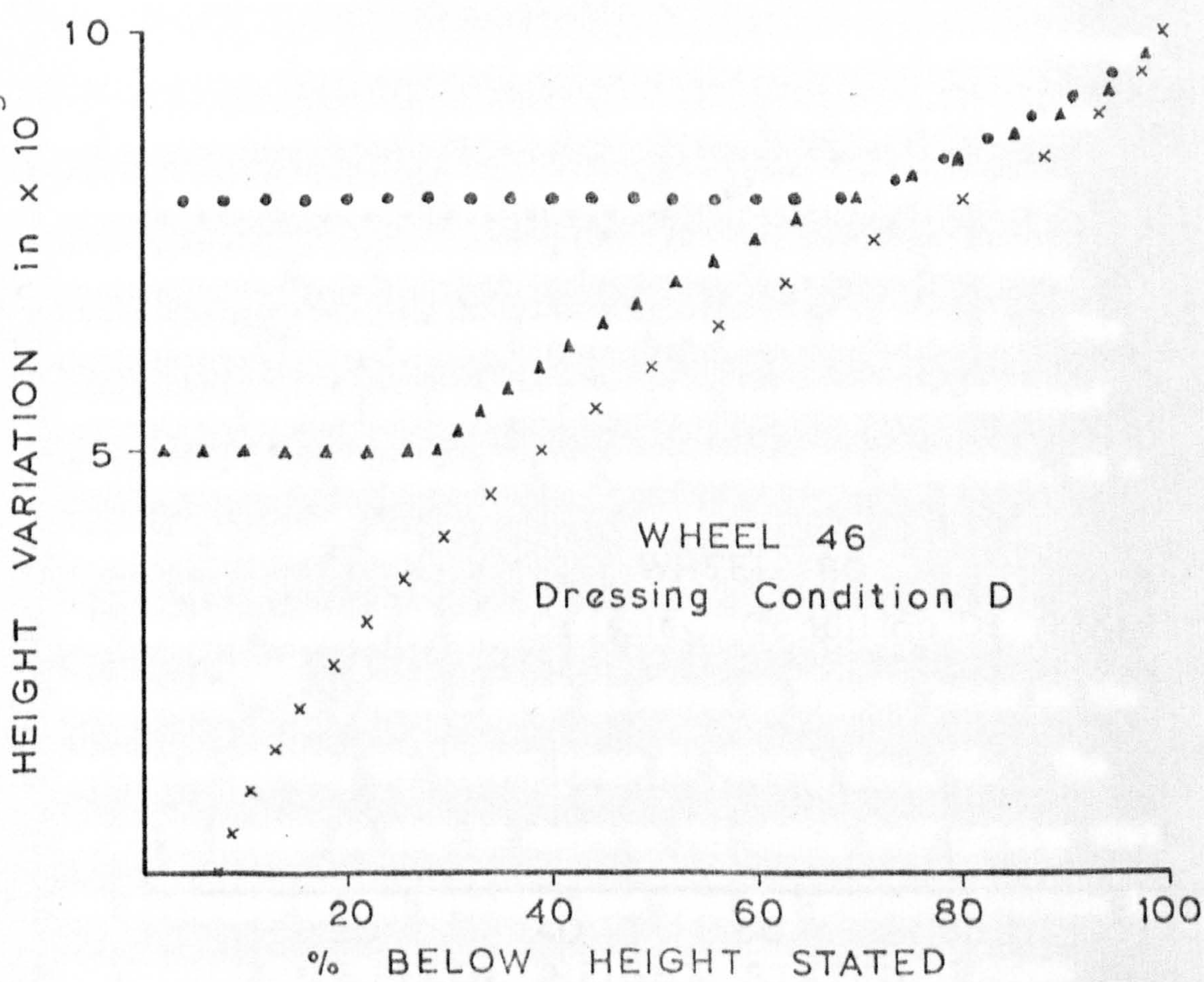

Fig. 41 Superimposed Bearing Area Curves (Wheel 46)

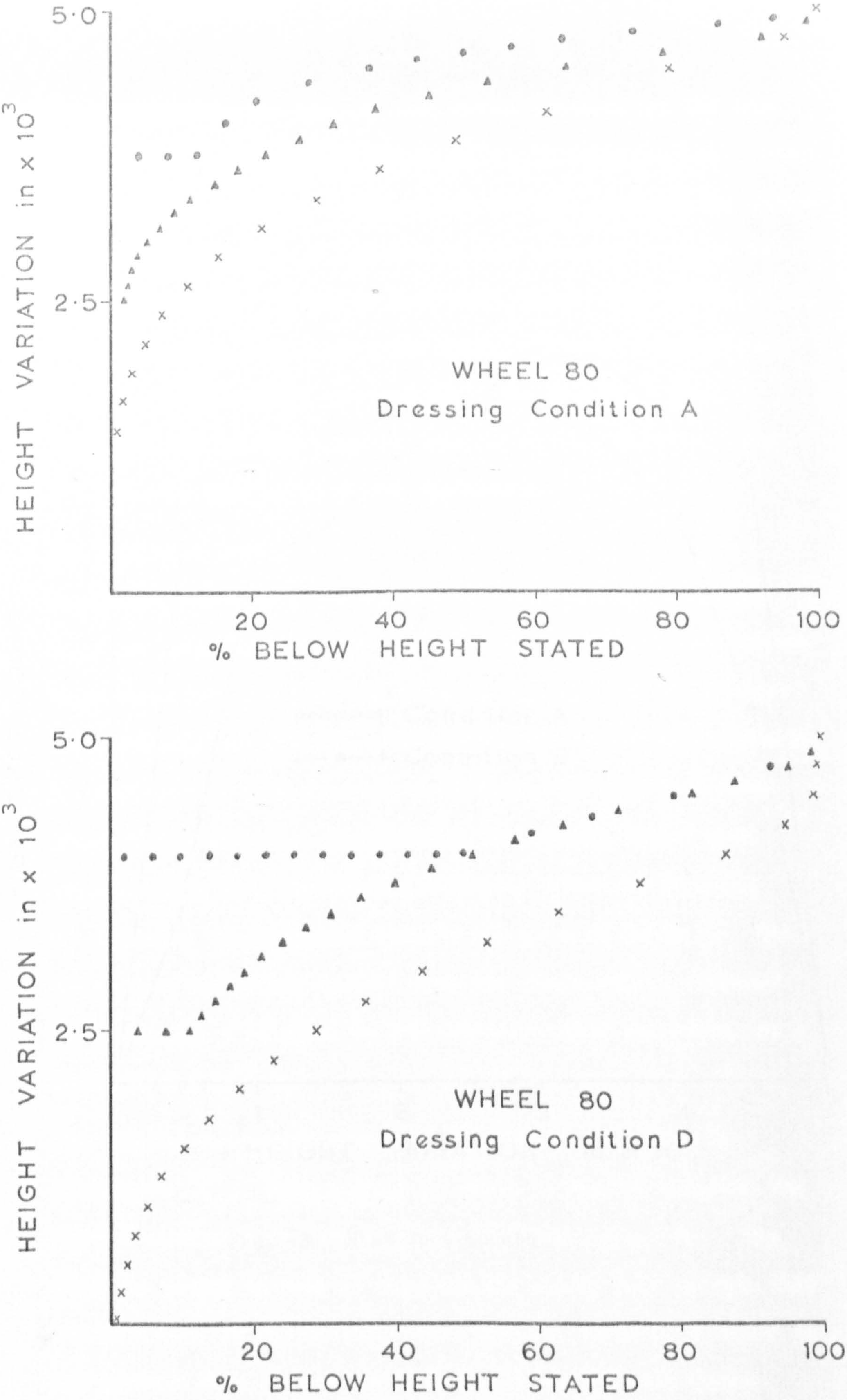

Fig. 42 Superimposed Bearing Area Curves (Wheel 80)

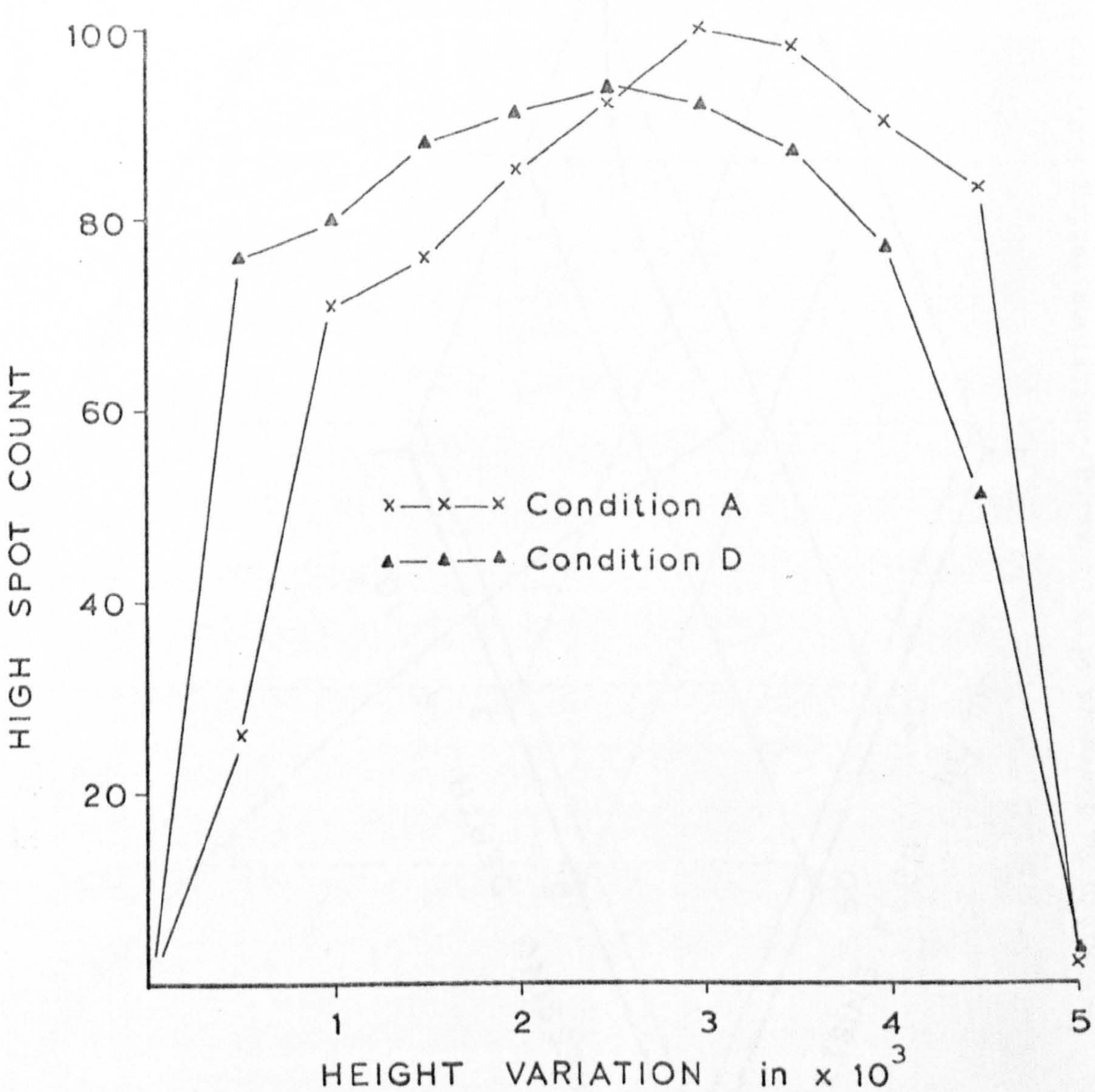

Fig. 43 High Spot Counts

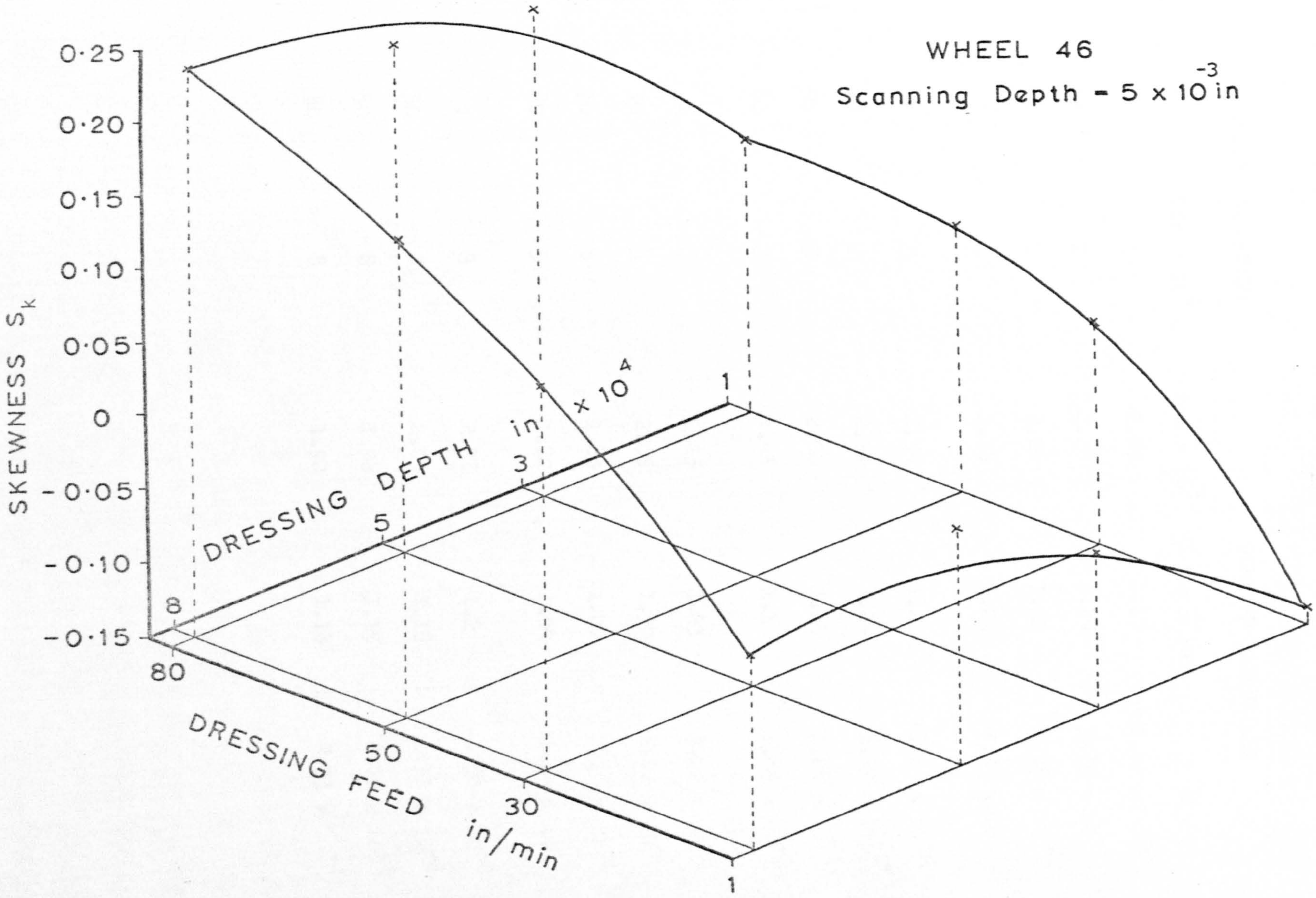

Fig. 44 Variation in Skewness with Dressing Conditions (using H.S. count technique)

TABLE 1

DRESSING CONDITION		DERIVED PARAMETERS		
f in/min	d in x 10^4	μ ins x 10^3	σ ins x 10^3	Sk
1	1	2.49	1.17	-1.42×10^{-1}
30	1	2.28	1.24	5.75×10^{-3}
50	1	2.26	1.21	2.36×10^{-2}
80	1	2.18	1.21	2.81×10^{-2}
1	3	2.34	1.21	-5.1×10^{-2}
30	3	2.21	1.24	6.17×10^{-2}
50	3	2.02	1.14	1.24×10^{-1}
80	3	1.93	1.1	1.89×10^{-1}
1	5	2.23	1.23	3.72×10^{-2}
30	5	2.06	1.30	5.72×10^{-2}
50	5	1.83	1.07	2.26×10^{-1}
80	5	1.82	1.04	1.84×10^{-1}
1	8	2.21	1.2	-1.98×10^{-2}
30	8	2.09	1.18	1.11×10^{-1}
50	8	1.98	1.15	1.76×10^{-1}
80	8	1.92	1.14	2.33×10^{-1}

3.3.2 CORRELATION AND SPECTRAL MEASUREMENTS

The previously described pdf measurements are essentially concerned with characterising abrasive surfaces in terms of the height ordinates. In order to investigate additional profile properties correlation measurements were undertaken.

Fig. 45 shows the ACF for the condition 80 A 0.5, obtained when using the dc cut-off. The function is typical of all correlation measurements utilising this mode, in that the presence of a dc level and the large amount of power at the very low frequency end of the spectrum cause a loss in information concerning the higher frequency data. (Appendix A1). For this reason, the correlator was operated entirely in the ac mode, i.e., cut-off frequency of 1 Hz. Unfortunately, the dc level is then lost, and an estimate of the mean height, μ, is not possible.

Figs. 46 and 47 give the ACF's for conditions 46 A 0.5 and 80 A 0.5 respectively, using the 1 Hz cut-off. The functions are seen to decay fairly rapidly and exhibit an apparent oscillatory component. Further observation shows that for the given conditions, the period of this component is close to the nominal grain diameter. For the 46 wheel, the approximate period is 1 sec. which is equivalent to 16.7×10^{-3} in. Similarly, for the 80 wheel, the period is 0.5 sec. equivalent to 8.3×10^{-3} in. These compare with the nominal diameters of 0.015 in. and 0.0075 in. for the 46 and 80 wheels respectively. Although in this case, the change in periodicity is almost certainly a function of grain size, in general, great care should be taken in drawing such conclusions. The reasons for this become clear when considering the case of a pure random signal (white noise). The theoretical ACF is a Dirac function at $\tau = 0$ (τ = time delay). The process of bandwidth limiting the noise (Fig. 48) changes the form

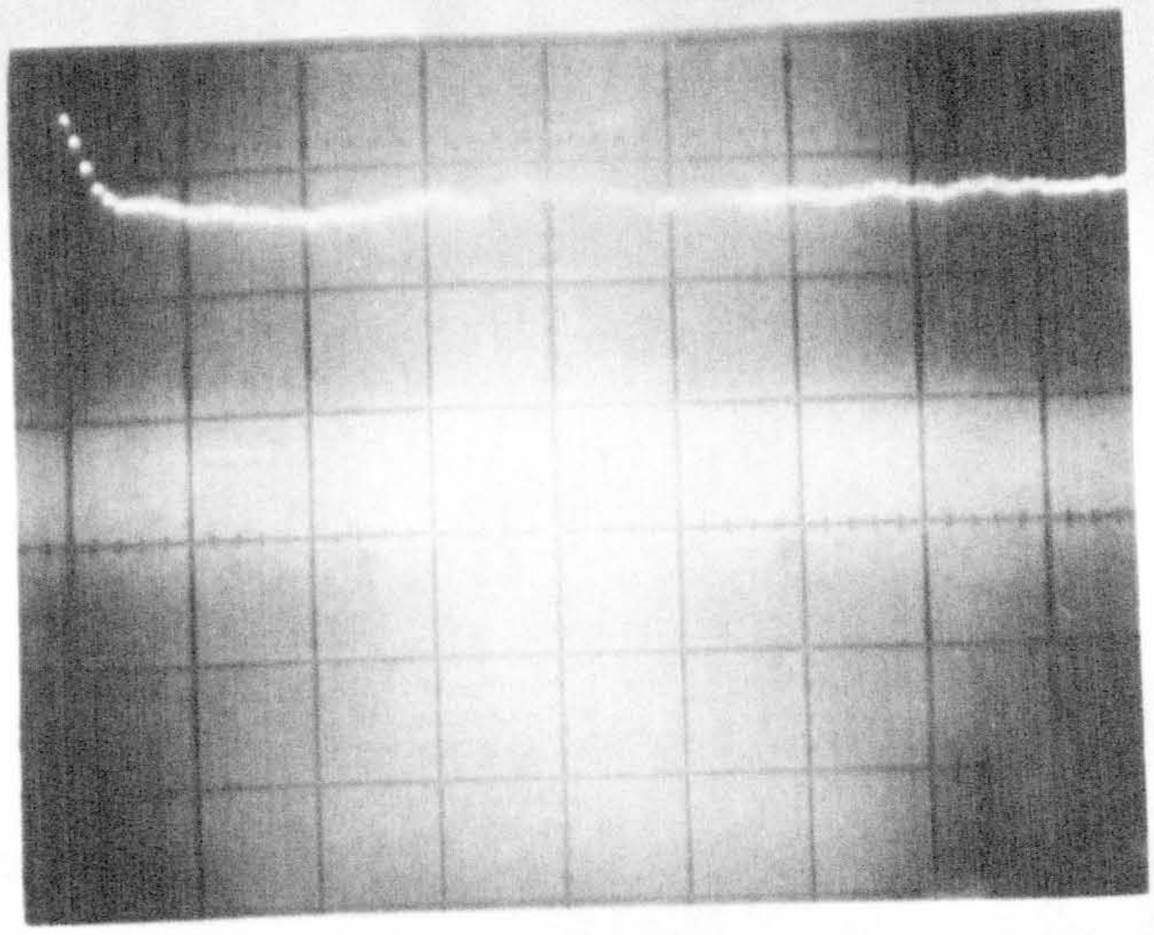

Fig. 45 ACF Condition 80A0.5 dc cut-off

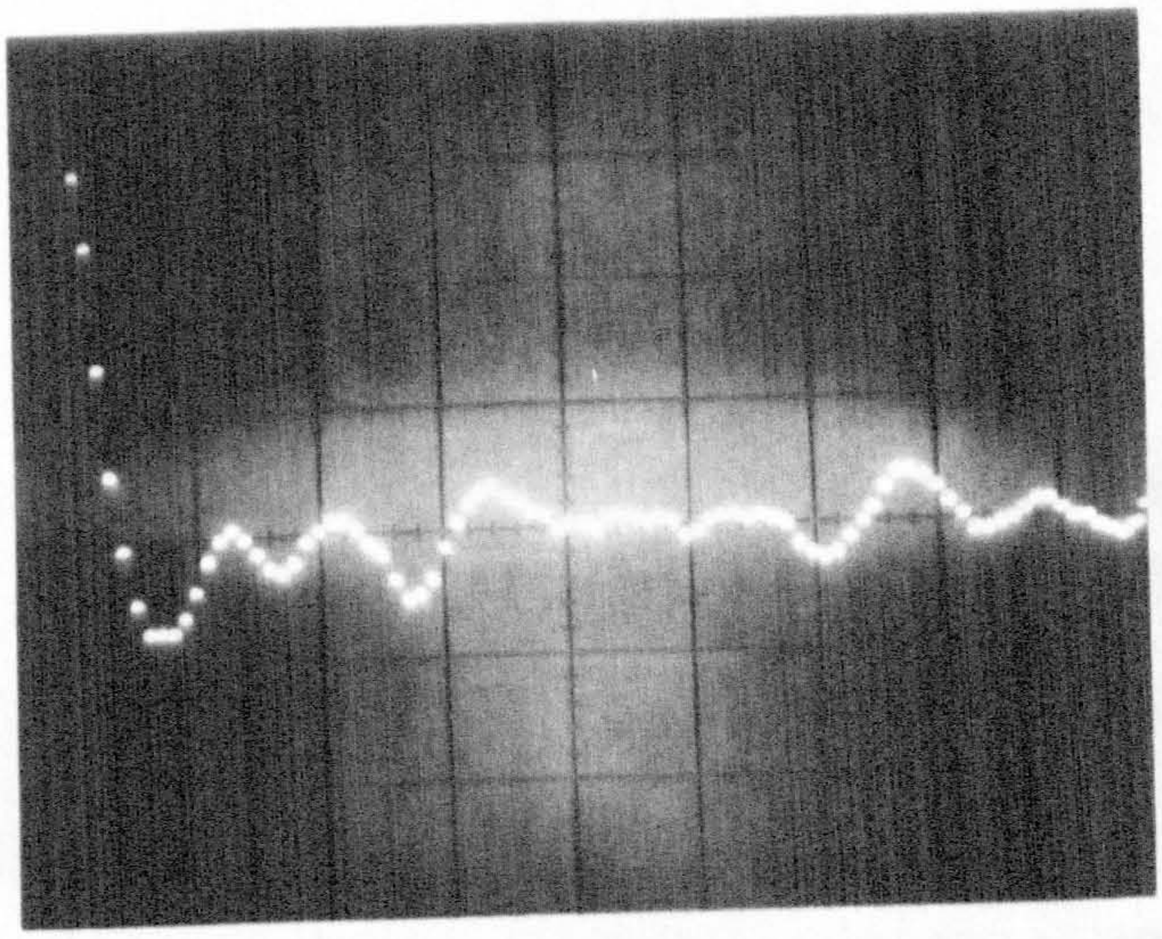

Fig. 46 ACF Condition 46A0.5 ac cut-off

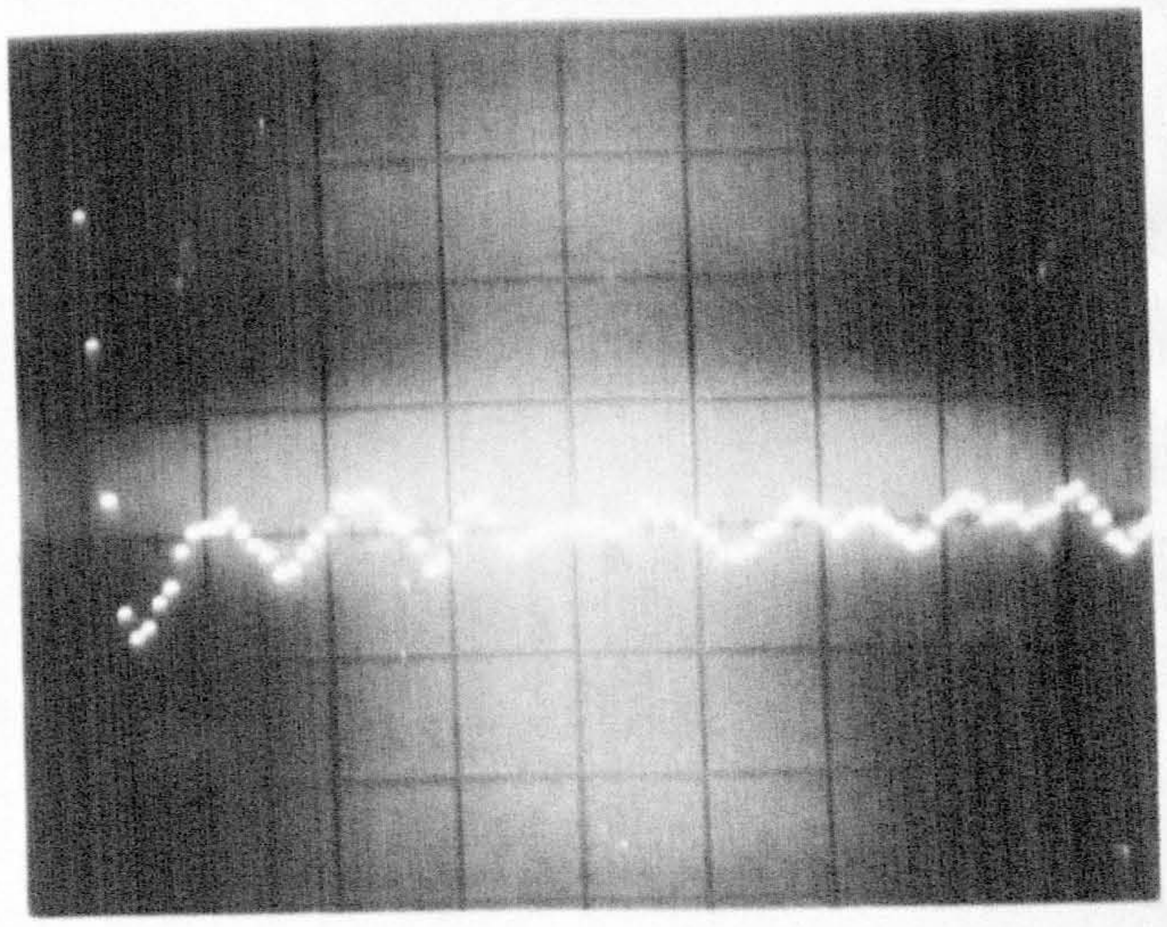

Fig. 47 ACF Condition 80A0.5 ac cut-off

of the ACF to

$$R(\tau) = \frac{dB \sin(\pi B \tau)}{\pi \tau} \times \cos(2\pi f_o \tau) \qquad \text{(Fig. 49)}$$

In practice, this is further distorted by the non rectangular characteristics of practical filters. As a check on the previous conclusions regarding the appearance of the grain size in the tail of the ACF, white noise of bandwidth 15 c/s was fed directly into the correlator and also via the tape and low pass filter. No change was apparent in the resultant ACF function, Figs. 50 a) and b) ((a) into correlator direct).

At this point it is worth comparing the general nature of the results with those obtained by Peklenik[18]. The ACF's are similar in form, Peklenik having suggested that his functions could be expressed by the relationship

$$R_{yy}(\beta) = Ae^{-\alpha\beta} \cos \gamma\beta + B$$

where A, B, α, γ, and β are constants. Unfortunately, no attempt was made to control the wheel parameters in an orderly fashion, the wheel specifications showing simultaneous changes in both hardness and grain size. The period of the oscillatory component did not appear to reflect the change in grain size. It should be pointed out, however, that a detailed comparison of two correlation studies is somewhat speculative unless one has prior knowledge of the filtering circuits, sampling lengths and computational procedures.

When used in the ac mode, the mean squared value of the signal, ψ^2, equals the (standard deviation, σ)^2. Thus the ACF's should provide a rapid estimate of σ. In Table 2 a comparison is made between σ values obtained from a range of pdf and correlation measurements (46 wheel, $\delta = 2 \times 10^{-3}$ in.)

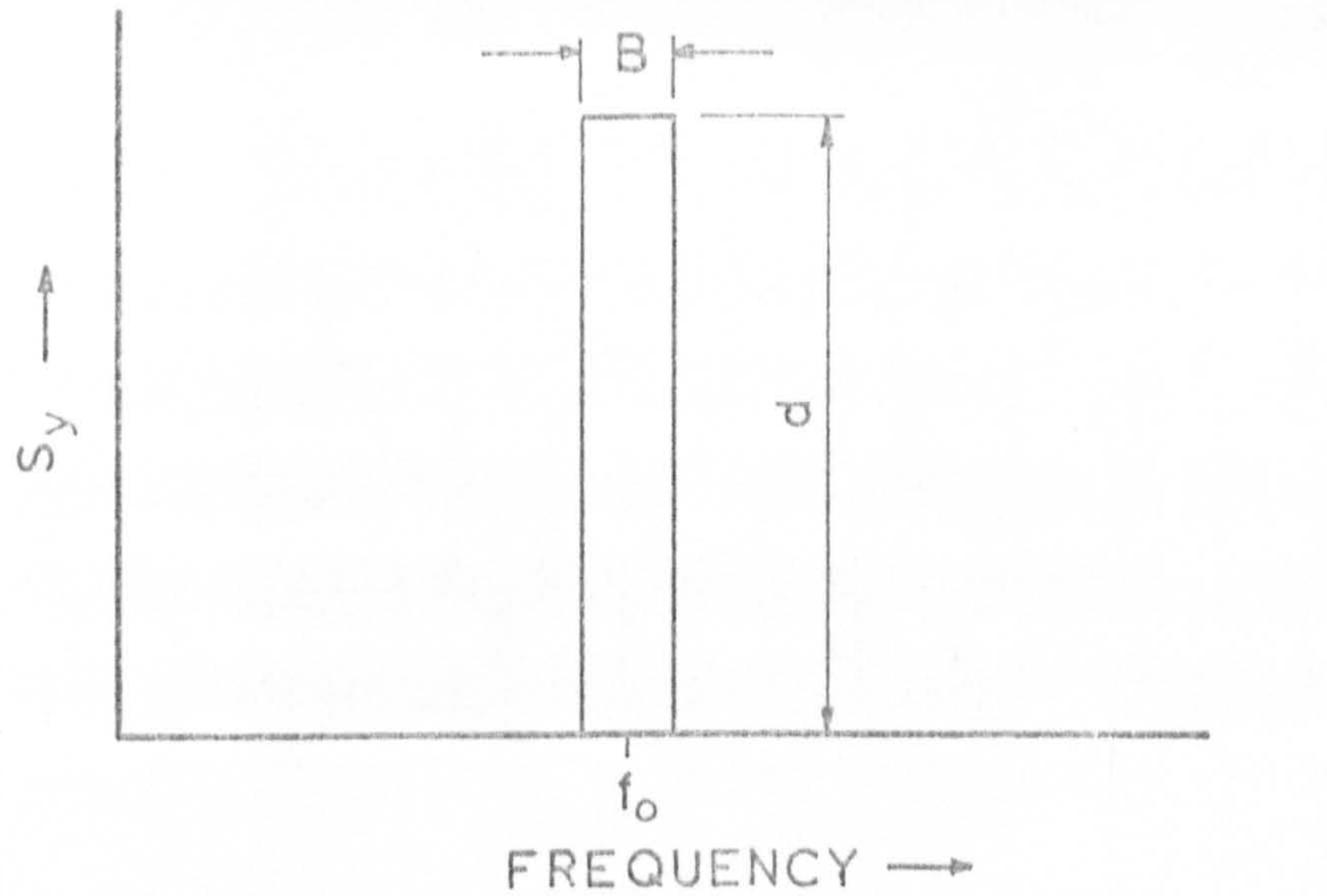

Fig. 48 Spectrum of Bandwidth Limited White Noise

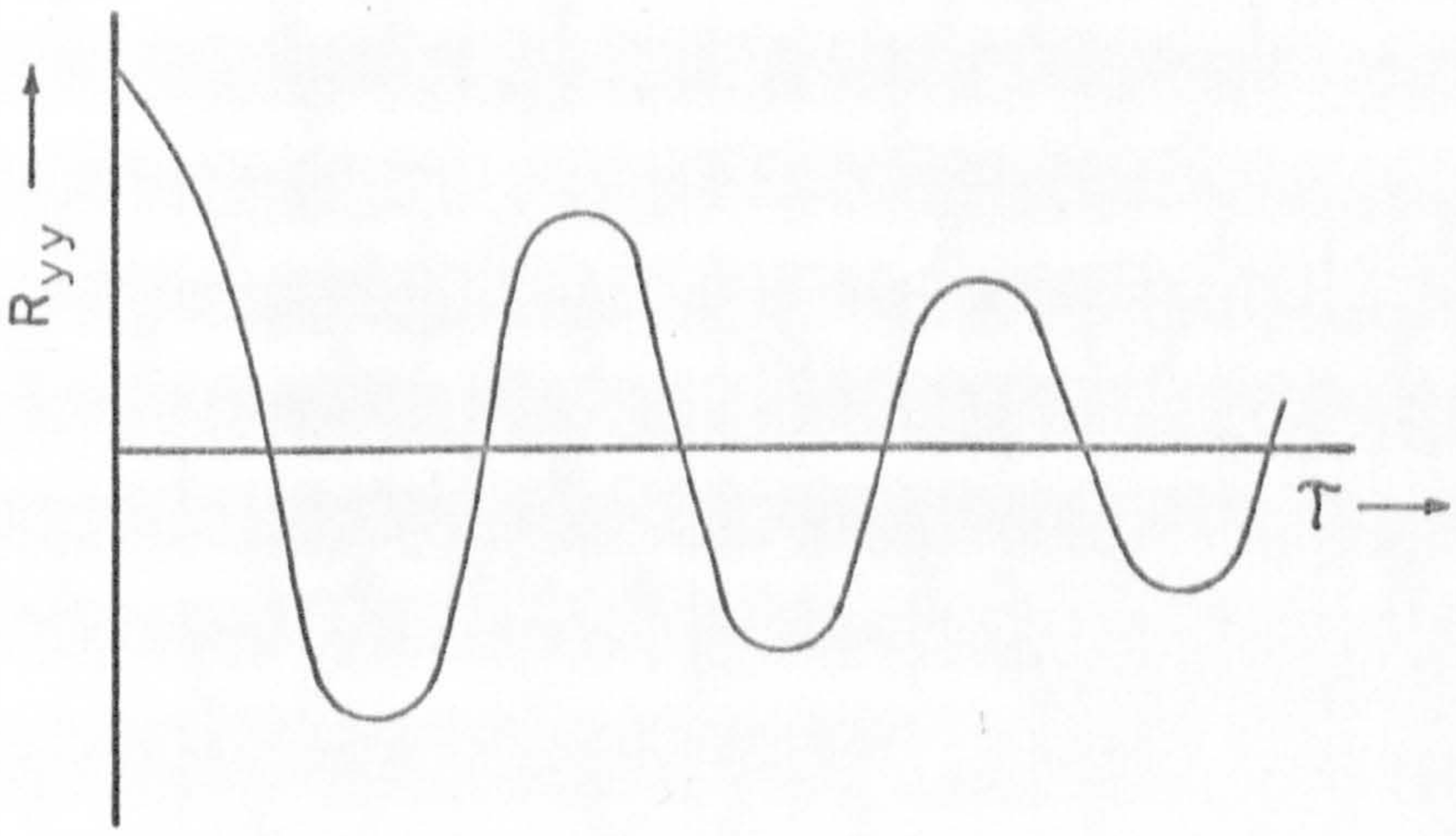

Fig. 49 ACF of Bandwidth Limited White Noise

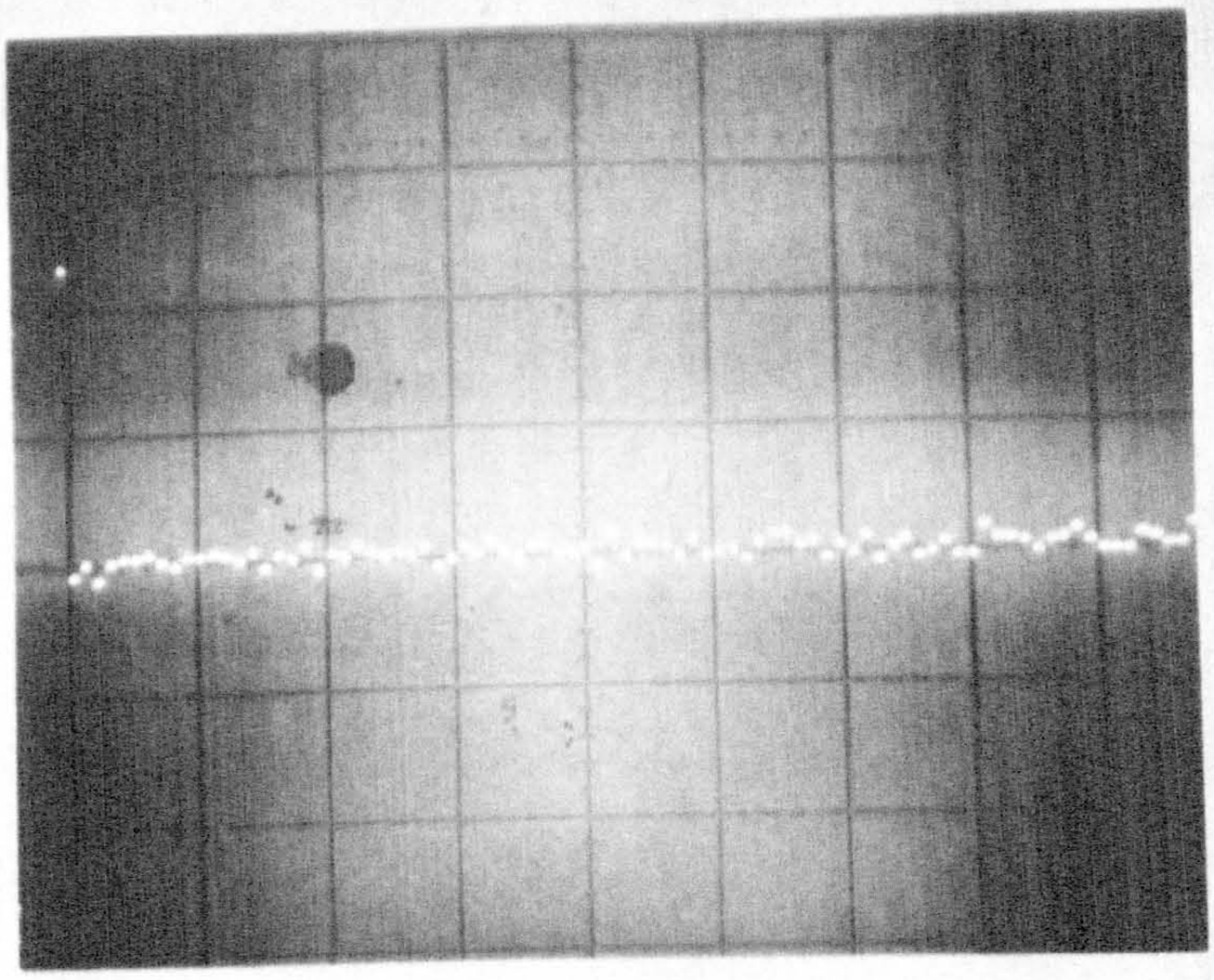

Fig. 50a ACF of White Noise (direct)

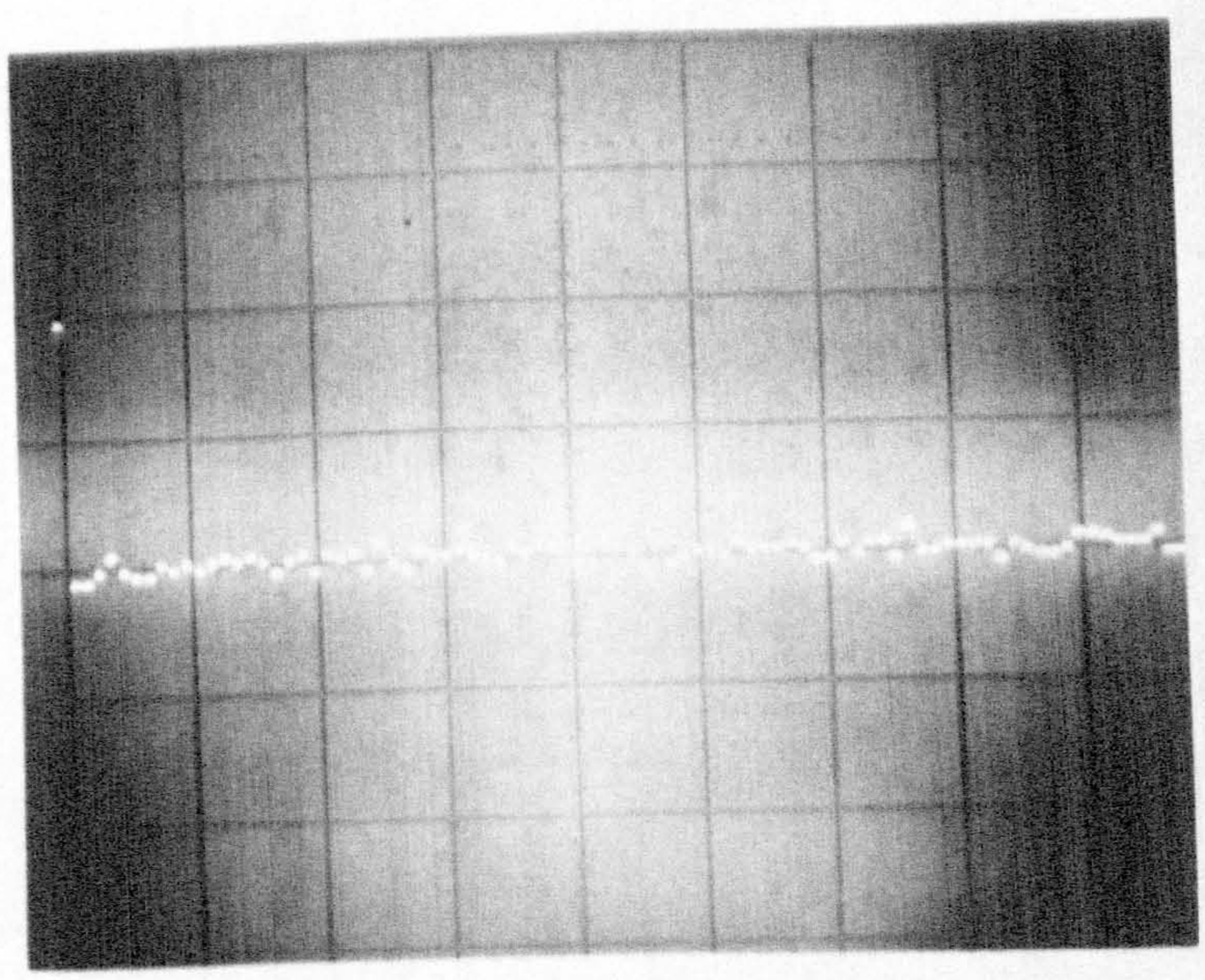

Fig. 50b ACF of White Noise (through measuring system)

TABLE 2

DRESSING CONDITION	STANDARD DEVIATION in. x 10^3 (pdf)	(ACF)	(mod)
A	0.88	0.49	0.84
B	0.75	0.44	0.71
C	0.62	0.39	0.61
D	0.47	0.32	0.5

The values of σ derived from the ACF's fall well below the values resulting from the pdf measurements. This was thought to be due to the considerable loss in power of the signal caused by the 1 Hz cut-off. In an attempt to overcome this and still maintain the higher frequency data, the profiles were recorded on the slowest tape speed and replayed into the correlator at the highest tape speed. This effectively raises all frequencies by a factor of 8, resulting in a larger proportion of the data escaping the lower cut-off point. With a corresponding reduction in sampling time (x10) the equivalent sampling interval is now 1.34×10^{-3} in. cf 1.67×10^{-3}. The modified values of σ are also shown in Table 2 where good agreement is obtained with the pdf results. Hence the ACF can be used to estimate the value of σ provided the above procedure is followed.

Although measurements of the rate at which the ACF decayed to 10% were made initially (Section 3.2.3), the results are not discussed here. This is because the measurements are essentially a function of the signal bandwidth, which is now analysed in more detail by considering the power spectrum, S_y, of the surface profile.

Since the area under the S_y curve is a measure of the total power in the signal, ψ^2, (σ^2 when using 1 Hz cut-off), the power spectra measurements will obviously reflect the previously determined variations in σ. Of more interest, however, is the change in power with frequency. Hence it is convenient to study the normalised values of $S_y = S_y/\sigma^2$, known as the spectral density. A typical spectral estimate is shown in Fig. 51 (condition 80 A 1). The frequency scale is calibrated in cycles/second and also in an equivalent cycles/inch. The results of the window closing technique as discussed in Appendix A 2 are also indicated. As more ACF points are used in the Fourier transform, greater resolution is obtained, but the reliability of the estimate unavoidably decreases. It must be pointed out that the apparent condition $S_y = 0$ at $f = 0$ is a result of the correlator lower cut-off frequency (1 Hz), and is not a property of the surface profile.

The influence of scanning depth, grain size and dressing condition upon the spectral density is now considered:-

a) Effect of δ

The influence of δ on the spectral density is shown in Figs. 52 and 53 for the 46 and 80 wheels respectively. As δ increases, the power at the high frequency end of the spectrum decreases. This is a direct result of the disappearance of the sharp asperity peaks which constitute the higher frequency components.

At the low frequency end of the spectrum, there is a tendency for the power to increase, as δ increases. This is attributable to the introduction into the profile of the longer wavelength structure of the surface.

b) Effect of grain size.

Comparison of Figs. 52 and 53 shows the marked influence of grain size upon the spectral density. The higher frequency components

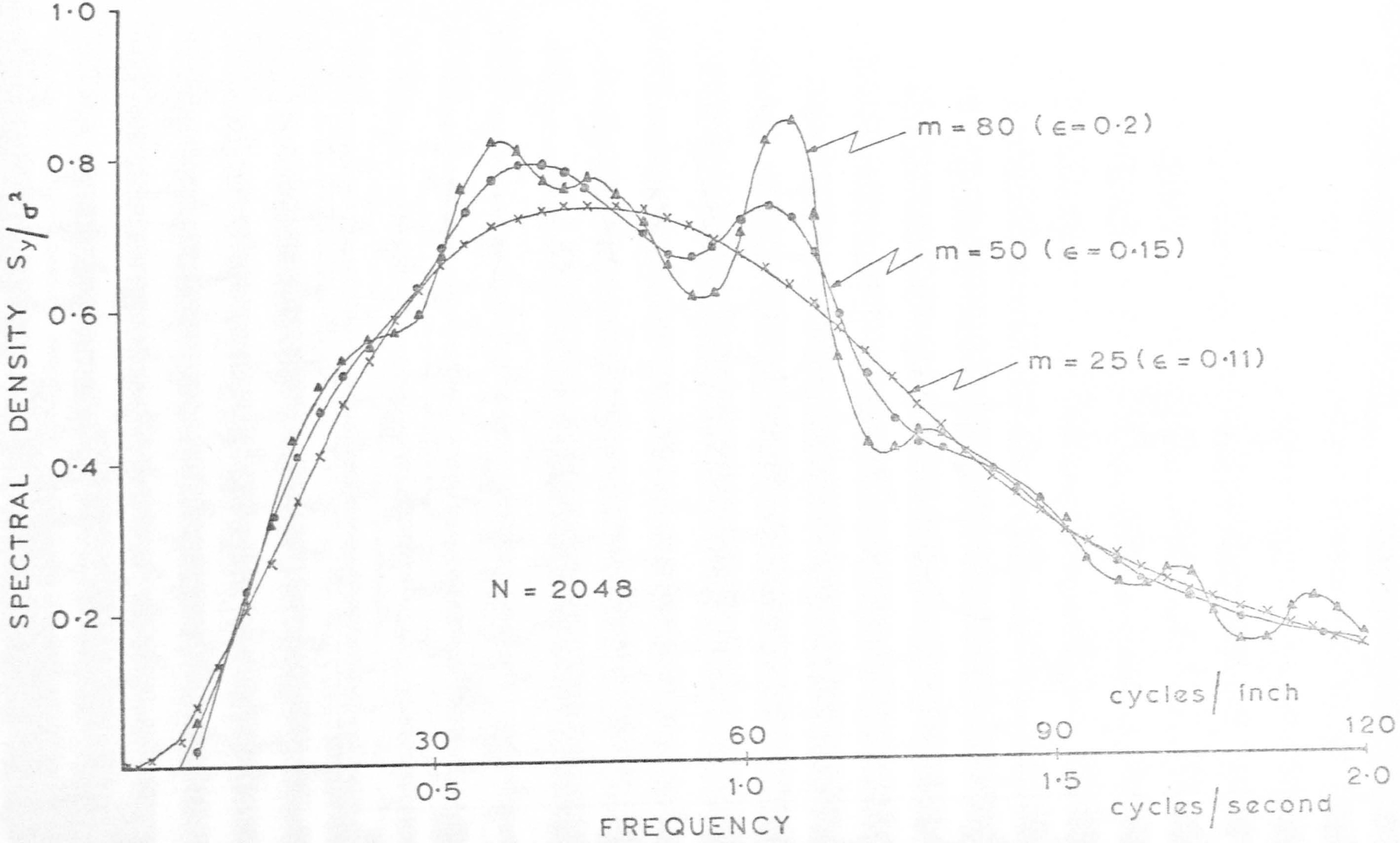

Fig. 51 Spectral Density Estimates

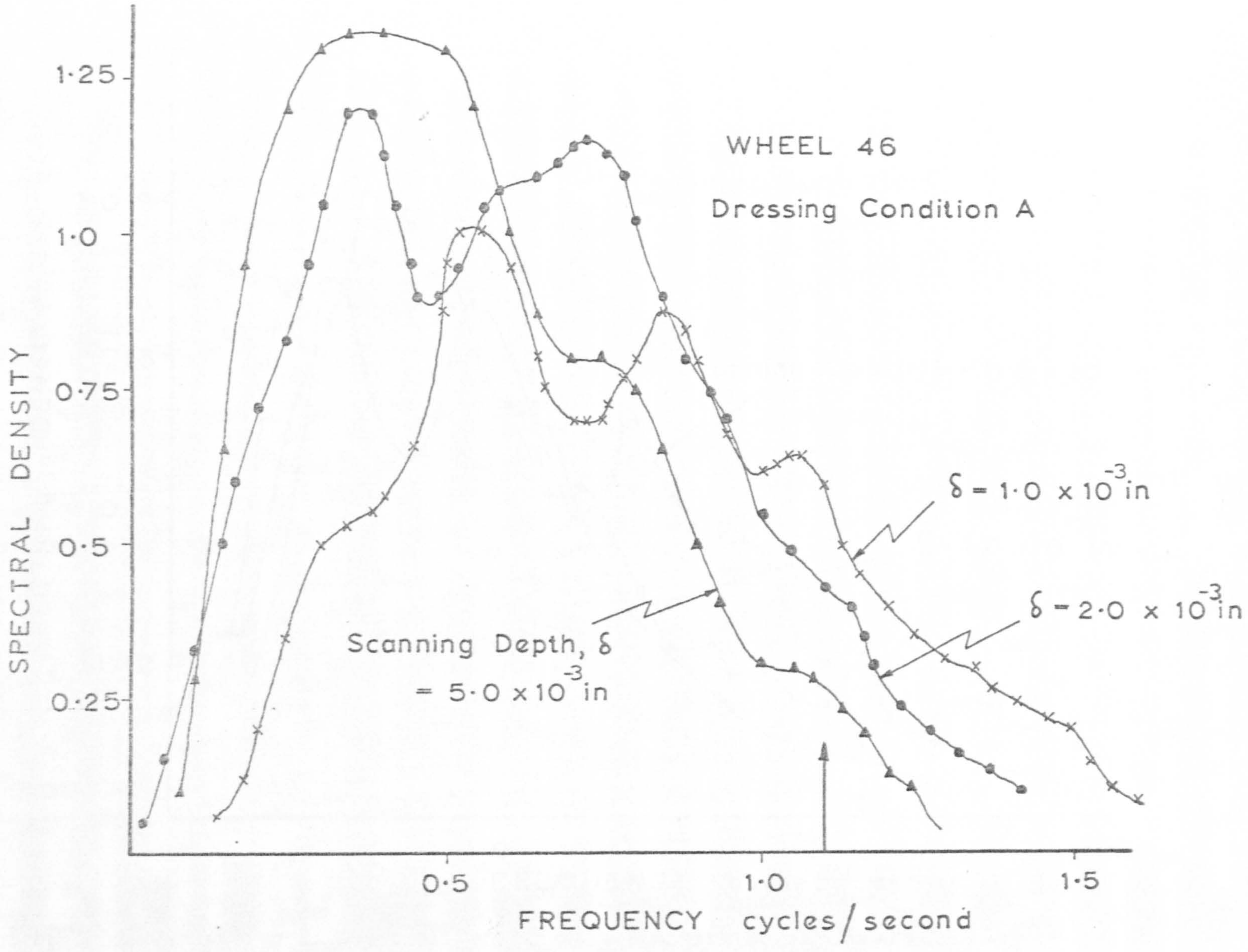

Fig. 52 Variation in Spectral Density with Scanning Level (46 Wheel)

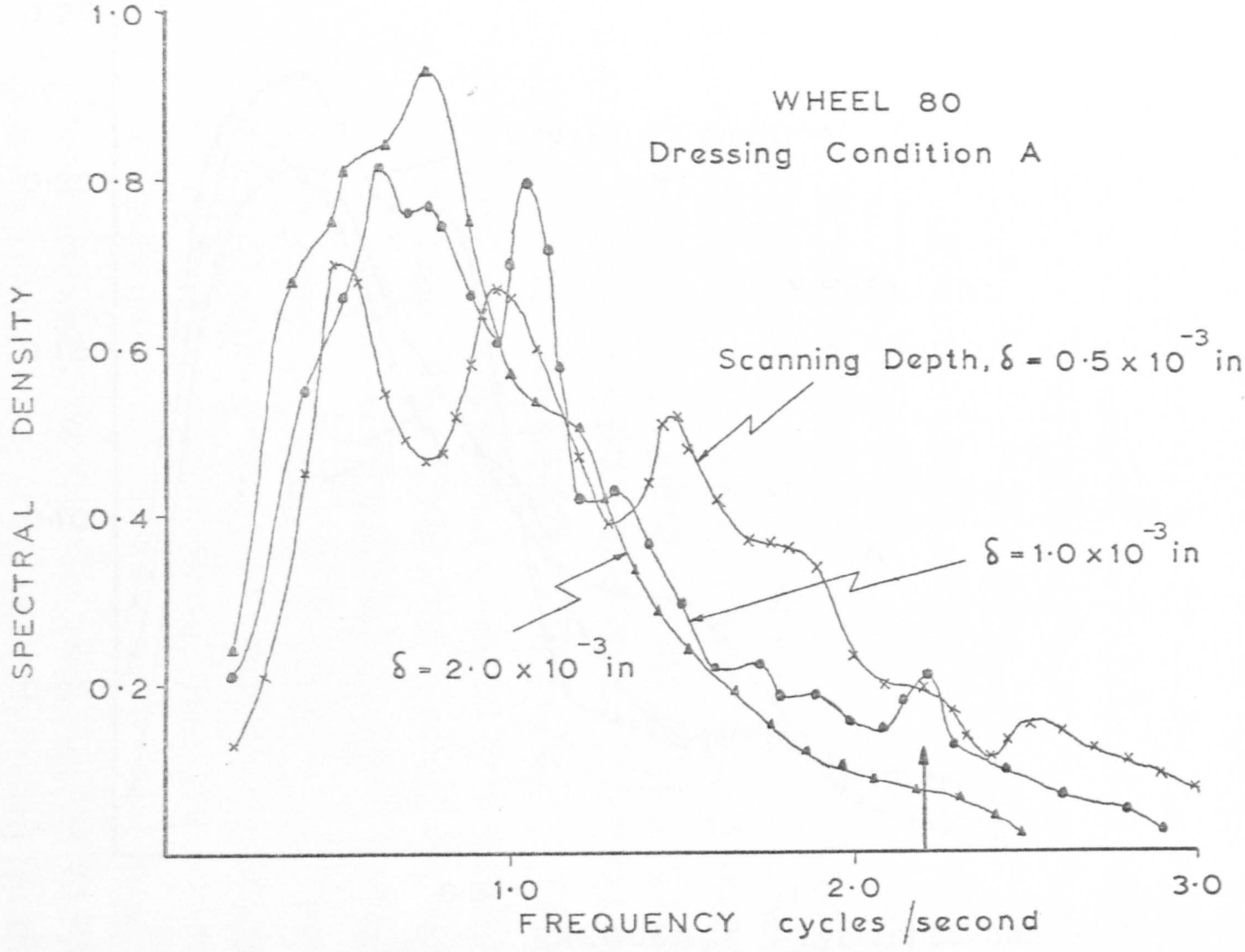

Fig. 53 Variation in Spectral Density with Scanning Level (80 Wheel)

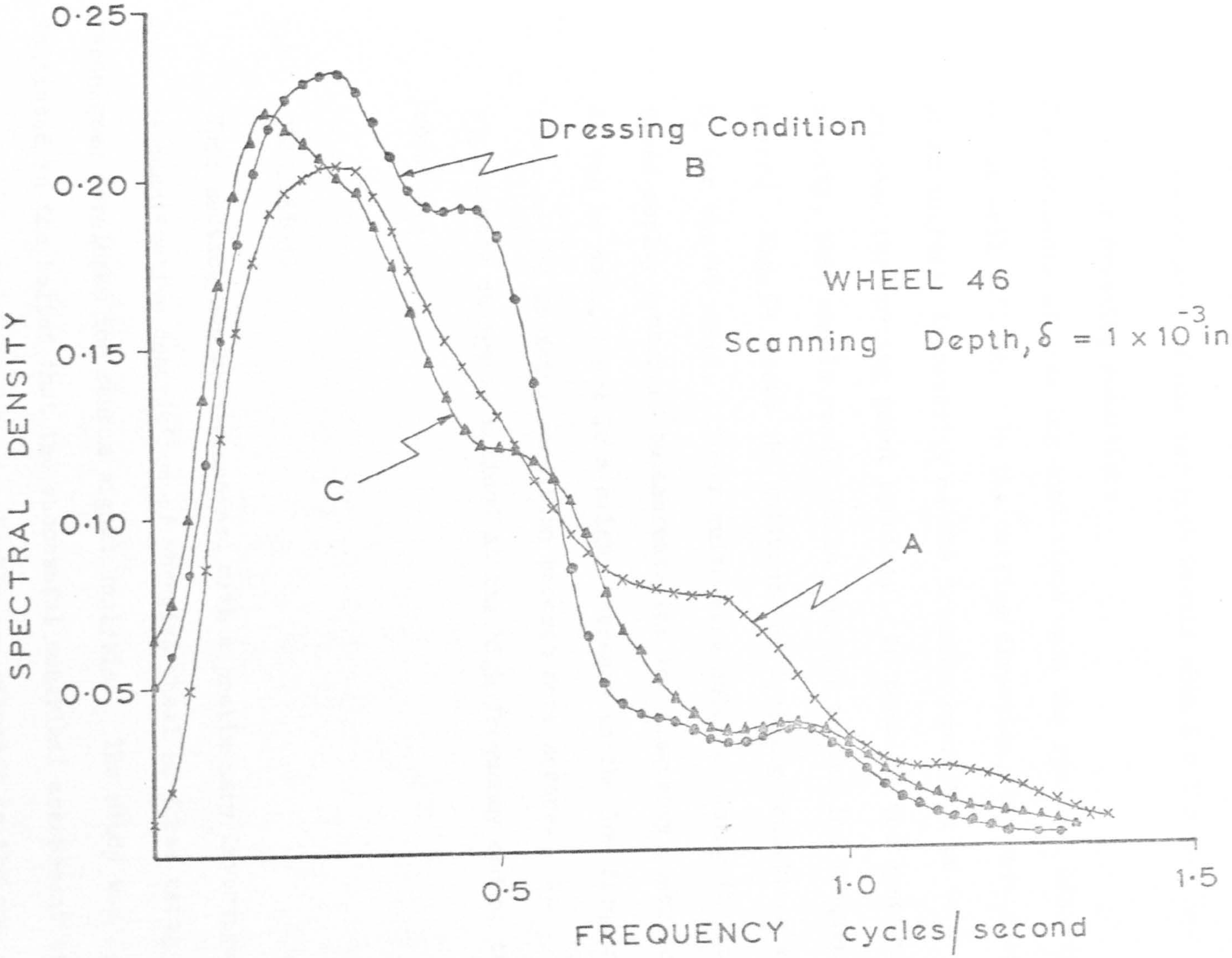

Fig. 54 Variation in Spectral Density with Dressing Conditions

of the finer wheel are clearly indicated. The arrows on the frequency axis are the equivalent periods of the nominal grain diameters. No definite peaks occur at this point although there is a resemblence of one for both wheels when $\delta = 1 \times 10^{-3}$ in.

c) Effect of dressing conditions

The influence of dressing conditions upon the spectral density is not well defined. In the cutting direction, the main result of an increase in severity of the dressing operation is to increase the cutting point spacing. In terms of the spectral density, this should result in an increase in the low frequency power. Fig. 54 shows the influence of dressing conditions on S_y for the 46 wheel. The results were obtained using the high speed replay procedure to decrease the low frequency power loss. As can be seen, there is a slight increase in the low frequency power as the dressing condition becomes more severe. No appreciable change is noticed at the high frequency end of the spectrum.

3.4 CONCLUSIONS

This section has been concerned with a preliminary investigation into the quantitative description of abrasive wheel surfaces using the techniques developed for random signal analysis. The study was initiated in the belief that the successful numerical assessment of abrasive topography would make a valuable contribution to the study and eventual prediction of abrasive wheel performance, e.g., metal removal rate, abrasive wear, etc.

Properties of the profile investigated are the statistical height distribution and derived parameters, the autocorrelation function

and the power spectrum. If such measurements are to be presented as realistic indicators of the wheel surface properties, they must obviously be sensitive to different wheel structures and superimposed dressing conditions. Hence, as a starting point, the influence of grain size and dressing conditions upon the above measurements was considered. The pdf estimates showed marked changes with both grain size and dressing condition and this was expressed through the change in percentage spacing, mean height, standard deviation and skewness. In physical terms, an increase in severity of the dressing operation has two distinct effects. The surface exhibits a wider range of amplitude fluctuations, and the spacing between individual cutting asperities is increased. This simple observation is used later (Chapter VI) in a computer simulation of the simple plunge grinding operation of Chapter V. With increasing grain size, the distribution became more negatively skewed, reflecting the bluntness of the abrasive asperities.

As far as correlation and spectral measurements are concerned, a great deal more work is required before their value as a measure of the surface properties can be completely assessed. Initial results seem promising, however, in that the effects of grain size and dressing conditions can be detected in both the ACF and spectral density estimates. A variation in total power of the signal is reflected by changes in the mean squared value of the ACF, and in addition, variations in power with frequency are also evident from the spectral estimates. Because of the importance of the sampling interval in terms of the scale of the information extracted from the surface, the implications of varying the interval must be studied further. For example, it may well be that the poorly defined low frequency changes associated with different dressing conditions could be accentuated by increasing the sampling interval. In addition, the present loss in power at the low frequency end of the

spectrum due to the correlator 1 Hz cut-off requires modifications. The problem could possibly be overcome by using the dc mode of operation in conjunction with an external filter operating at a lower cut-off frequency of, say, 0.01 Hz. Alternatively, if a proximity type transducer could be used instead of a stylus, scanning could be carried out at high speeds thus raising the signal frequencies above the lower cut-off frequency. As regards the present transducer, the errors due to profile distortion caused by the finite dimensions of the stylus have been indicated. The method can be satisfactorily employed as long as the wheel structure is fairly open and the scanning depth small.

An ideal conclusion to the investigation ultimately would be the realisation that the abrasive surfaces can be exactly defined by 'x' simple numerical parameters. In a very recent investigation into the representation of machined surfaces, Whitehouse and Archard[70] suggested that, for their particular model, the surface could be completely defined by two parameters, viz., the standard deviation, σ, and the correlation distance, β^*. In the abrasive measurements reported here, although the profile can theoretically still be represented completely by the pdf and ACF, it is unlikely that the latter will simplify to two straightforward parameters as in ref. 70. This is because in the first place, the distribution is not always Gaussian and in order to express the degree of skewness, etc., the measurements must be related to the scanning depth. Also, the ACF would appear to be of the more complex form as suggested by Peklenik[18].

In terms of a complete definition of the wheel surface, the pdf and correlation measurements do not give any direct information regarding the number and shape of individual asperities. This is a definite limitation of the present work because, as already indicated

(Section 2.2.2) the geometry of an abrasive grit is likely to be a critical factor in determining the mode of metal deformation during asperity - workpiece interaction. In ref. 70, however, an attempt was made to derive the slopes and curvatures of asperities from pdf and ACF measurements by theoretical means. When using a sampling interval that was sufficiently large to overcome the effects of stylus distortion, good agreement was obtained with experimental observations derived from a digital analysis of the profile. The feasibility of similar measurements being derived from abrasive wheel profiles could well form a useful continuation of the present work, but it may well be that the only successful way of determining the shape of individaul abrasive grits is by examination under a microscope.

One undeniable advantage of the present measuring system is the speed at which surfaces can be investigated. Sampling intervals, averaging modes, etc., can be rapidly adjusted to give the required information in its most satisfactory form. Hence an extensive investigation of a wide range of wheels can be contemplated as a practical reality. This is in sharp contrast to the scope of previous investigations which have been unavoidably limited to an extremely narrow range of wheel parameters.

Another attractive possibility arises as a continuation of the present work in that if a suitable fast response proximity transducer can be obtained, the change in abrasive properties during a grinding operation could be studied. The correlator would then be used in its "on line" capacity, showing variations in statistical properties as the grinding operation proceeds.

Having established a measuring technique, the next step is to investigate the cutting performance of a wheel in terms of the statistical properties of its profile. This is the main subject of Chapter V, where experimental observations on the mechanics of a simple controlled force plunge grinding system are interpreted in the light of the initial abrasive surface properties. However, as a necessary corollary to this work, the influence of abrasive asperity geometry upon the resultant mode of metal deformation is considered in the next chapter.

CHAPTER IV

THE INFLUENCE OF ABRASIVE GRIT GEOMETRY ON THE MODE OF METAL DEFORMATION

The study of metal removal during grinding can be facilitated by using tools of known geometry to simulate the action of abrasive grits. Previous investigations of this nature (Section 2.2.2) have indicated that in a practical grinding operation, the interaction of abrasive grit and workpiece can result in three main types of metal deformation:-

a) Elastic deformation, associated with the rubbing of grits along the workpiece surface.

b) Plastic deformation or ploughing where material is displaced without being removed.

c) Microcutting, resulting in the formation of metal chips as in a conventional milling or turning operation.

All the above types of deformation may occur simultaneously during grinding because of the varying geometries of the many individual grit - workpiece interactions. In addition, the mode of deformation associated with any one interaction may change as the grit passes through the workpiece surface forming a groove.

In this chapter, a simulation is used to study the influence of abrasive asperity geometry and wheel speed, on the type of metal deformation obtained. A single tool is arranged to interact with a stationary test piece, with the emphasis on reproducing conditions which are realistic of the grinding process, e.g., impact speed and duration, minute scale of deformation, and workpiece material. The forces developed and the energy consumed during the impact are

analysed in an attempt to correlate the mode of deformation with these fundamental parameters. Of particular interest is the influence of tool geometry and speed on the transition from plastic displacement to microcutting.

The findings are then substantiated by further experimental work involving an analysis of the groove side swell, observation of a fine grid on the test material surface, and high speed photography of the entire period of tool - test piece engagement.

4.1 APPARATUS

4.1.1 GENERAL ARRANGEMENT

The main experimental set-up (Fig. 55) was designed to reproduce as accurately as possible the path traced by a single abrasive grit during a practical grinding operation. A standard Churchill surface grinder (horizontal spindle, Model 'OSB') was used and a special holder constructed to take the small simulated tools. The test material was held stationary, the rotating tool thus forming a single continuous groove (Fig. 56). Under these conditions, the path of the tool relative to the material is seen to be circular, and not trochoidal as in practice. The difference in the resulting groove geometry is very small however, and the grooves approximate closely to Types 4 and 5 as defined by Reichenbach[45] and reproduced in Fig. 17 (Section 2.3.1).

It was found possible to obtain a practical range of impact speeds by accelerating the tool from different angular settings, β, by means of the standard wheel head motor assembly.

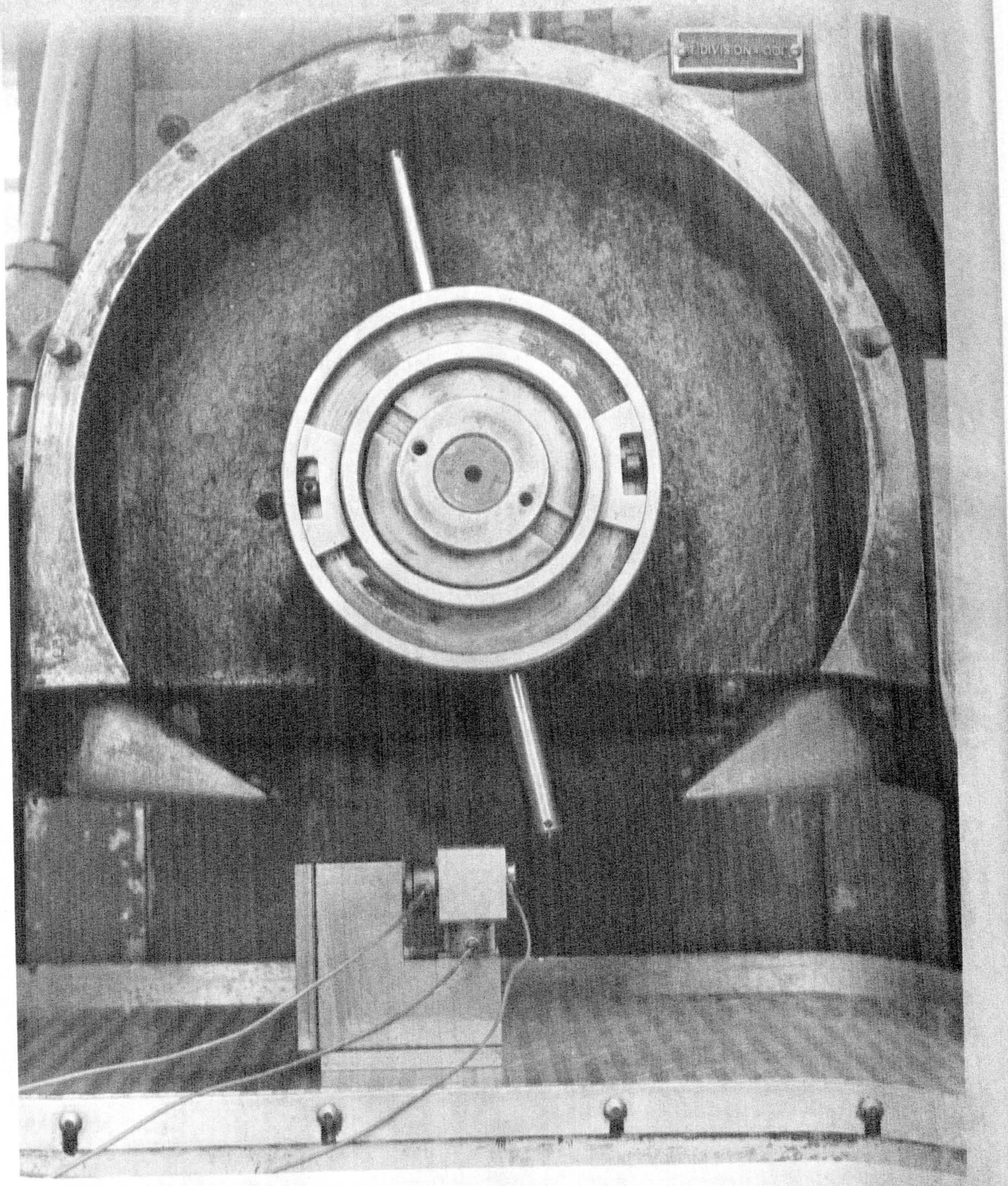

Fig. 55 Experimental Apparatus

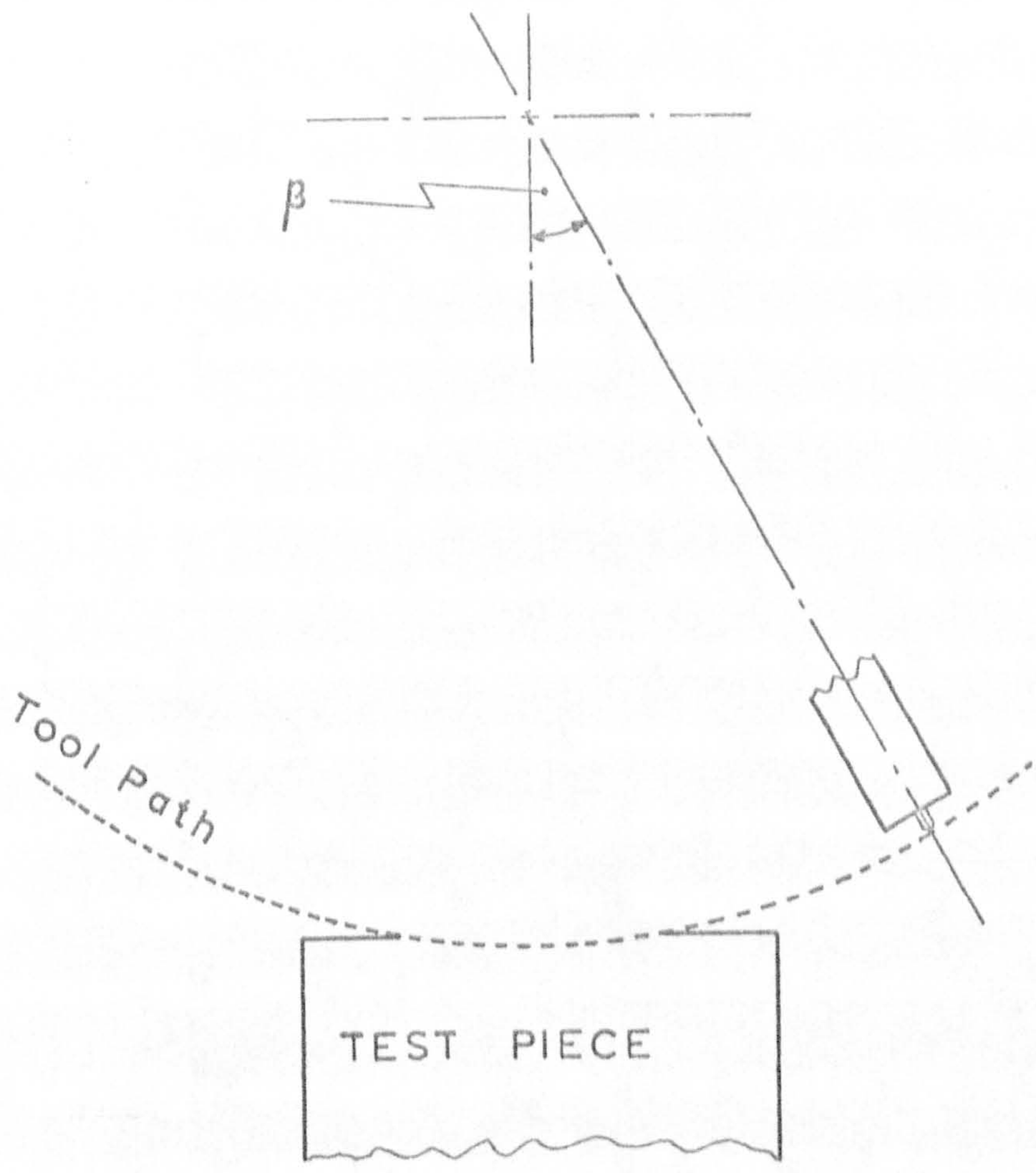

Fig. 56 Geometry of Groove Formation

4.1.2 THE DYNAMOMETER

A dynamometer possessing a very high natural frequency is an essential requirement for the accurate measurement of short duration impacts. This has been pointed out by Crisp et al[40] who suggested that for satisfactory performance, the natural period of vibration should not be greater than one third of the minimum impact time experienced during tests. Using the above criterion and an estimated minimum impact duration of 0.27 millisec, a required natural frequency of 11 k Hz was obtained. The impact time was evaluated from the geometry of the interaction assuming a maximum speed of 4,000 ft/min and a minimum depth of tool penetration of 0.001 in. In order to achieve this high natural frequency the test piece was made an integral part of the two component dynamometer (Fig. 57). Two Kistler load washers having a resonant frequency of 50 k Hz (Type 902 A - quartz crystal transducers) provided the pressure sensitive elements. These were insulated from the main body of the dynamometer in order to provide a triggering circuit for the Tektronic 564 B storage oscilloscope on which the impact forces were recorded.

Initially, commissioning tests were carried out on the dynamometer to determine the natural frequencies in both the horizontal and vertical directions, and the cross sensitivity:-

a) Natural frequencies, fn.

These were determined experimentally by observing the dynamometer response to an external periodic force of the form $P = P_o \sin wt$. A Goodman Vibrator was used in conjunction with a standard signal generator, this combination giving a peak force output of 1.5 lb f up to a frequency of 20 k Hz. Fig. 58 shows the response of the dynamometer in both the vertical and horizontal

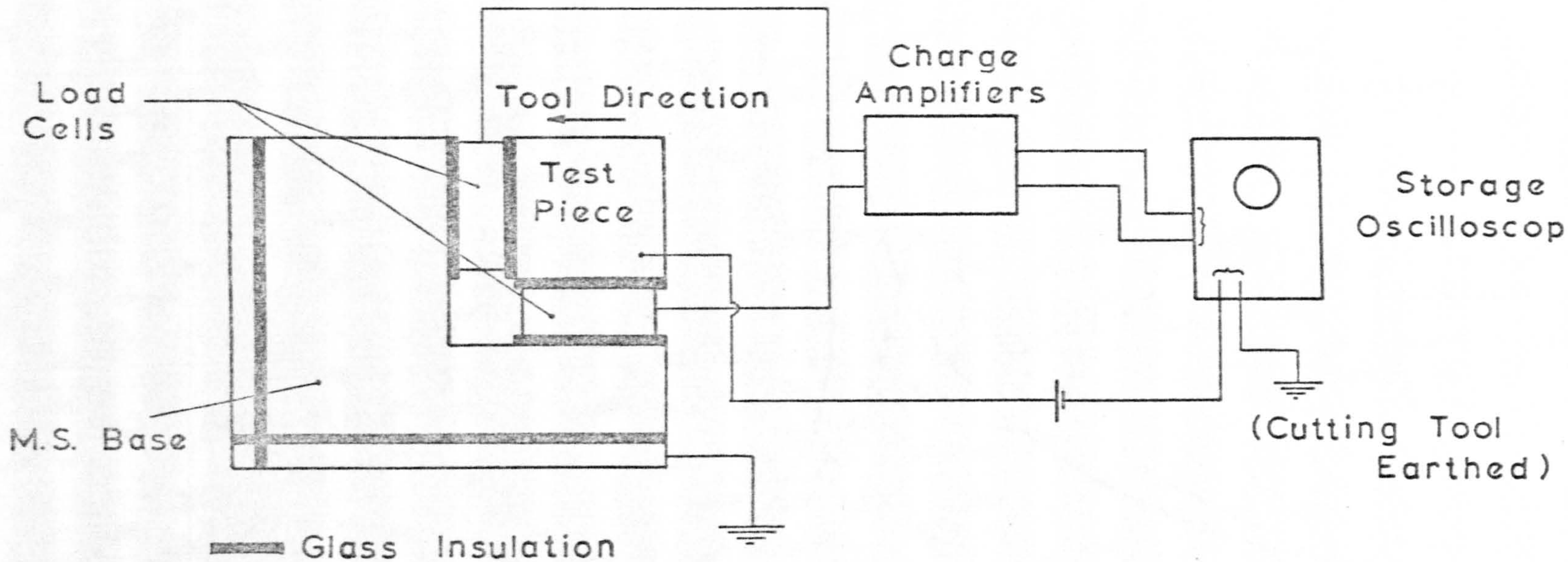

Fig. 57 Dynamometer and Associated Electronics

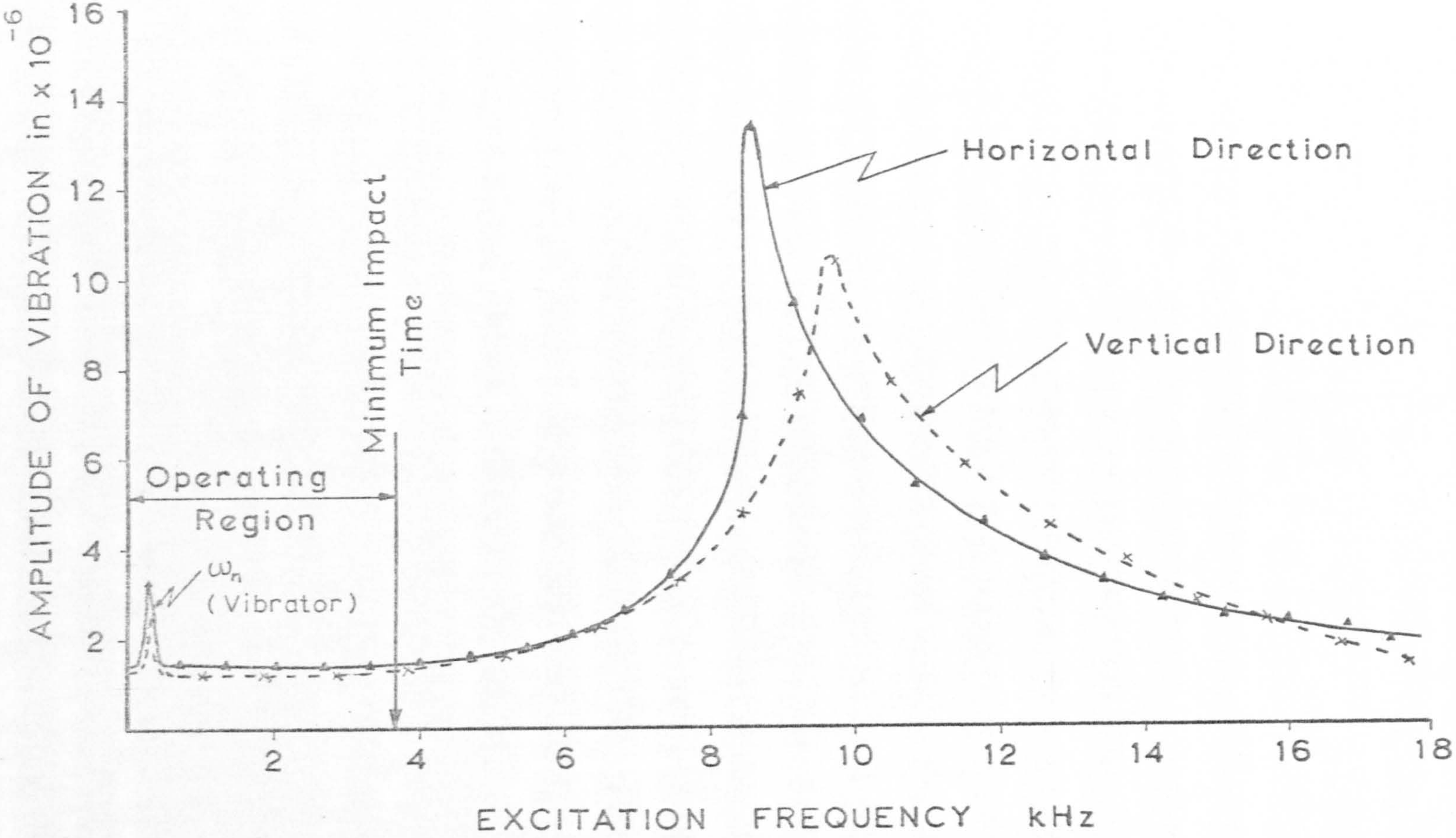

Fig. 58 Dynamometer Response

directions and the natural frequencies occurring at 9.7 and 8.6 k Hz are indicated. These high values were achieved by ensuring good contact at the various mating surfaces of the dynamometer and by using glass as the insulation material.

Although less than the ideal figure initially estimated, i.e., 11 k Hz, the response of the dynamometer is seen to be negligible over the anticipated working range, signified in Fig. 58 by the limiting frequency value based on the minimum impact time of 0.27 millisec.

The resulting natural frequencies of the assembled dynamometer are seen to be considerably less than the stiffness of the load cells. This is due to the added mass of the test material and elasticity effects at the various contacting surfaces. Because of this unavoidable reduction in frequency a simple arrangement whereby the test piece is mounted on a standard composite two component load washer is not feasible, since the natural frequency of such a device is only 10 k Hz.

b) Cross sensitivity.

In order to determine an accurate estimate of the cross sensitivity, the two component dynamometer was subjected to an impulsive force. This was achieved by dropping a steel ball onto the test piece surface from a known height. The position and direction of the impact force relative to the axis of the load cells could therefore be accurately controlled. The dynamometer was assumed to behave as a simple mass spring system with viscous damping (Fig. 59a). The theoretical expressions for the force exerted by the ball on the test piece and the duration of the impact (Fig. 59b) were derived from dynamic

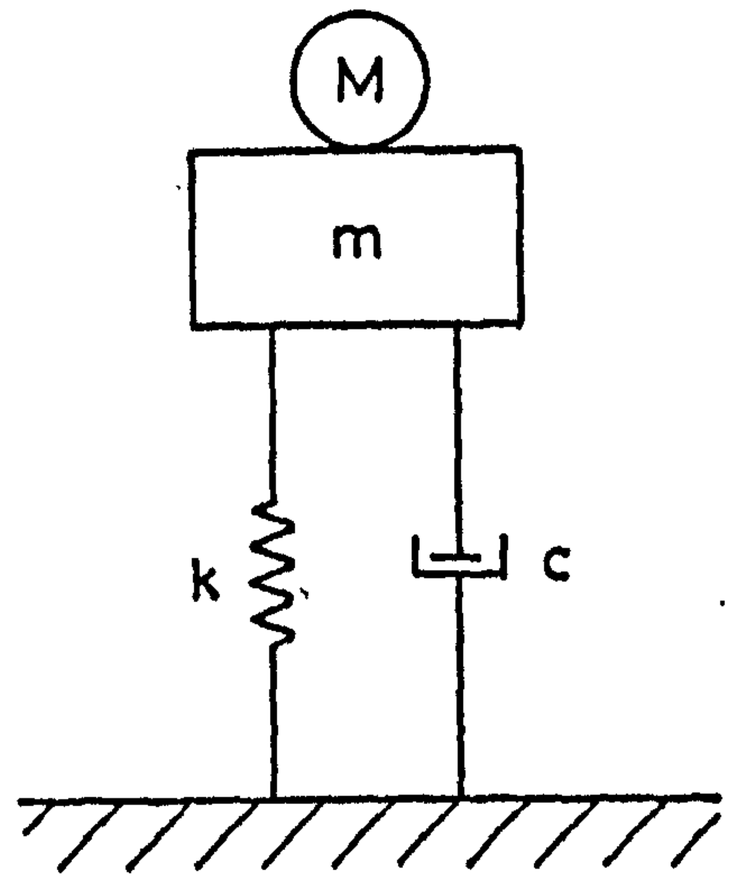

Fig. 59a Simple Mass Spring System with Viscous Damping

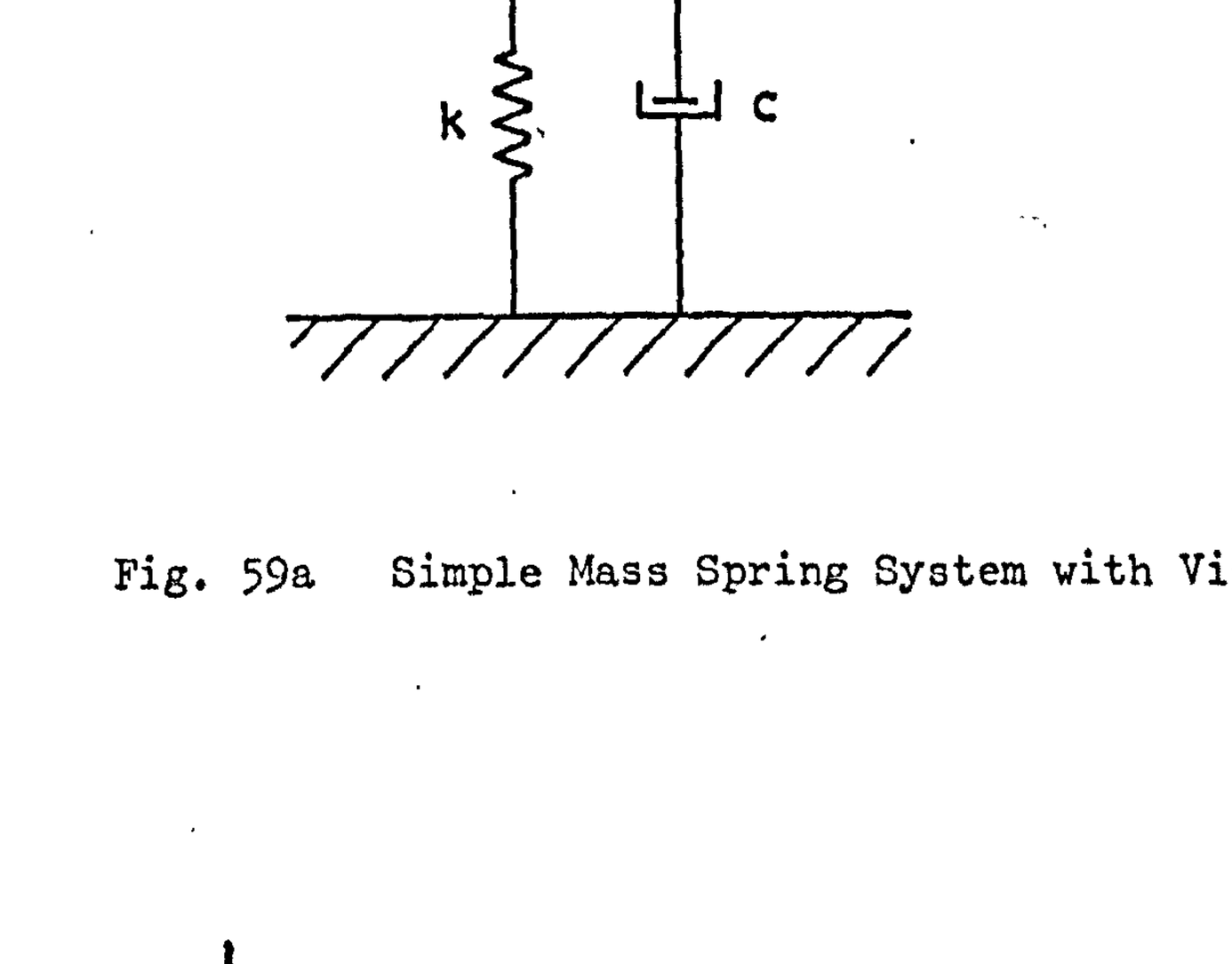

Fig. 59b Force Exerted on the Test Piece

and elasticity considerations at the point of impact[40]:-

$$P_{max} = 1.143\, n^{0.4}\, M^{0.6}\, V_o^{1.2}$$

$$T = 3.215\, (M/n)^{0.4}\, V_o^{0.2}$$

where $n = ER^{\frac{1}{2}}/1.364$

and E = Young's modulus for the ball material

R = Ball radius

M = Mass of ball

V_o = contact velocity = $(2gh)^{\frac{1}{2}}$

h = drop height

Fig. 62a shows the cross response of the horizontal load cell when a peak force of 80 lbf is applied in the vertical direction. Allowing for the difference in scope sensitivity settings, the horizontal force, T, = 6.8 lbf, i.e., a cross sensitivity of 8.5%. The effect of T upon the vertical force, N, was found to be of similar magnitude. The results of a large number of tests where the ball was dropped at different points on the test material surface, indicated that the cross sensitivity was always less than 10%. In addition, for a given drop height, the change in the measured value of P_{max} was negligible, indicating that grooves could be formed anywhere on the test piece surface with the same measurement accuracy.

4.1.3 TOOL GEOMETRY

Detailed qualitative examinations of abrasive surfaces using stereoscan techniques have revealed that the individual asperity geometry is extremely complex. Past experimental and theoretical

investigations have often simplified the true situation by approximating the asperity geometry to idealised mathematical shapes. In general, these have taken the form of angular structures such as pyramids, truncated wedges, etc. In this investigation, two tool geometries have been used, viz., pyramidal and spheroidal. Spheroidal tools have been included because, although the macro-structure of a wheel tends to be decidedly angular, the asperity tips which are responsible for the actual metal removal often display a pronounced curvature. In fact, Redko[14] has presented a graphical relationship between nominal grain size and asperity radius based on the investigation of a large number of taper sections of ground surfaces.

All tools were made from tungsten carbide, the initial filaments being rough ground to shape and then finished by diamond lapping in specially designed holders. The profile details are:-

a) Pyramidal. These tools are characterised by the angles α° and θ° (Fig. 60). There is a deliberate positive clearance on both the sides and trailing edge, to ensure that tool-test piece contact occurs exclusively on the rake face, thus eliminating any interference effects.

Two sets were used, and are given below together with the resultant groove width to depth ratios (form factor) assuming a maximum depth of penetration of 0.001 in.

SERIES A $\theta = 90^{\circ}$, $\alpha = -75^{\circ}, -60^{\circ}, -40^{\circ}, -20^{\circ}, 0^{\circ}, +15^{\circ}$

FORM FACTOR 7.75, 4, 2.6, 2.13, 2, 2.07

SERIES B $\alpha = -40^{\circ}$ $\theta = 150^{\circ}, 120^{\circ}, 90^{\circ}, 60^{\circ}$

FORM FACTOR 9.7, 4.5, 2.6, 1.5

The rake angles selected are predominantly negative. This is because, although there may be a considerable diversity of

opinion on the basic geometry of asperities, it is generally believed and accepted that the vast majority possess large effective negative rake angles.

b) Spheroidal. These were prepared by lapping the required radius on the apex of a 90° cone. The tool radii and corresponding form factors assuming a maximum penetration of 0.001 in. are:-

TOOL RADIUS, R in x 10^3	2	6	10	20	30	40	50
FORM FACTOR	4	6.3	89	12.6	15.5	17.9	20

4.1.4 TEST MATERIALS

It was decided to carry out the majority of tests on a ductile material and an aluminium alloy, BS HP 15WP, having the following mechanical properties was eventually selected:-

0.1% Proof stress = 60×10^3 lb/in^2

Young's modulus = 10×10^6 lb/in^2

% Elongation = 12.6

The low density of the alloy is an advantage in view of the detrimental effect of the test piece mass upon the resultant natural frequencies of the dynamometer, as discussed earlier. The intricate tools also withstood the impact forces satisfactorily with this material.

Some additional tests were also carried out on cast iron and brass to compare the behaviour of ductile and brittle materials.

In the case of the surface grid deformation tests, specimens were specially prepared from stainless steel EN 58J. This is discussed in detail in Section 4.2.2.

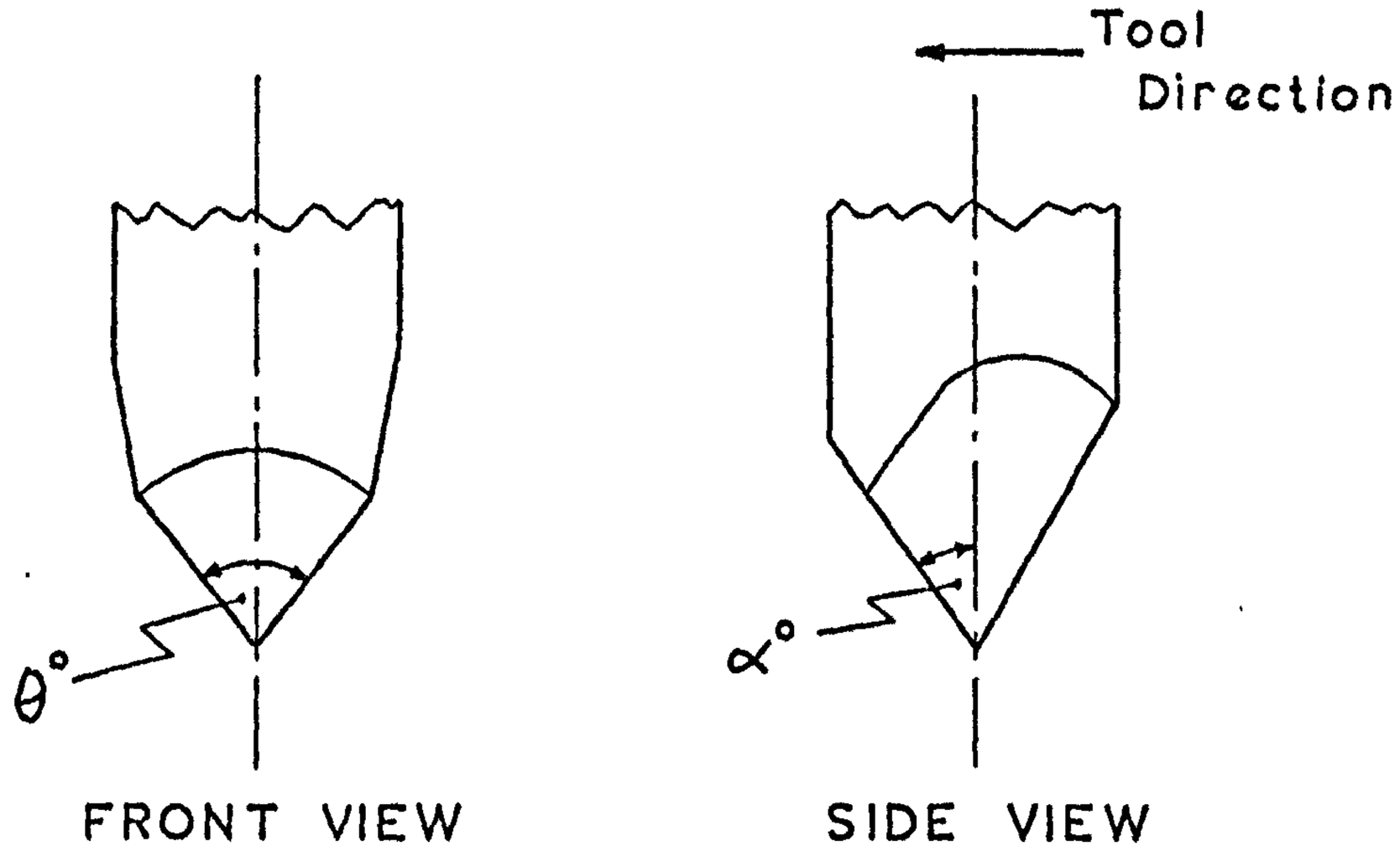

Fig. 60 Pyramidal Tool Geometry

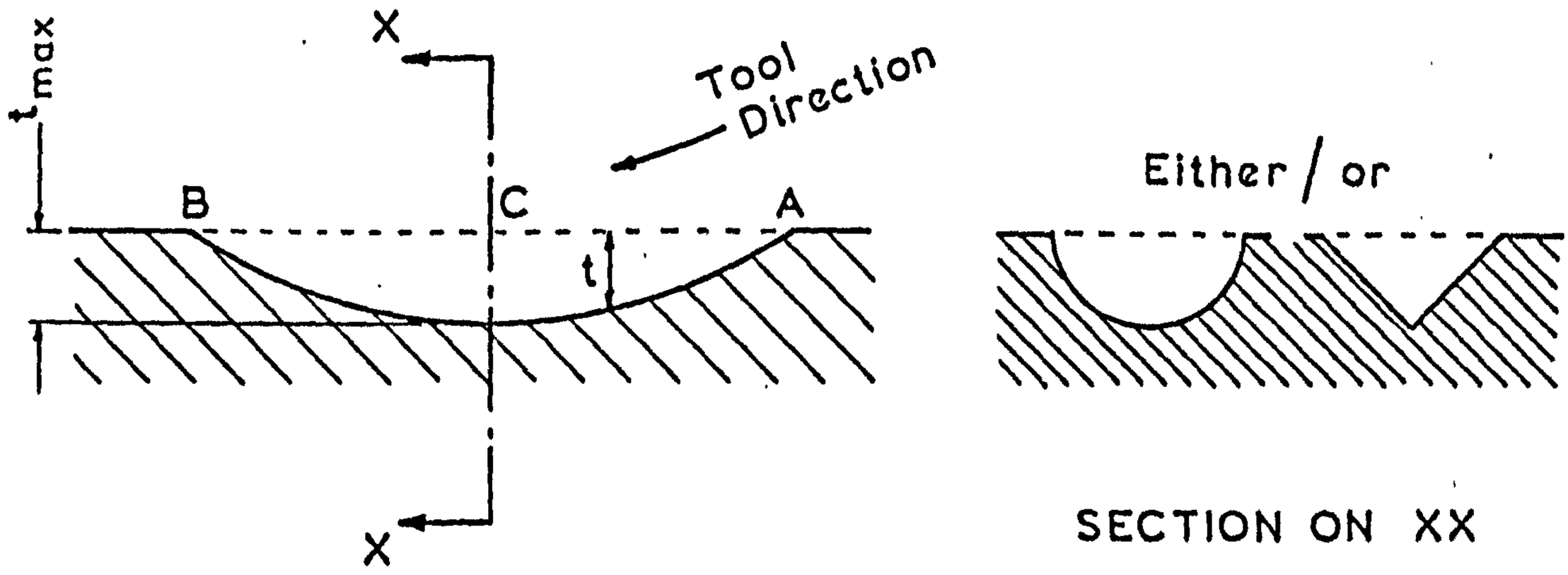

Fig. 61 Groove Geometry

4.2 EXPERIMENTAL PROCEDURE

4.2.1 FORCE MEASUREMENTS

In order to obtain an accurately aligned surface of good texture (< 10 CLA), the test material was ground in situ on the grinding machine table. The abrasive wheel was then removed and replaced by the special tool holder. The maximum tool depth of penetration, t_{max}, was then set as follows. The rotating tool was lowered slowly until the circuit triggered the oscilloscope indicating tool-test piece contact at the point C (Fig. 61). The tool was halted and the desired depth of penetration obtained by lowering the wheelhead assembly, noting the downfeed on a Rank Taylor Hobson Magna-gauge. In this way, t_{max} could be set to $\pm$ 2.5% over the desired operating range.

The impact speed which depended on the initial angular setting was calculated by estimating the time taken for the tool to travel the distance AB (Fig. 61). The oscilloscope was assumed to trigger when the tool first contacted the test piece surface at the point A. The time taken to reach B was then determined from the width of the force traces recorded on the oscilloscope. The calculation which assumes the velocity to be constant along the length of the groove introduces only a small error because of the small arc of contact.

In view of the negligible dynamometer response (Fig. 58) over the desired operating range, a static calibration for the dynamometer was considered acceptable and this was carried out at frequent intervals for a range of sensitivities.

4.2.2 SURFACE GRID DEFORMATION TESTS

The stainless steel test pieces were originally ground and lapped to give a high surface finish coupled with flatness (2 CLA and ± 0.0001 in over 2.5 in.). The specimens were then lapped again using a slightly coarser paste, the relative movement of the lap and specimen being restricted to one direction. This had the effect of producing a fine grid of parallel lines (5 CLA) on the test piece surface. Grooves were then produced normal to these lines, and examined under a microscope.

If metal is displaced by plastic deformation only, it is fair to assume that the grid lines will remain visible on the groove base. On the other hand, microcutting can be expected to erase any trace of the original grid.

4.2.3 GROOVE SIDE SWELL

These measurements were made on the grooves cut in the aluminium alloy, using a standard Talysurf instrument. Profiles were obtained of the groove cross sections in the nominal regions of entry and exit, and at the groove centre.

4.2.4 HIGH SPEED PHOTOGRAPHY

This involved a straightforward observation of the metal removal process along the entire groove length. In order to obtain the required number of frames with the camera and lighting equipment available, the impact speed was limited to 250 ft/min in the case of these tests. With this limitation in mind, provision was made to trigger the wheelhead motor using the camera, thus synchronising the impact with the film speed required.

Details:- Camera - Fastax WF 17 with Weinberger Control Equipment

Film - Ilford FP4

Settings - aperture f2.8, pictures/sec 5,000

4.3 RESULTS AND DISCUSSION

4.3.1 FORCE AND ENERGY CONSIDERATIONS

Fig. 62 b and c show typical impact forces for pyramidal and spheroidal tools (lower trace - tangential force, T; upper trace - normal force, N, i.e. relative to the test material surface)

For comparison, the forces obtained when using an authentic abrasive grit are given (Fig. 62 d, $Al_2 O_3$ grit, mesh size 46). In all cases, both T and N rise sharply on initial contact suggesting the absence of a proliminary rubbing regime. This was later confirmed by observations of the surface grid deformation (Section 4.3.2), and is attributed to the high rigidity of the system employed.

The traces can best be discussed in terms of the important basic parameters which have become well established in practical grinding investigations, i.e., specific energy, etc. (Section 2.3.1)

(i) EVALUATION OF THE SPECIFIC ENERGY, S.E.

The S.E. is generally defined as

$$\text{S.E.} = \frac{\text{Work done in removing material}}{\text{Volume of material removed}}$$

In the present investigation however, the S.E. at any stage of the impact can be determined by applying the relationship

$$\text{S.E.} = T_i/A$$

where T_i = instantaneous tangential force

A = corresponding groove cross-sectional area.

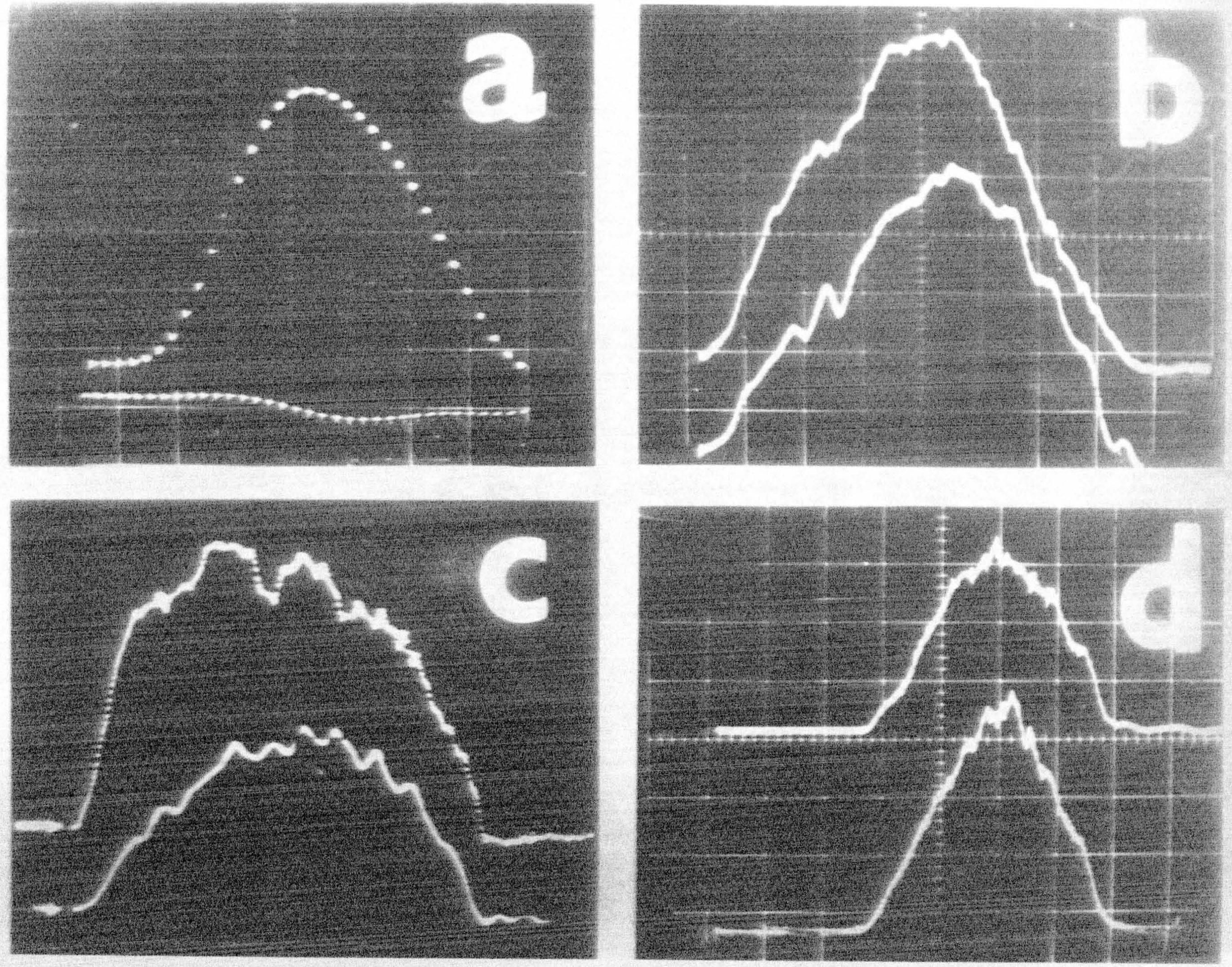

Fig. 62 Force Measurements

In the discussions which follow, however, the S.E. is based essentially on the values relating to the maximum tangential force and the maximum groove cross-sectional area, both of which occur nominally at the mid-position. It should be noted that in situations where severe ploughing and large transverse deformations occur, A will not in fact represent the amount of metal "removed". Nevertheless, the definition provides a realistic parameter for determining the energies associated with the different modes of metal deformation.

(ii) EFFECT OF TOOL GEOMETRY ON THE SPECIFIC ENERGY

Fig. 63 a shows the variation in S.E. with rake angle, α, for pyramidal tools. The impact speed in this case is 750 ft/min. The S.E. is seen to increase as α becomes more negative. This can be explained by increases in both the extent of the plastic shear deformation and the frictional force at the tool - test piece interface.

An interesting result occurs in the case of the ductile aluminium alloy, where a sharp increase in energy, in the region of $\alpha = -55^{\circ}$, suggests a transition in the mode of metal deformation. This value of α compares favourably with the figure of -60° suggested by Rubenstein[36] for a transition from microcutting to plastic deformation (SAE 1020 Steel). In addition, the apparent absence of any similar effect with cast iron and brass substantiates his conclusion the α_{crit} is greater for brittle materials, since in the present tests α_{crit} must be greater than -75°.

A similar change in S.E. is observed in the case of aluminium alloy when spheroidal tools are used (Fig. 63 b), and again a transition is evident in the region of R = 0.02 in. The groove

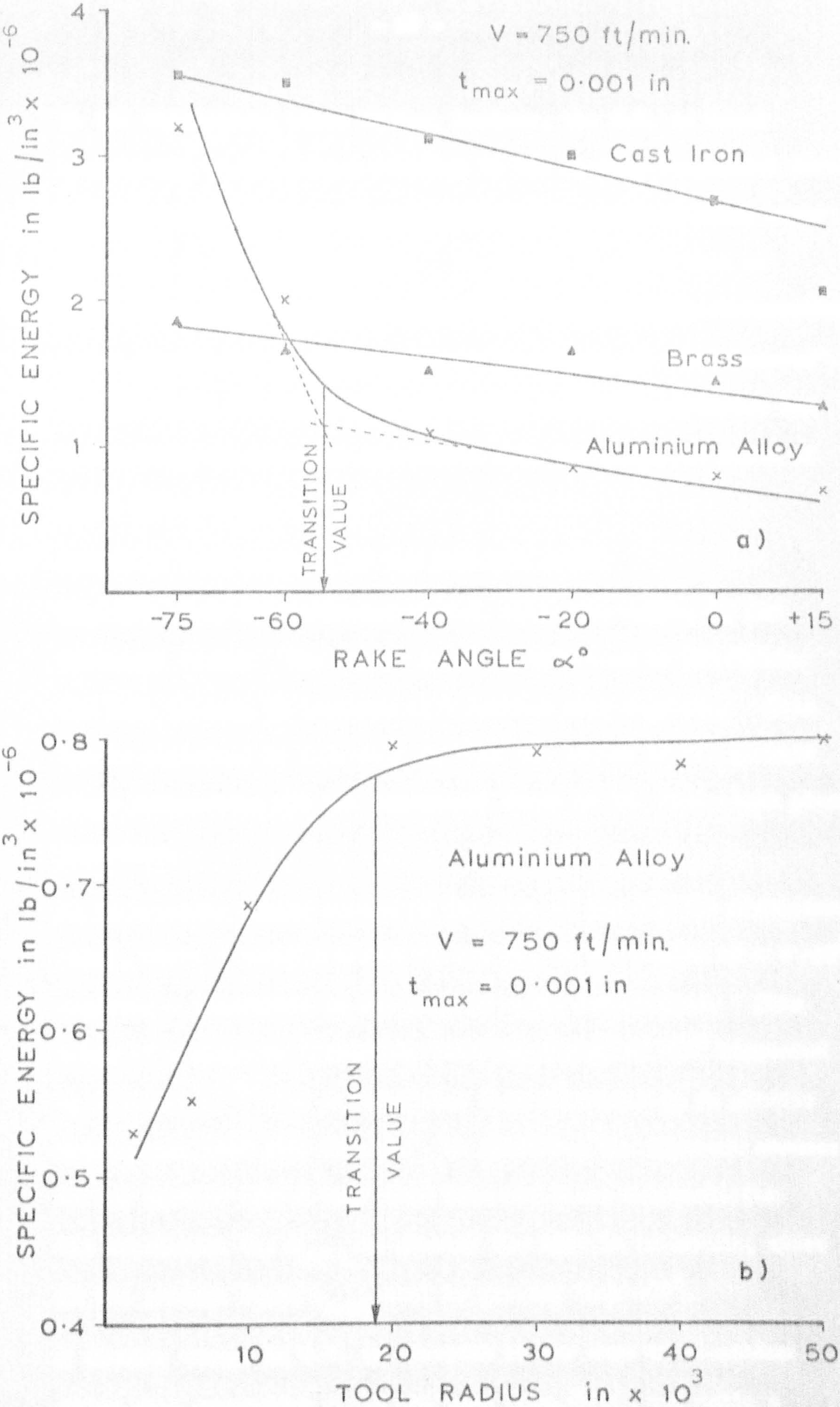

Fig. 63 Effect of Tool Geometry on the S.E. (Showing Transition Points)

width to depth ratio or form factor is considered to be the significant factor in this case, high values being associated with metal ploughing and increased energy consumption. If the effective rake angle of a spheroidal tool is defined as $-\tan^{-1}(\frac{w}{2t_{max}})$ where w is the groove width, the transition is seen to occur in the region of -75°.

(iii) EFFECT OF TOOL GEOMETRY ON THE $^{T}/_{N}$ RATIO

For pyramidal tools the $^{T}/_{N}$ ratio is seen to decrease as the rake angle becomes more negative (Fig. 64). Similarly with spheroidal tools, the $^{T}/_{N}$ ratio decreases with an increase in radius. This confirms the opinion that predominantly ploughing mechanisms associated with high negative values of α and large radii (high form factors) are characterised by low $^{T}/_{N}$ ratios.

In metal removal operations, e.g., turning, the $^{T}/_{N}$ ratio generally falls within the range 1.5 to 2.0. In comparison, the range of values encountered in grinding is considerably lower:- 0.5 to 0.75. If it is assumed that a grinding wheel consists of pyramidal tools only, from the evidence presented in Fig. 64, values of mean rake angle in the range -60° to -45° could be expected. This is at variance with earlier estimates (e.g., $\alpha = -30^{\circ}$ ref. 28). Alternatively, if the wheel is assumed to consist only of spheroidal grits, the mean effective rake angle could be expected to fall within the limits -45° to -75°. The close proximity of these values to the transition values described earlier and shown in Fig. 63, suggests that although metal grinding is essentially a complex combination of rubbing, plastic displacement, and microcutting under slightly unfavourable

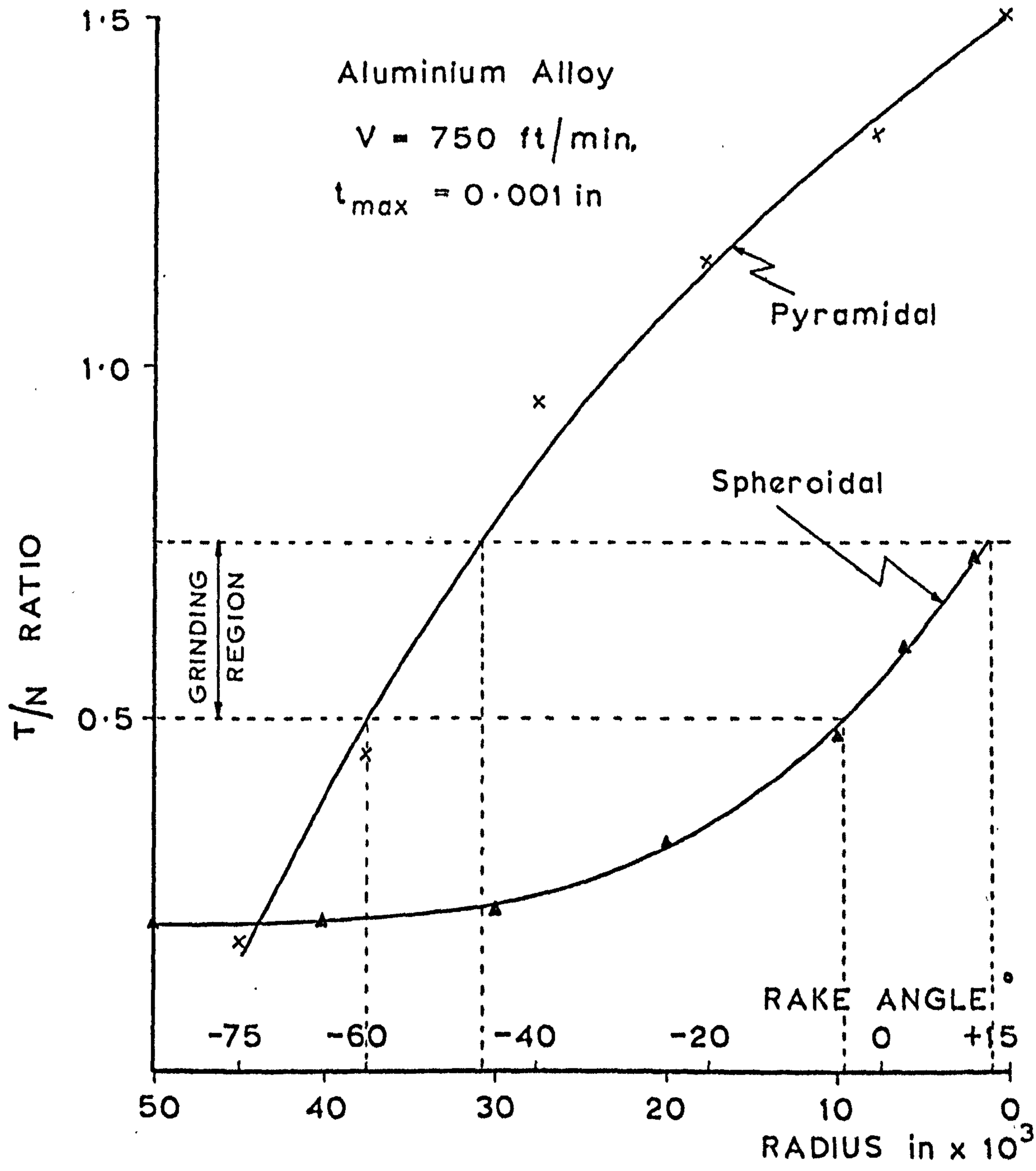

Fig. 64 Effect of Tool Geometry on the $^{T}/_{N}$ ratio

conditions, in the case of ductile materials, ploughing could easily predominate, resulting in poor grindability.

(iv) EFFECT OF IMPACT SPEED ON THE $^{T}/_{N}$ RATIO

The $^{T}/_{N}$ ratio is seen to increase significantly with increasing speed for the pyramidal tool, but to decrease slightly in the case of spheroidal tools (Fig. 66). To explain this anomaly it is necessary to consider the apparent coefficient of friction, μ, at the tool-test piece interface as given by Merchant's expression[34]

$$\mu = \frac{N + T \tan \alpha}{T - N \tan \alpha}$$

From the above expression it can be shown that for small negative values of α, μ is approximately equal to $^{N}/_{T}$. Similarly, for extremely high negative values of α (characteristic of spheroidal tools) the value of μ becomes more a function of $^{T}/_{N}$. Hence both trends are indicative of a reduction in the apparent coefficient of friction with speed.

(v) EFFECT OF IMPACT SPEED ON THE SPECIFIC ENERGY

An increase in impact speed results in a considerable decrease in S.E. values (Figs. 65a and b). This can be attributed mainly to the reduction in friction at the tool-test piece interface as shown already in (iv). The reduction in energy can also be explained by a decrease in the extent of the plastic deformation with speed (as discussed in the following Section 4.3.3), and the possible occurrence of thermal softening effects.

Although the present results terminate in the region of conventional grinding speeds, the trends exhibited suggest that

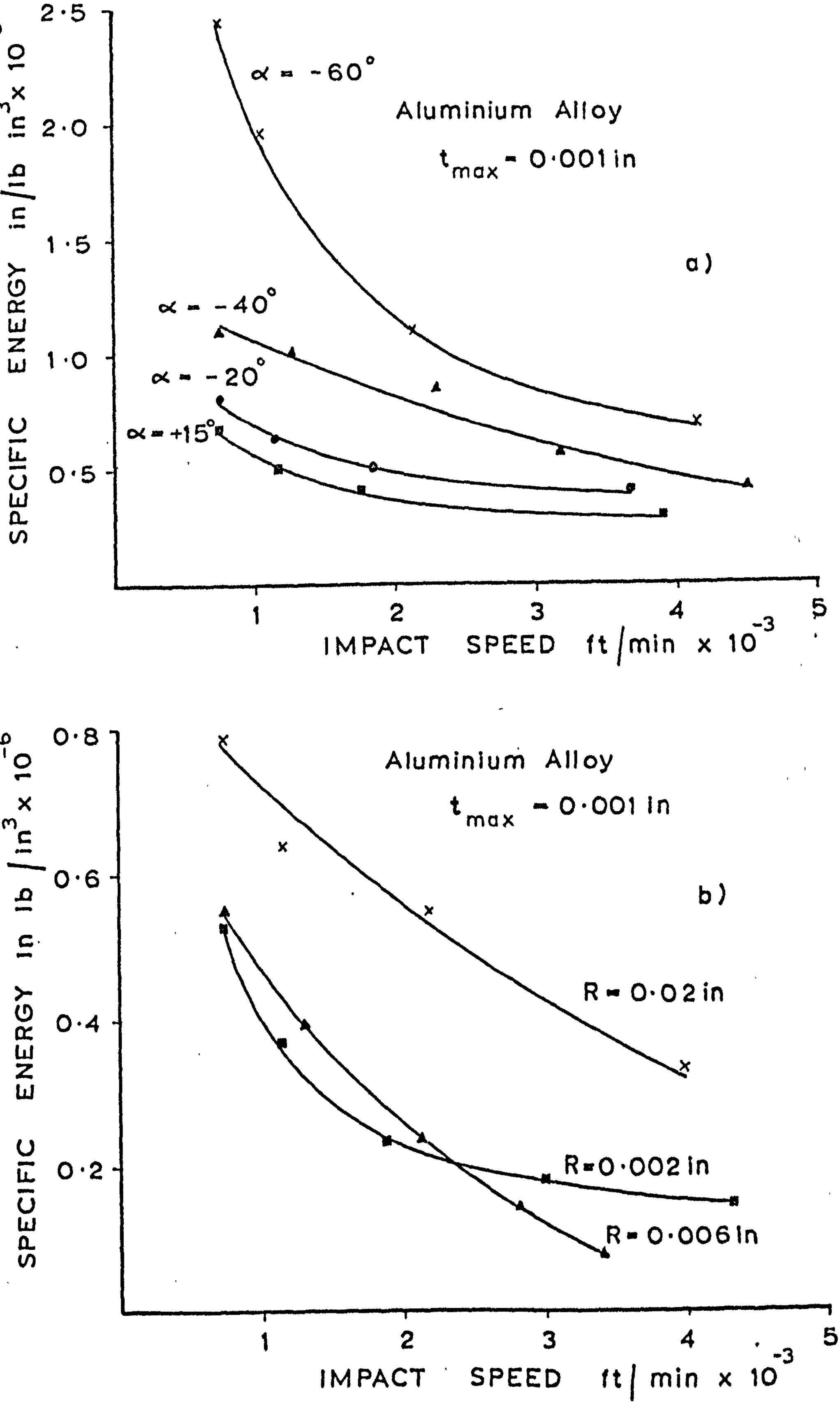

Fig. 65 Effect on Impact Speed on the S.E.

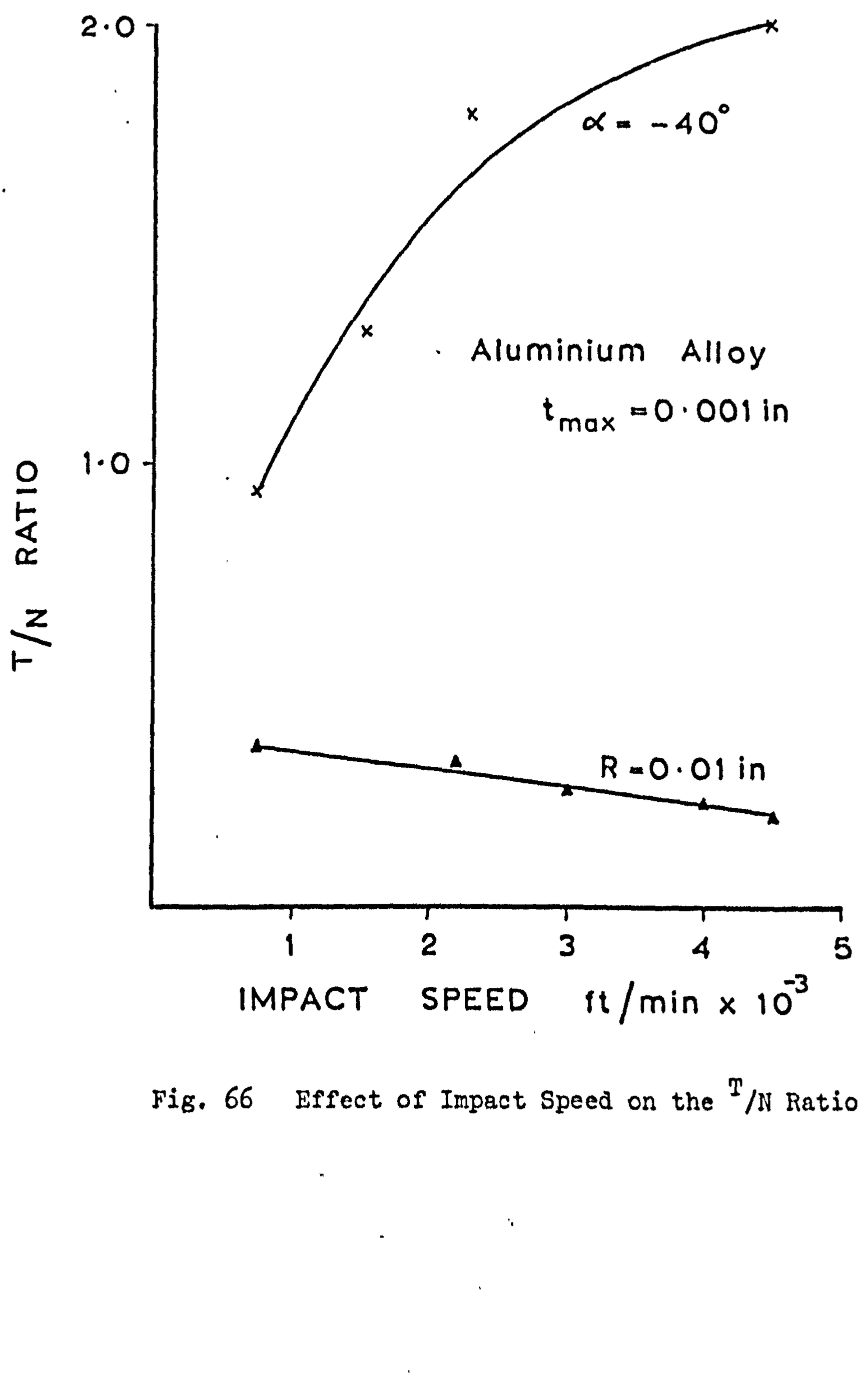

Fig. 66 Effect of Impact Speed on the $^{T}/_{N}$ Ratio

further reductions in S.E. are possible at higher speeds, thus highlighting one of the possible advantages of grinding at higher speeds.

The considerable variation in S.E. over the speed range investigated also suggests that considerable care should be exercised when relating the results of slow speed simulation tests[32,35,37] to actual metal grinding operations.

(vi) THE SIZE EFFECT

Fig. 67a shows the change in S.E. with maximum groove cross-sectional area, A, as a result of a variation in the tool depth of penetration. For both pyramidal and spheroidal tools, the S.E. is seen to increase with a reduction in A giving evidence of the so-called size effect[12,29]. Previous investigations[12] have tended to concentrate on rectangular tools where A is a linear function of the penetration depth. The size effect has then been expressed as a function of depth. In the present tests however, A is a non linear function of depth and the S.E. must therefore be considered in terms of A. The importance of this is illustrated by the results from tests carried out with the 'B' series of tools. Here the tool penetration depth remained constant, and the area changed by virtue of the different values of Q influencing the groove widths. As can be seen from Fig. 67b, a size effect is still evident.

The size effect in grinding was first discussed by Backer et al[12]. They proposed that the reduction in strength of a metal below a certain theoretical value, based on atomic considerations, was due to the presence in the material of inhomogeneities,

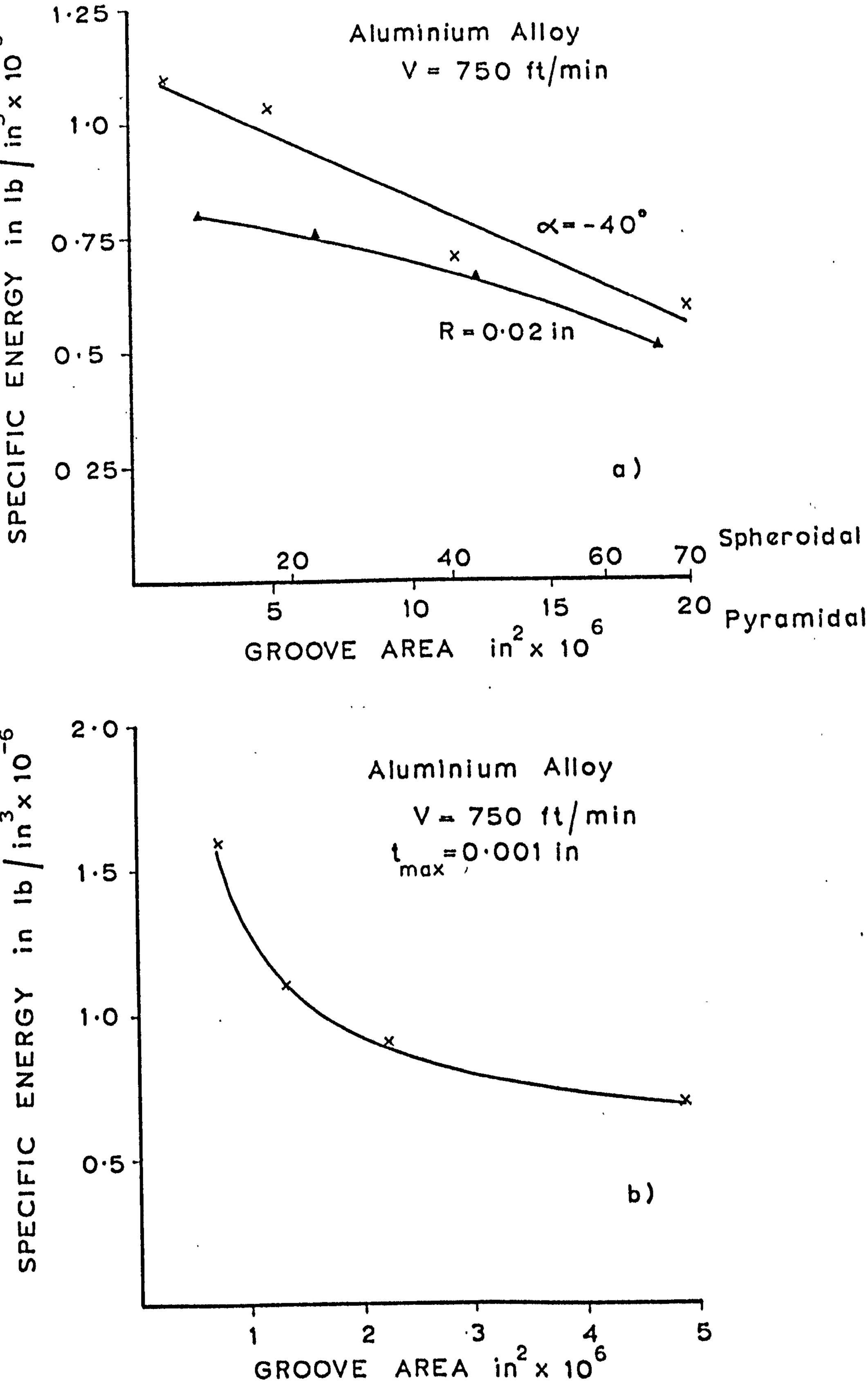

Fig. 67 Evidence of the Size Effect

e.g., grain boundaries, crystal defects, impurities, etc. Thus as the grit penetration decreases, the probability of a chip being formed between these defects increases, and the strength of the metal tends towards its theoretical value. By considering grinding, micromilling and turning, the variation in shear energy was seen to extend to relatively large values of chip thickness (Fig. 68). That the above hypothesis should explain the variation in energy for larger depths of tool penetration (0.01 in) is not entirely convincing, especially when the mean spacing of the inhomogeneities is quoted as lying in the range 4 to 40 μin.

In the tests described here, the above argument based on material imperfections could be applied in view of the small scale of the deformations involved. There is however, another important aspect associated with the decrease in grit penetration during a grinding operation. In general, such a decrease would result in an increase in the groove width to depth ratio which, as indicated earlier, would generally lead to an increase in the relative amount of plastic deformation, and hence the energy consumed. Further reductions in the penetration would tend to produce extensive rubbing with a further significant increase in the S.E. Within the scope of the present investigation it would not be possible to attempt to obtain the relative magnitudes of these effects.

(vii) FORCE AND ENERGY CONSIDERATIONS ALONG THE GROOVE

The previous energy measurements were all obtained at the groove mid-point. By comparing values for the different tool

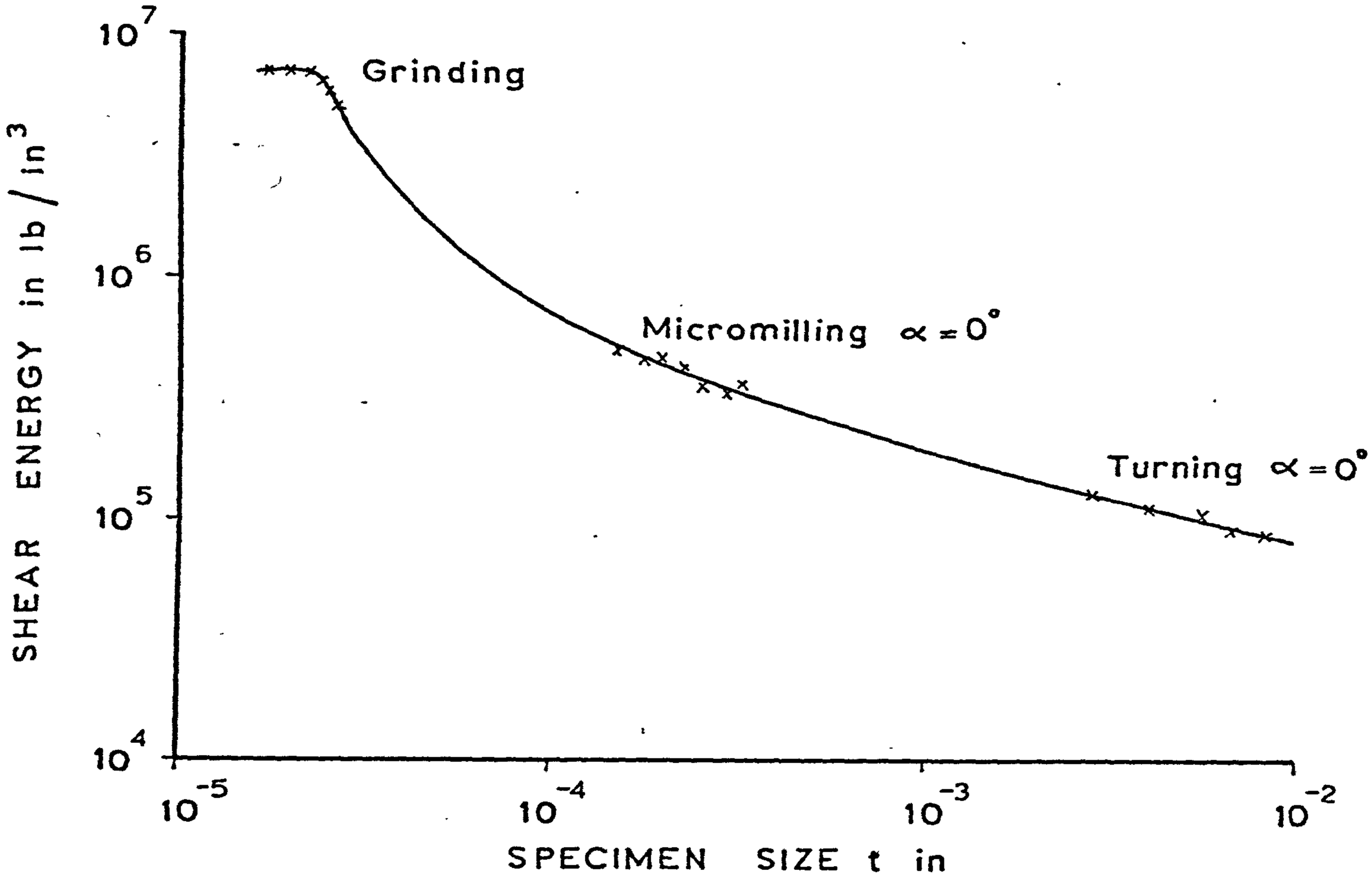

Fig. 68 Variation of Shear Energy with Specimen Size (After Backer et al[12])

geometries, a transition in the mode of metal deformation as α becomes increasingly negative has been indicated. In order to discover whether a transition is also evident along the groove, i.e., as the depth of penetration increases, values of the instantaneous tangential and normal forces were plotted for a number of positions along the groove.

Typical results for both the pyramidal and spheroidal tools are given in Fig. 69 and 70 respectively. As can be seen, the general trend of the curves is the same. This is to be expected, for although tool geometry may influence the shape of the curves, fundamental changes are unlikely. The tangential force follows the law $T = Ct^n$ where t is the penetration depth and C and n are constants. For all tests, the value of n was found to be in the range $1 < n < 1.3$. This range is similar to that quoted by previous workers (as reported in ref. 65) when investigating coarse grinding operations.

The energy curves show a decrease in S.E. as the penetration increases, giving further evidence of the previously discussed size effects. Contrary to what might be expected[38,39,40], the curves do not indicate a sudden transition in the mode of metal deformation along the groove. However, since there is already a decrease in energy with penetration due to the size effect, the S.E. curve may not be the most suitable criterion for indicating the presence of a transition point. For this reason, a closer examination of the force traces was undertaken.

It is suggested that in the case of spheroidal tools, the first significant dip in the tangential force and the corresponding

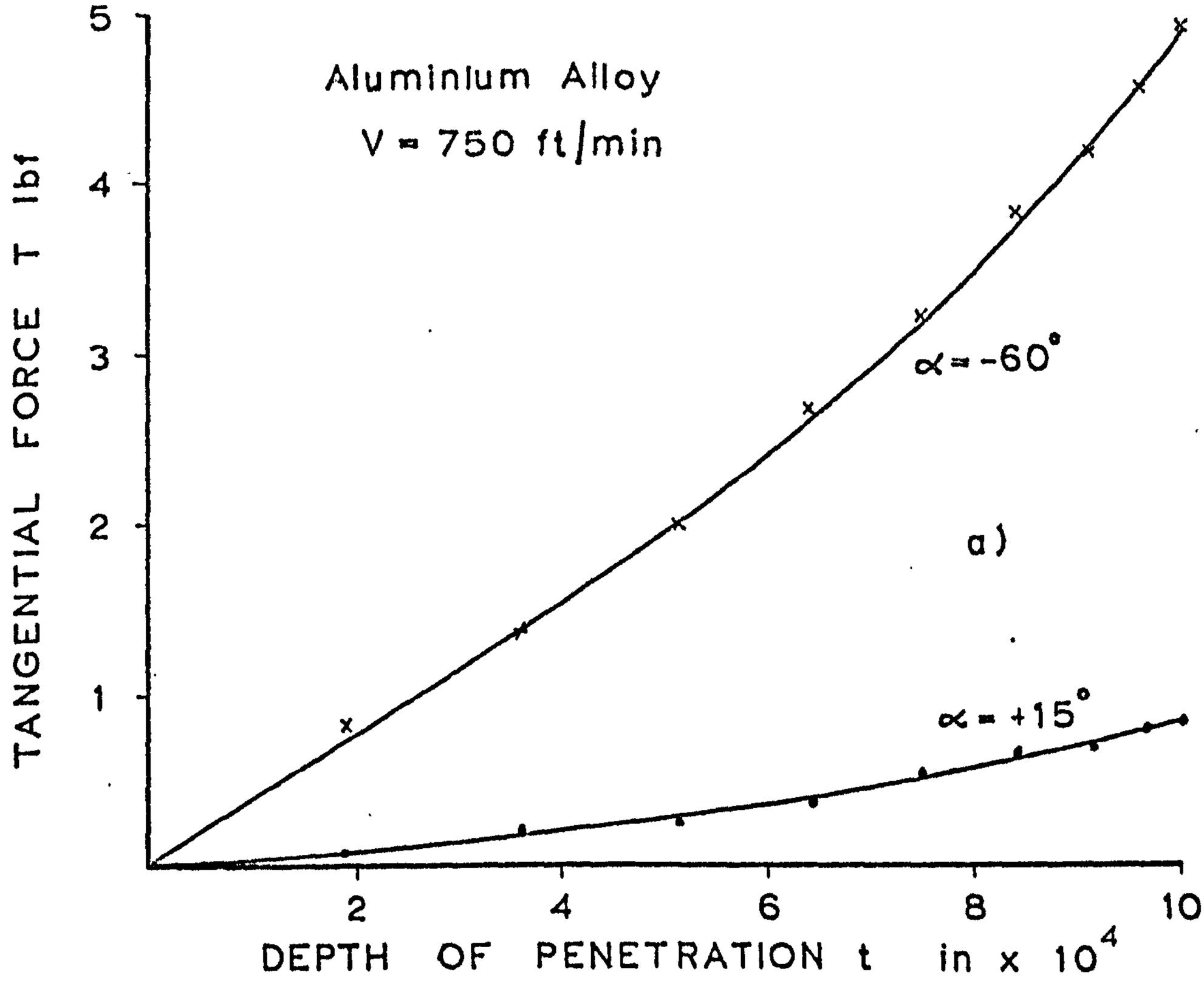

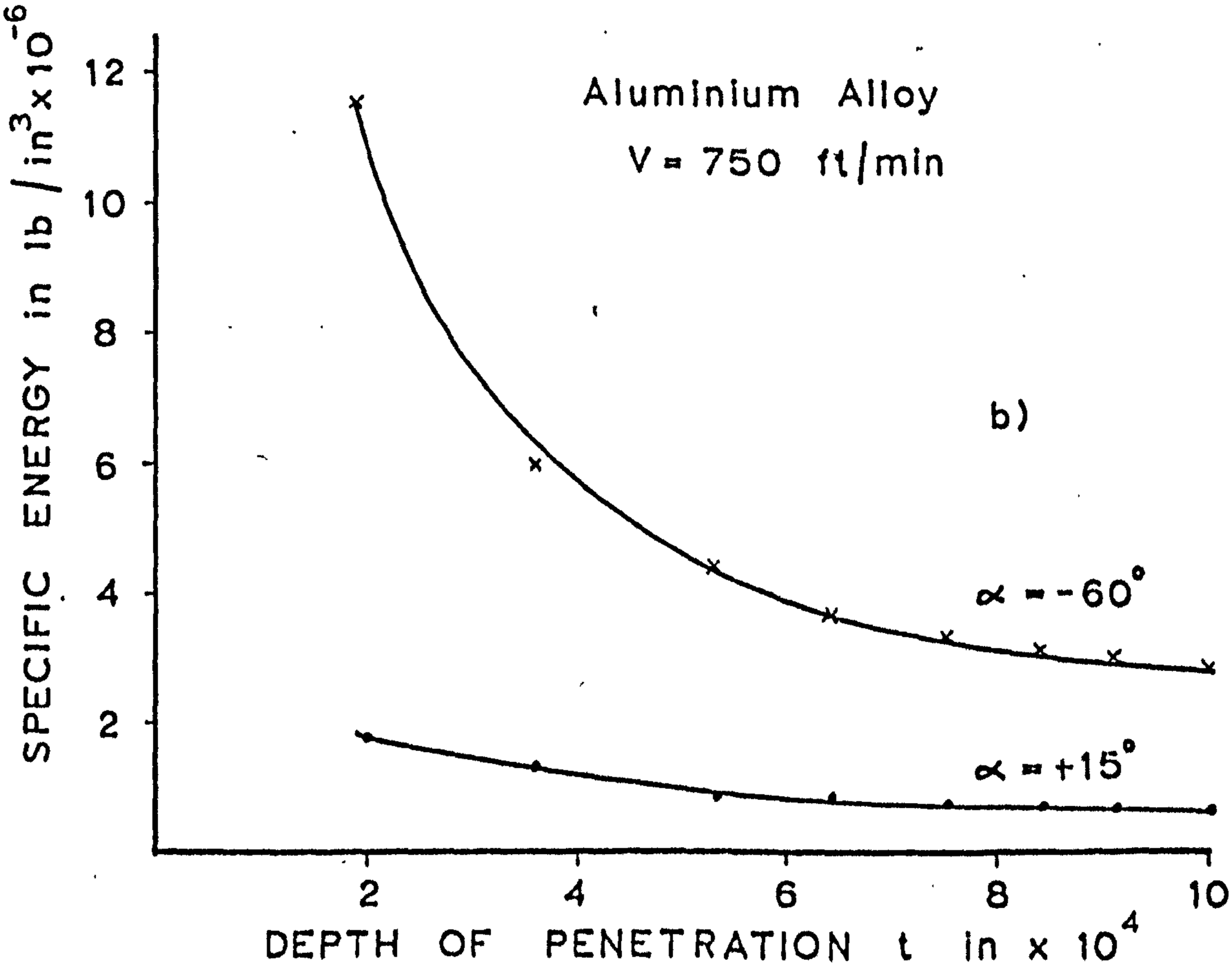

Fig. 69 The Tangential Force and the S.E. along the Groove (Pyramidal)

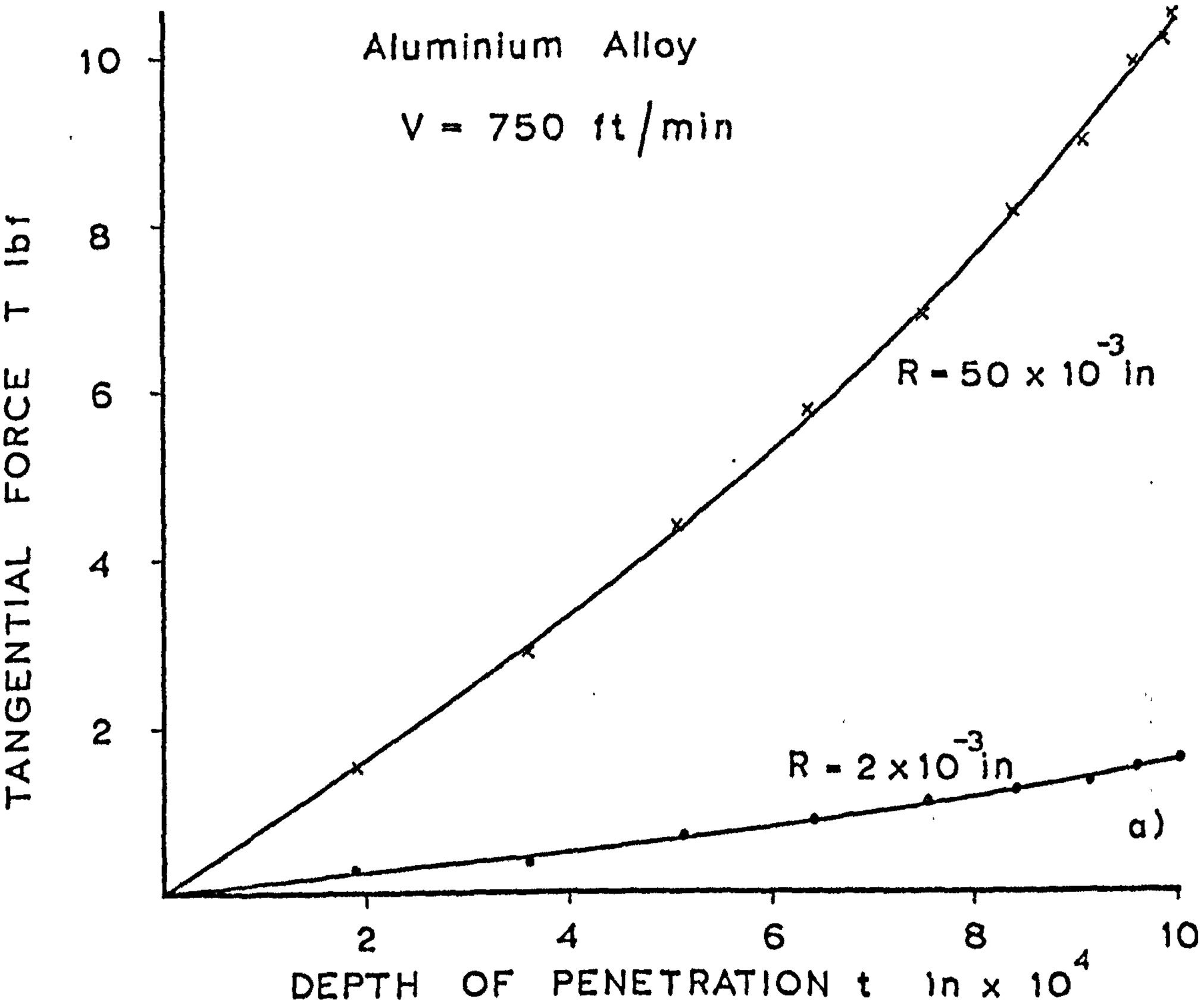

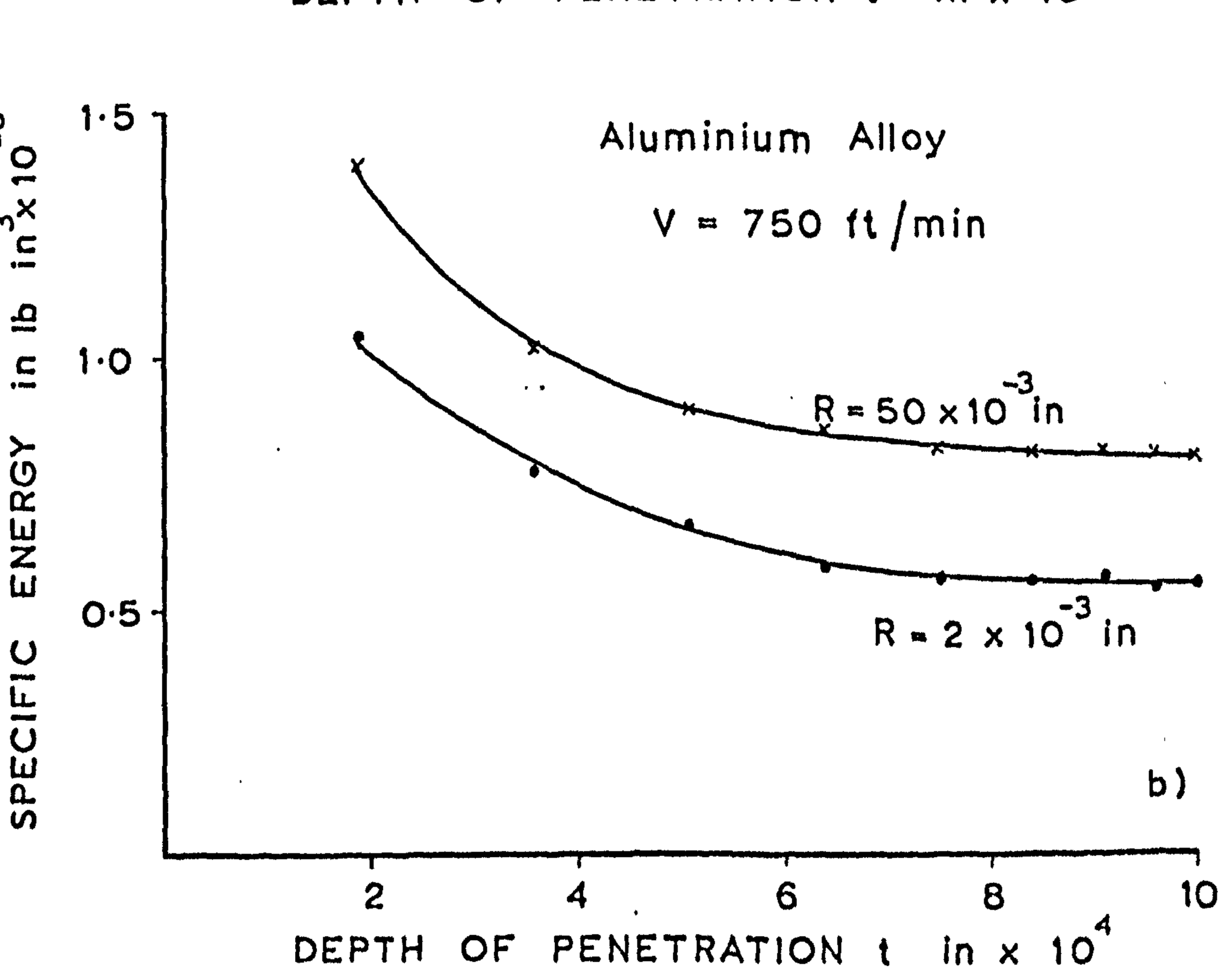

Fig. 70 The Tangential Force and the S.E. along the Groove (Spheroidal)

change in gradient of the normal force (Fig. 62c) indicate a possible change in the mode of metal deformation. The position can be determined with reasonable accuracy by plotting the $^{T}/_{N}$ ratio as a function of t as shown in Fig. 71 for R = 0.006 in. This gives a critical penetration depth, t_c, = 2×10^{-4} in. The force discontinuity was seen to move to the right of the traces with increasing radius until virtually smooth traces were obtained for R = 0.04 in. If the transition is assumed to be from plastic deformation to microcutting, the increase in t_c with radius agrees in principle with the slow speed results reported by Kragelskii[26]. In a similar manner, t_c was seen to decrease with an increase in impact speed confirming the results of the grinding experiments undertaken by Tanaka[38].

The above transition along the groove was not observed with pyramidal tools and indeed the value of $^{T}/_{N}$ was seen to be constant, Fig. 71. The explanation for this can possibly be found by examining the basic difference between the two tool geometries. For pyramidal tools, except for a small change in angle caused by the circular tool path, the rake angle is constant along the entire groove length. With spheroidal tools, however, the effective rake angle is a function of the penetration depth. In the case of the tool relating to Fig. 71, the rake varies from a theoretical -90° at entry to a value of approximately -70° at the mid-position, and as shown earlier this could be expected to lead to the observed increase in the $^{T}/_{N}$ ratio as the penetration increases.

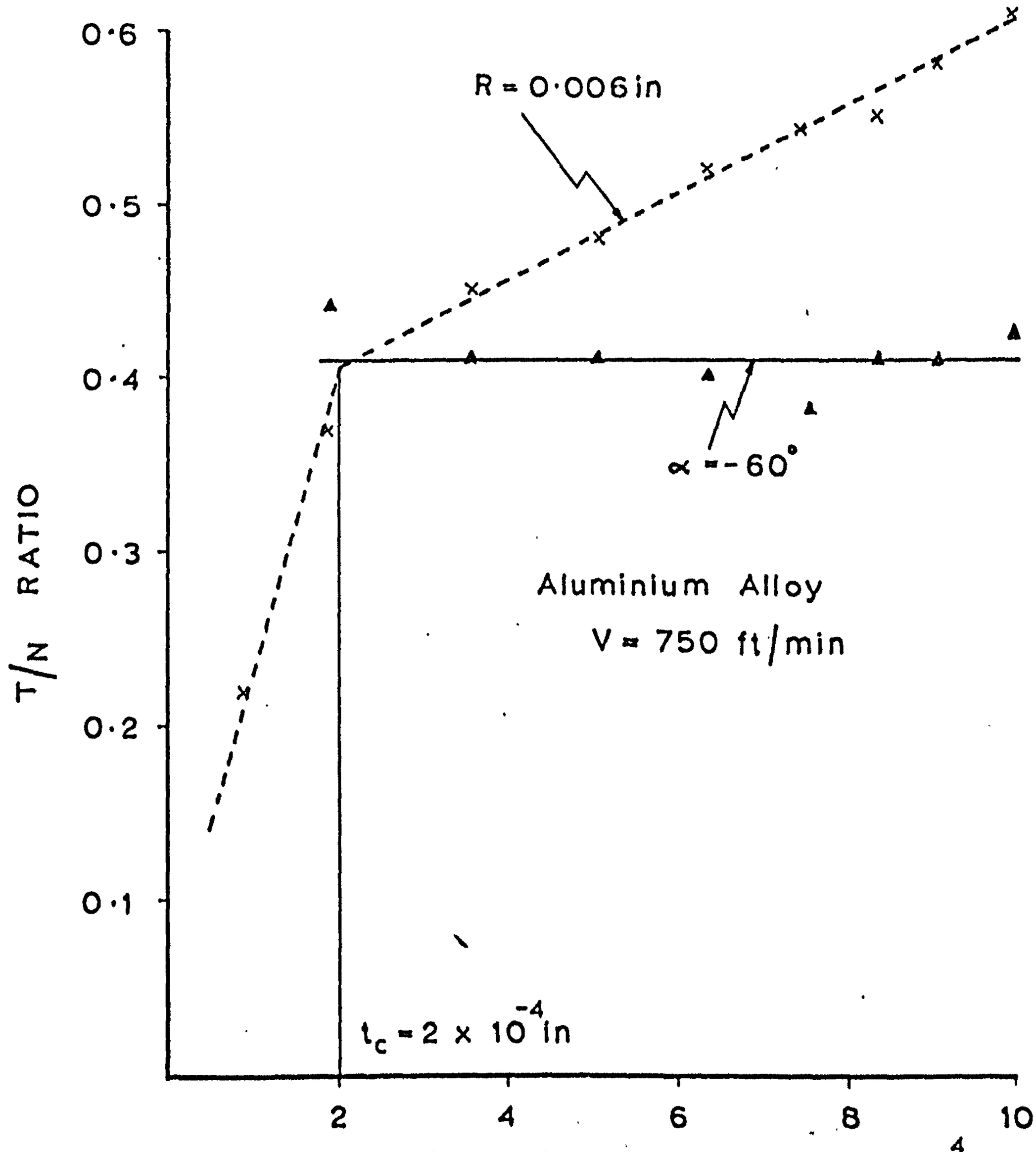

Fig. 71 Determination of the Critical Transition Depth
(force measurements)

To investigate further the suggested transition along the groove exhibited by spheroidal tools, the results of three further experiments are now discussed.

4.3.2 SURFACE GRID DEFORMATION TESTS

Typical results for the ploughing and microcutting regimes are shown in Fig. 72 a and b respectively. The striations are clearly seen on the groove base when the tool is ploughing, whereas lines are visible only in the cutting direction when microcutting occurs. By estimating under a microscope the distance along the groove at which the transition occurs, a value of the critical penetration depth, t_c, was obtained. Fig. 73 shows the plot of $^{t}c/t_{max}$ against tool radius for tests with t_{max} = 0.001 in. For $R \geqslant 0.03$, $^{t}c/t_{max}$ takes the value of unity as grid lines were in evidence as far as the groove centre. Since it is unlikely that cutting would occur as the tool emerges from the test piece, in these cases $^{t}c/t_{max}$ indicates total ploughing. The value of $^{t}c/t_{max} = 0.2$, i.e., $t_c = 2 \times 10^{-4}$ in for R = 0.006 in. compares very favourably with the result of Section 4.3.1 (vii) based on the analysis of the tangential impact force.

Fig. 72 c shows the tendency for metal immediately adjacent to the groove to be drawn in the direction of the tool, indicating the considerable extent of the plastic deformation. It is also interesting to note that grid lines are sometimes visible on the groove walls but not on the base. This would suggest that some form of transition with depth may also be operating in the transverse direction.

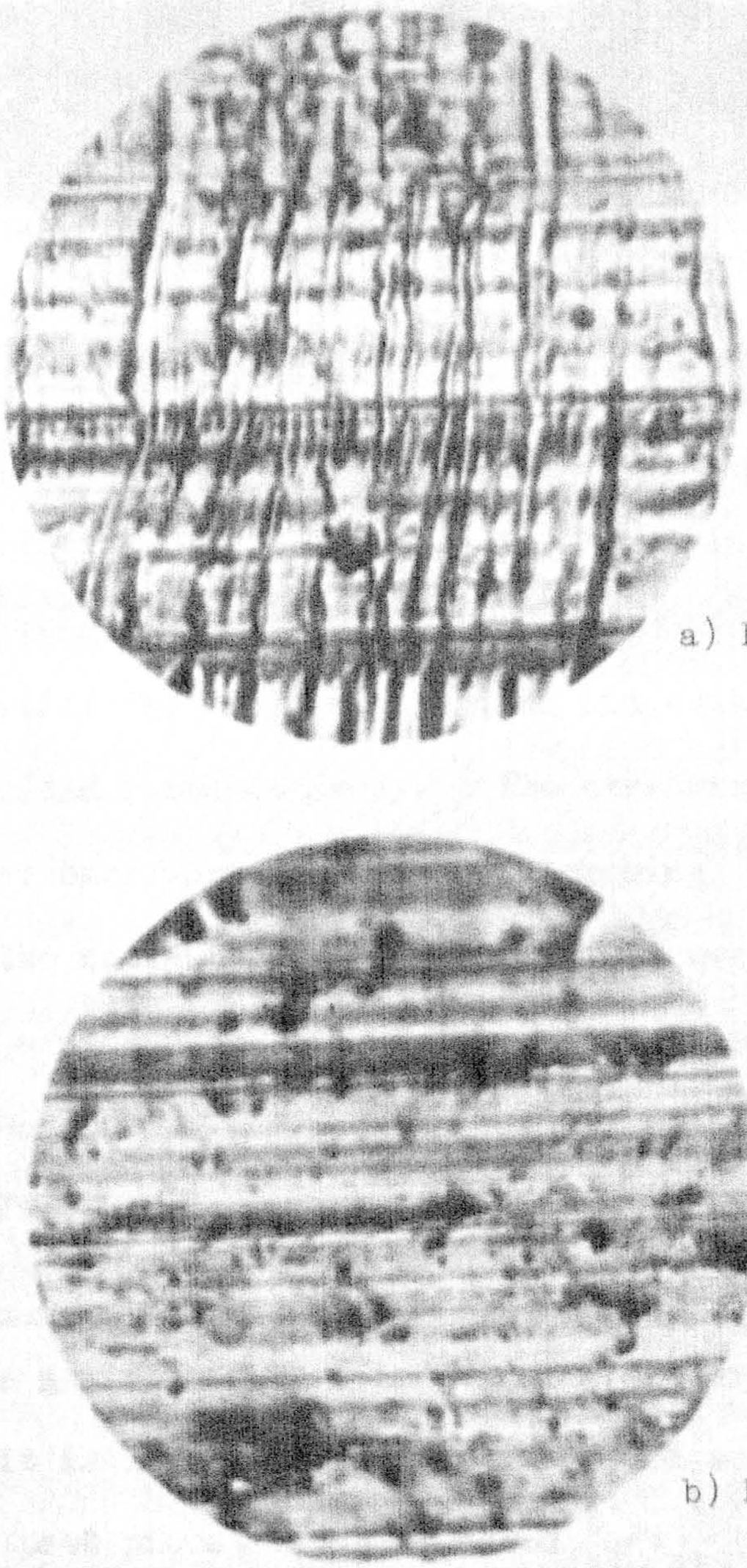

a) Ploughing Regime

b) Microcutting Regime

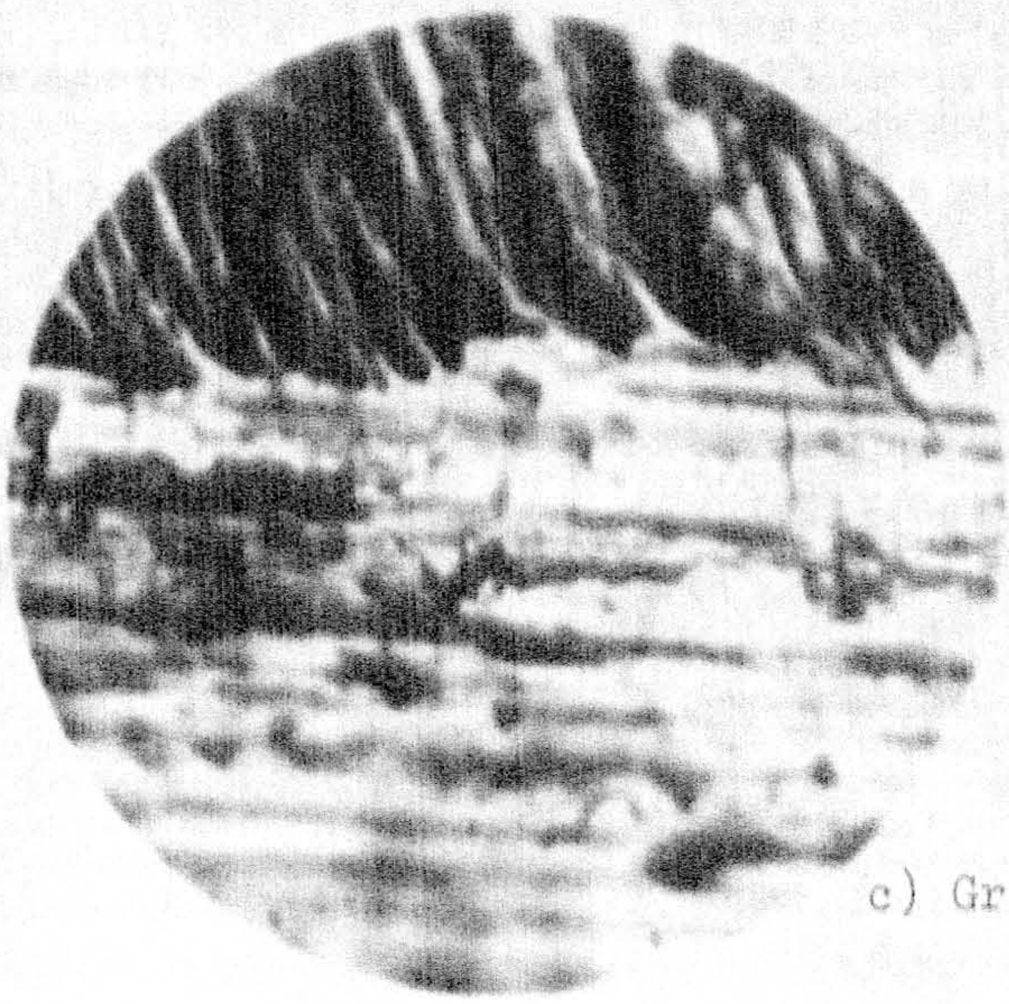

c) Groove Edge

Fig. 72 Surface Grid Deformation Tests

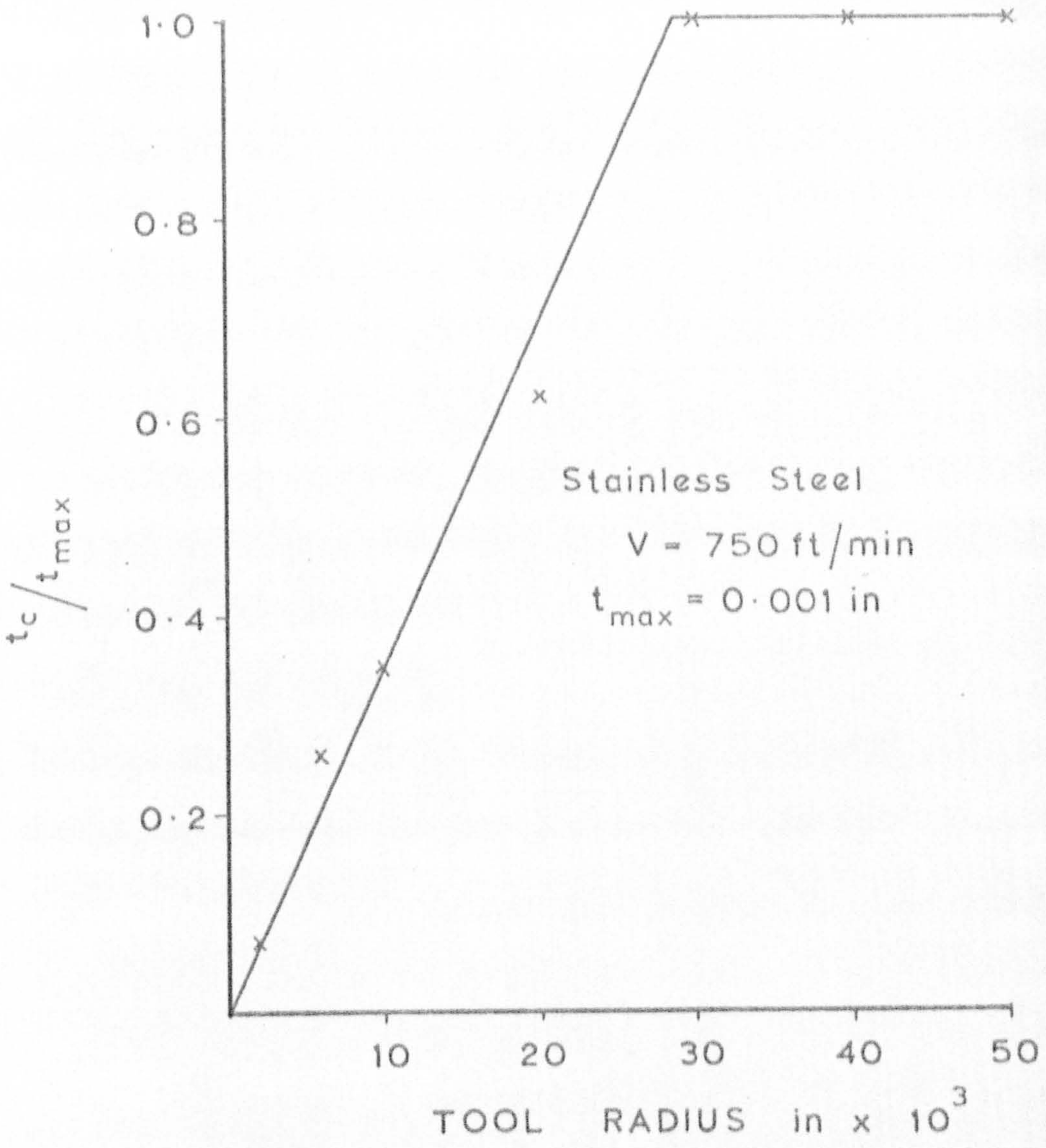

Fig. 73 Determination of the Critical Transition Depth
(grid deformation tests)

4.3.3 ANALYSIS OF SIDE SWELL

The ratio of the area of side swell to the total groove area (A_p/A_g) is given for different positions along the groove and for varying values of R (Fig. 74 a). For R $\leqslant$ 0.02 in. the amount of transverse deformation is seen to first increase and then decrease as microcutting occurs. For R $>$ 0.02 in. however, A_p/A_g increases along the full length of the groove but at an increasing rate in the exit section. This would suggest an overall transition in the mode of metal deformation in the region of R = 0.02 in. For the smaller radiused tools a transition also occurs at some point along the groove as indicated by the rise and fall of the A_p/A_g curve.

The magnitude of A_p/A_g also decreases with an increase in the impact speed (Fig. 74 b) suggesting a reduction in plastic deformation with speed. This would confirm the earlier assumption concerning the reduction in S.E. with speed.

NOTE: Values of A_p/A_g above 100% could be caused by metal being dragged along the groove. Alternatively, the estimate of A_p may be in error as a result of the side swell being "overlapped" as opposed to a solid displacement.

4.3.4 HIGH SPEED PHOTOGRAPHY

The results obtained with the high speed camera are shown in Fig. 75. To assist the interpretation of the photographs, a schematic representation of the interaction is given in Fig. 76. The results can be summarised as follows:-

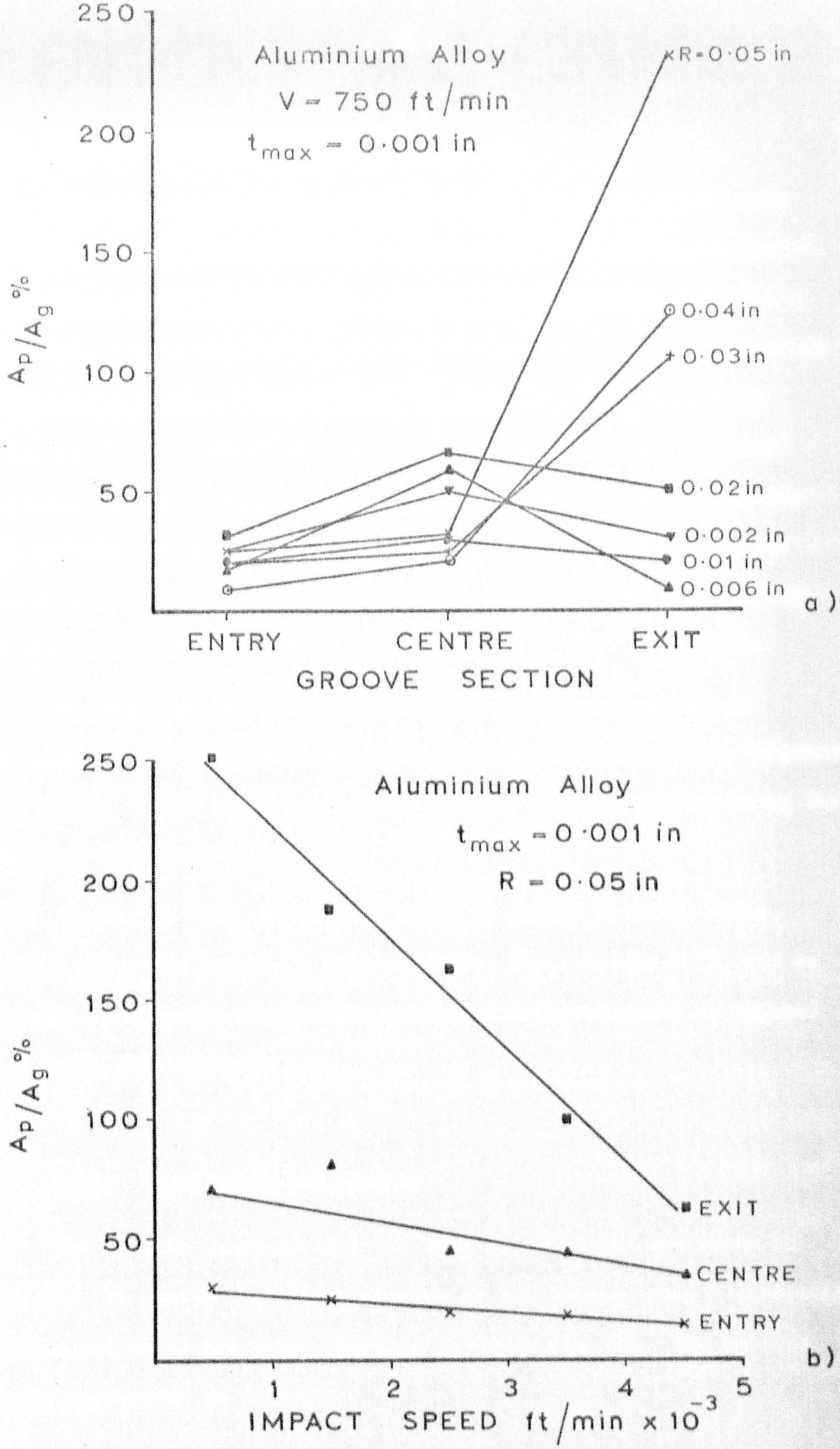

Fig. 74 Analysis of Groove Side Swell

(i) PYRAMIDAL TOOLS

Fig. 75 a $\alpha = +15^{\circ}$ Continuous chip formation

Fig. 75 b $\alpha = -40^{\circ}$ Again a continuous chip is formed with an expected reduction in chip length ratio. This value of α has been postulated by several workers to be within the region of plastic deformation. Although microcutting has also been observed, this has often been attributed to the formation of a prow in front of the tool effectively producing a positive rake. In this case, it is not clear why a prow should necessarily induce a positive rake, and why it should also adhere to the tool when the latter starts to emerge from the test piece.

Fig. 75 c $\alpha = -60^{\circ}$ Microcutting is not evident. The suggested transition of $\alpha = -55^{\circ}$ has been exceeded and the metal deformation is essentially plastic.

(ii) SPHEROIDAL TOOLS

Fig. 75 d R = 0.006 in. The previous sections have provided fairly conclusive evidence that with this tool a transition in the mode of metal deformation will occur at some point along the groove path. This photograph shows the initial entry into the test piece surface and the subsequent build up of material.

Fig. 75 e R = 0.006 in. The pile up in front of the tool has steadily increased until fracture occurs, and a piece of metal is seen to break away from the test material surface. The subsequent mode of metal deformation is not obvious from the photographs. Although a transition has occurred, the continued formation of a conventional chip is not evident. It can be concluded, however, that the conditions of the interaction were

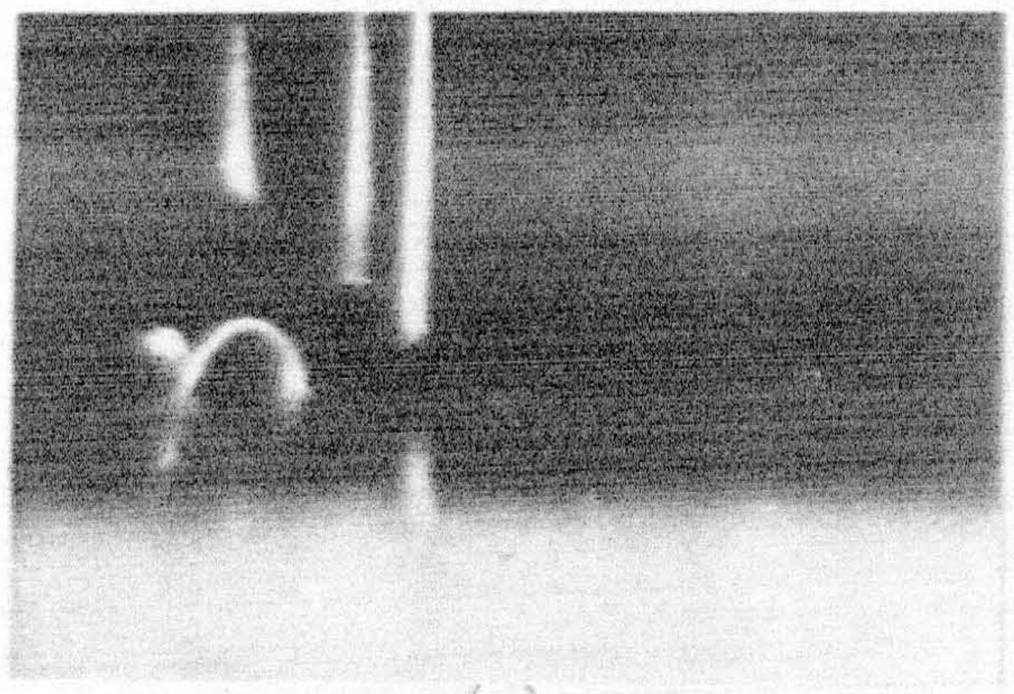

(a)

(b)

(c)

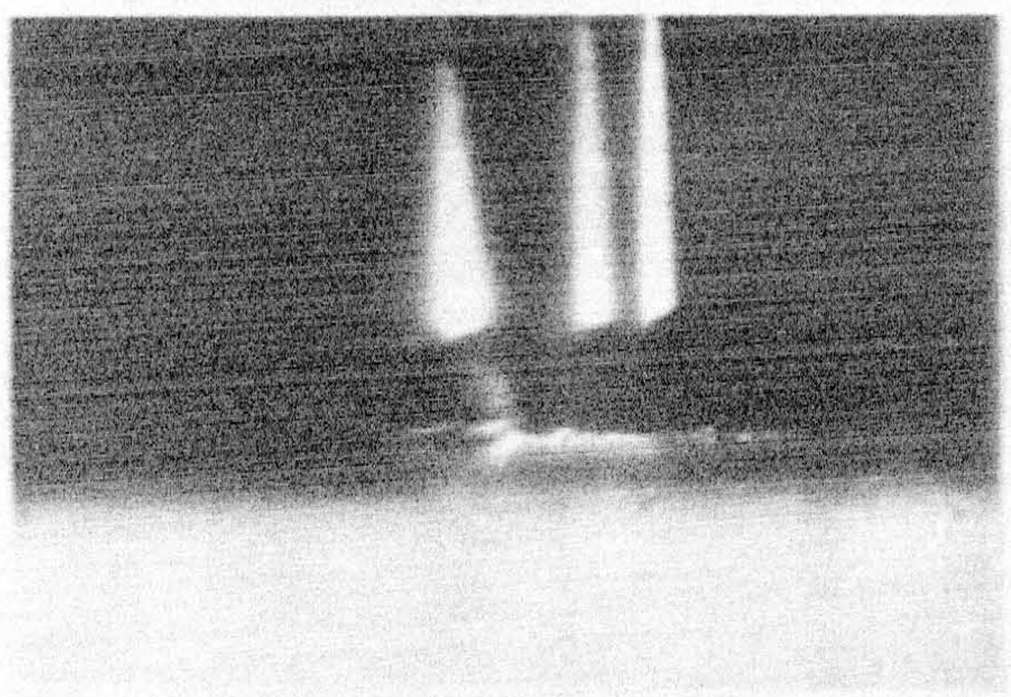

(d)

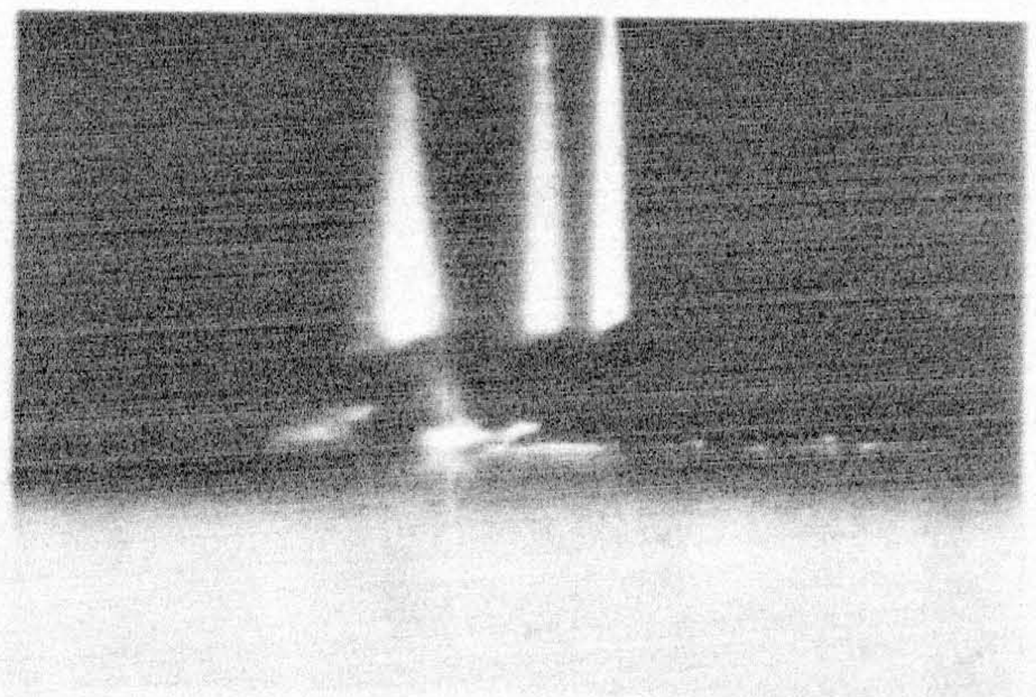

(e)

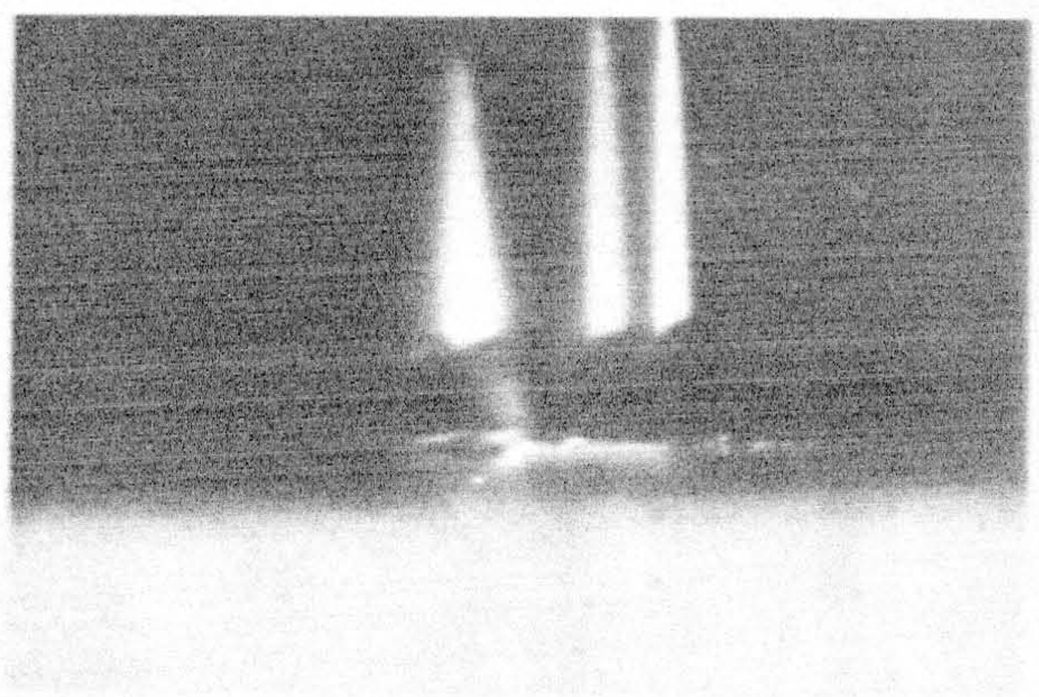

(f)

Fig. 75 High Speed Photography Results

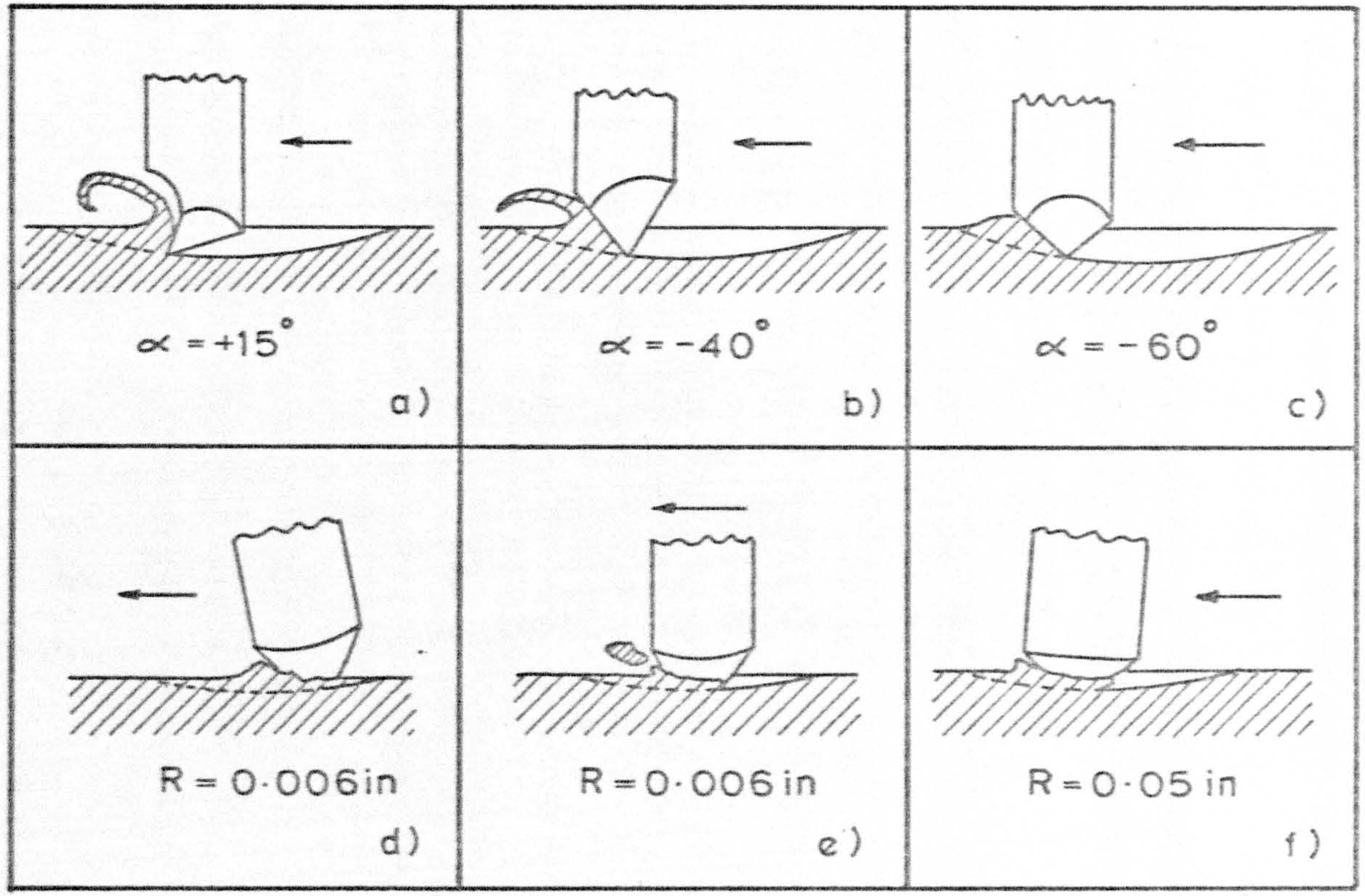

Fig. 76 Schematic Representation of the High Speed Photographs of Fig. 75

such as to induce fracture in the free plastic surface preceding the tool. The likelihood of such a fracture occurring in a practical grinding operation has already been suggested as an important criterion in determining the grindability of metals[30]. In addition, the presence of highly irregular shapes in grinding swarf[71], suggests that the above mechanism is indeed an integral part of the grinding process.

Fig. 75 f R = 0.05 in. The groove width to depth ratio is very high and plastic deformation occurs along the full length of the groove.

4.4 CONCLUSIONS

Previous investigations of this nature involving force measurements have, in general, been carried out at very low speeds well outside the practical range of grinding, or at speeds more appropriate to conventional metal cutting operations. In addition, the scale of deformation has often been greater than that resulting from the interaction of a single abrasive grit in metal grinding.

In contrast, the present tests have been designed to give a realistic simulation of the abrasive grit-workpiece interaction. The tests have shown that the tool geometry, impact speed, and scale of deformation all have a very significant influence on the S.E. For both types of geometry, the S.E. increased with an increase in the negative rake angle and a decrease in the impact speed and scale of deformation. These results immediately suggest that considerable care should be exercised when evaluating and interpreting the findings of simulated tests performed under conditions unrealistic of practical grinding operations.

The S.E. was found to correlate well with the mode of metal deformation, higher values being associated with extensive plastic ploughing type deformation and high interface friction. The energy curves also signified a change in the type of metal deformation at $\alpha = -55^{\circ}$ and $\alpha_{effective} = -75^{\circ}$ for pyramidal and spheroidal tools respectively. This was later confirmed to be a transition from microcutting to plastic deformation as α becomes increasingly negative. The correlation of energy with the mode of metal deformation confirms the opinion of Marshall and Shaw[46] that the former is an important consideration in grinding mechanics.

The behaviour of spheroidal tools is interesting in that if characterised by an effective negative rake angle, they function in the same way as pyramidal tools. In addition with R $\leqslant$ 0.02 in., a transition in the mode of metal deformation was evident at some point along the groove. A similar effect was not observed with pyramidal tools, this being attributed to the basic difference in geometry between the two profiles. If the transition point is defined by a critical depth of penetration, t_c, then the latter was seen to increase with an increase in tool radius and with a reduction in impact speed.

The simulation of an abrasive wheel surface using spheroidal asperities is adopted later (Chapter VI) to derive a simple mathematical model of the plunge grinding discussed in Chapter V. It will be seen that the mathematical description of the surface is straightforward (cf randomly orientated pyramids, etc.) and that the overall S.E. can be estimated by considering the outcome of individual grain-workpiece interactions using the experimental data of this section.

The absence of a rubbing region at the tool entry position would suggest that the stiffness in the normal direction of the present system employed is higher than that of bonded grits in grinding wheels. The results of the simulation can only be compared, therefore, with very hard grinding wheels, i.e., those containing a large percentage of bond. In addition, the geometry of the groove formation as defined by Reichenbach's[45] classification, represents an extreme in operating conditions. In order to extend the simulation to cover the more practical range of wheels and operating conditions, two modifications are suggested. Firstly, an elastic module could be introduced into the tool support system to simulate the elasticity of the grain mounting. Secondly, a simple variation in experimental procedure would enable the complete range of groove types to be reproduced. This could be accomplished by forming a circular groove as at present, and then indexing the workpiece along a distance x in the horizontal direction (Fig. 17, Section 2.3.1). By varying x, the different groove types could be simulated and their influence upon the mode of metal deformation and S.E. determined. It is expected that both modifications would increase the probability of obtaining an initial rubbing regime, since small values of x and increased elasticity would effectively reduce the rate of tool penetration into the test piece surface.

In conclusion, the present simulation has provided a convenient means of studying metal removal in grinding. Of particular importance has been the observed influence of tool geometry on the mode of metal deformation and the energy consumed. There would appear to be considerable scope for future investigations. In addition to the modifications already mentioned, the range of materials could be extended, the impact speeds increased, and simple theoretical considerations introduced.

CHAPTER V

THE BASIC MECHANICS OF A SIMPLE PLUNGE GRINDING OPERATION

This chapter is concerned with an investigation into the basic mechanics of a simple grinding operation, viz., the plunge grinding of metal strip under constant load.

The study was initiated to assess the value of the previous abrasive surface measurements (Chapter III) and simulation tests (Chapter IV) as a contribution to the understanding of the mechanics of the grinding process, with particular reference to the influence of abrasive surface topography.

The chapter also contains information relating to the effect of cutting fluids on the process, and a brief indication of how the measurement techniques developed in Chapter III might be used in a quantitative study of abrasive wheel wear is given.

5.1 APPARATUS

5.1.1 TEST RIG

The advantages of studying a controlled force system as opposed to a fixed feed operation have already been discussed by Hahn[31]. He suggested that since the grinding action itself, i.e., the stock removal rate, the surface finish and the wheel wear, depends directly on the instantaneous force between the wheel and the workpiece, it is appropriate to relate these variables to the force directly. As a

consequence, the grinding process is made independent of the wheel-workpiece system rigidity and the determination of functional relationships between the grinding variables is simplified.

In designing the test rig the following considerations were taken into account:-

a) The rig must be adaptable for use with the Jones Shipman cylindrical grinder discussed in Section 3.1.1.

b) Provision must be made for loading the test piece (metal strips of cross-section $\frac{1}{8}$" x $\frac{1}{2}$") onto the wheel under a constant load in the range 0 - 30 lbf.

c) Arrangements must be made for measuring the applied normal load, the tangential force developed during grinding, and the metal removal rate.

d) Both the friction between moving parts and the inertia of the parts themselves must be minimised. The former improves the repeatability of test conditions by reducing the indeterminate frictional behaviour, whilst both effects ensure adequate sensitivity to a sudden change in operating conditions at the wheel-workpiece interface.

e) All moving parts require protection to prevent undesirable effects caused by the penetration of coolant, swarf, and spent abrasive material between the bearing surfaces.

The final design is shown in Fig. 77 and a diagramatic representation of the configuration adopted is given in Fig. 78. The test piece was mounted directly onto a two component dynamometer attached to a counterbalanced arm. This assembly was then supported on an air bearing positioned high above the cutting zone, thus preventing

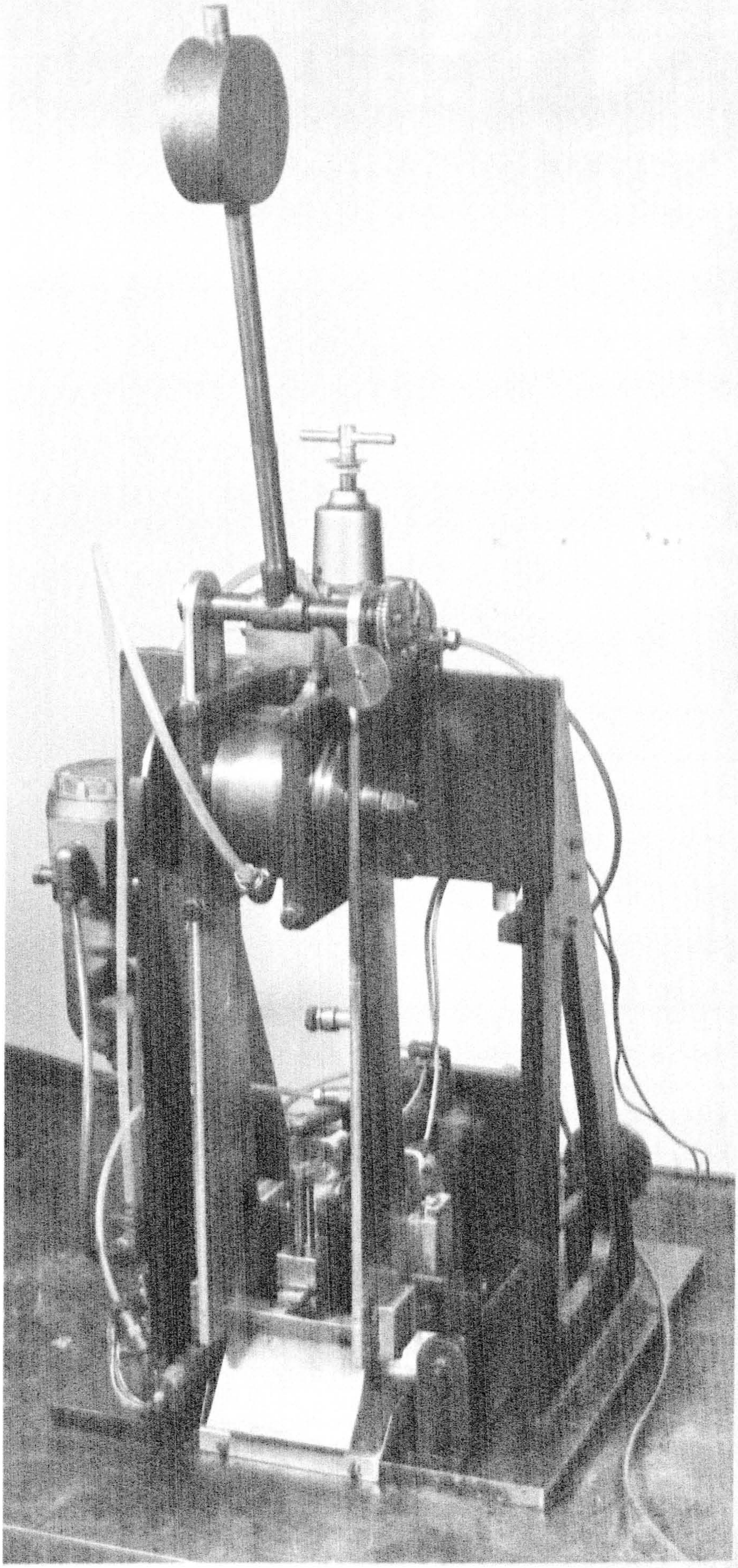

Fig. 77 Rig for the Controlled Force Plunge Grinding of Metal Strip

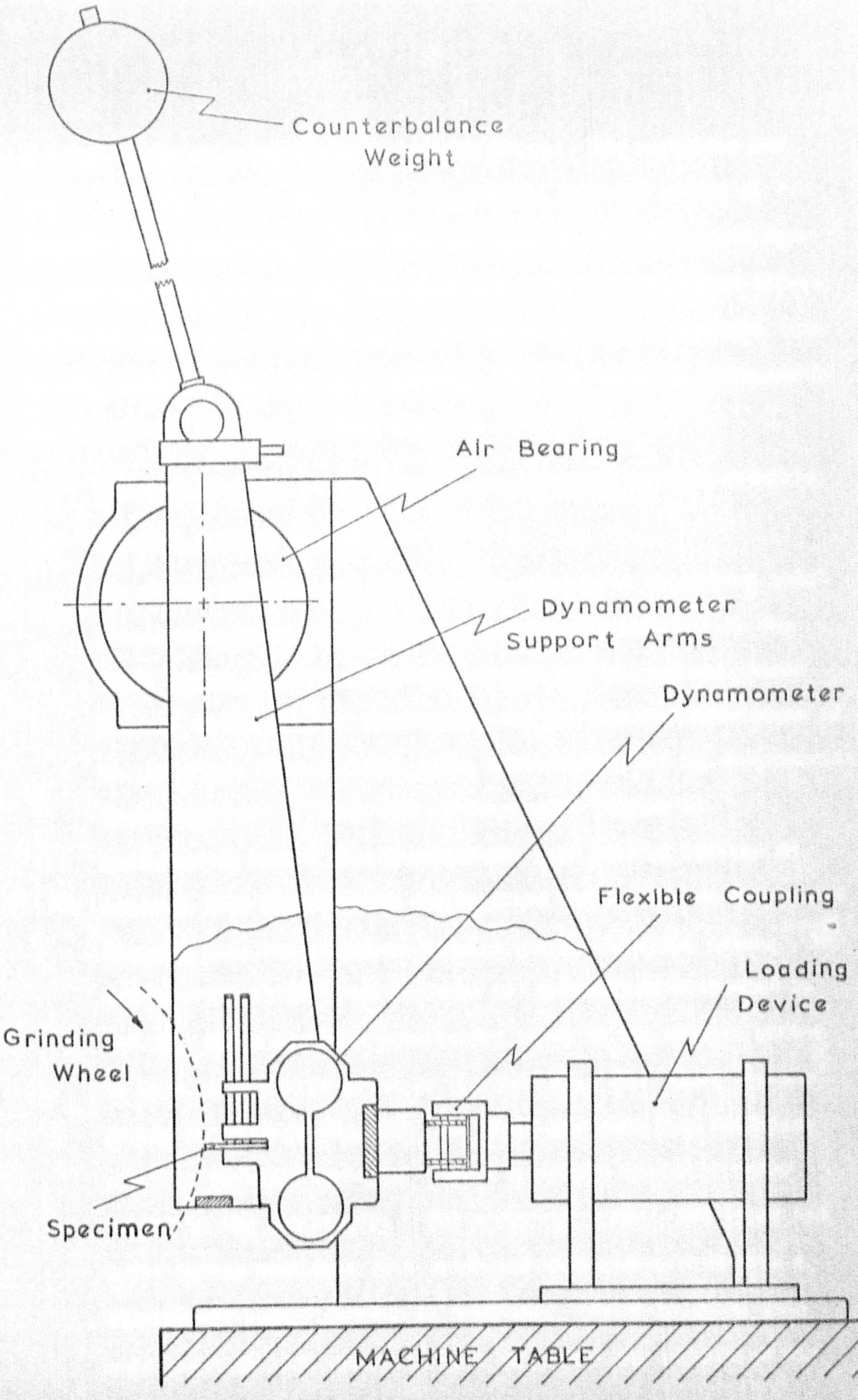

Fig. 78 General Configuration of the Grinding Rig.

foreign bodies entering the main bearing areas. The workpiece was loaded onto the wheel using a simple hydraulic cylinder acting at the back of the dynamometer. With this arrangement, the test piece does in fact approach the arm on a circular path, but over the short infeed distances considered (max. 0.2 in.) the departure from a straight line is only 0.001 in. and can be neglected. The rig could be conveniently mounted on the grinding machine table as seen in Fig. 78.

The main features of the rig are now discussed in more detail:-

(i) THE MAIN SUPPORT BEARING

For design purposes the shaft can be considered stationary which greatly simplifies the problem of bearing selection. In the final design, an internally compensated gas bearing was chosen because of the ease of manufacture and the inherent advantages of an air supply over a fluid, i.e., availability and no recirculation system required. This type of bearing is simpler in construction than a more conventional pool bearing because no external flow restrictions are employed and the air is introduced directly into the clearance through straight-drilled holes. The design criteria for such bearings are extensively discussed in ref. 72, and a specimen calculation based on the example quoted in this reference is given in Appendix B1. The final bearing design is given in Fig. 79. The shaft was made from stainless steel to minimise corrosion caused by minute traces of water vapour in the air supply. For a similar reason, the inner and outer bushes were made from brass and were designed to give a central air supply annulus on assembly. Axial location pads were provided with suitable slots to permit the exhaust of air from the bearing clearance.

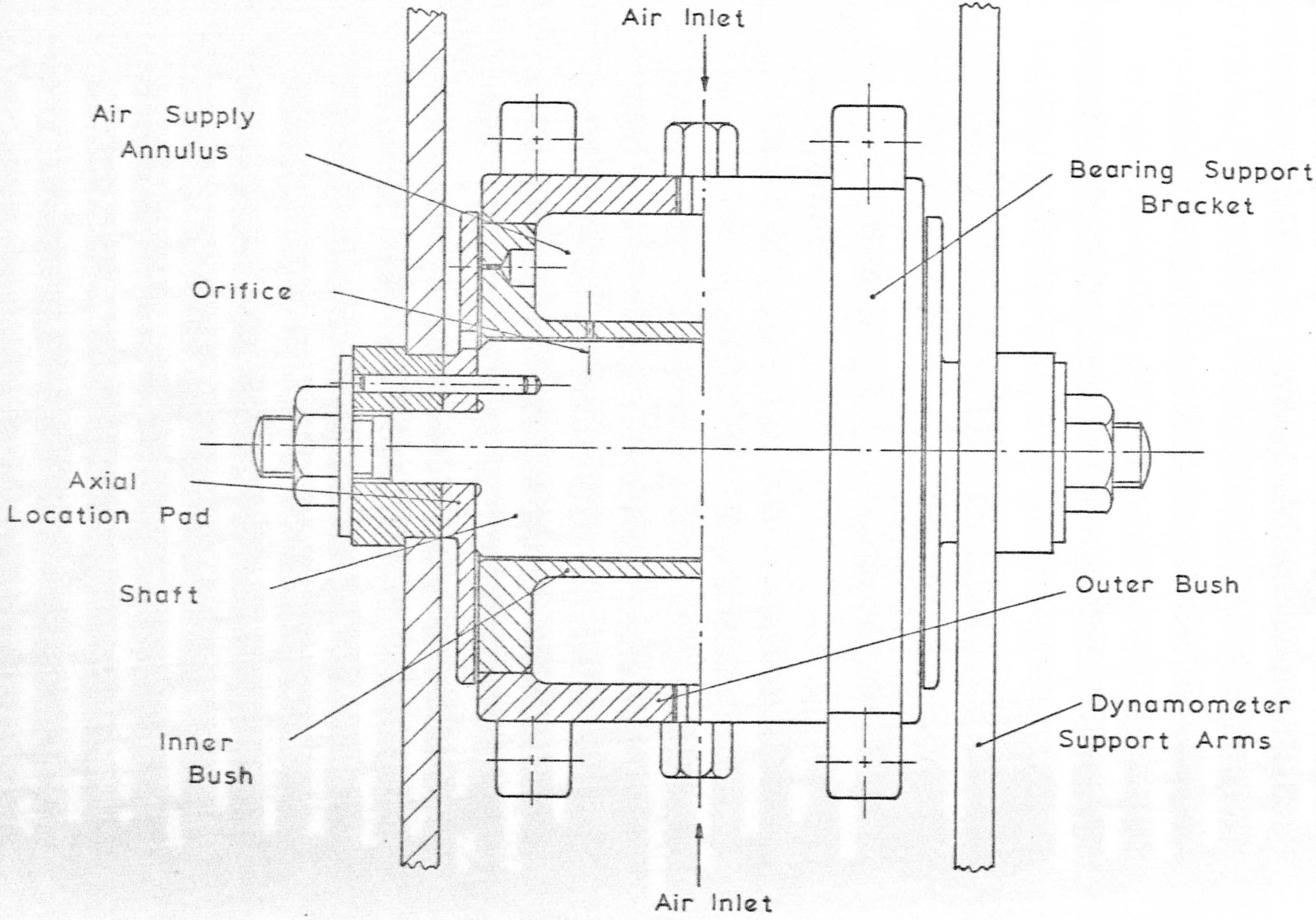

Fig. 79 Air Bearing

An extensive investigation into the bearing properties was not undertaken in view of the elementary function which it performed. It was noted, however, that the bearing was able to support a load of 70 lbs before metal to metal contact occurred. This figure is considerably higher than the total load which the bearing will encounter during actual tests.

(ii) THE LOADING MECHANISM

This consisted of a simple single acting hydraulic cylinder (Fig. 80) acting at the base of the suspended arm. Oil was allowed to flow freely out of the cylinder thus reducing friction caused by sealing. The piston was supported by P.T.F.E. bushes, since at low loads the oil pressure may not be great enough to ensure full film lubrication. The oil supply system is shown in Fig. 81. Oil was pressurised in a primary reservoir using the laboratory compressed air supply. By varying the air flow regulator valve, A, the oil supply pressure could be varied from 0 to 100 psi giving a corresponding load range of 0 - 35 lbf. Returning oil was piped into the secondary container which could then be alternatively pressurised to refill the primary reservoir.

The piston was attached to the base of the support arm by a flexible coupling. This effectively absorbed the non-linear movement of the arm and any misalignment errors incurred during assembly. The coupling simply consisted of a steel ball moving between two sets of cylindrical runners. The runners were fixed on the mating parts and positioned at right angles, thus permitting relative movement in any direction. The two sections were then held together by light springs.

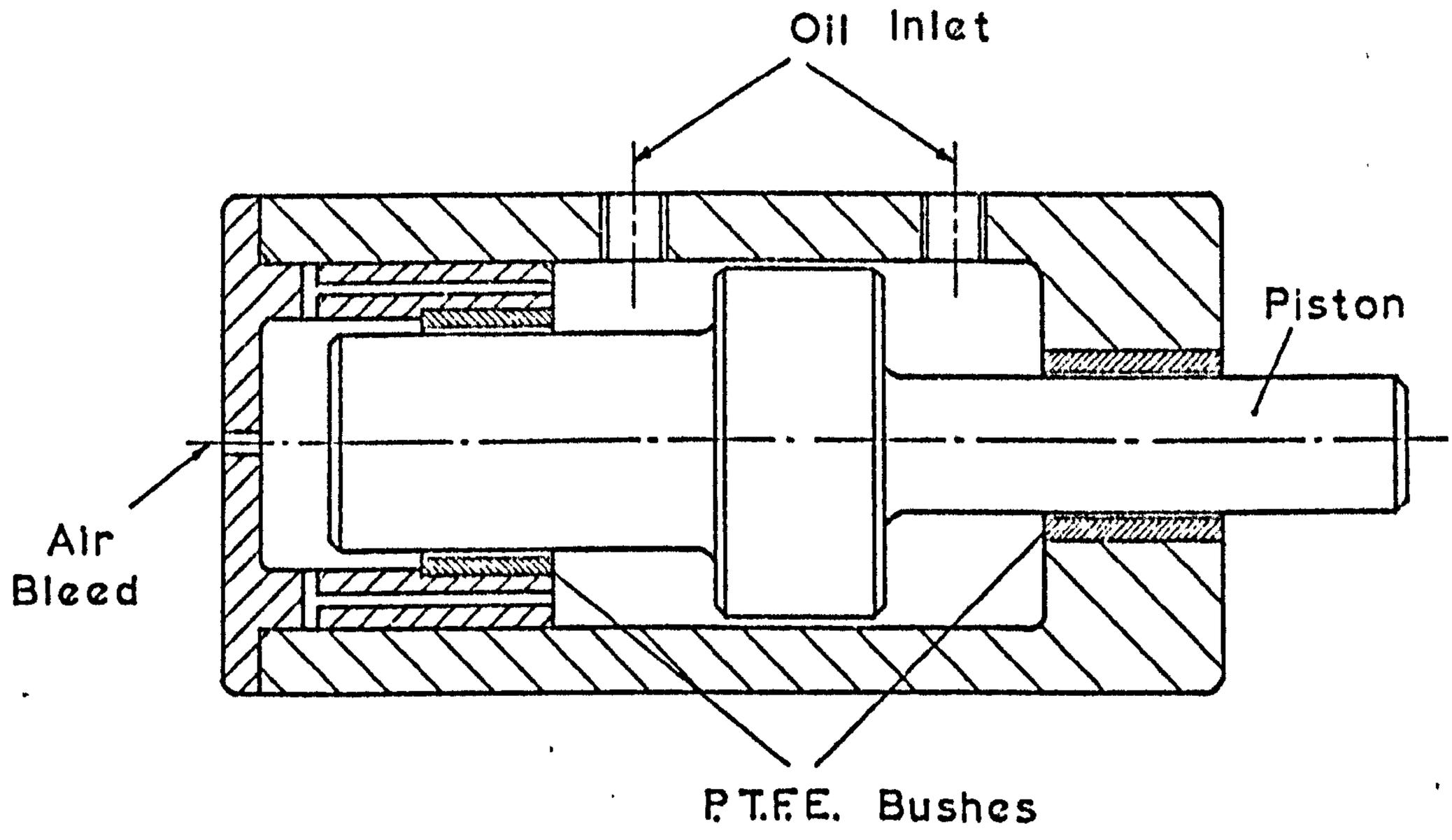

Fig. 80 Hydraulic Loading Device

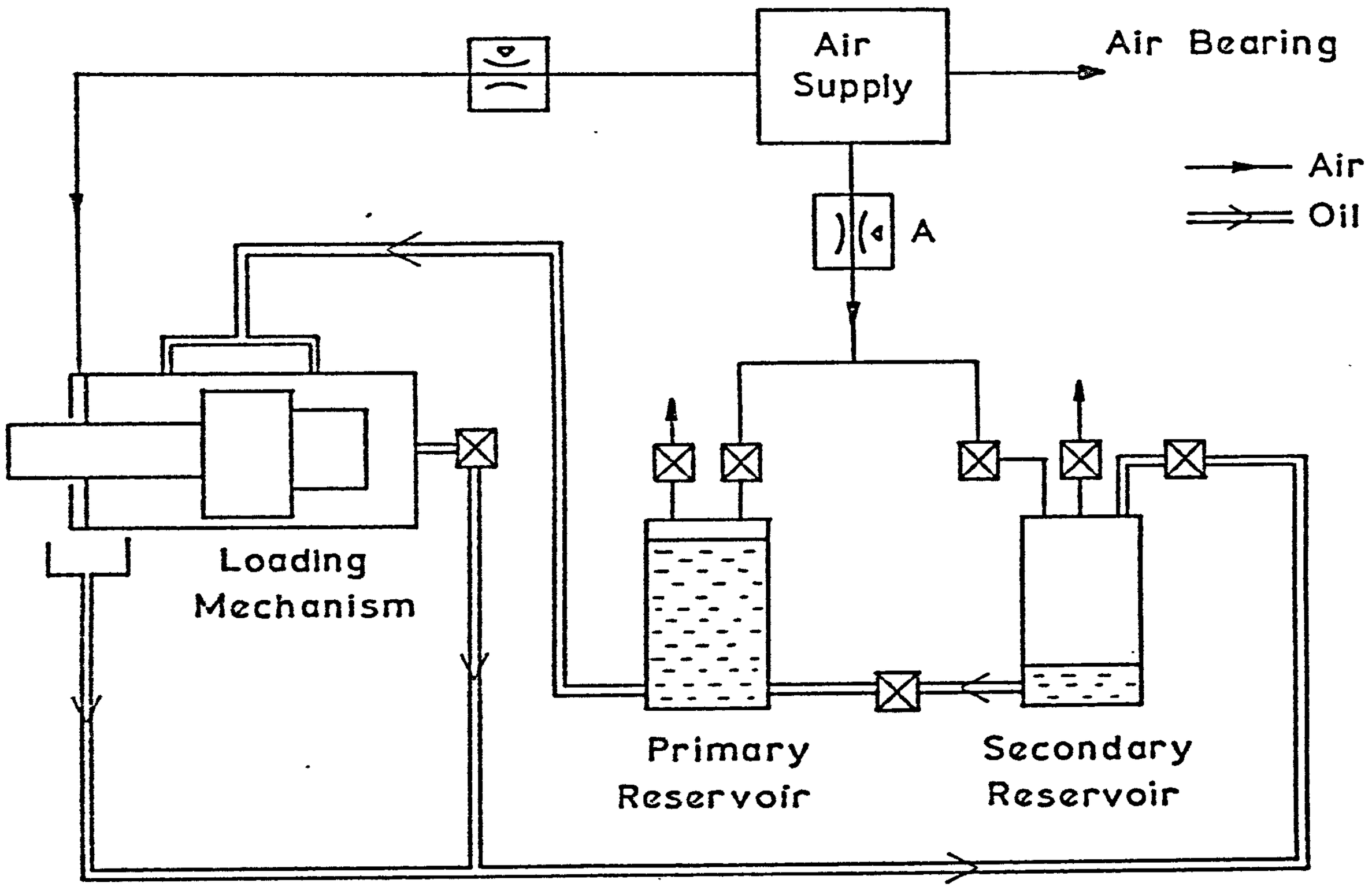

Fig. 81 Oil Supply System

(iii) MEASUREMENT FACILITIES

a) Force measurement

The final dynamometer design enabled the simultaneous measurement of both the normal applied load, N, and the tangential force, T, and was based on the properties of thin circular rings when subjected to two forces which are mutually perpendicular.

When a circular ring, built in at the bottom (Fig. 82) is subjected to a vertical force, N, on the axis AA the two points on the outside diameter will be in tension and the two points on the inner diameter will be in compression. Points on the axis B_1B_2 and B_3B_4 are not stressed. Similarly, when a horizontal force, T, is applied to the top of the ring, on the outside diameter points at B_1 and B_2 are in compression, and points at B_3 and B_4 are in tension. Points on the axis AA are not stressed (These positions apply to points prior to deformation). Consequently, with suitable positioning of strain gauges and the appropriate electrical bridge, the strains resulting from the forces N and T can be measured independently without any cross-sensitivity. In practice, the rings are elongated to facilitate mounting of the workpiece, and assume an octagonal shape, the horizontal force gauges being located at 45° to the vertical (Fig. 83).

The final dynamometer design was similar to the ring shown in Fig. 83 with slight modifications for mounting purposes. The value of L is not critical and was chosen to suit the overall design. The final dimensions and their method of selection based on a procedure given in ref. 73 can be found in Appendix B2.

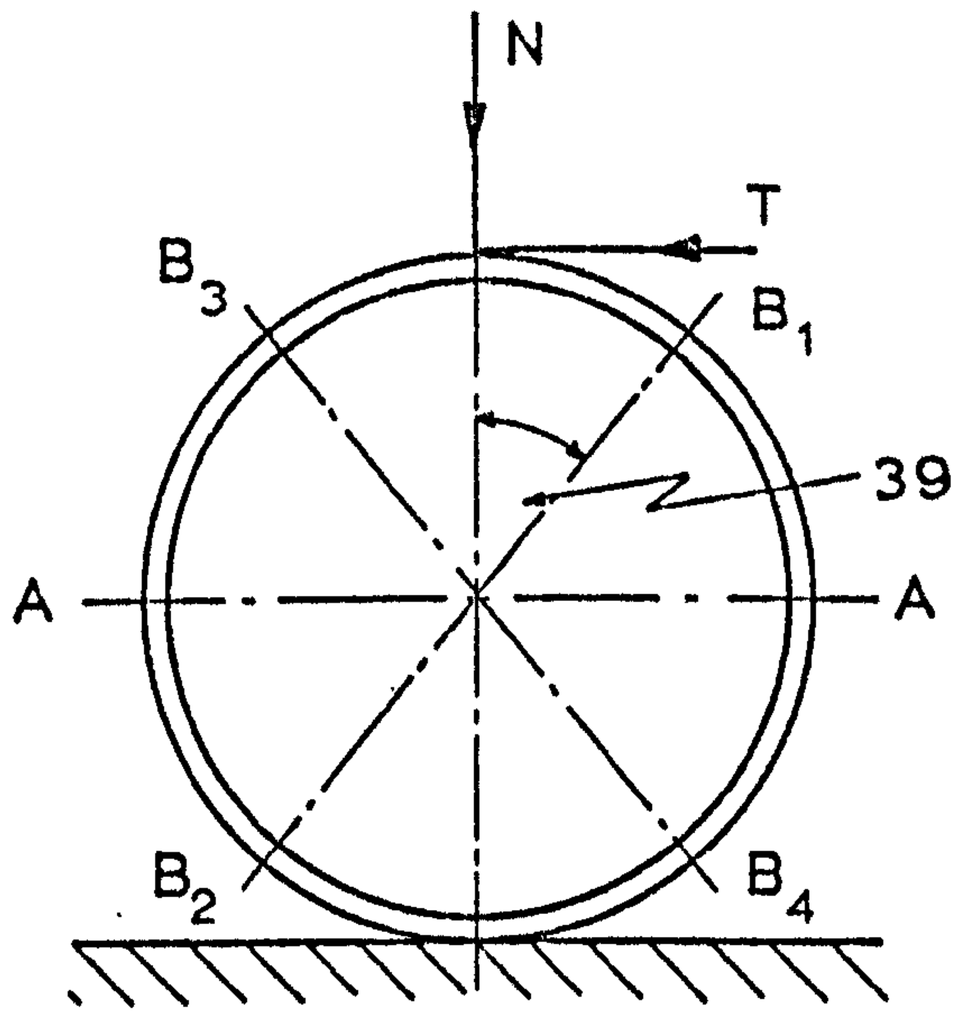

Fig. 82 Deformation of a Thin Circular Ring

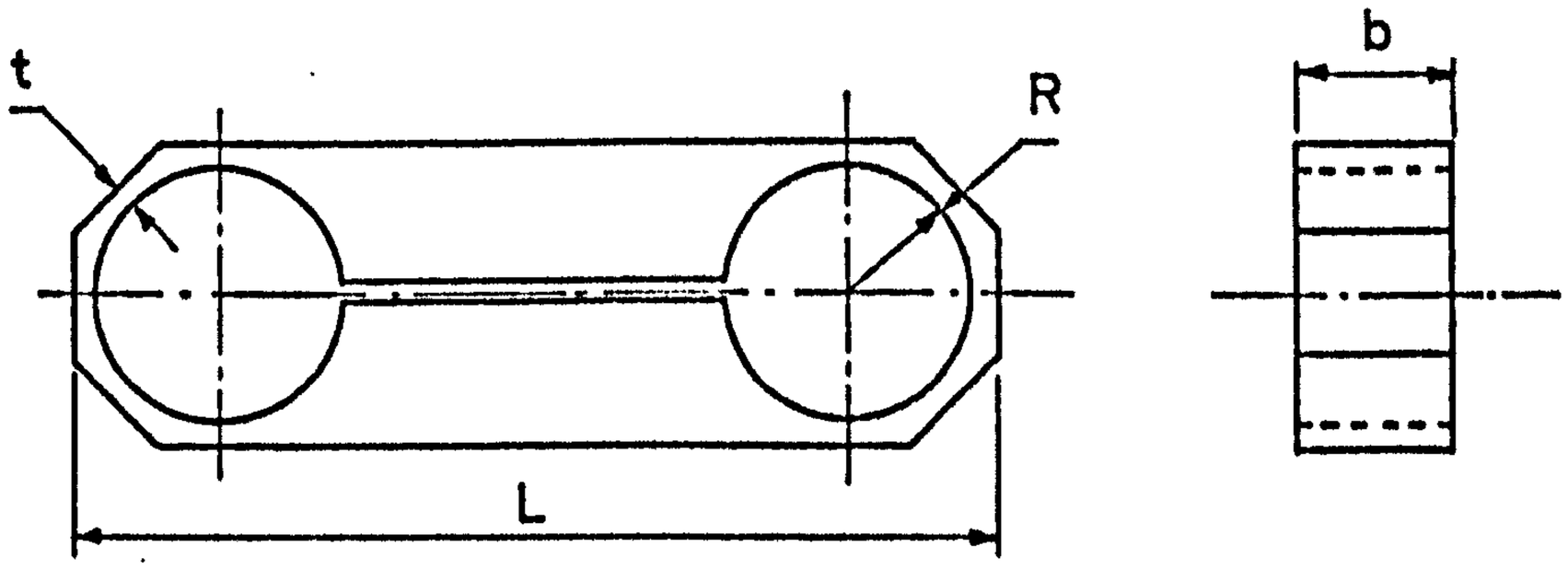

Fig. 83 Practical Shape for Dynamometer

The dynamometer was used in conjunction with a 6 channel carrier amplifier (carrier signal 4V rms and 3kHz) and a UV recorder. The appropriate electrical bridge circuits are shown in Fig. 84.

NOTE: With the general rig configuration adopted, certain following precautions had to be taken to prevent undesirable turning moments influencing the values of N and T at the wheel-test piece interface:-

i) The interface should be vertically below the air bearing centre. This was implemented during the experimental procedure.

ii) The support arm should be statically balanced about the air bearing centre. An approximate balance was first achieved by using a large mass operable on an extended arm capable of angular movement. Small weights located on a disc at the centre of the arm were then employed to effect a finer adjustment, in a manner similar to the standard technique for balancing grinding wheels.

b) Measurement of the metal removal rate

During a plunge grinding operation, the infeed of the workpiece is a function of:-

i) metal removal rate

ii) abrasive wear rate

iii) thermal expansion of the workpiece

iv) system elasticity

In the short duration tests performed here, the last three effects are neglected, the metal removal rate then being

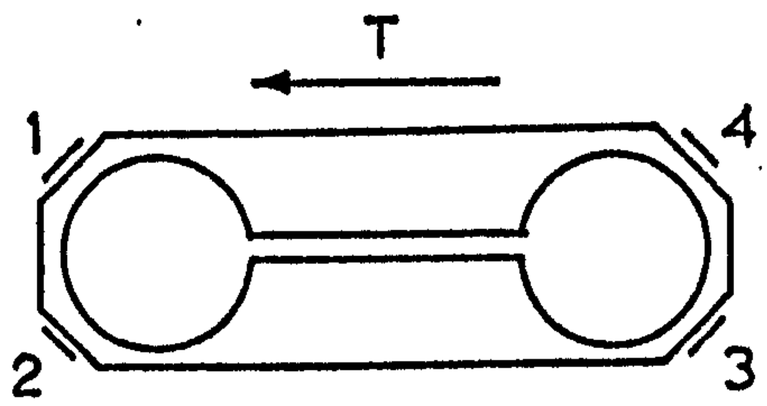

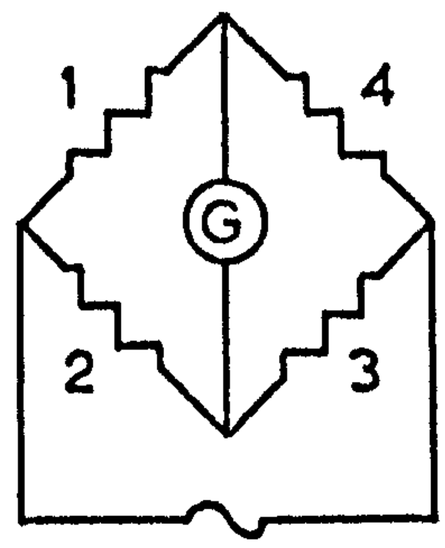

TANGENTIAL FORCE

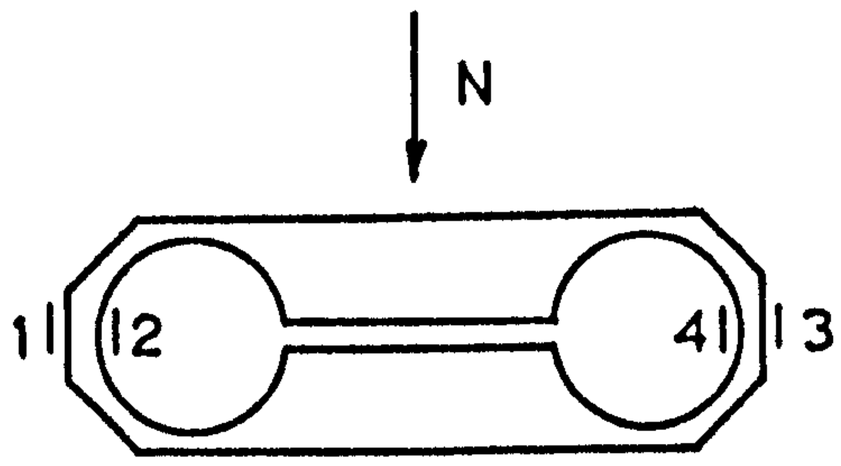

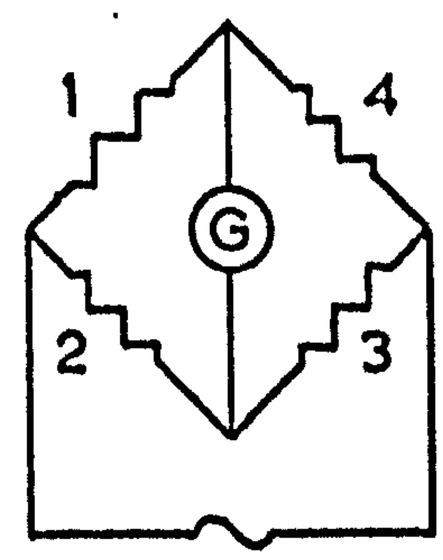

NORMAL FORCE

Fig. 84 Electrical Bridges for Force Measurements

a direct function of the infeed velocity. The velocity was measured using a Schaevitz Standard Linear Variable Differential transducer. This is an electromechanical transducer which produces an electrical output proportional to the displacement of a separate moveable core. There are no contacting sliding surfaces and hence detrimental frictional effects do not occur. The transducer was again used in conjunction with the carrier amplifier and UV recorder and gave a linear calibration of 0.05 in. infeed/inch galvo deflection.

5.1.2 INITIAL RIG COMMISSIONING TESTS

Before beginning the experimental programme, initial tests were undertaken to determine certain characteristics of the completed system. These were combined with theoretical considerations to gain information relating to the limiting infeed velocity of the test piece, and the sensitivity of the system to sudden changes in resistance at the wheel - test piece interface. The system was also loaded dynamically to investigate the response to vibrations obtained in practice as a result of the grinding wheel out-of-roundness. The results of these tests and the conclusion drawn are discussed in detail in Appendix B3.

5.1.3 TEST PIECE MATERIAL

Three materials were used, in the form of $\frac{1}{2}$ in. x $\frac{1}{8}$ in. strip:-

a) EN 8 - Rockwell hardness 20

Approximate U.T.S. 49 tons/in^2

b) TOOL STEEL - Composition: 0·90% C, 1.1 - 1.3% Mn,
0.1 - 0.3% Si, 0.4 - 0.6% Cr
0.1 - 0.2% Va, 0.4 - 0.6% W
0.03% maximum S and P

Used in the fully hardened condition
(hardened 800°C and oil quenched)

Rockwell hardness 64
Approximate U.T.S. 148 ton/in^2

c) TUNGSTEN CARBIDE

Since the maximum amount of metal which could be removed during a grinding test was very limited (only 0.2 in. length of strip), the corresponding abrasive wear was negligible. In order to induce wheel wear using the test rig, the grinding of tungsten carbide was attempted, resulting in rapid wear rates with virtually no stock removal.

5.1.4 WHEEL SPECIFICATIONS

Three different wheels were selected with a view to considering the influence of grain size:-

23 A 46 - K5 - VBE
23 A 80 - K5 - VBE
38 A 150 - K8 - VBE

5.1.5 GRINDING FLUIDS

Two series of tests were undertaken to determine the influence of grinding fluids on the grinding action:-

a) A general investigation using the soluble oil Shell Dromus B, in a 40:1 concentration with water.

b) A more detailed study on the influence of lubricant concentration using tap water, 60:1 and 30:1 concentrations of Shell Dromus D soluble oil, and Sintolin S.B.2 - a synthetic lubricoolant containing E.P. additives.

In all cases the rate of fluid supply was approximately three gallons/minute.

5.2 EXPERIMENTAL PROCEDURE

5.2.1 DYNAMOMETER CALIBRATION

The dynamometer was calibrated by separately applying incremental loads in the normal and tangential directions, and observing the corresponding output from both measurement bridges. Fig. 85 shows a typical calibration for amplifier settings of 27 db and 24 db in the N and T bridges respectively. In both cases, the cross-sensitivity is seen to be small, the actual value depending on the relative magnitudes of N and T. In practice, several amplifier settings were used to give maximum sensitivity over the entire working range.

5.2.2 WHEEL DRESSING

All experiments were carried out with newly dressed wheels, three tests being possible at intervals across the wheel surface prior to

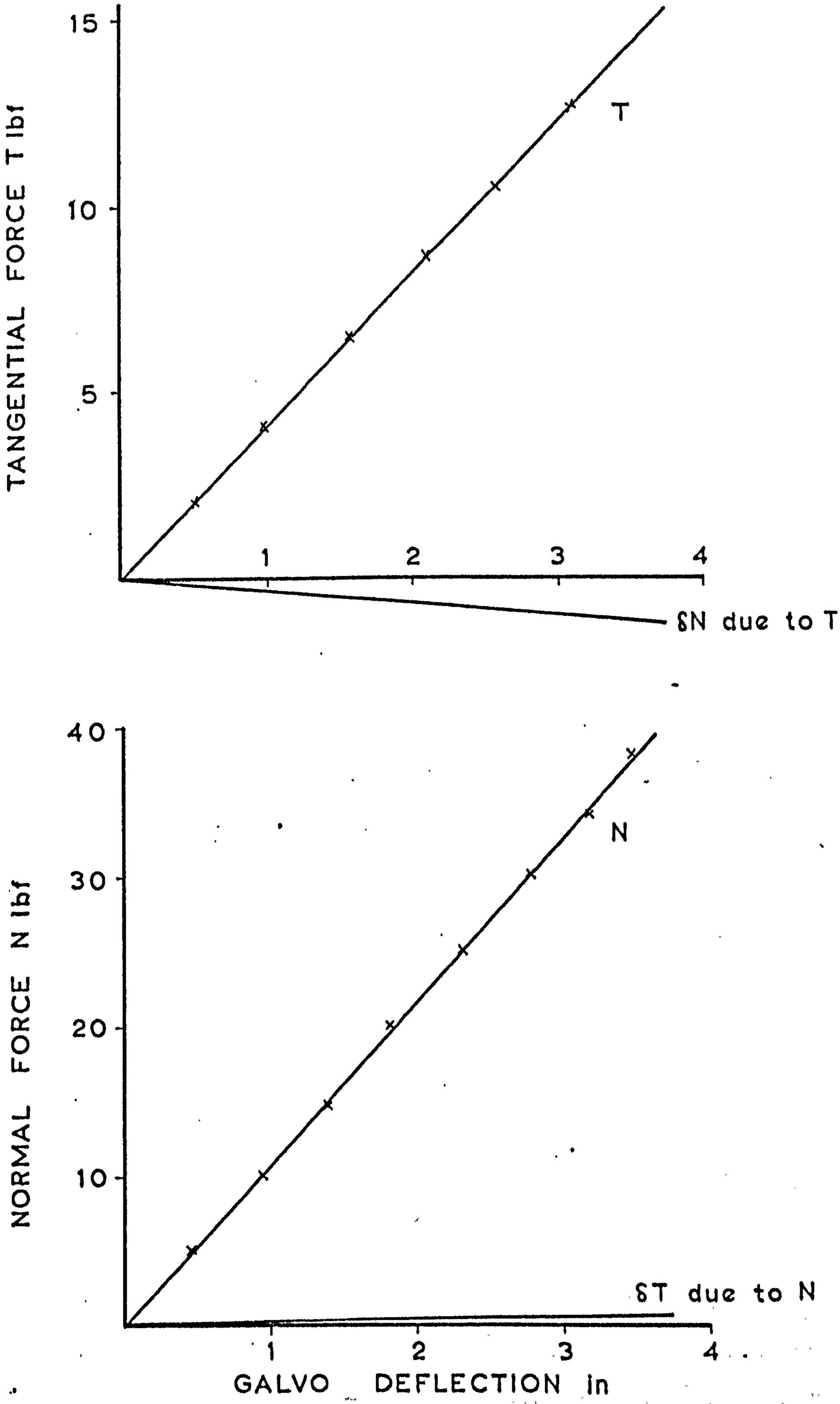

Fig. 85 Dynamometer Calibration

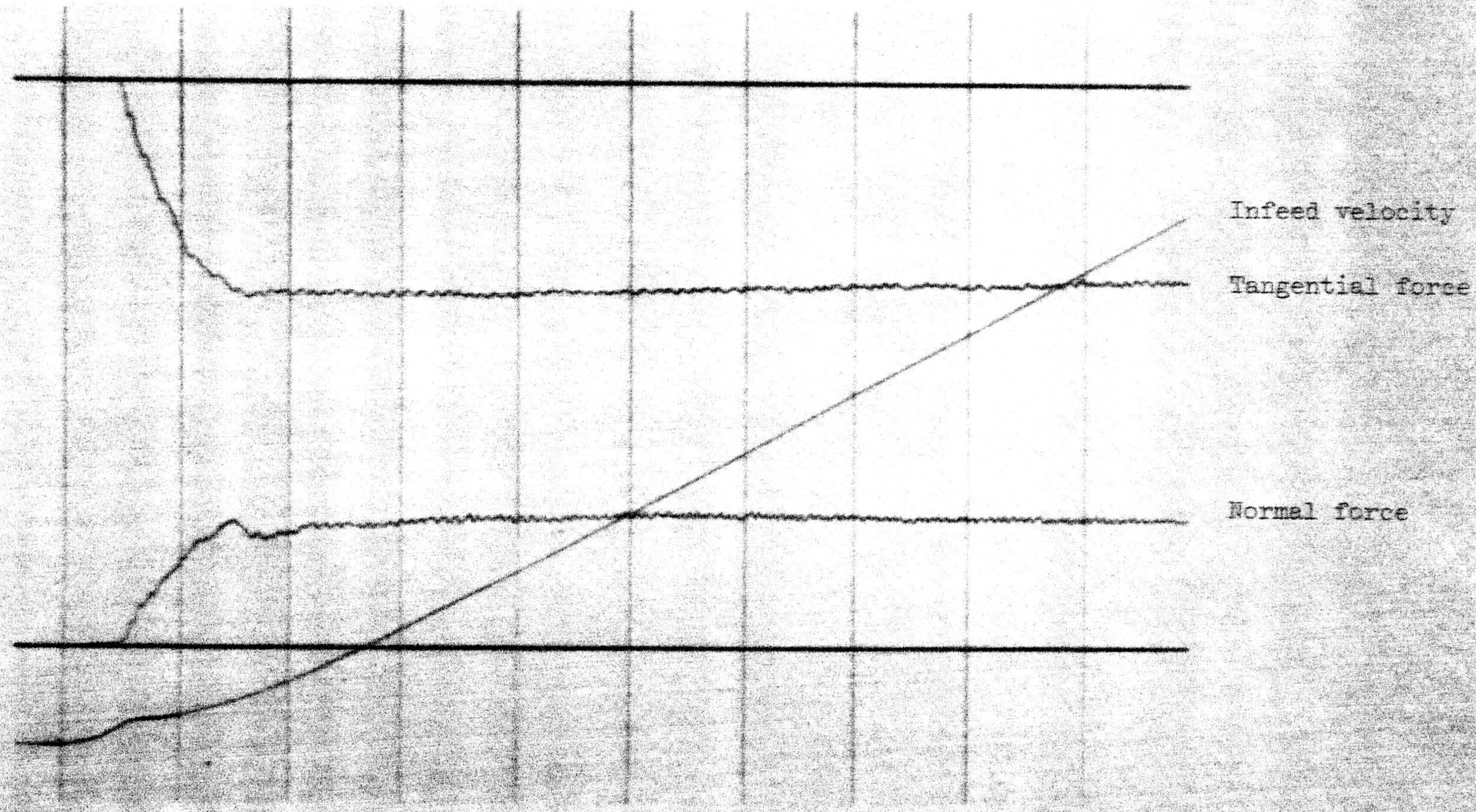

Fig. 86 UV Trace

redressing. The dressing operation was standardised as indicated in Section 3.2, and the same range of conditions was employed:-

Condition	Dresser feed f in/min	Dresser penetration d in x 10^4
A	1	1
B	30	3
C	50	5
D	80	8

5.2.3 TEST PROCEDURE

The test piece was mounted onto the dynamometer and the position of the grinding wheel adjusted until the wheel-test piece interface was vertically below the air bearing centre, (Section 5.1.1(iii)). The test piece was then loaded onto the stationary wheel and the applied load selected by adjusting the air flow valve, A (Fig. 81), noting the corresponding galvanometer deflection on the UV recorder. The test piece was then momentarily retracted whilst the wheel was set in motion, and then reloaded. The normal and tangential force traces and the test piece time-displacement curve were then recorded on UV paper.

5.3 RESULTS AND DISCUSSION

The experimental results are again discussed in terms of two basic grinding parameters, i.e., the specific energy and the grinding ratio ($^T/_N$).

In this case, the S.E. is given by:-

$$S.E. = \frac{2\pi RnT}{60v_i A} \text{ in lb/in}^3$$

where R = Abrasive wheel radius, in.

n = Wheel speed, r.p.m.

T = Tangential force, lb f

A = test piece cross-sectional ares, in^2

v_i = test piece infeed velocity, in/sec.

Thus $S.E. = 1.76 \times 10^4 \times \frac{T}{v_i}$ in lb/in^3

It is interesting to note that the energy is proportional to T and inversely proportional to v_i. Thus, in addition to the energy variations resulting from changes in T (as in Chapter IV), the metal removal rate will also have an effect on the final computed value of the S.E. This effect is seen to be compatible with the already observed variations in S.E. arising from changes in the mode of metal deformation. Extensive plastic deformation will result in little metal being actually removed, the infeed velocity will be low, and the energy will be correspondingly high. On the other hand, microcutting will cause high test piece infeed rates, and low energy consumption.

In the results that follow, except where given as a function of time, average values of S.E. and $^T/N$ are used, as determined from the UV traces (Fig. 86).

5.3.1 DRY TESTS

In this first set of tests, carried out in the absence of a grinding fluid, the effect of dressing conditions, grain size, applied normal load and material hardness upon the resultant mode of metal

deformation is discussed:-

(i) EFFECT OF DRESSING CONDITIONS ON THE S.E.

Fig. 87 shows the S.E. as a function of applied load for the different dressing conditions and grain sizes. It can be seen that as the severity of the dressing operation increases, there is a dramatic decrease in the S.E. The reason for this can be explained by considering the change in abrasive surface properties with dressing conditions, as discussed in Chapter III. With finely dressed wheels, the individual asperity peaks tend to fall at the same level, and the concentration of potential cutting edges in the outermost levels of the wheel surface is correspondingly high. In a controlled force-free infeed operation, this will result in the normal loads supported by individual contacting asperities being relatively low. As a consequence, the grit penetration depths are also low, and the individual grit - test piece interactions are characterised by high groove width to depth ratios (form factors). In Chapter IV it was shown that such conditions favour extensive plastic deformation and high energy consumption.

As the severity of the dressing conditions increases however, the asperity peaks display a wide range of amplitudes, and the concentration of potential cutting edges in the outermost levels decreases. Consequently, the individual groove width to depth ratios are lower than those experienced with fine dressing conditions. As discussed in Chapter IV, the extent of the plastic deformation will decrease, the number of grits actively engaged in microcutting will increase, and there will be a corresponding reduction in the S.E.

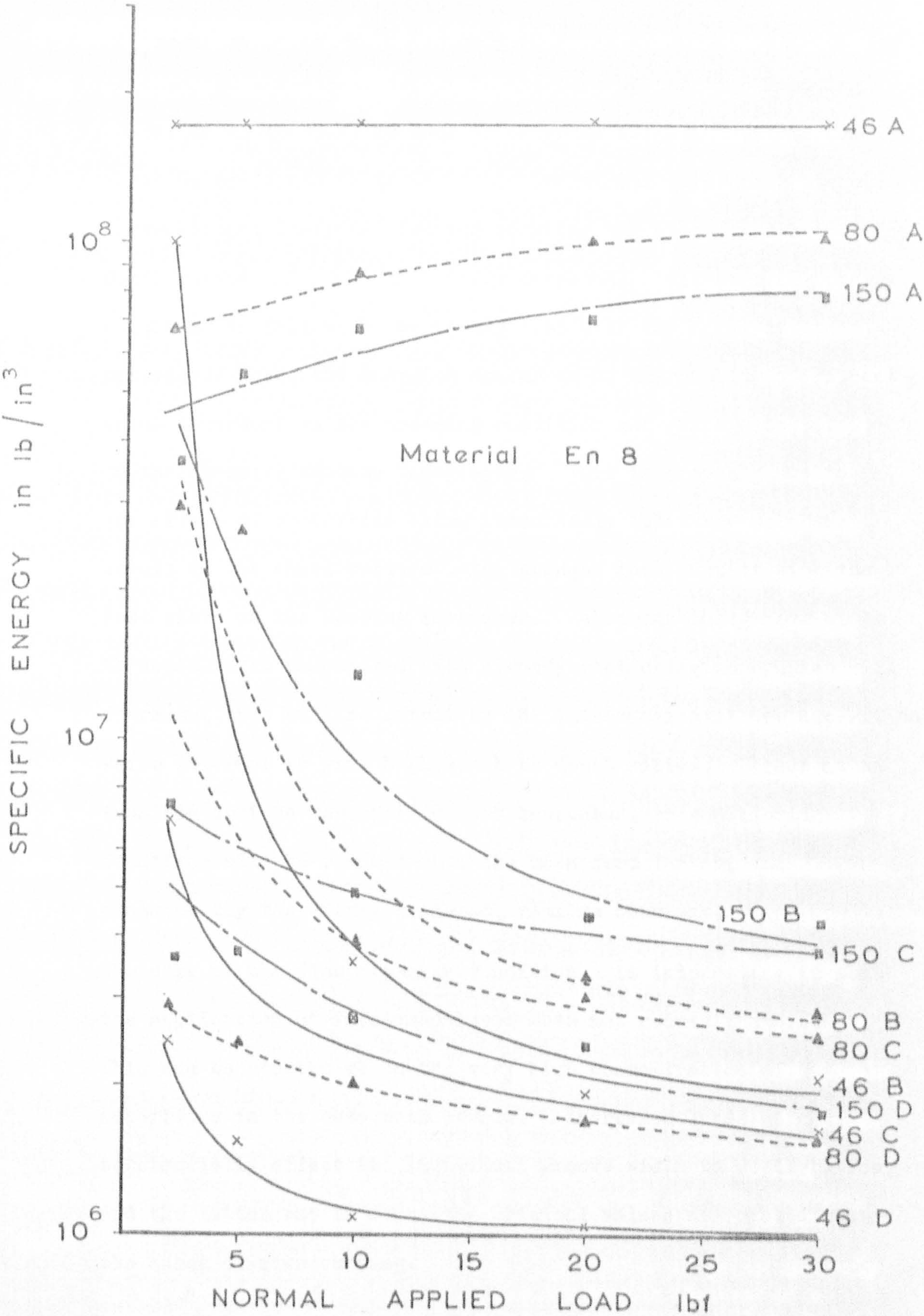

Fig. 87 The Effect of Grain Size, Dressing Conditions and Normal Applied Load upon the Resultant S.E. Values

(ii) EFFECT OF THE APPLIED NORMAL LOAD ON S.E.

As the load increases, except in the case of the fine dressing condition A, the S.E. is seen to decrease (Fig. 87). This can again be explained in terms of the individual grit - test piece interactions, increased loading reducing the groove width to depth ratios and hence the energy consumed. Although the energy continues to fall with increasing load over the range of loads considered here, the energies appear to be approaching a constant value dependent on the dressing condition and grain size, i.e., on the abrasive surface topography. This is probably due to the effect of asperities lying immediately below the outermost levels of the wheel surface being brought into contact with the test piece as the loading increases. Although the groove width to depth ratio associated with already contacting asperities will decrease, this will be offset by the introduction of new asperities which interact to give high width to depth ratios. Hence it is feasible that as the applied load increases, an equilibrium condition will be reached when the mean form factor, and consequently the energy consumed, remains constant.

The case of the fine dressing condition A is interesting in that the application of increased loads does not reduce the S.E. This can be attributed to the very high concentration of asperities in the outermost levels. Increased loads do not substantially effect the individual groove width to depth ratios, and the latter ramain above the critical values associated with the onset of microcutting.

(iii) EFFECT OF GRAIN SIZE ON S.E.

Further examination of Fig. 87 reveals that the S.E. is also a function of grain size, although the effect is secondary to that of dressing conditions. For fine dressing associated with extensive plastic deformation, the S.E. is seen to decrease with a decrease in the nominal grain size. With coarse dressing conditions however, the reverse effect occurs, the S.E. decreasing with an increase in the nominal grain diameter. The reasons for this anomalous behaviour can be explained by again considering the geometry of the individual grit - test piece interactions. The individual groove width to depth ratios are influenced by two main factors, viz., the geometry of the grit and the depth of penetration into the metal surface. As the grain size decreases, the mean effective rake angle increases in a positive sense, resulting in relatively small width to depth ratios. However, the number of asperities in contact with the test piece surface also increases, resulting in decreased penetration depths and larger width to depth ratios. Thus the nett result of a change in grain size depends on the outcome of two conflicting effects, which in turn will depend on the exact nature of the abrasive surface topography.

For fine dressing conditions it can be assumed that the conditions of interaction are such that a decrease in grain size results in a nett decrease in the individual groove width to depth ratios, with a corresponding decrease in S.E. For coarse conditions however, the reverse effect occurs, the width to depth ratios decreasing because of the greater penetration depths. This causes the S.E. to fall with an increase in the

grain size. In addition, the more open structure of a larger grain size wheel may be conducive to "free" cutting conditions, with negligible interference between neighbouring grits. This could be expected to cause a further reduction in the S.E.

(iv) EFFECT OF DRESSING CONDITIONS, GRAIN SIZE, AND APPLIED LOAD ON THE $^{T}/_{N}$ RATIO

The effect of the above variables on the $^{T}/_{N}$ ratio is seen from the typical results reproduced in Fig. 88 and 89. An increase in the severity of the dressing operation causes a corresponding increase in the $^{T}/_{N}$ ratio (Fig. 88). This is a further confirmation that the number of grits actively engaged in microcutting increases with coarser dressing conditions, since it was shown in Chapter IV that predominantly microcutting operations are characterised by high $^{T}/_{N}$ ratios.

The effect of grain size upon the $^{T}/_{N}$ ratio was less predictable (Fig. 89) and showed no definite trends. This is probably to be expected in view of the small energy change resulting from a variation in grain size.

It can be seen from Figs. 88 and 89 that the influence of applied load upon $^{T}/_{N}$ is again not well defined. This is somewhat surprising in view of the considerable change in S.E. with applied load. It was noticed, however, that the S.E. values were much more a consequence of a change in infeed velocity than tangential force, and hence in this case, the $^{T}/_{N}$ ratio may not be sensitive to changes in the mode of metal deformation.

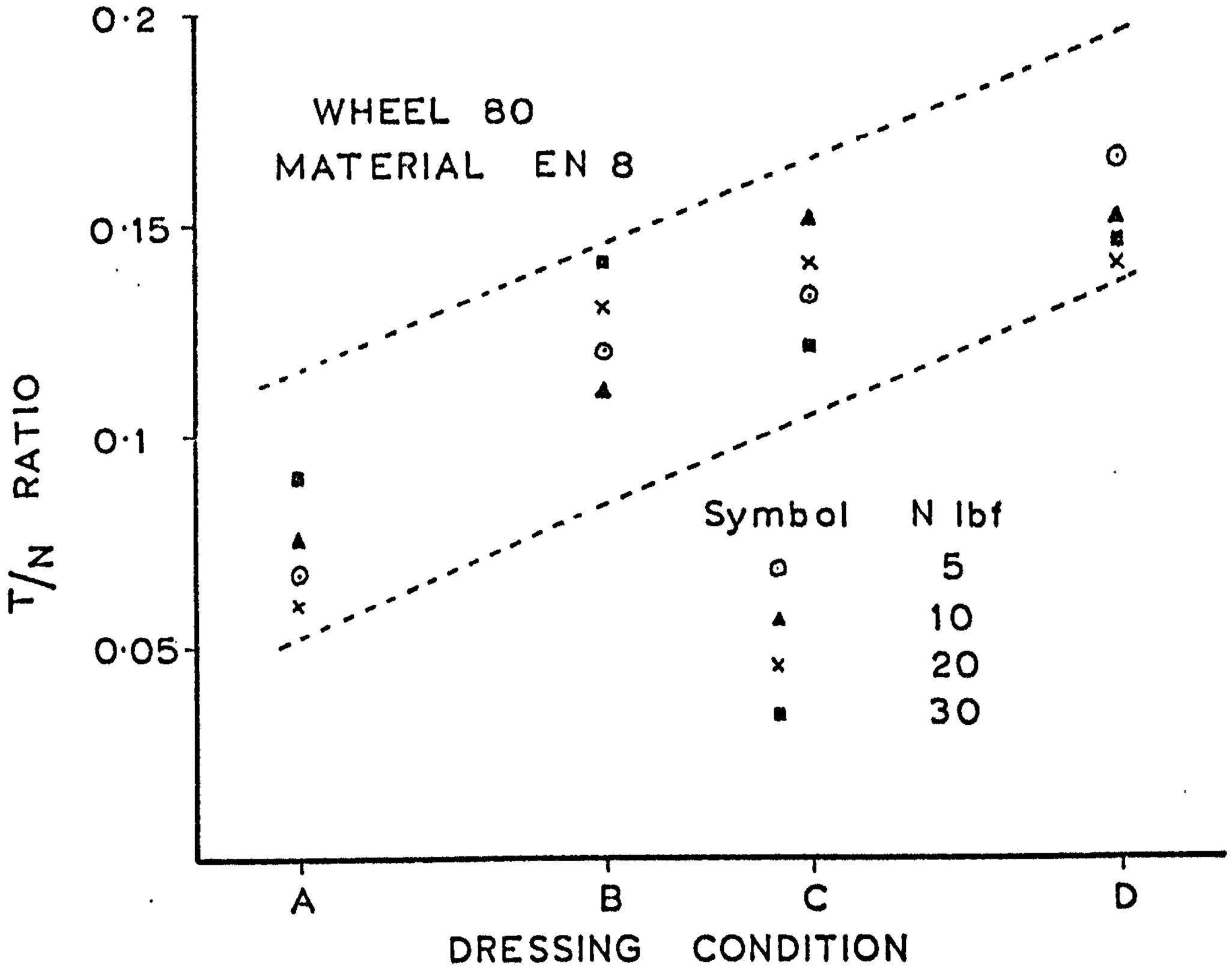

Fig. 88 Variation in $^{T}/_{N}$ Ratio with Dressing Conditions

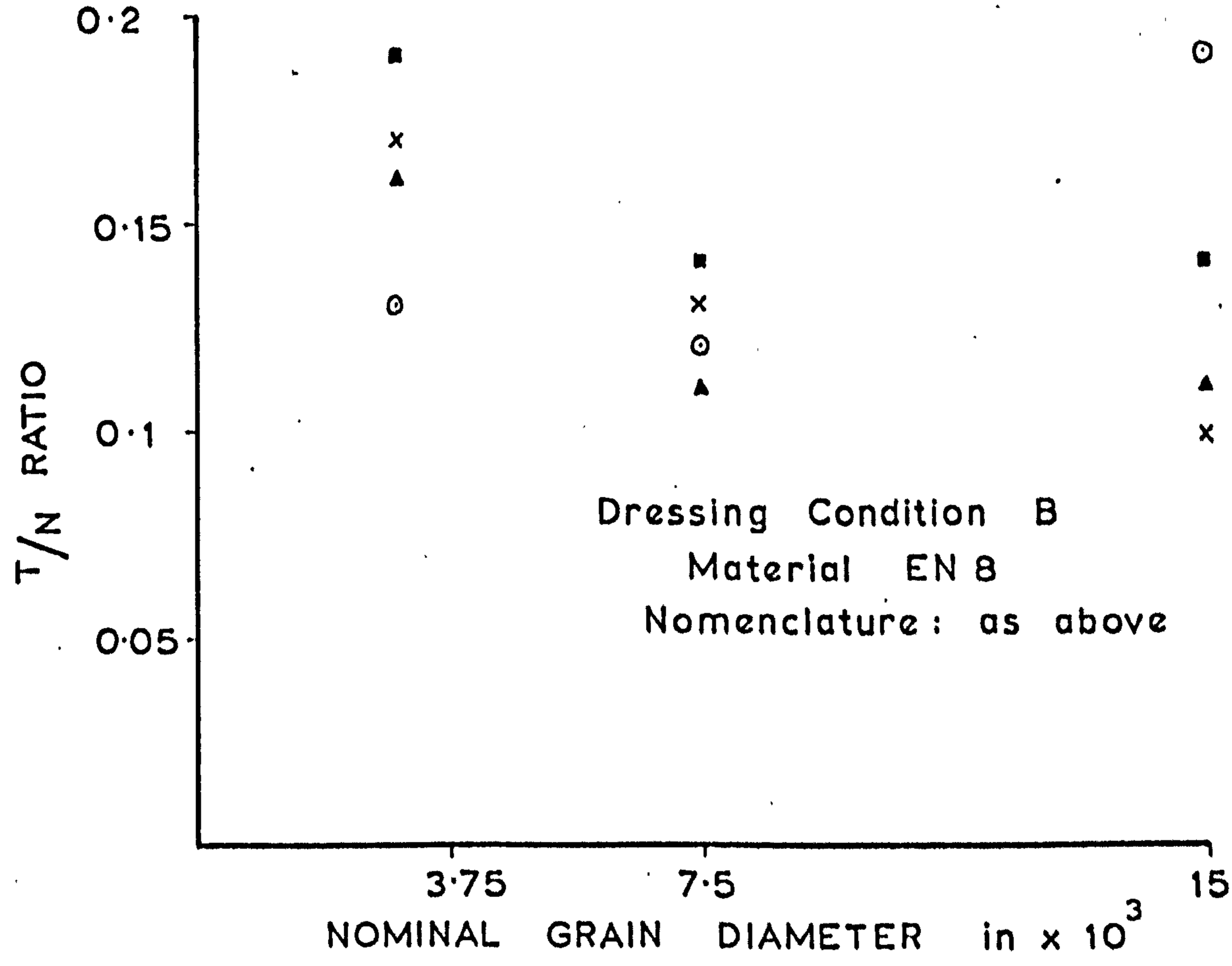

Fig. 89 Variation in $^{T}/_{N}$ Ratio with Grain Size

(v) EFFECT OF MATERIAL HARDNESS ON THE S.E.

The S.E. was first condidered as a function of hardness by Marshall et al[46]. They concluded that the S.E. was independent of hardness and attributed this to the small thickness of chips, causing metals to effectively exhibit the same theoretical strength. In the discussion of the report however, Tarasov indicated that the experimental conditions were such that the thickness of chips was unnaturally low, and reported that for tests carried out under commercial conditions, the S.E. varied appreciably with material hardness.

In the present tests, the S.E. is again seen to vary with material hardness (Fig. 90). With the exception of the fine dressing condition A, the energy associated with tool steel is less than that of EN 8 for low applied loads, and greater for high loads. This effect is interesting in that it gives a possible indication of a change in metal deformation with hardness. On account of the high hardness of the tool steel, it could be expected that the individual groove geometries will not change significantly with load. Consequently, the S.E. should remain virtually insensitive to load, which is seen to be the case from Fig. 90. In addition, it seems reasonable to assume that the extent of plastic displacement will be lower with the tool steel. This is confirmed by the lower energy consumption with tool steel when grinding in the predominantly ploughing regime associated with low applied loads. As the load increases however, the penetration depths increase with the softer EN 8, and due to the increased microcutting, the energy falls below the corresponding value for tool steel.

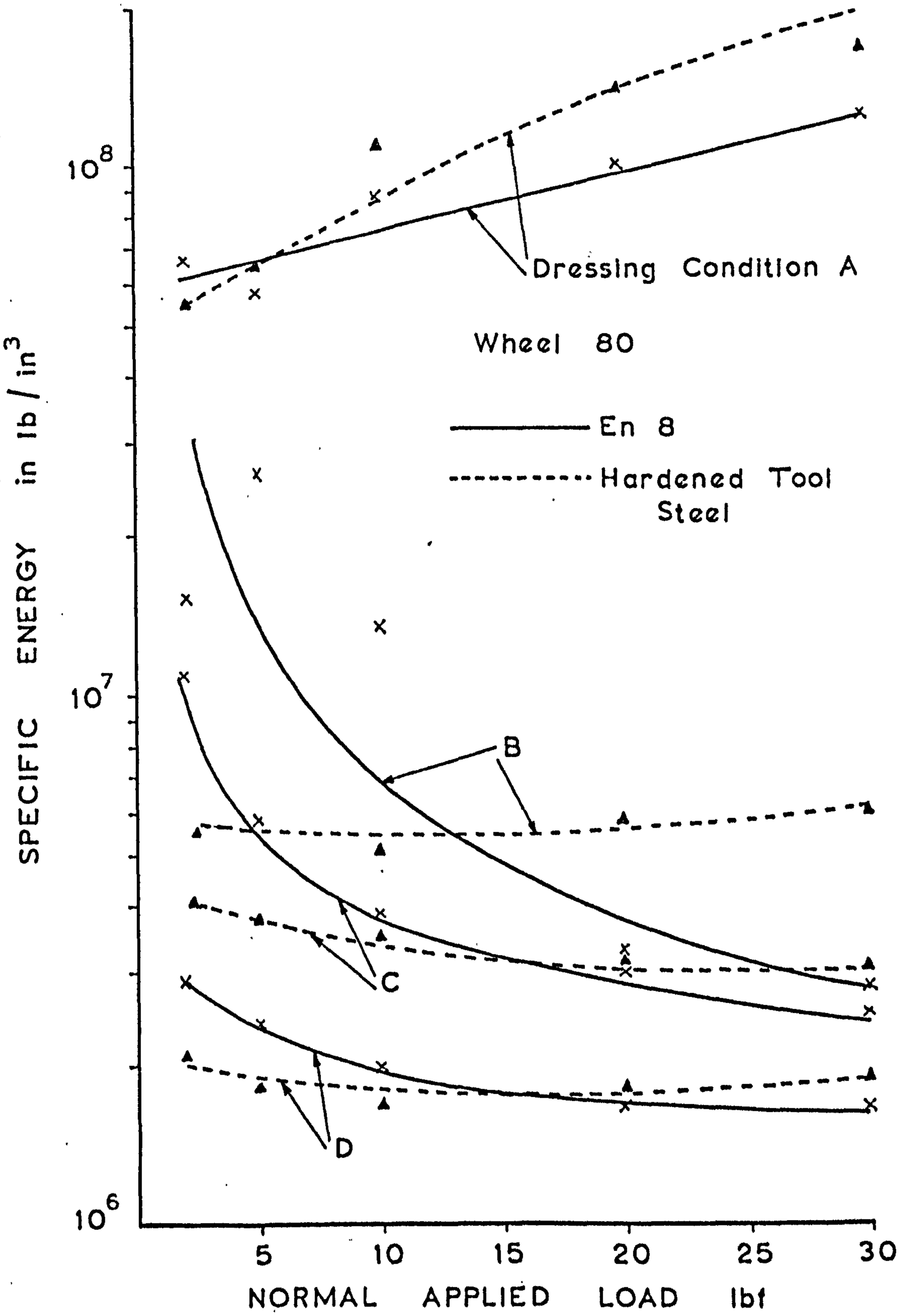

Fig. 90 Effect of Material Hardness on the S.E. Values

5.3.2 EFFECT OF APPLYING GRINDING FLUIDS

All tests were undertaken on the hardened tool steel using an 80 grit size wheel. The results are initially discussed in terms of the general effects, and then later, the more specific effect of lubricant concentration.

(i) GENERAL EFFECT

In terms of the S.E., the general effect of applying a grinding fluid can be seen in Fig. 91. For conditions associated with extensive plastic deformation, i.e., fine dressing and low applied loads, the application of a fluid increases the S.E. However, for coarse dressing conditions and high applied loads where microcutting is predominant, the S.E. is reduced.

The increase in energy for operations characterised by extensive plastic deformation can be attributed to two main effects:-

a) A hydrodynamic effect. Since it has already been established that under these conditions, the normal load supported by contacting grits is small, a hydrodynamic pressure generation at the wheel-test piece interface could cause a marked reduction in the grit penetration with a corresponding increase in S.E. The effect has already been observed by Hahn[53], when investigating the influence of cutting fluids on an internal grinding operation. The fact that grinding wheels can support hydrodynamic loads has also been demonstrated by Baul[74] when investigating a technique for applying fluids to the grinding zone when using high cutting speeds. In the present tests, the hydrodynamic effect has probably been

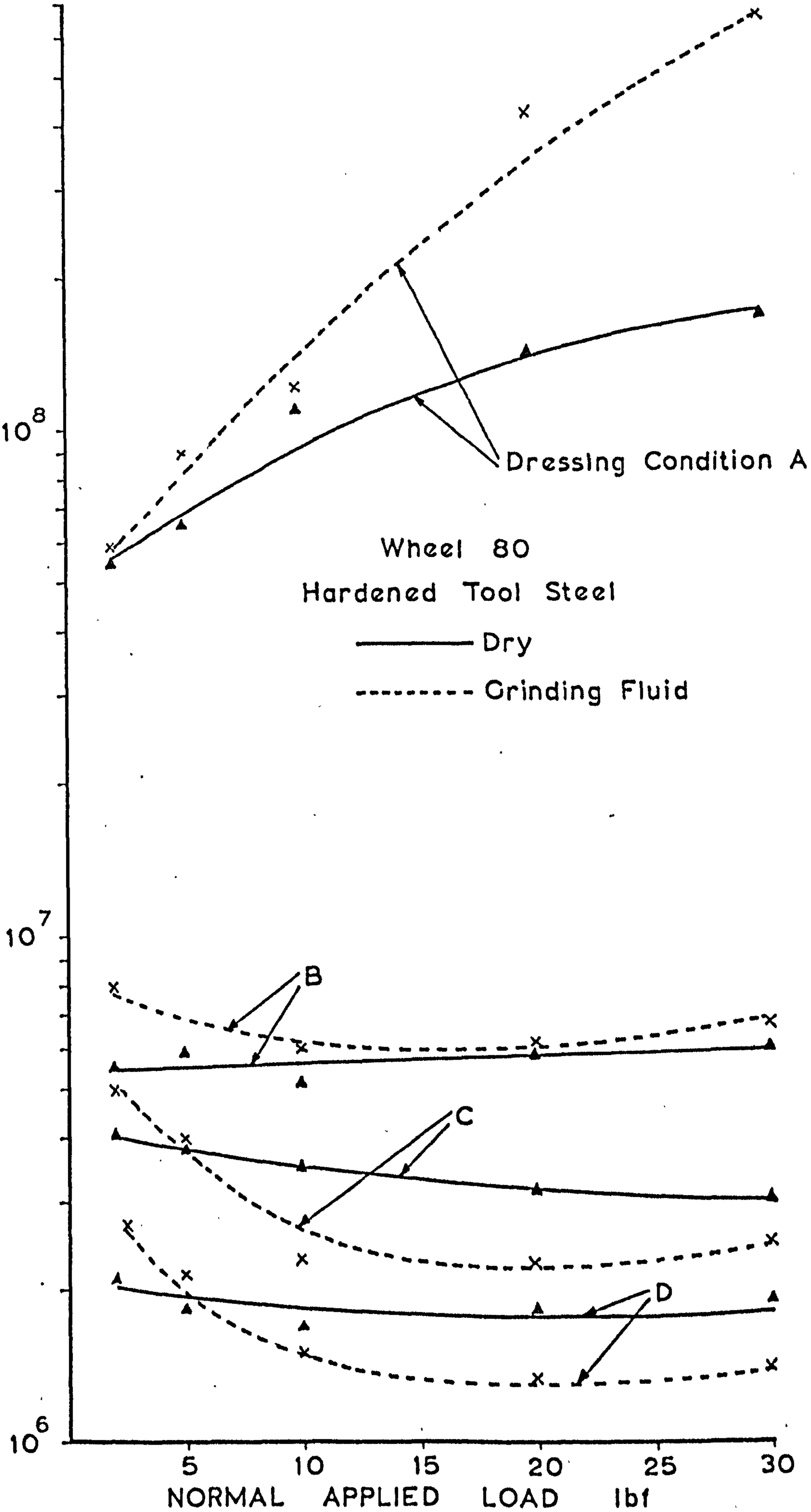

Fig. 91 The General Effect on S.E. Values of Applying a Grinding Fluid

exaggerated on account of the large area of conformity between wheel and test piece. Nevertheless, as grinding speeds are increased, it is anticipated that there will not only be a problem in transporting the fluid to the cutting zone, but also in overcoming the decrease in grinding efficiency due to considerable hydrodynamic effects.

b) A lubricating effect. The application of a lubricant to the grinding zone will cause a decrease in the true molecular coefficient of friction between the abrasive grits and test piece. In the previously discussed slow speed tests undertaken by Kragelskii[26] (Section 2.2.1) a reduction in friction was seen to increase the transition depth between plastic deformation and microcutting. This effect would also explain the experimental results since an increase in the transition depth would automatically be accompanied by an increase in S.E. It was considered beyond the scope of this project however, to obtain evidence to support Kragelskii's initial hypothesis.

Evidence of the above two effects is given in Fig. 92 where the $^{T}/_{N}$ ratio is plotted as a function of time for the wheel dressed in the fine condition, A. The $^{T}/_{N}$ values are seen to decrease with the application of a fluid, indicative of both a reduction in friction and grit penetration.

The observed decrease in S.E. when fluid is applied to operations where microcutting is the predominant mode of metal deformation, can be explained in terms of a reduction in the abrasive wear. As grinding proceeds, the cutting ability of individual grits gradually deteriorates as the edges become worn or dulled. The

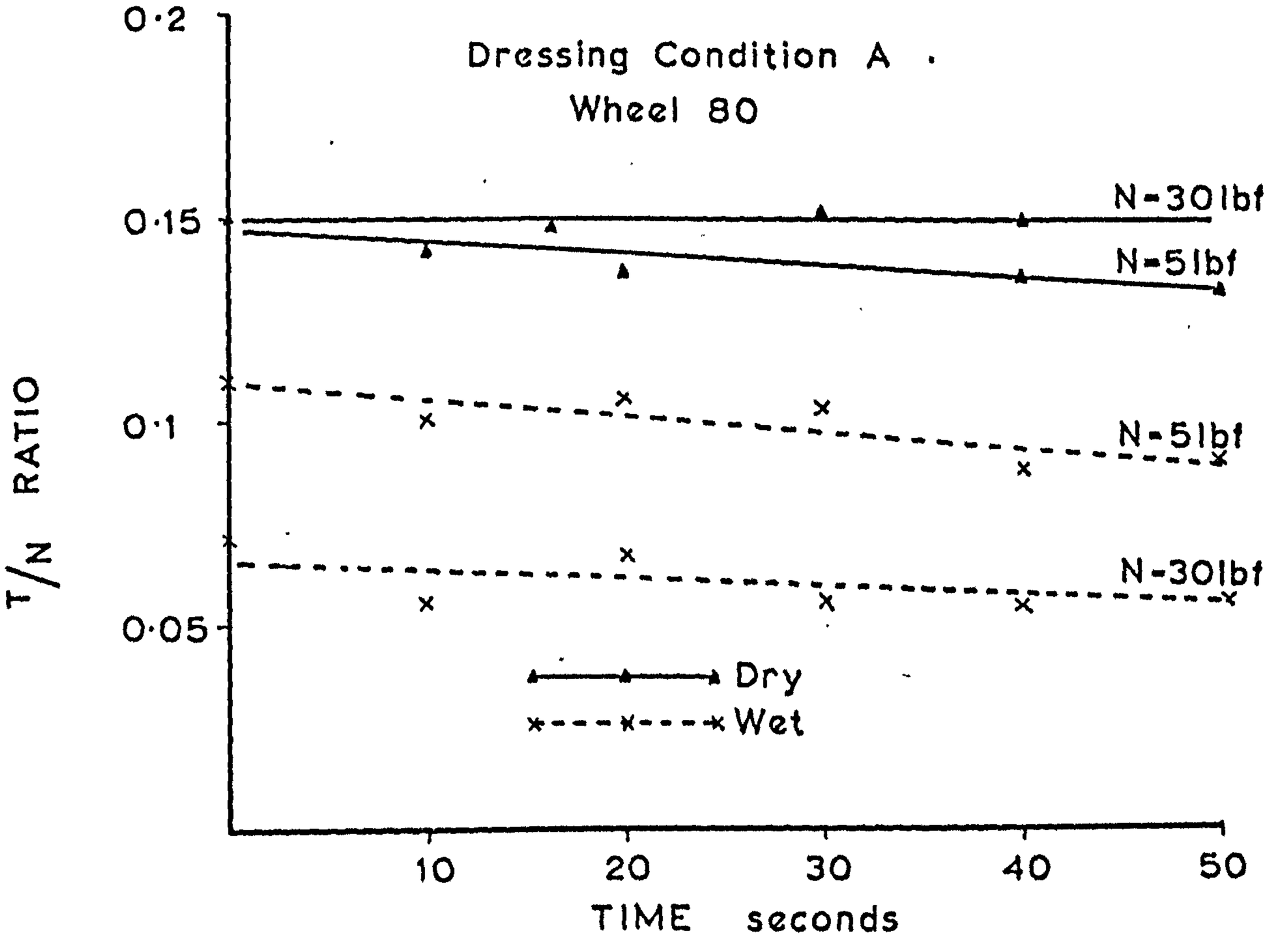

Fig. 92 Effect of Grinding Fluids on $^{T}/_{N}$ Ratio

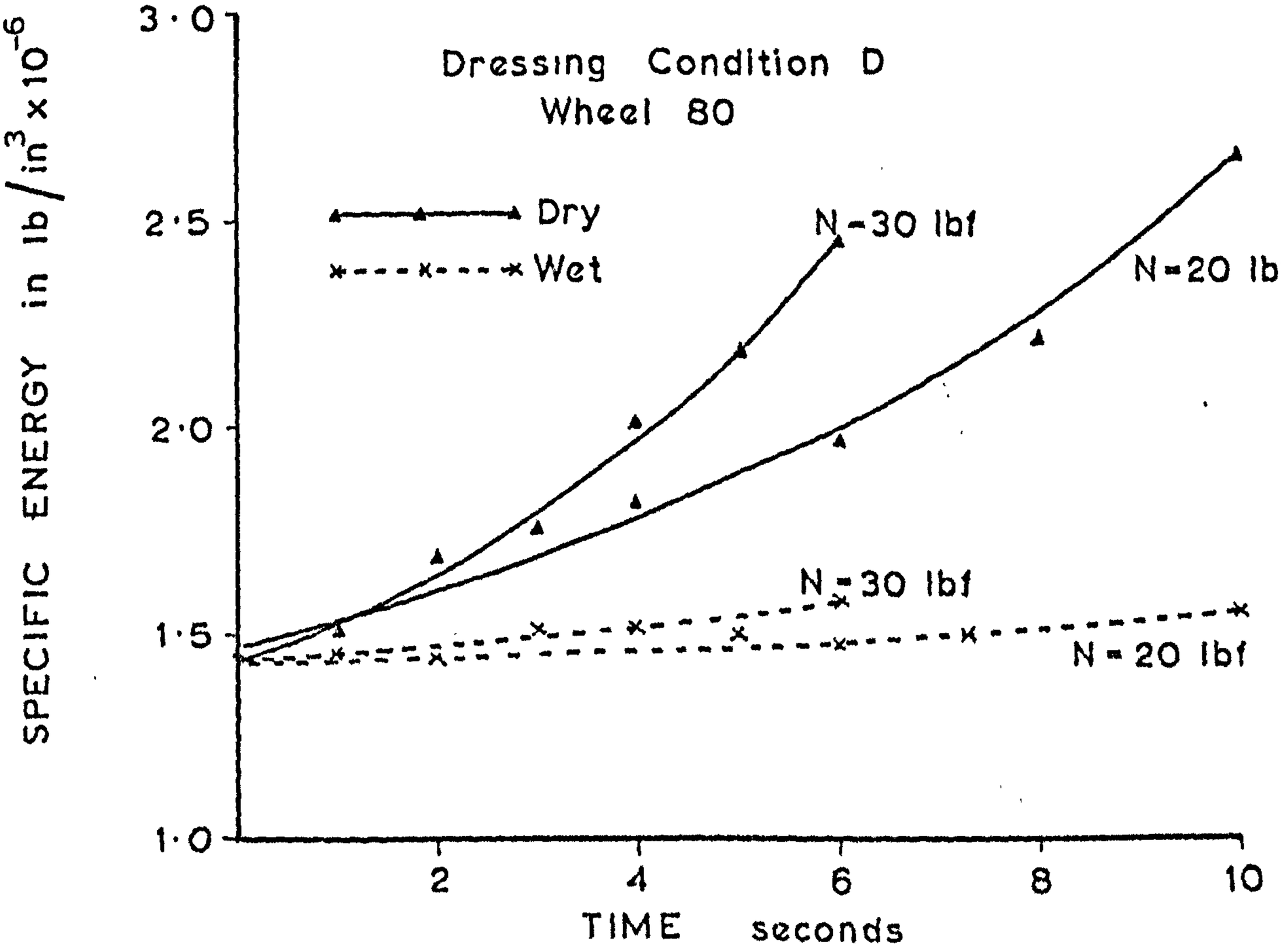

Fig. 93 The Reduction in the Rate of Increase in the S.E. with Time when Grinding Fluids are Applied

application of a grinding fluid preserves these edges by a combined lubricating and cooling effect (as discussed in Section 2.3.4). Thus, the rate of increase in S.E. with time, caused by the loss of cutting ability should be reduced when a fluid is applied. This is confirmed by the results presented in Fig. 93 where the S.E. is given as a function of time for the wet and dry conditions.

It can be assumed that when operating within the microcutting regime, the hydrodynamic and transition depth effects applied to plastic deformations are negligible.

(ii) EFFECT OF LUBRICANT CONCENTRATION ON S.E.

Considering the previous discussion on the general effects of grinding fluids, it seems reasonable to assume that an increase in the lubricating properties of a fluid will again have two different effects, depending on operating conditions. With predominantly ploughing mechanisms, the detrimental hydrodynamic and transition depth effects are increased with an increase in lubricant concentration. This is evident from the decrease in the $^{T}/_{N}$ ratio with lubricant concentration when using fine dressing conditions (Fig. 94). The S.E. also increases as seen from the energy values associated with low applied loads (Fig. 95).

On the other hand, with predominantly microcutting operations, an increase in the lubricant concentration results in a decrease in S.E. (Fig. 95). The energy curves suggest that there will be some optimum lubricant concentration depending on dressing conditions and applied load, i.e., on the mode of metal deformation. This agrees in principle with the work of Furuchi et al[62] who suggested that the optimum concentration is a function of dressing conditions.

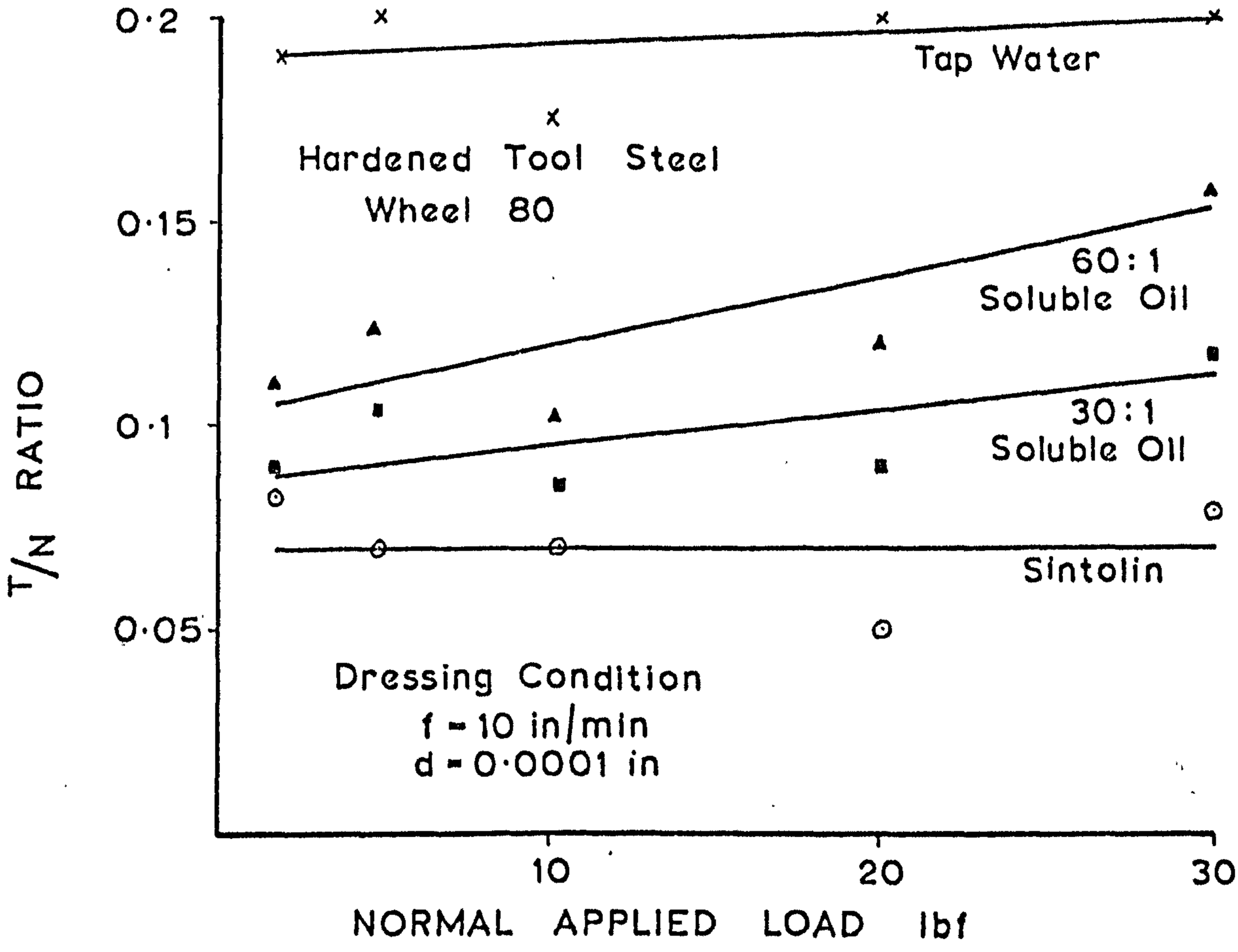

Fig. 94 Effect of Lubricant Concentration on the $^{T}/_{N}$ Ratio

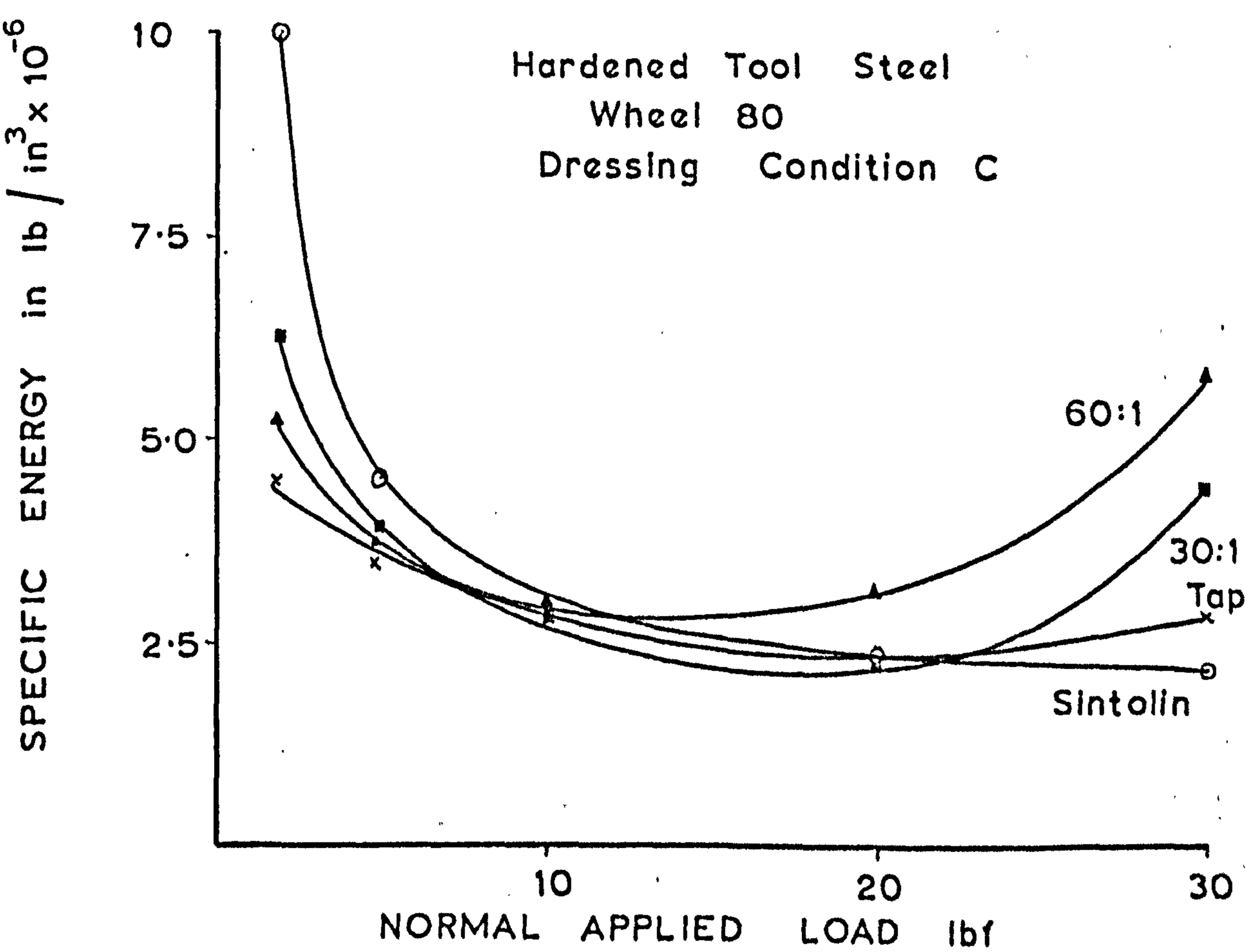

Fig. 95 Effect of Lubricant Concentration on the S.E.

The characteristic U-shape of the energy curves obtained when using Shell Dromus D soluble oil is also of interest, the rise in S.E. with increasing applied loads being an indication of the comparative failure of the lubricant properties at high pressures. In contrast, the continued down trend of the Sintolin curve demonstrates the effectiveness of an E.P. additive when operating at high pressures.

NOTE: The anomalous behavior of tap water at high values of applied load (Fig. 95) was caused by bulk thermal softening of the test piece due to intensive frictional heating.

5.3.3 MEASUREMENT OF ABRASIVE WHEEL WEAR

The interpretation of the S.E. values obtained during the previous tests has been assisted by initial measurements of the abrasive surface topography. During the discussion on the grinding fluid tests however, it was indicated that the S.E. steadily increased as the grinding operation proceeded. This was attributed to a gradual wearing of the abrasive grits causing a progressive loss in cutting ability. The complexity of this wear process has already been discussed in Section 2.3.3, and in order to study the process in detail, an accurate measurement of the change in abrasive surface properties as grinding proceeds is an obvious requirement. Although a detailed investigation of this problem was considered beyond the scope of this project, the application of the measurement techniques developed in Chapter III is now briefly discussed.

As already indicated, appreciable wear rates cannot be obtained with the present strip grinding operation. Thus, in order to induce a measurable amount of wear, the unorthodox grinding of tungsten carbide was considered. As would be expected using a 23A 80-K5-VBE wheel, the abrasive surface rapidly deteriorated with virtually no stock removal. In Chapter III it was shown that the probability density function and the power spectrum were two significant properties of the abrasive surface, and are consequently used here.

Fig. 96 shows the change in pdf as grinding proceeds for the operating conditions N = 20 lbf, Dressing condition A. The scanning depth was 1×10^{-3} in. relative to the newly dressed wheel, the stylus remaining stationary as wear proceeded. The measurements were carried out using the exponential averaging mode, the meaningless zero probability being omitted from the figure. As expected, the newly dressed wheel shows a high probability at the outermost levels of the wheel surface. At t = 30 seconds however, this probability peak has moved to the left, the distance 'x' being a measure of the radial wheel wear. The peak has also increased in amplitude, signifying an increase in the concentration of height ordinates at the outermost level. This can be directly attributed to the development of wear flats on the abrasive grits. At t = 1 min. the picture has changed completely. The outermost probability peak has decreased in amplitude, this being accompanied by a general increase in probability over the lower height range. This suggests that the surface now displays a wide variety of amplitudes and has effectively increased in roughness. This change in surface properties indicated by the pdf measurements agrees in principle with previous observations

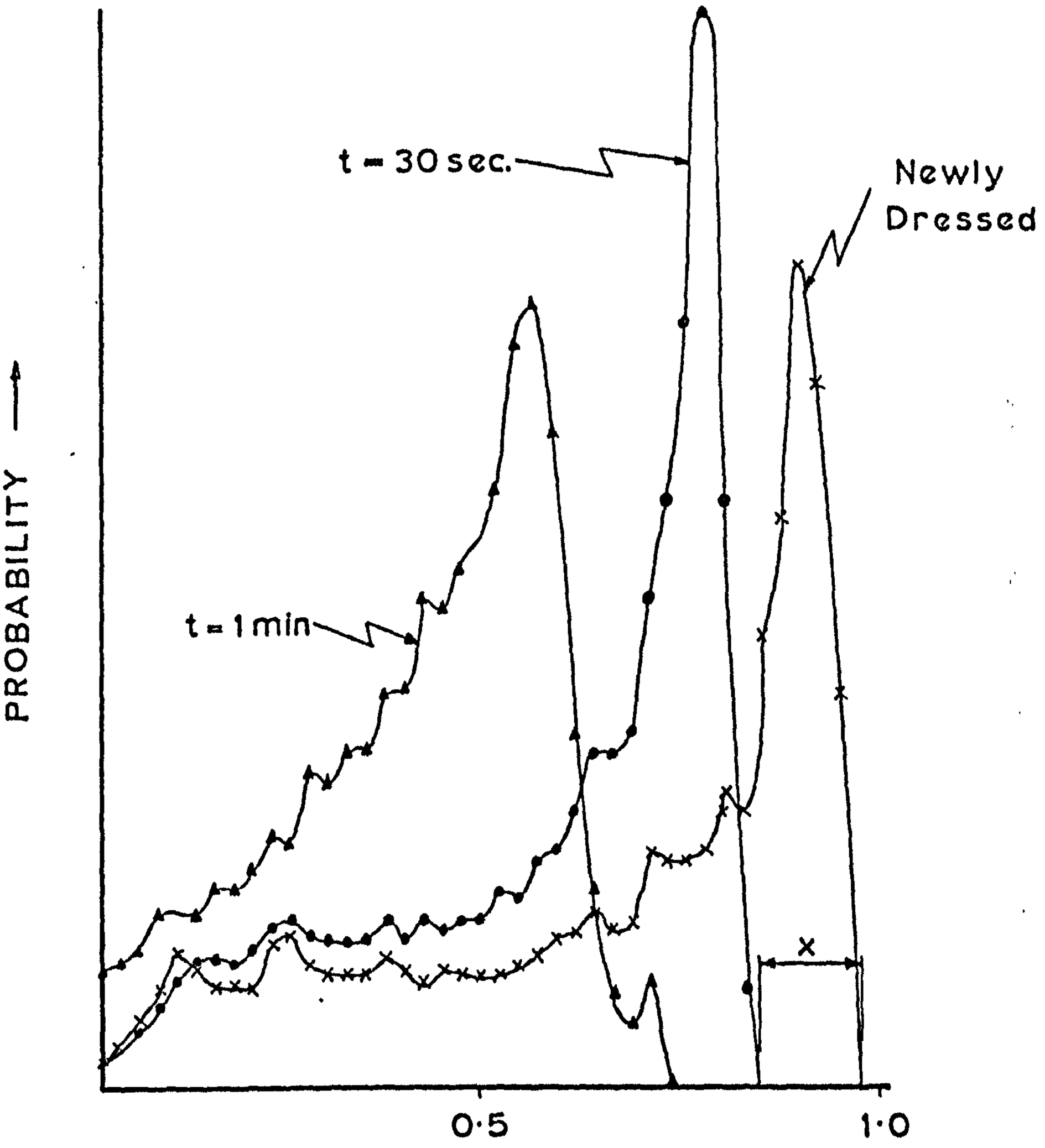

Fig. 96 Effect of Abrasive Wear on the Probability Density Function

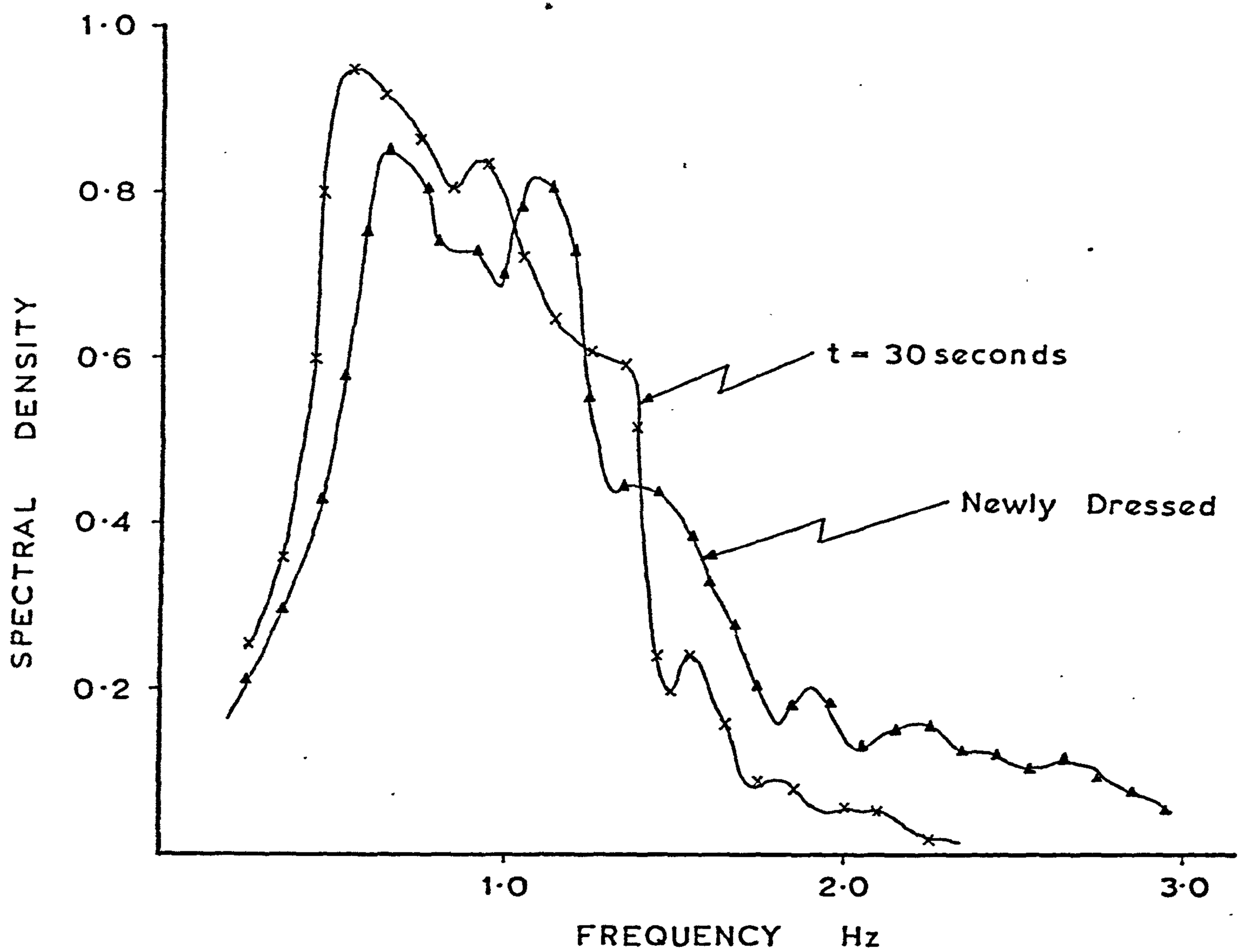

Fig. 97 Effect of Abrasive Wear on the Spectral Density

on severe breakdowns of this type. Extensive wear flats are known to develop causing an increase in both the force on the grain and the heat input to it. A rapid deterioration then occurs, as a combination of mechanical and thermal stress fracture mechanisms causes grains to break away from the wheel surface.

The change in surface properties as described above is also reflected in the power spectrum measurements. The variation in total power of the profile as a consequence of the radial wheel wear is indicated by a change in area under the S_y curve. The change in power with frequency is demonstrated by the spectral density functions shown in Fig. 97 where the reduction in higher frequency components with time signifies the development of wear flats.

Because of experimental limitations, the above wear process was unavoidably severe and not representative of normal wear rates. There would appear to be no reason however, why the pdf and power spectra measurements could not be used with considerable success in the analysis of more practical wear processes.

5.4 CONCLUSIONS

The basic mechanics of a simple controlled force plunge grinding system have been investigated with particular reference to the influence of abrasive surface topography resulting from the initial wheel specifications, superimposed dressing conditions, and the normal applied load. The experimental data was again discussed in terms of the two well established grinding parameters, viz., the specific energy

and the grinding ratio ($^{T}/_{N}$). It was found that the dressing conditions, grain size, and applied load all influenced the resultant S,E. values, although the effect of grain size was secondary to the other two. The S.E. was seen to decrease with an increase in both the severity of the dressing operation and the normal applied load. The effect of grain size was not straightforward and depended to a large extent on dressing conditions. The material hardness was also secn to exert a considerable influence on the energy consumed.

The above variations in energy with operating conditions were attributed to changes in the dominant mode of metal deformation, high energy values being associated with extensivo plastic deformation, low energies with microcutting. The reasons for these changes were explained by considering thc indivldaul abrasive grit - test piece interactions. The abrasive surface topography measurements of Chapter III were first consulted to establish the likely geometry of the groove formations, mainly in terms of the width to depth ratios. The experimental findings of Chapter IV were then used to determine the probable mode of metal deformation, and hence the energy consumed. Thus, although during a grinding operation all modes of metal deformation will occur simultaneously, by adopting the above procedure, the effects of different operating conditions can be determined in terms of a general swing towards either the high energy consuming plastic deformation or the low energy microcutting.

The influence of cutting fluids upon the S.E. was seen to depend on the dominant mode of metal deformation. On applying fluid to operations characterised by extensive plastic deformation, the

energy was seen to increase. With predominantly microcutting operations however, the energy decreased. Further tests related to the influence of lubricant concentration suggested that in terms of a minimum energy consumption, an optimum concentration will exist depending on operating conditions.

Although the results have provided valuable information regarding the mechanics of metal grinding, it is important to realise the limitations of this simplified process when drawing conclusions regarding the more conventional grinding operations. In these tests, the test piece was held stationary resulting in small grain depths of penetration. This tended to extend the range of conditions over which large scale elastic and plastic deformations occurred and the S.E. values were correspondingly high. This is evident from the maximum value of the grinding ratio obtained during the tests (0.2), which is considerably less than the values obtained in normal practice. It is therefore suggested that for future work, whilst still maintaining the concept of a controlled force process, a more practical grinding operation should be considered.

In the introduction to this project it was stressed that modern grinding practice could only be improved by a more detailed understanding of the metal removal process. To this end, the different modes of metal deformation occurring in grinding have been identified, and the influence of various operating factors upon these modes considered. From a practical point of view however, the successful prediction of the likely mode of metal deformation is not sufficient. The deformation must then be related to the important process parameters

such as workpiece surface finish, quality of the surface, dimensional accuracy, rate and nature of the abrasive wear, etc. In experimental terms, this may simplify to a straightforward determination of the relationship between the S.E. and the above mentioned parameters. (On the subject of abrasive wear, suitable measurement techniques have already been indicated) Such investigations would undoubtedly provide a valuable intermediate stage before undertaking the more complex studies relating to the interdependence of process parameters, e.g., the correlation between abrasive surface profile and workpiece surface.

CHAPTER VI

THE COMPUTER SIMULATION OF A SIMPLIFIED CONTROLLED FORCE PLUNGE GRINDING OPERATION

This chapter is concerned with a computer simulation of the previously discussed controlled force metal strip grinding operation. A simple mathematical model of the process is established which incorporates the results of the earlier surface topography and simulated abrasive grit investigations. Although the exact reproduction of the complex wheel workpiece interaction by means of a simple model is unlikely, it has been shown that the effect of different process parameters upon the mechanics of the grinding operation can be predicted with reasonable accuracy. These parameters include the dressing conditions, the normal applied load, and the grain size.

This theoretical work was initiated so as to bring together the earlier experimental sections of the project in an attempt to substantiate as far as possible the conclusions already drawn.

6.1 ESTABLISHING THE MODEL

6.1.1 PRELIMINARY ASSUMPTIONS

i) The abrasive wheel surface is assumed to consist of idealised rigid spheres, the radii, spacing and height distribution of these spheres being functions of the initial wheel specifications and dressing conditions.

ii) The workpiece is considered isotropic and homogeneous, and is characterised by a metal flow pressure, p, determined from a straightforward hardness test using a spherical indentor.

iii) The effect of elasticity in the wheel - workpiece system is neglected.

iv) Consideration is given only to the plastic and microcutting modes of metal deformation.

v) The effect of a continual deterioration in the cutting profile as a result of abrasive wear is neglected.

6.1.2 GENERATION OF THE ABRASIVE SURFACE

The general configuration of the strip grinding operation is given in Fig. 98. The strip is seen to conform to the wheel surface and hence the apparent area of contact between wheel and workpiece is equal to the cross-sectional area of the strip. The important assumption is now made that the wheel - workpiece behaviour can be determined by considering the instantaneous contact of the strip with a segment of the wheel surface bounded by the strip perimeter (shaded area, Fig. 98). Such a segment is shown in Fig. 99.

The abrasive asperity radii are assumed constant and equal to the nominal grain radii as reported by Baul[69]. The spacing and height distributions of the grits are assumed to be dependent on the grain size and the dressing conditions as discussed in Chapter III. The distributions are also assumed to be constant in the axial and circumferential directions and are determined in the following manner:-

i) Grit spacing

The grits are assumed to be equally spaced at a distance, s (Fig. 99)

For the fine dressing condition, A, the grits are considered

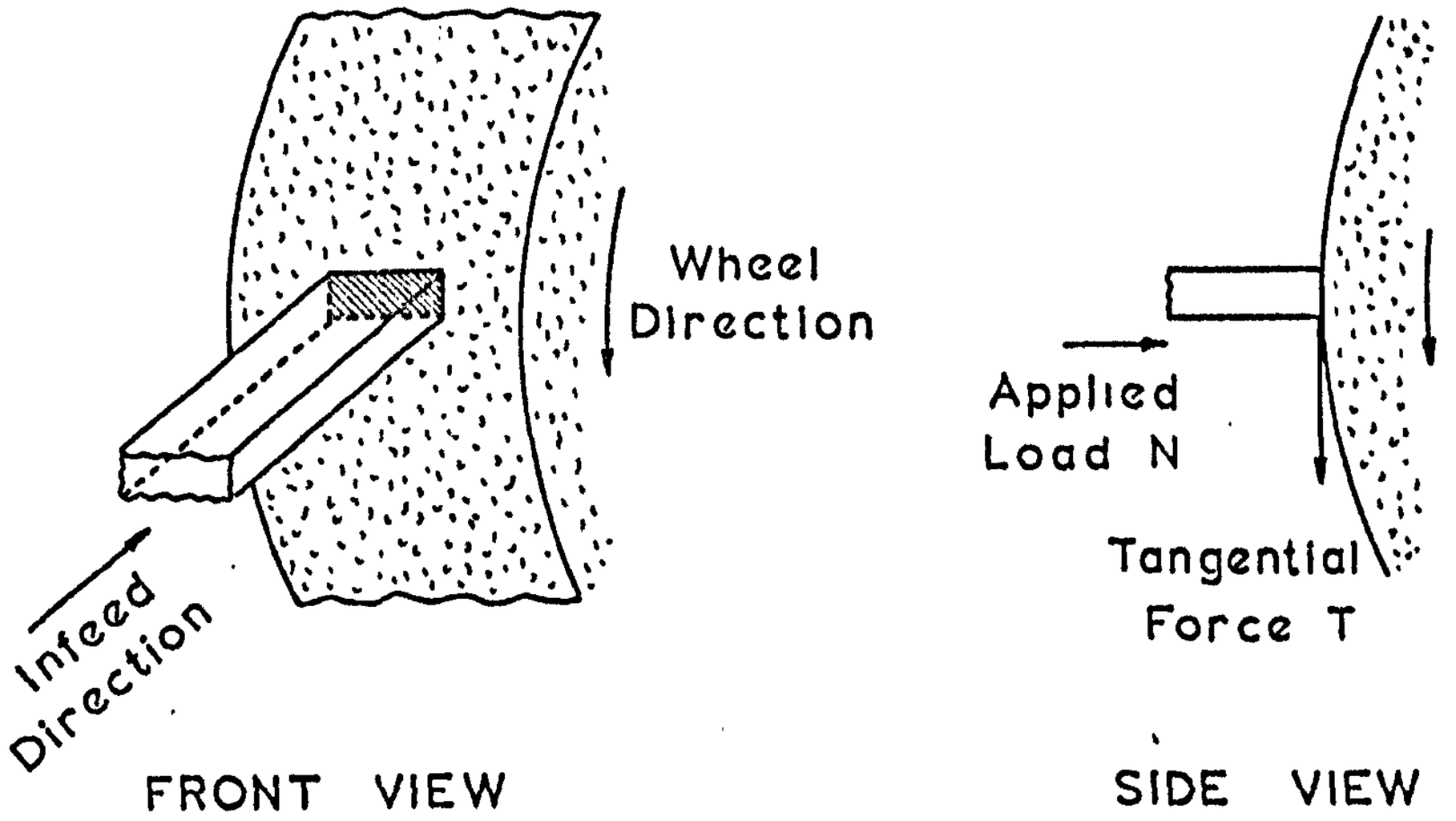

Fig. 98 The Strip Grinding Configuration

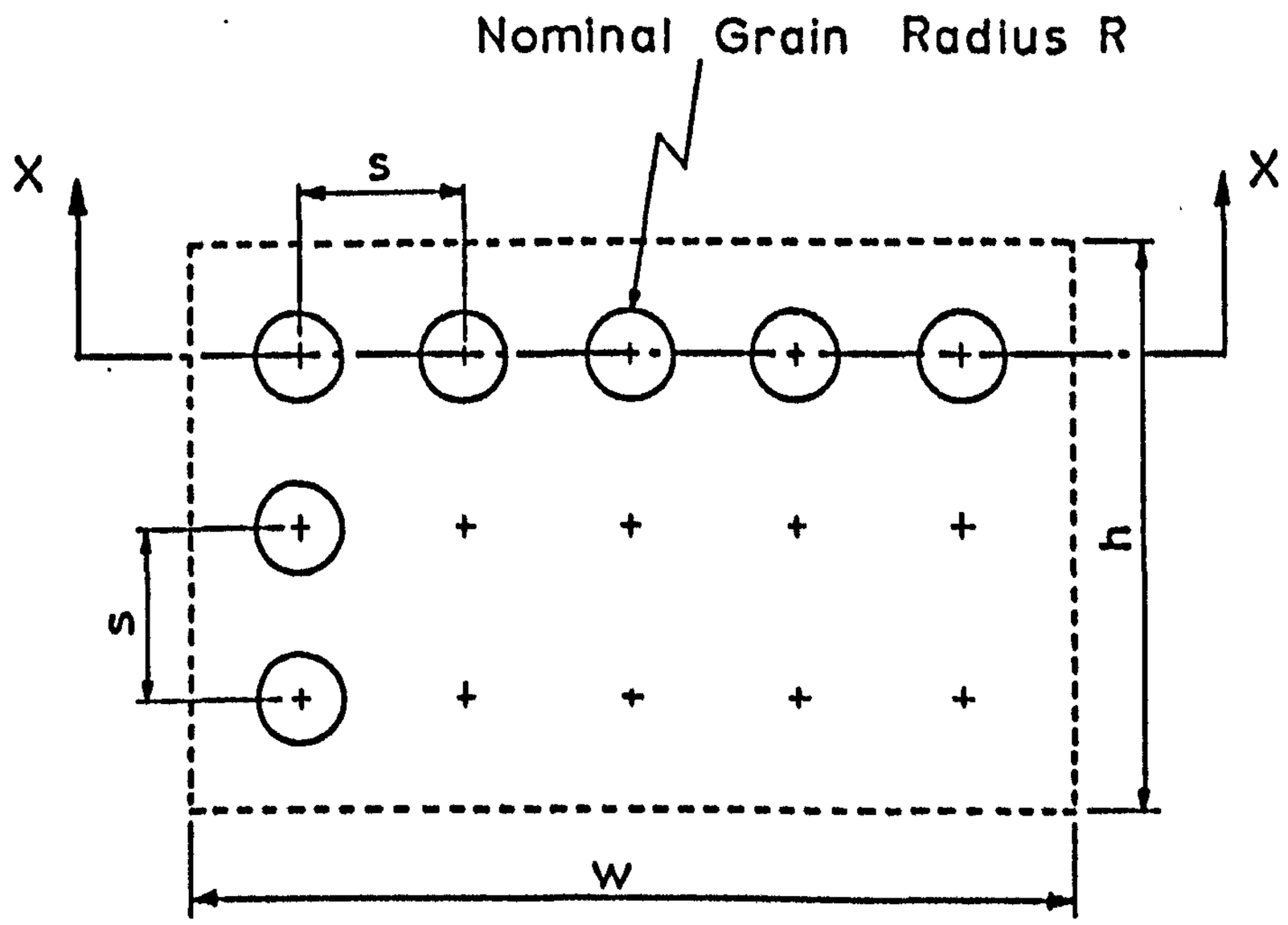

Fig. 99 Simulated Abrasive Surface

to be spaced at intervals of s = nominal grain diameter. This gives the total number of potential cutting edges, n, = $(\frac{w}{2R} \times \frac{h}{2R})$
A check on this assumption can be made by considering the experimentally derived values of the percentage spacing, S, (Chapter III) with the theoretical figures, for different scanning levels. Assuming all grits to fall at the same level with the fine dressing condition A, a typical abrasive profile (Section XX Fig. 99) would be as shown in Fig. 100. From Fig. 100;

$$\text{Percentage spacing, } S = 100y/R$$

$$= 100\left(1 - \frac{(2R - \delta)\delta}{R}\right)$$

The theoretical and experimental values of S are shown in Table 3 for different values of δ. (In establishing the model, the behaviour of the 46 wheel is considered, in view of the greater accuracy of the topography measurements resulting from minimal stylus distortion.)

TABLE 3

WHEEL 46

SCANNING DEPTH, δ in x 10^3	S (theoretical)	S (experimental)
1	50.3	49
2	32	32
3	20	25

As can be seen, the agreement between experiment and theory, assuming s = 2R, is extremely good.

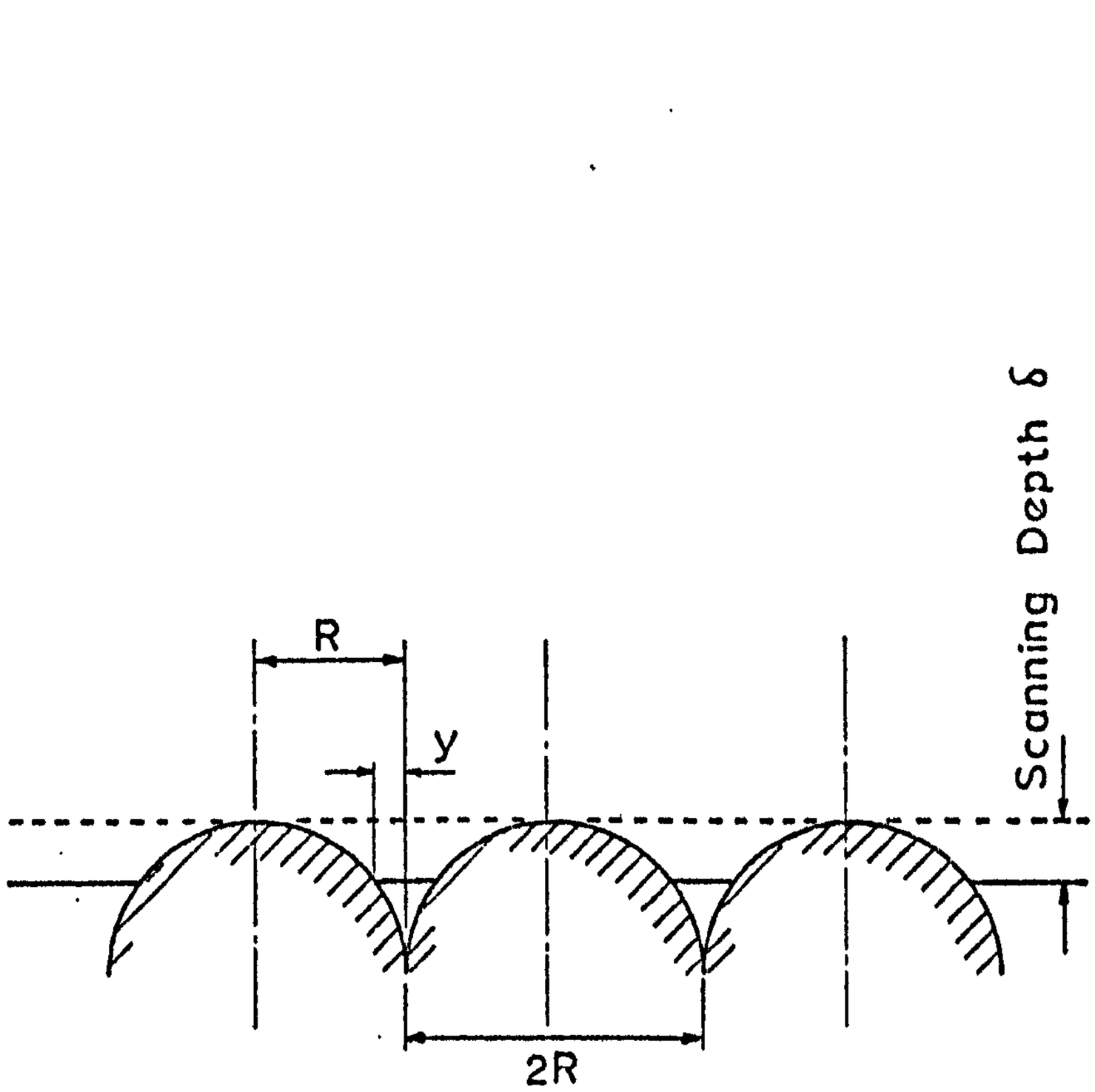

SECTION ON XX (Fig. 99)

Fig. 100 Simulated Abrasive Profile

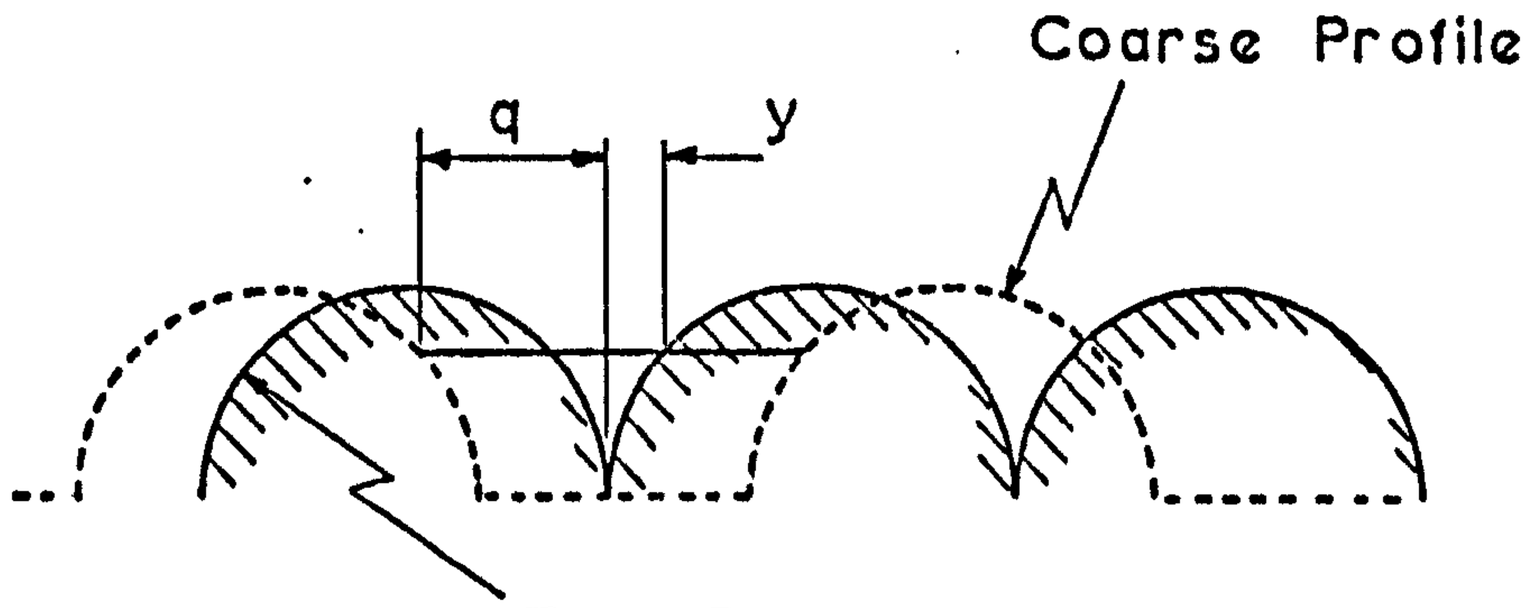

Fig. 101 Simulation of an Increase in the Severity of the Wheel Dressing Conditions

For coarser dressing conditions, the value of s is adjusted according to the experimental values of the percentage spacing, S. Let the value of S for dressing condition, A. be S_1. Then if the percentage spacing for a coarser condition is given by S_2, in Fig. 101,

$$q = \frac{S_2}{S_1} \times y$$

and the size of the roughness array, N, is $n = \frac{wh}{4(R + q - y)^2}$

Table 4 gives the size of the roughness array for the different dressing conditions (Wheel 46).

TABLE 4

DRESSING CONDITION	A	B	C	D
SIZE OF ROUGHNESS ARRAY, n	264	203	156	110

The above derivation of n assumes that the increase in S with coarser conditions is mainly a consequence of grits being fractured from the surface. In practice, S may also vary because of changes in the height distribution of the existing grits. However, the assumption does permit the simulation of the observed decrease in potential cutting edges with coarse dressing conditions as reported by Tsuwa[51] and Pattinson et al[15].

ii) Height distribution

The peak height distribution of the simulated grits is assumed to be equal to the overall height ordinate distribution as determined by the earlier pdf measurements of Chapter III. The heights are generated using a continuous random number generator having a discrete distribution corresponding to the experimental

probability measurements. The method of generating such numbers using a digital computer is outlined in Appendix C1. To illustrate the procedure a simple example is also given.

To summarise, the abrasive topography is completely defined in terms of the following parameters:-

a) The number of abrasive grits, n, constituting the roughness array

b) The peak height distribution

c) The radius of the grits, assumed constant and equal to the nominal grain radius.

NOTE The assumption regarding the spheroidal nature of the abrasive grits is also seen to fulfill the volumetric considerations of the wheel structure. The volumetric proportions of grain and bond, and the porosity, for a 46 wheel of hardness grade K and structure number 5 are:-

Grain = 52%

Bond = 7.5%

Porosity = 40.5%

(Reported by L.V. Colwell from V.J. Yobomudov - Grinding work materials and their manufacture, MASGIS 1953).

In the model, the wheel is assumed to consist of uniformly packed spheres representing the abrasive grains. Consider one grain of nominal radius R:

$$\text{Volume of grain} = \frac{4}{3}\pi R^3$$

For a 46 wheel, $R = 15 \times 10^{-3}$ in.

and Volume of grain $= 1.77 \times 10^{-6}$ cu.in.

Volume of bond $= 0.075 \times (2R)^3$

$= 0.25 \times 10^{-6}$ cu.in.

Volume (grain and bond) $= 2.02 \times 10^{-6}$ cu.in.

$\therefore$ Volume of air $= (2R)^3 - 2.02 \times 10^{-6}$

$= 1.36 \times 10^{-6}$ cu.in.

$\therefore$ Porosity $= \frac{1.36}{(2R)^3} = \underline{\underline{40.3\%}}$ cf. 40.5%

6.1.3 THE MECHANICS OF THE WHEEL - WORKPIECE INTERACTION

Consider the static indentation of the workpice by a single abrasive grit (Fig. 102)

Assuming $d \ll R$

$$r^2 = 2Rd$$

and the normal projected area $A_n = 2\pi Rd$. A simple empirical relationship for the tangential projected area is:- $A_t = 1.32\,rd$

Now consider the contact of the wheel surface and the workpiece as indicated in Fig. 103 (for a typical section XX Fig. 99).

It is assumed that the abrasive grits will penetrate the metal surface until the total normal area of contact, $\sum A_n$, is sufficient to support the applied load, N. In terms of the model, this equilibrium position is determined by adjusting the value of b (Fig. 103) until $\frac{N}{p} = \frac{2\pi R \sum d}{2}$. (The normal area of contact is divided by 2 since it is assumed that when the wheel is rotating, the normal load will be supported on the front half of the grains only)

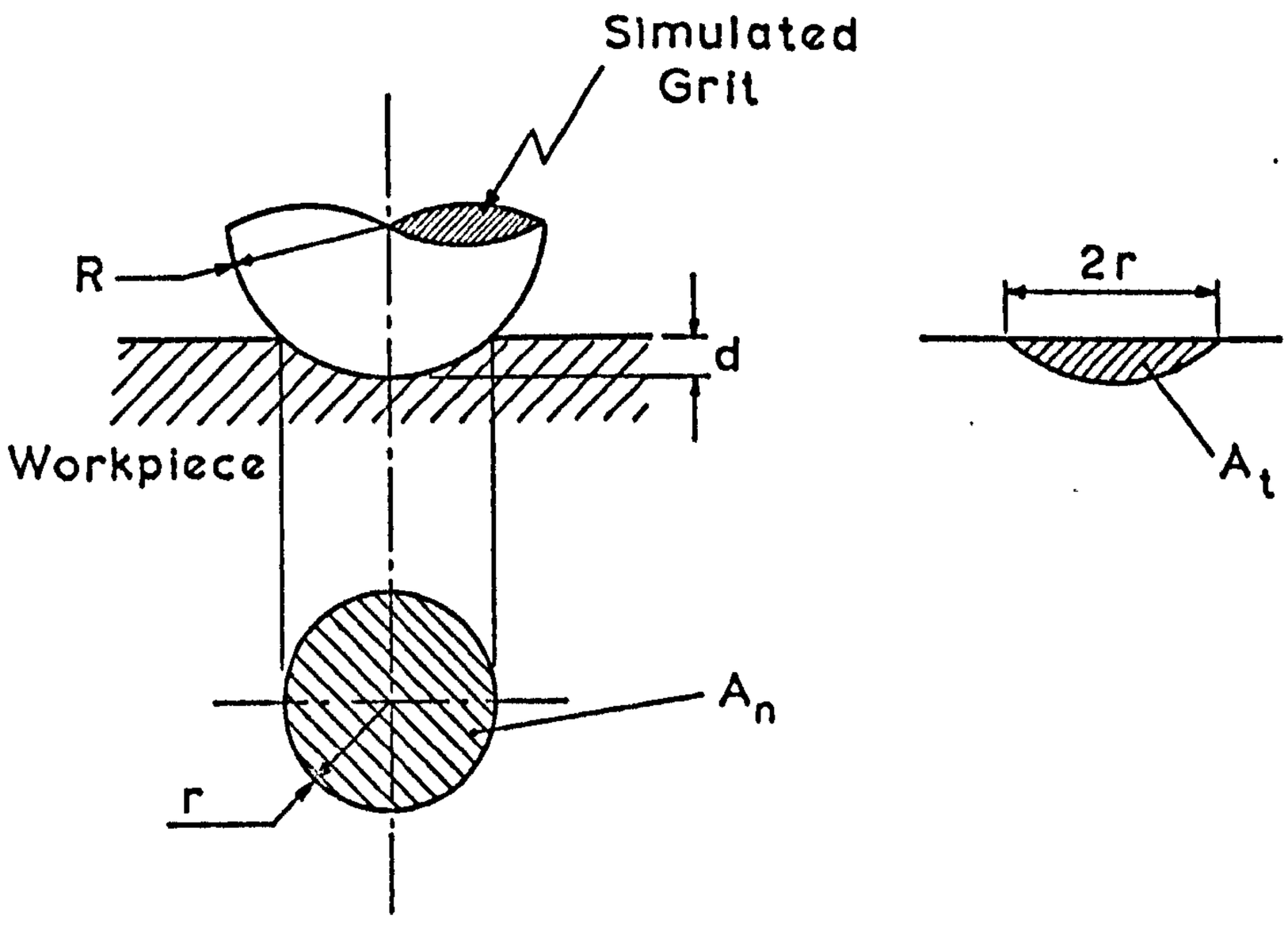

Fig. 102 Indentation of Workpiece Surface by a Spherical Indentor

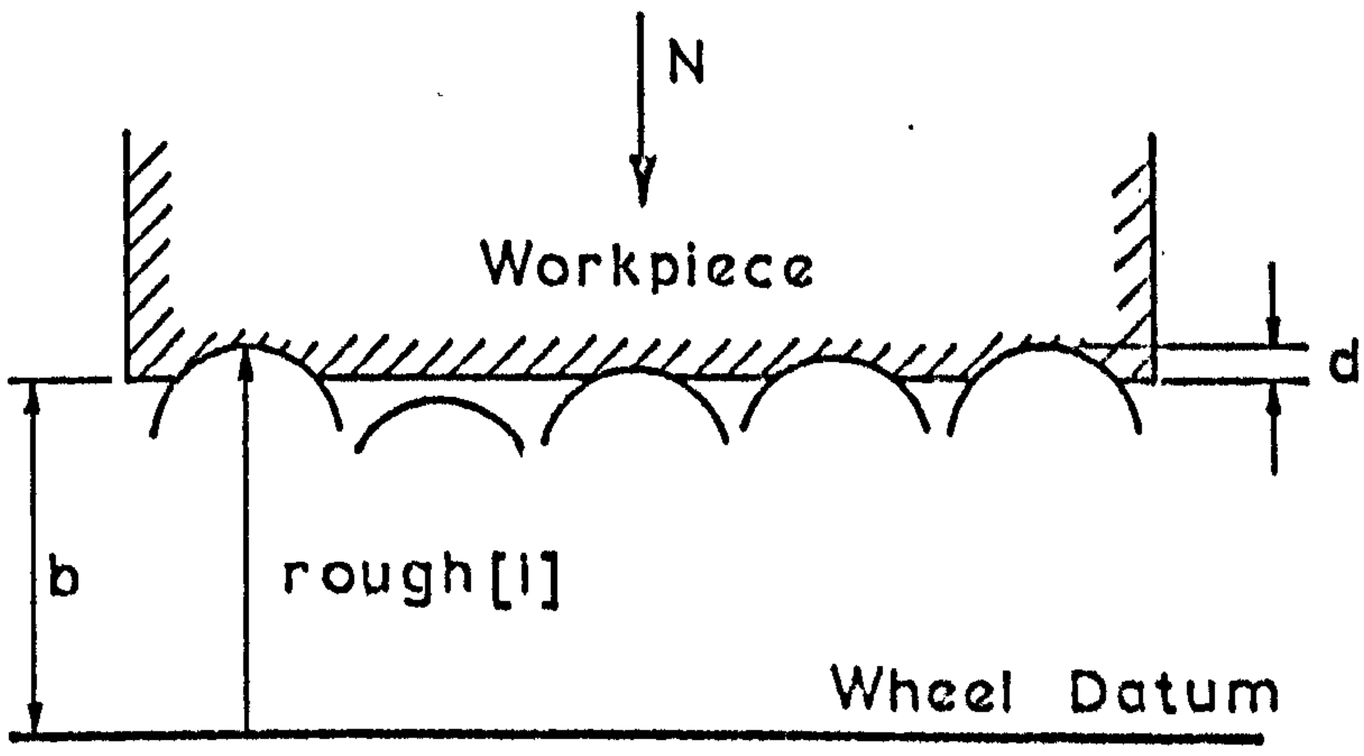

Fig. 103 Simulated interaction of Wheel and Workpiece

By considering the geometry of the individual penetrations, the following parameters can now be determined:-

i) The number of contacts, co

This is a straightforward measure of the number of abrasive grits actively engaged with the workpiece.

ii) The average form factor or groove width to depth ratio

This is an average value of the form factors associated with 'co' individual contacts.

iii) The tangential force, T

This is defined by $T = p\sum A_t = 1.32\, p\,(2R)^{\frac{1}{2}} \sum d^{3/2}$

iv) The infeed velocity, v_i

It seems reasonable to assume that the amount of metal removed by a segment of the wheel length, h, (Fig. 99) will also be a function of the total tangential projected area. Thus the average infeed of the strip may be written as $\sum A_{t/w}$

If the nominal wheel diameter is 12 in. and the wheel speed is 1500 rpm then the time taken to remove $\sum A_{t/w}$ material is given by:-

$$\delta_t = \frac{60}{1500} \times \frac{h}{12\pi} \text{ seconds}$$

For h = 0.125 in.

$$\delta_t = 1.33 \times 10^{-4} \text{ seconds}$$

$$\text{and } v_i = \frac{1.32 \times (2R)^{\frac{1}{2}} \times \sum d^{3/2}}{0.5 \times 1.33 \times 10^{-4}} \text{ in./sec}$$

v) The specific energy S.E.

Having obtained estimates of the tangential force and the infeed velocity, the relationship already applied in Chapter V can be used to determine the S.E., i.e., S.E. = $1.76 \times 10^4 \times T/v_i$ in.lb/in^3

6.2 RESULTS AND DISCUSSION

6.2.1 INITIAL RESULTS

The results reported in this section represent the average of five sets of readings, obtained by considering five consecutive segments of the wheel surface. In practice, the readings did not differ appreciably as seen in the specimen output shown in Appendix C[2]. The simulation is representative of the grinding of EN 8, characterised by a value of $p = 0.3 \times 10^6$ lb/in^2. The results are considered in terms of the effects of dressing conditions and applied load upon the output parameters listed in the previous section. The influence of grain size is discussed later in Section 6.2.3.

i) Number of contacts, co

Fig. 104 shows the variation in 'co' with applied load for the different dressing conditions. In general, an increase in load results in an increase in the number of contacts but the increase takes place at a far greater rate in the case of fine dressing conditions. The number of active grits is seen to increase with a decrease in the severity of the dressing operation. These observations are in keeping with the assumptions made in Chapter V when interpreting the effects of dressing conditions and load upon the specific energy values. In addition, if the number of contacts associated with increased values of N is taken to give an indication of the underlying nature of the wheel surface, the results agree with the findings of Tsuwa[51] and Pattinson[15] concerning the influence of dressing conditions upon abrasive wear.

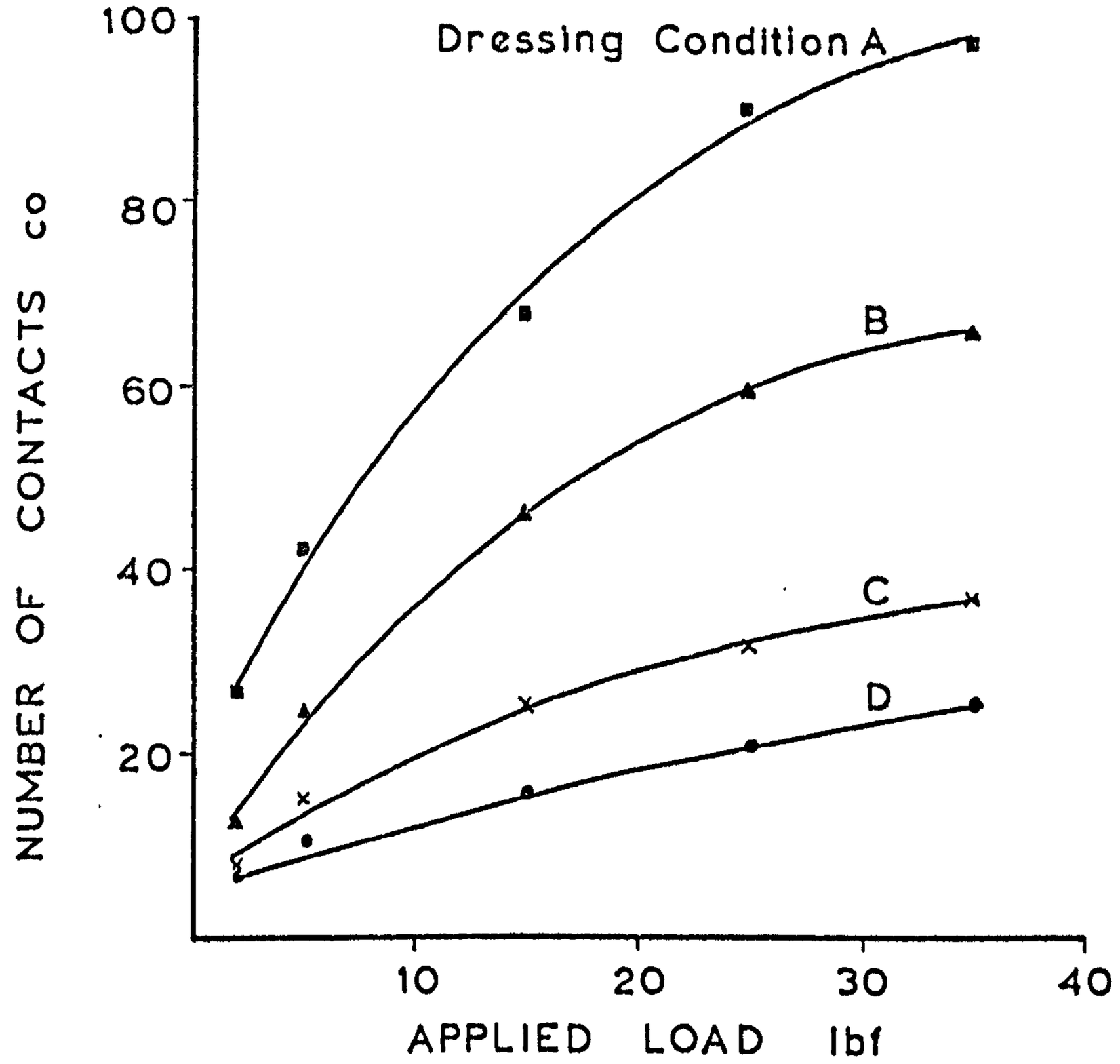

Fig. 104 Number of Grit-Workpiece Contacts

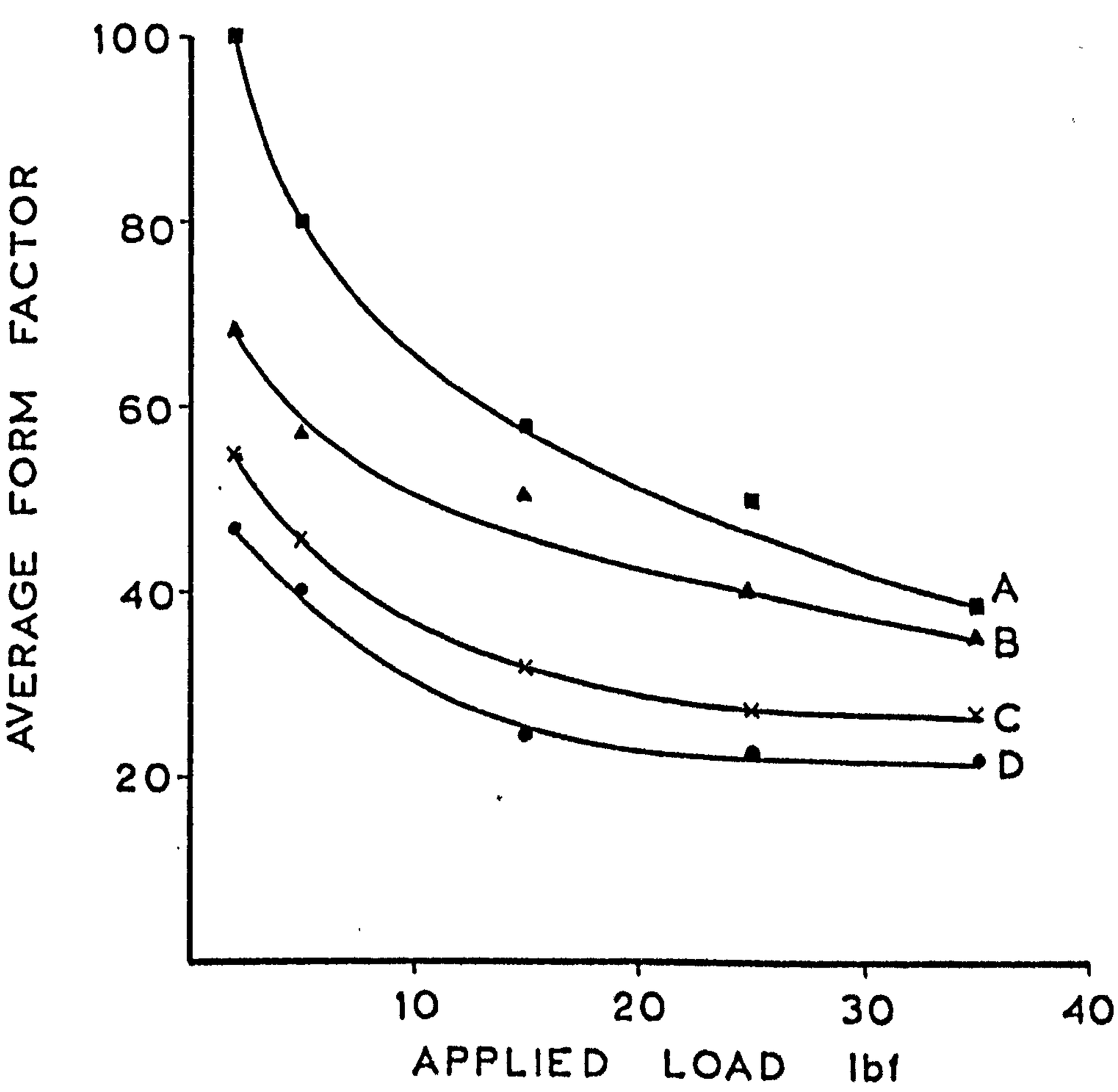

Fig. 105 Average Form Factor Values

ii) Average form factor

The average form factor values are given in Fig. 105. The curves again justify the previous assumptions (Chapter V) regarding the influence of dressing conditions and applied load on the individual form factors. The factor is seen to increase with coarser dressing conditions, this being a direct consequence of the lower density of potentially active grits associated with coarse dressed wheels. The form factor also decreases with an increase in applied load, the curve tending to a constant value depending on the dressing condition. In Chapter V this effect was suggested as a possible explanation for the levelling out of the S.E. curves at high loads (Fig. 65). The effect was attributed to the attainment of an equilibrium as N increases, between the decrease in form factor associated with grits already engaged with the workpiece, and the higher values characteristic of the newly contacting grits. In the case of the model, there is another contributary factor to the shape of the form factor curves, since from geometrical considerations of the abrasive grit alone, the form factor = $f(N^{-\frac{1}{2}})$.

iii) Tangential force, T

The theoretical and observed experimental values of T are given in Fig. 106 (the experimental values being only approximate in view of the poor correlation of T with N as discussed in Chapter V). As can be seen, the curves are in good agreement although this may be somewhat fortuitous in view of the many simplifying assumptions inherent in the model derivation.

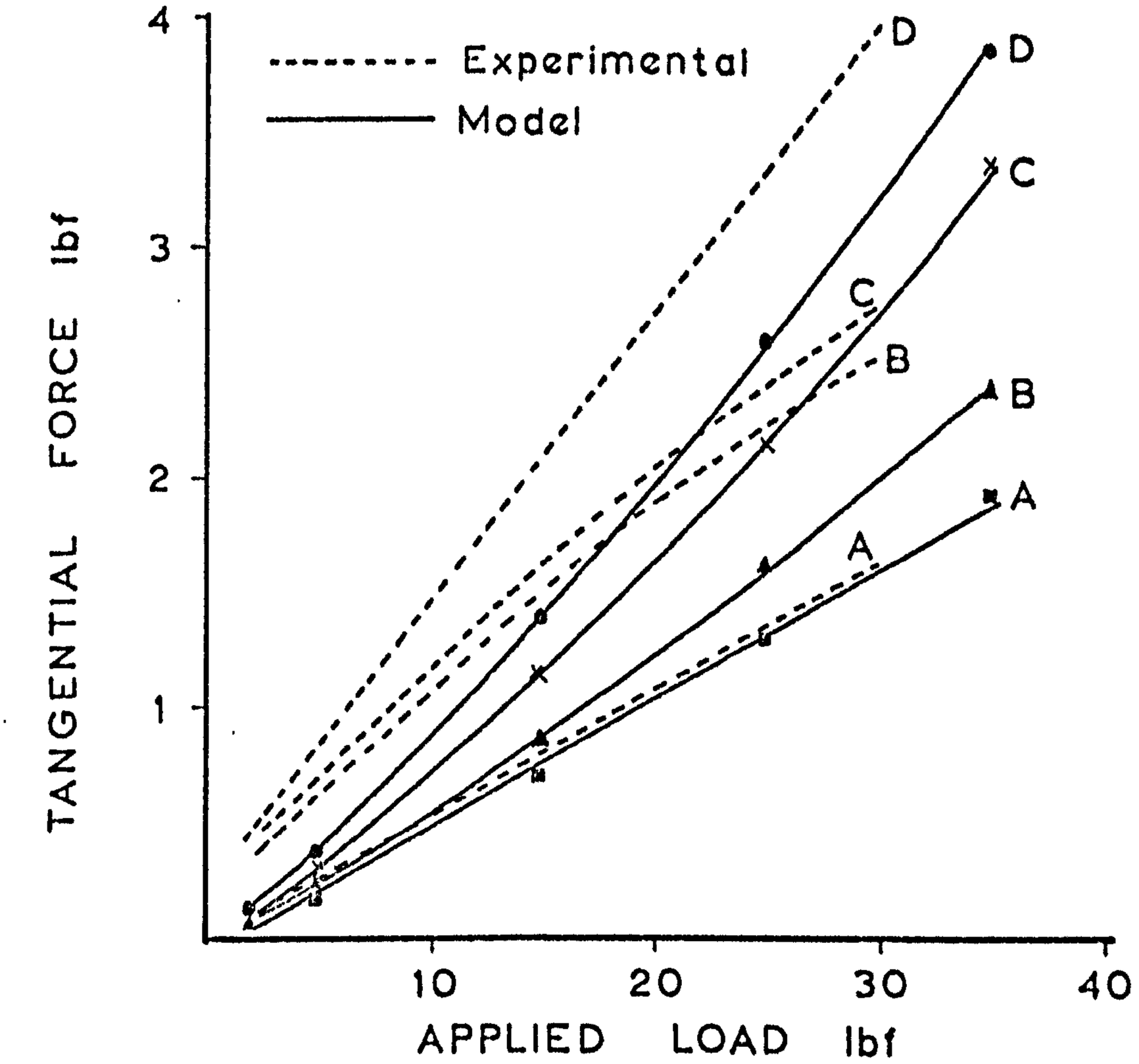

Fig. 106 Experimental and Theoretical Tangential Force Values

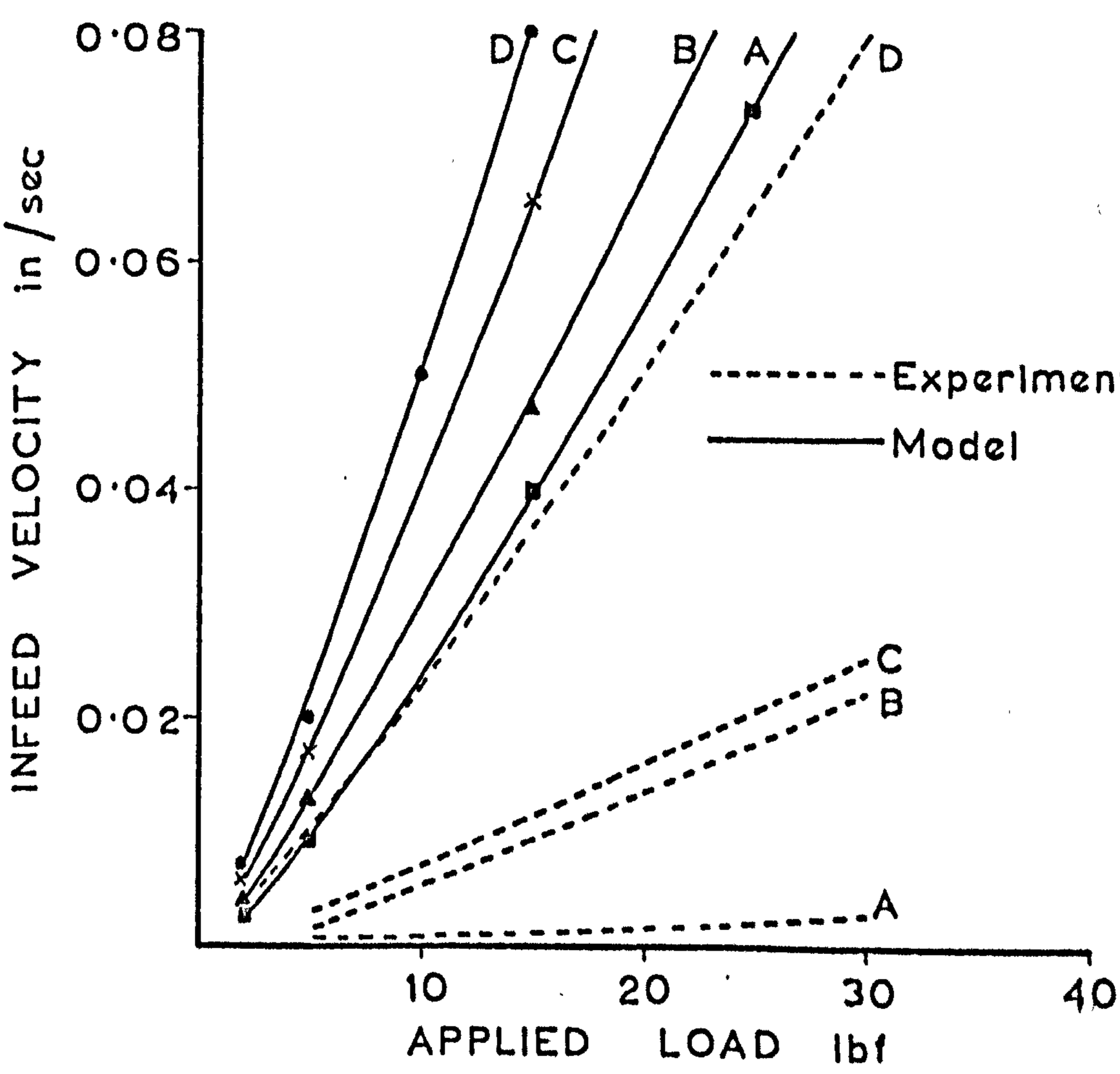

Fig. 107 Experimental and Theoretical Infeed Velocity Values

iv) Infeed velocity, v_i

Model and experimental values of the infeed velocity, v_i, are shown in Fig. 107. The model values are seen to be far in excess of the experimental results which suggests a fundamental error in the model derivation of v_i.

v) Specific Energy, S.E.

Since by definition S.E. = $f(\frac{T}{v_i})$, and from the model,

$T = f(\sum d^{3/2})$ and $v_i = f(\sum d^{3/2})$

S.E. = constant

For $p = 0.3 \times 10^6$ lb/in^2, S.E. = 0.35×10^5 in.lb/cu.in.

This result is in sharp contrast to the experimental results of Chapter V where the S.E. was found to be strongly dependent on the normal applied load and wheel dressing conditions.

In view of the failure of the model to predict the above effects, the derivation of the S.E. expression was reconsidered.

6.2.2 MODIFICATIONS TO THE MODEL

The investigation into the metal removal by simulated abrasive grits (Chapter IV) has shown that the resultant S.E. is influenced by the following factors:-

i) The effective rake angle of the abrasive grit

ii) The size effect

iii) The impact speed

iv) Material hardness

v) The actual mode of metal deformation resulting from a combination of the above effects.

In this case, effects iii) and iv) can be neglected since the simulation is concerned with the grinding of one material, viz., EN8 at constant speed. However, effects i) ii) and v) may influence the S.E. to a considerable degree and cannot be disregarded.

The results of the previous section have shown that the major discrepancy between the model S.E. predictions and the observed experimental values is due to the considerable error in the infeed velocity estimates. This may be caused by neglecting, in particular, the mode of metal deformation, since extensive plastic deformation will result in only a small amount of material being physically 'removed' from the surface. On the other hand, microcutting could be expected to produce high infeed rates. Hence it was decided to consider the mode of metal deformation in the following manner.

The important conclusion has already been drawn that the mode of metal deformation associated with individual grit - workpiece contacts is largely a consequence of the geometry of the interaction. In the case of the simulated spheroidal tools of Chapter IV, as R increased, a transition from microcutting to plastic displacement was observed in the region $R = 0.02$ in. Since $d = 0.001$ in., an equivalent critical form factor can be derived equal to 12.5. In the model, the form factor of each individual interaction is examined and compared with some critical factor, cff. If the form factor is less than 'cff' then microcutting is assumed to occur. Alternatively, if the factor is greater than 'cff', plastic displacement is the assumed mode of metal deformation, the metal being displaced without actual removal. The effect of this is then simulated by not including the tangential projected area of that particular interaction in the general expression for the infeed velocity.

In the simulation, the value of cff was adjusted until the predicted S.E. values were in the same range as the experimental results. This was finally accomplished with a cff value of 30. The reason for this figure being much higher than the observed value of 12.5 lies in the original assumption that the wheel surface consists of idealised spheres of radius 0.015 in. This tends to inflate the range of form factors above those obtained in a practical grinding operation, since in reality, some grits in the wheel surface will undoubtedly possess small cutting radii which will interact with the workpiece to give individual grooves characterised by low form factor values. It is obvious when the speed of the wheel is taken into account, that only a few microcutting interactions would be required per revolution to produce a measurable infeed velocity.

NOTE 1. The expression for the tangential force associated with an individual interaction, i.e., $T = pA_t$ was also re-examined, by applying the relationship to the spheroidal tool data of Chapter IV. Fig. 108 shows the theoretical and experimental values of T plotted against groove cross-sectional area for the tool R = 0.02 in. interacting with aluminium alloy at a speed of 750 ft/min. (R = 0.020 being the nearest value to the model equivalent of 0.015 in.) As can be seen, $T = KpA_t$ where K is a constant considerably greater than unity. This difference is due mainly to the work hardening and frictional effects, etc., not previously considered. (Related work on slow speed tests in the fields of friction and wear has shown K to lie typically in the range 1 to $10^{(26)}$) It can be seen also, that K is not

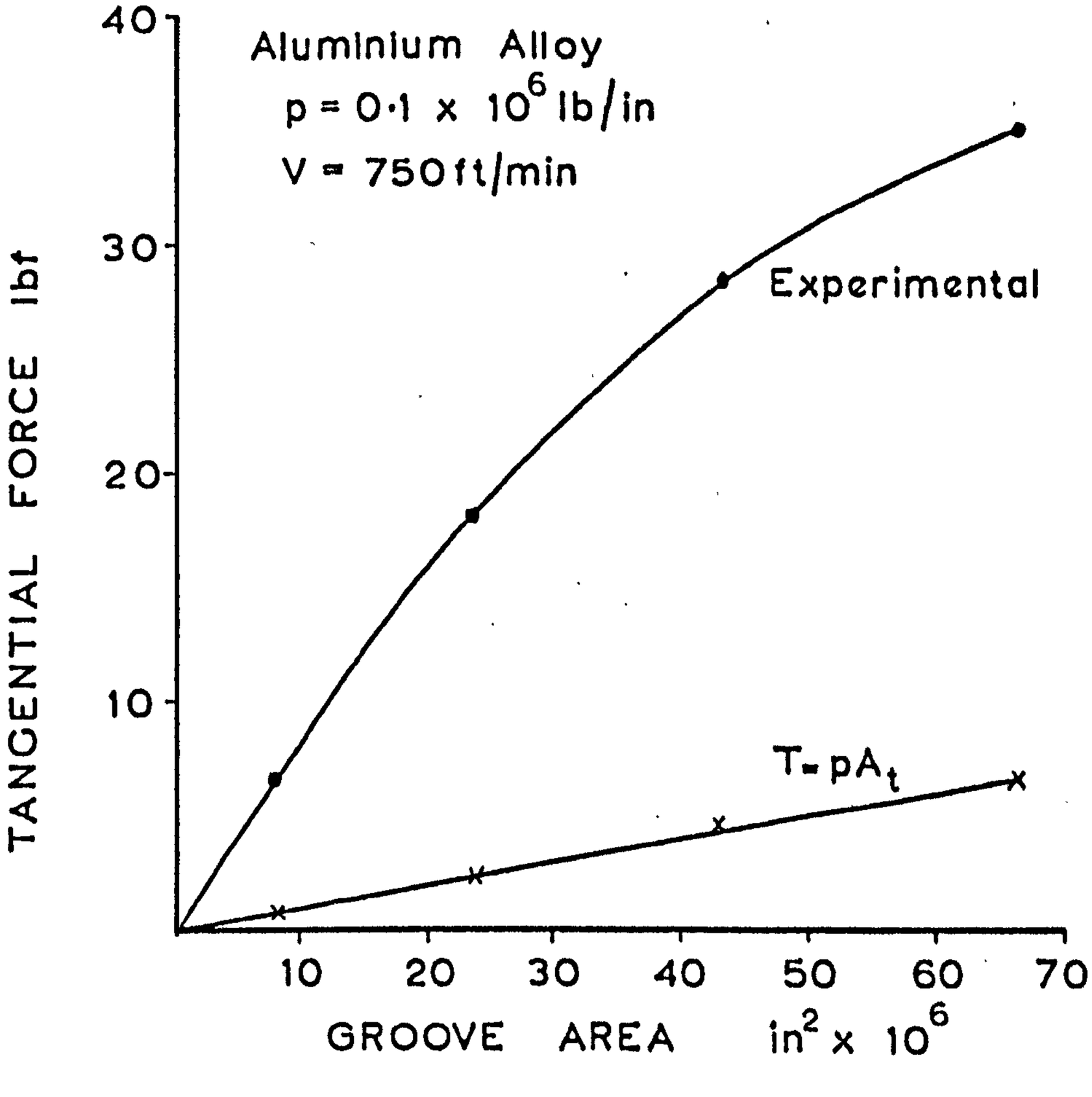

Fig. 108

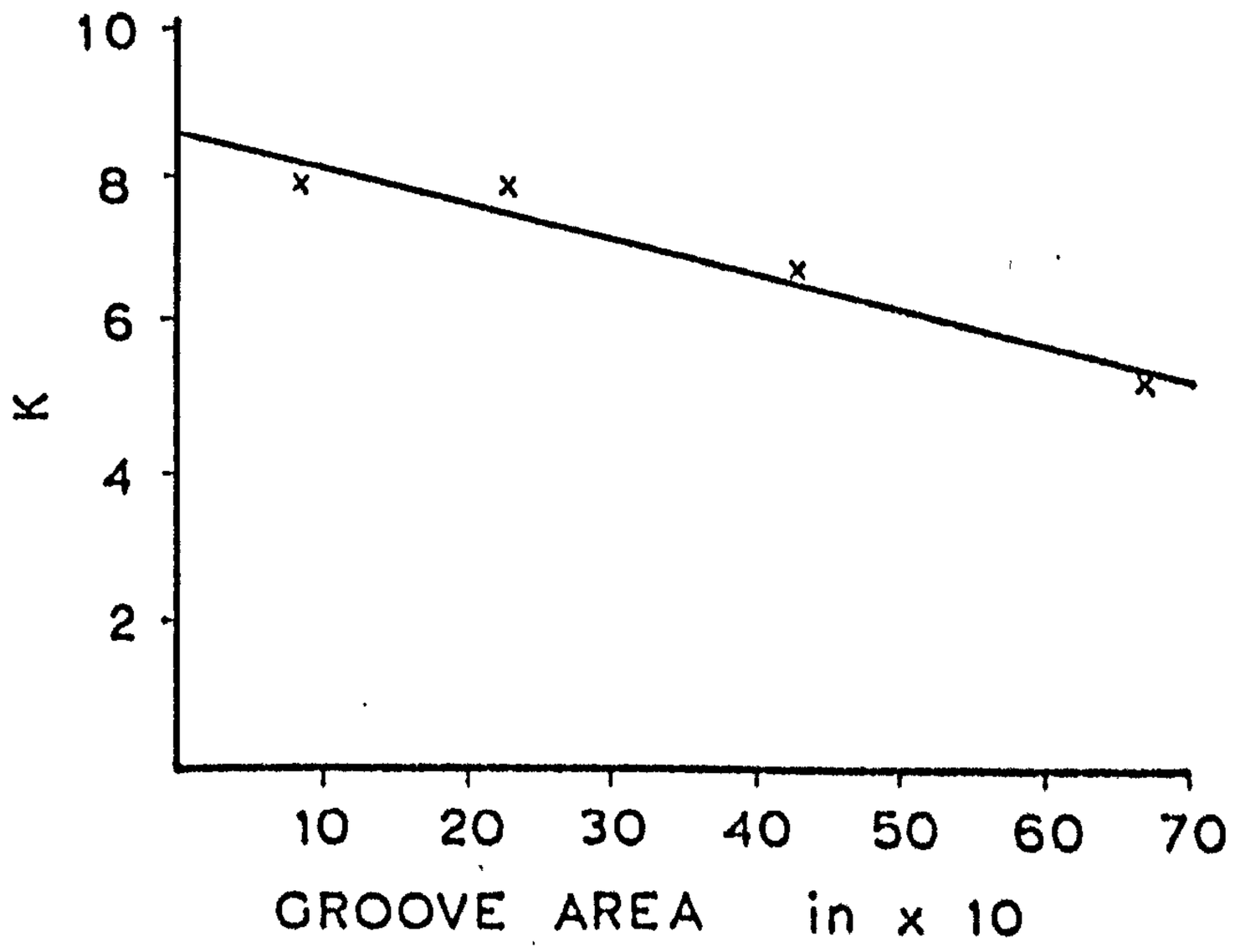

Fig. 109

constant and depends on the groove area as a result of the size effect. However, an approximate value of $K = 8.5$ can be obtained by plotting K against the groove area (Fig. 109) and assuming a value when the area is extremely small, as in practice. This value is then further modified by introducing a speed factor to compensate for the lower speed of the single point data. This was derived from Fig. 65 and effectively reduced the value of K to 2.5.

$$\text{Thus } T = 2.5\, p\, A_t$$

$$= 0.75 \times 10^6 A_t$$

2. The assumption that the normal applied load is effectively supported on only the front half of the simulated grits was also checked using the previous single point data. Table 5 gives the experimental and theoretical ($N = pA_{n/2}$) values of N for the test discussed in Note 1.

TABLE 5

GROOVE AREA $in^2 \times 10^6$	N(experimental) lbf	N(theoretical) lbf	K
15.7	17.5	1.57	11
31.8	34	3.18	10.7
47	42.5	4.7	9
62	60	6.2	9

The range of values of K compares favourably with those obtained in the tangential direction suggesting the relationship for N to be satisfactory.

6.2.3 FINAL COMPUTED ENERGY VALUES

A copy of the final program is given in Appendix C2 together with a typical output for the conditions stated.

The complete set of energy values is shown in Fig. 110. As can be seen, the predicted values are in remarkably good agreement with the experimental results. (Dressing condition A is not shown since, in this case, the individual form factors are always greater than the critical form factor thus giving an infeed velocity of zero and an infinite energy comsumption) The reproduction of the dependence of S.E. on the applied normal load and the wheel dressing conditions has two important implications. Firstly, the results reaffirm the conclusion that the S.E. in a practical grinding operation is very much a function of the mode of metal deformation. Secondly, the results would indicate that the mode of deformation is primarily a function of the abrasive surface topography.

In Fig. 111 the S.E. values for the 80 grain size wheel are shown relative to the 46 wheel for the same critical form factor of 30. As seen, the model fails to predict the observed decrease in energy with increased grain size associated with coarse dressing conditions. (Fig.87 and discussed in Chapter V) The results do not support the argument based on topography which was presented in Chapter V as a possible reason for this effect. However, although the more open structure of the wheel could be an explanation as also suggested in Chapter V, the effect may be due to the 'size effect' since the cross-sectional area of the individual grooves was seen to be much smaller in the case of the 80 wheel. Possible evidence for this

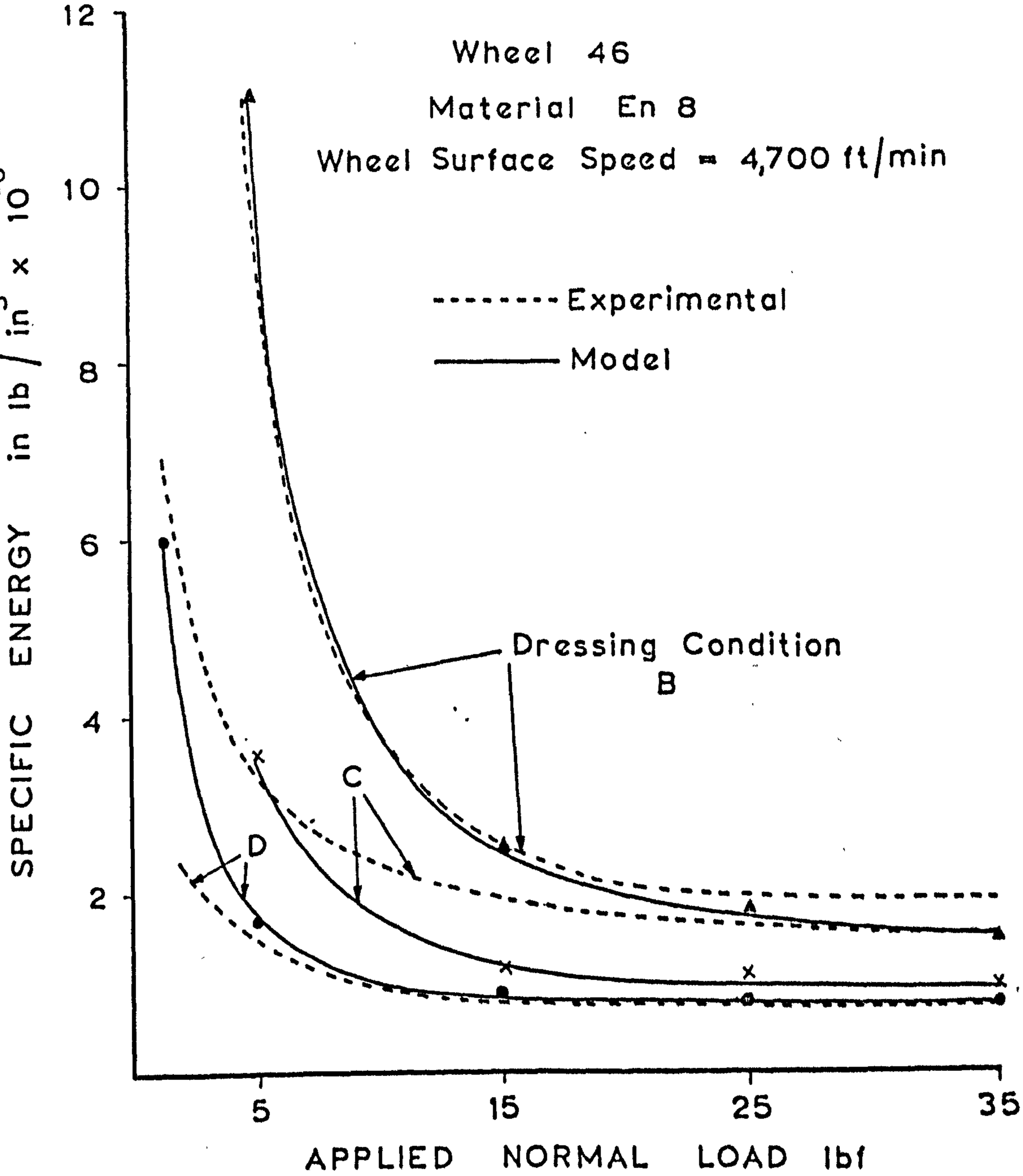

Fig. 110 Final Comparison between Experimental and Theoretical S.E. Values

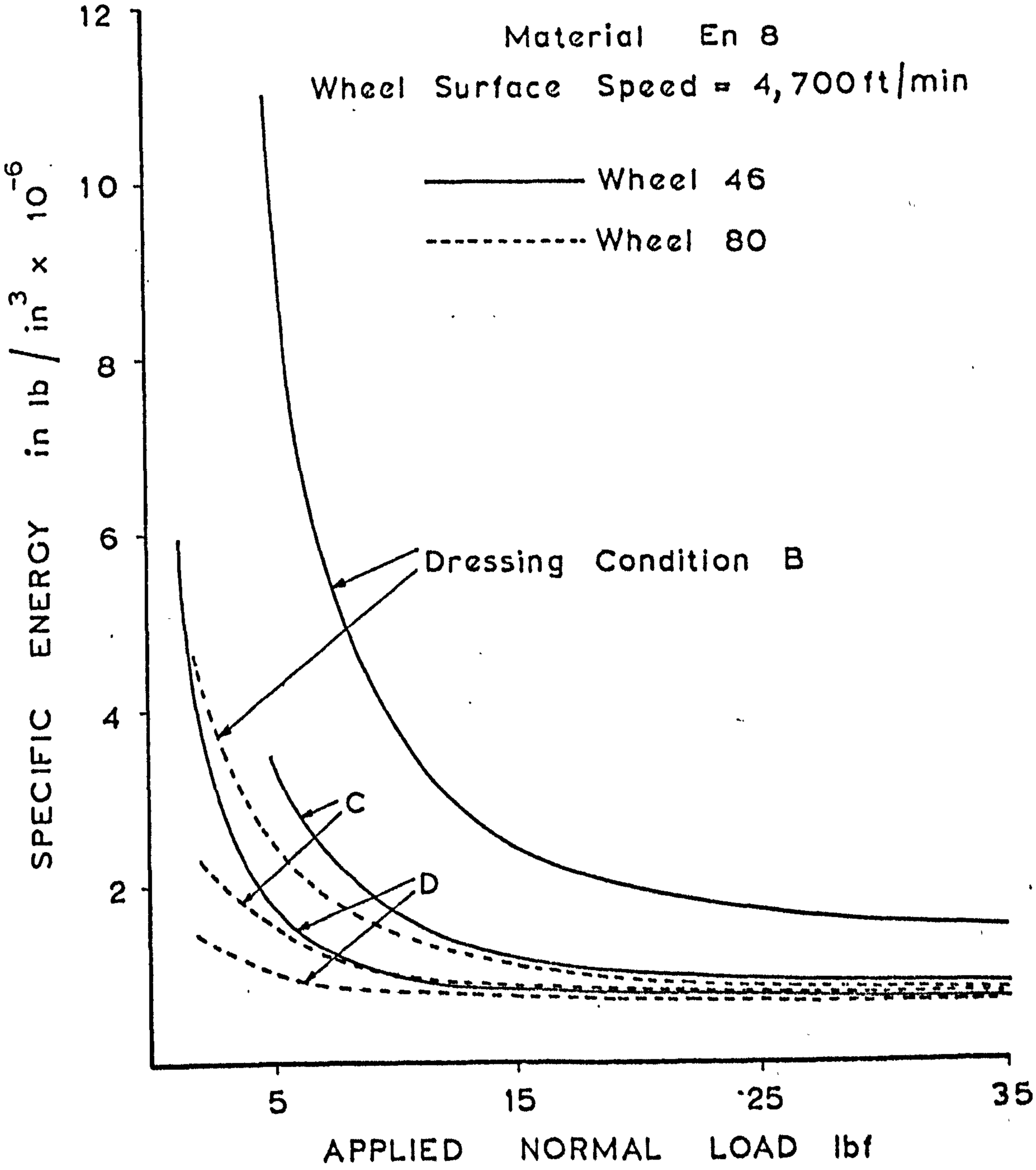

Fig. 111 Theoretical Influences of Grain Size on S.E. Values

is given by the fact that the error between the experimental and theoretical values of T is significantly greater in the case of the 80 size wheel.

6.3 CONCLUSIONS

A simple mathematical model has been established which is capable of predicting specific energy values which are in good agreement with practical values. The model was based essentially on considerations of the individual asperity workpiece interactions and utilised experimental data from the earlier surface topography measurements and simulation tests. The results have confirmed many of the previously drawn conclusions regarding the influence of abrasive surface topography on the grinding action. In addition, it is important that the results also confirm the value of an approach based on the study of the likely outcome of individual grit - workpiece interactions when attempting to predict the influence of various parameters on the mechanics of the grinding process.

From the point of view of further work, it would seem that the future value of such a modelling technique will depend to a large extent on the accuracy with which the true wheel topography can be simulated. This concerns not only the highly irregular shapes constituting the surface, but also the scale of measurement. This is because it can be strongly argued that for simple models in which wear and elastic effects are neglected, etc., the relevant profile information is contained in a range bounded by the maximum grit

penetration (recorded at 2.5×10^{-4} in. in this model). However, the model could possibly be extended to cover a more practical grinding operation, thus providing the opportunity to study the influence of different groove types on the mechanics of the metal removal.

CHAPTER VII

CONCLUSIONS

This project has been concerned with the influence of abrasive surface topography on the basic mechanics of the metal grinding process. The work was initiated in the belief that a detailed investigation of the mode of metal removal, and its dependence on various operating parameters, would make a valuable contribution to the study and eventual prediction of abrasive wheel performance. The investigation has been conveniently divided into sections covering a quantitative description of the abrasive wheel surface, the influence of abrasive grit geometry on the mode of metal deformation, and the analysis and subsequent computer simulation of a simplified grinding operation. Although detailed conclusions and recommendations have been presented at the end of each section, the main points are now summarised:-

1. The abrasive surface can be successfully defined using the techniques developed for random signal analysis, i.e., in terms of the probability height distribution, the autocorrelation function and derived power spectrum. The measurement procedure adopted facilitates the rapid computation of the above functions, thus permitting the analysis of a wide variety of abrasive wheels. In addition, the possible observation of the change in wheel properties as grinding proceeds has also been discussed.

2. Realistic simulations of the abrasive grit-workpiece interactions have shown that in grinding three distinct modes of metal deformation are possible, viz., elastic displacement, plastic

displacement, and microcutting. The geometry of the grit-workpiece interaction has been found to be the most important single factor in determining the deformation mode. This geometry has in turn been found to be dependent on the overall distribution and size of abrasive grits, and the geometry of individual grit profiles.

3. It has been shown experimentally that grooves formed by grits having large negative rake angles or edges of large radius involve extensive plastic deformation. On the other hand, as the rake angles become increasingly positive and the radii smaller, conditions favourable for microcutting prevail. A transition between these two modes of metal deformation was observed and defined in terms of a critical rake angle or equivalent groove width to depth ratio.

4. The surface topography measurements have shown the initial wheel specifications and superimposed dressing conditions have a significant effect on the distribution of abrasive grits in the wheel surface. Consequently, the mode of metal deformation is strongly dependent on these two considerations, as indicated by the analysis of the controlled force plunge grinding operation.

5. The importance of the specific energy and the grinding ratio in the study of metal grinding mechanics has been underlined. Both parameters correlate well with the mode of metal deformation. High S.E. values and low $^{T}/_{N}$ ratios are associated with extensive plastic deformation, whereas low values of S.E. and high $^{T}/_{N}$ ratios are associated with microcutting.

6. The effect of applying grinding fluids is dependent on the dominant mode of metal deformation, increased lubrication being advantageous in microcutting situations, but detrimental to operations characterised by extensive plastic deformation. When grinding under severe contact conditions, extreme pressure additives are desirable.

7. The energy values observed when studying the controlled force grinding operation have been predicted using a simplified computer simulation. The results confirm the conclusions regarding the influence of surface topography on the mechanics of metal removal, and underline the value of considering the nature of individual grit-workpiece interactions when determining the influence of various process parameters on the grinding operation.

8. It is recommended that future investigations based on the findings of this project should be concerned with one of the well established practical grinding operations. Priority should be given to establishing the relationship between the mode of metal deformation and important process parameters such as surface finish, abrasive wear, dimensional accuracy and quality of workpiece surface.

APPENDIX A

A1 THE CORRELATOR

Before discussing the operation of the instrument in terms of the basic measurement requirements, it is convenient to consider the averaging procedure, since both probability and correlation measurements are processes in which the final computed functions are the average of many samples. The correlator possesses two distinct averaging modes:-

a) Summation averaging. This operates by summing N samples and then dividing the total by N, which may be selected in the range 2^7 to 2^{17}. This mode anticipates the number of samples contributing to the final value of the function and is therefore a process of predetermined length.

b) Exponential averaging. This is a continuous filtering process. If A_{p-1} is the current value of the running average and a new sample I_p arrives, the new average would be given by

$$A_p = A_{p-1} + (I_p - A_{p-1})/N$$

In fact, this running average algorithm is the digital equivalent of an RC smoothing filter.

Although both modes should eventually give the same answer, they do have separate uses. In general, the summation mode is suitable when the amount of data is limited. On the other hand, the exponential mode can be used as a "quick look" facility, since a rough approximation to the final function is given immediately, the value being steadily refined as the measurement proceeds. The mode can also be used as a test for stationarity as the change in statistical properties with time can be freely observed.

The two measurement facilities of interest to this project are now considered:-

1. PROBABILITY MODE.

This is capable of computing either of two functions:-

a) amplitude probability density function (pdf)

b) the integral of the pdf, or, the cumulative probability density funotion (cdf)

In both cases, the signal amplitude is represented by the horizontal axis of the display, whilst the vertical direction is a measure of the amplitude probability.

The main instrument settings are:-

HORIZONTAL SENSITIVITY. Variable from 0.05 to 4 V/cm depending on the maximum amplitude of the signal.

HORIZONTAL RESOLUTION. One hundred discrete levels across 10 cm wide display, i.e., 10 levels/cm.

VERTICAL SENSITIVITY. This depends on the averaging mode. When summation averaging is used, the process will automatically stop when any one level reaches full scale deflection = 8 cm. This corresponds to N events having occurred at that particular level.

VERTICAL RESOLUTION. 256 discrete levels in 8 cm high display, i.e., 32 levels/cm.

SAMPLING RATE. This can be set from 1 Hz to 3 kHz. These correspond to sampling times, t of 1 second and 0.33 millisec.

BANDWIDTH. The instrument bandwidth is dc to 250 kHz. Two lower cut-off frequencies are available, viz., dc and 1 Hz. In terms of the probability measurements, the centre of the horizontal scale represents the zero voltage

level. Thus, when used in the DC mode, only 50 points on the CRT are utilised.

2. CORRELATION MODE.

Consideration is given here to the autocorrelation function (ACF) only. The instrument computes and simultaneously displays 100 values of the ACF. The vertical axis is a measure of the correlation, and the horizontal axis represents the time delay.

The instrument settings are:-

HORIZONTAL SENSITIVITY. This is calibrated in time/mm and is variable from 1μs to 1 sec. This gives a total delay span of 100 μs to 100 sec.

HORIZONTAL RESOLUTION. One hundred points across 10 cm.

VERTICAL SENSITIVITY. This is calibrated in V^2/cm and is automatically displayed on an illuminated panel at the side of the instrument. Values can be selected from 5×10^{-6} V^2/cm to $5V^2$/cm.

VERTICAL RESOLUTION. This depends on the display sensitivity, the minimum resolution being 25 levels/cm.

SAMPLING RATE. The sampling time, t, is automatically equal to the horizontal sensitivity setting, t/mm.

BANDWIDTH. Same as for probability measurements.

When used in the dc mode, information is obtained over the entire frequency range. However, in situations where the signal contains a dc level or powerful low frequency components, the vertical sensitivity has often to be set at a low value to keep the displayed function within the confines of the CRT. This usually results in a loss of information regarding the higher frequency data.

This can be overcome by operating the instrument in the ac mode (1 Hz cut-off), but information is then lost concerning the dc level. Also, the low frequency data is unavoidably attenuated by an amount depending on the filter characteristics.

A2 ESTIMATION ERRORS

Errors associated with the analysis of sample records of random data may be divided into three main categories:-

a) estimation or statistical errors

b) instrument errors

c) usage or personnel errors

Estimation errors are now briefly discussed, but it must be remembered that these are over and above instrument and usage errors.

The estimation error obtained when measuring a random process is in itself random and consists of a mean component called the bias error, and a fluctuating component termed the variance. A common measure of the error introduced by measurement is the normalised error, ϵ given by,

$$\epsilon = \left(\frac{\text{variance of parameter estimate}}{(\text{parameter})^2}\right)^{\frac{1}{2}}$$

For a continuous signal, the error associated with the measurement of a parameter is given by $\epsilon = f(BT)^{-\frac{1}{2}}$ where B = signal bandwidth in c/s and T is the length of the sample in seconds.

1. Errors in the probability measurements

A detailed account of the estimation of statistical errors when using digital analysis techniques is given in ref. 67. It seems that in general, the estimation errors associated with probability measurements are not major considerations. This is because one

sample of the signal is generally used to determine all the statistical properties, and the sampling time Δt and the sample size, N, are selected to give the desired accuracy for the later spectral measurements. In the present work also, a rigorous analysis of the errors associated with the pdf measurements was not conducted. However, it is reasonable to assume that the likely value of ϵ will be less than 0.05 for the conditions quoted in Section 3.2.3.

2. Errors in correlation and spectral measurements

As already indicated in Section 3.2.3, it is necessary to smooth the spectral estimates determined from the raw correlation measurements. This is generally accomplished by weighting the original correlation function non-uniformly. This is carried out using what is known as a spectral window of which several different types are in common use. In the present work, a Tukey window[6] is used, mainly because the available computer program (Appendix C) for determining the Fourier transform of the ACF incorporated this particular window.

The equivalent resolution bandwidth, B_e, of this window is given by

$$B_e = \frac{1.33}{\Delta t \times m}$$

With Δt = 100 millisecs, and m chosen equal to 80, an adequate resolution bandwidth of 0.167 c/s was obtained.

If the sample size is N, an estimate of the normalised error for spectral calculations is given by $\epsilon = (m/N)^{\frac{1}{2}}$.

With a sample size of N = 2048 giving a corresponding trace length of 3.4 in., ϵ = 0.2. The value of ϵ could be reduced by taking larger samples. For a fixed smaple size, however, the accuracy could be steadily increased by increasing the resolution bandwidth, i.e., reducing m. The value of m can then be adjusted to give acceptable resolution consistant with the maximum permissible error. This is the window closing technique discussed in ref. 68

APPENDIX B

B1 SPECIMEN CAICULATION FOR AIR BEARING DESIGN (reference 72)

Specifications:-

i) Maximum load carrying capacity - 75 lbs

ii) Maximum available supply pressure - 100 psi

iii) Design for minimum bearing diameter consistent with economy of fluid supply

Nomenclature:-

h = radial clearance, ins

k_s = static stiffness of full journal bearing, lb/in

b = circumferential spacing of orifices, ins

D = bearing diameter, in

L = bearing length, in

A_e = effective area, in^2

P_s = supply pressure, psi

a_1, a_2 = dimensionless flow pressure sensitivities

b_1, b_2 = dimensionless displacement flow sensitivities

k = ratio of specific heats = 1.4 for air

g = acceleration due to gravity = 386 in/sec^2

R = gas constant, ft lbf/lb ^oR

T_s = bearing supply temperature, ^oR

μ = viscosity, lbf sec/sq.ft

C_d = orifice discharge coefficient

d = diameter of inlet orifice, in

W = mass flow rate, lb/sec

A = flow area of compensating orifice, in^2

A^* = area of hypothetical choked orifice permitting flow W_i, in^2

To conserve supply fluid, the bearing clearance should be as small as possible and a value of $h = 0.0008$ in. is taken here as a practical minimum.

For design purposes, the maximum allowable load $= 0.5\, k_s h$

i.e. $k_s = \frac{150}{0.0008} = 1.875 \times 10^5$ lb/in

For an I.C. bearing $b_1 = 1$, and for laminar flow in the clearance, $b_2 = 3$.

Three inlet regions were chosen giving $b = \frac{\pi D}{3}$

$$A_e = \frac{\pi DL}{4}$$

Eq.(16) becomes

$$\frac{k_s h}{A_e P_s} = \frac{6}{\pi DL} \leqslant \frac{P_{m_1}}{P_s} \left(\frac{2}{a_1 + a_2}\right)$$

$\frac{P_{m_1}}{P_s} \times \frac{1}{(a_1 + a_2)}$ has a maximum at $\frac{P_{m_1}}{P_s} = 0.8$ and then $a_1 + a_2 = 3.5$

Hence $DL \geqslant 4.2$

Select $\underline{D = 1.5}$ and $\underline{L = 3}$

From (36)

$$0.35 = \left(\frac{k-1}{2gkRT_s}\right)^{\frac{1}{2}} \times \frac{P_s D}{192 \mu C_d} \times \frac{h^2}{LD}$$

i.e. $d = 6.5 \times 10^{-3}$ in.

In practice, two sets of three orifices were chosen situated 0.75 in. from the ends of the shaft. As a very rough approximation, this was assumed to correspond to a bearing with one set of three orifices, having an $\frac{L}{D}$ ratio = 1.

Thus $d = 0.013$ in. $= \underline{\frac{1}{64} \text{ in. approx.}}$

As an estimate of the mass flow rate

$$W = \pi\, dh\, C_d \times \frac{0.532\, P_s}{(T_s)^{\frac{1}{2}}} \times \frac{A^*}{A}$$

for $\frac{P_{m_i}}{P_s} = 0.8$, $\frac{A}{A^*} = 1.21$

and $\underline{W = 5.65 \times 10^{-5}\ \text{lb/sec}}$

B2 SPECIMEN CALCULATION FOR DYNAMOMETER DESIGN (reference 73)

Nomenclature:-

t = thickness of ring, in.

R = radius of ring, in.

b = width of ring, in.

K_r = effective spring constant, lb/in

M = spring mass

N = normal applied load, lbf

T = tangential cutting force, lbf

E = Young's Modulus lb/in^2 (M.S. = 30×10^6 lb/in^2)

ϵ_a = strain on axis AA (Fig. 82, Section 5.1.1)

ϵ_b = strain at points B

f_n = natural frequency, Hz

From elastic ring theory,

$$\epsilon_a = \frac{1.1\, NR}{E\, b\, t^2}$$

$$\epsilon_b = \frac{2.2\, TR}{E\, b\, t^2}$$

Assume $R = 0.75$ in. which gives sufficient space to affix the strain gauges on the octagonal flats. Put $\underline{b = 1\text{ in.}}$ and $\underline{t = \frac{3}{32}\text{ in.}}$

Then for $N = T = 1$ lbf.

$$\epsilon_a = \underline{3.05 \times 10^{-6}}$$

and $$\epsilon_b = \underline{6.1 \times 10^{-6}}$$

These were considered to be of sufficient magnitude to give the required sensitivity.

The spring stiffness, $K_r = \frac{1.39\, E\, b\, t^3}{R^3} = 8.15 \times 10^4$ lb/in

The natural frequency, $f_n = \frac{1}{2\pi}\sqrt{\frac{k_r}{M}}$

For $M = 2.5$ lbs

$$f_n = \frac{1}{2\pi}\sqrt{\frac{8.15 \times 10^4 \times 384}{2.5}}$$

$$= \underline{560\text{ Hz}}$$

NOTE: The natural frequency of the dynamometer was determined experimentally and found equal to 450 Hz, the discrepancy between theory and practice probably being due to the minor modifications for retaining the specimen. In reference 73 it was suggested that an optimum value for f_n is 500 Hz, which is slightly higher than the observed experimental value. Despite this fact, the dynamometer performed satisfactorily with the dimensions and characteristics quoted above.

B3 RIG COMMISSIONING TESTS

Nomenclature:-

P = oil pressure

A = effective cross sectional area of piston

x = lateral displacement of piston

θ = angular displacement of suspended arm

M_1 = mass of piston

M_2 = mass of suspended arm

k = radius of gyration of arm

I = moment of inertia of arm = M_2k^2

R = perpendicular distance of line of action of applied load from the bearing centre

V = infeed velocity

V_L = limiting infeed velocity

K_1, K_2 = constants of proportionality

t = time

f_n = natural frequency of vibration

i) THE LIMITING INFEED VELOCITY

As metal is removed during the grinding action, the test piece will move towards the wheel, a limiting velocity being reached when equilibrium conditions exist between the contact resistance and the applied load. If the rig is assumed to approximate to the idealised arrangement of Fig. 1b, then for a frictionless system the equation of motion is

$$F - K_1V = M_1\ddot{x} + \frac{I}{R}\ddot{\theta}$$

assuming the resistance forces to be proportional to the infeed velocity. The limiting velocity occurs when the acceleration is zero and is given by

$$V_L = \frac{F}{K_1} = \frac{PA}{K_1}$$

In the case of metals with poor grindability the resistance forces may not be a linear function of V and may not pass through the origin[31].

Thus $$V_L = \frac{(PA - B)^n}{K_1}$$

where B is the threshold value of the force required for initial metal removal, and n is the exponent of the force/infeed velocity curve. In addition, the effectiveness of the applied load will be reduced by the inevitable frictional resistance inherent in the mechanism. If these frictional forces are assumed to be purely viscous and proportional to velocity then,

$$V_L = \frac{\left[(PA - K_2V_L) - B\right]^n}{K_1}$$

It is important to note that the dynamometer measures directly the magnitude of $(PA - K_2V_L)$. Consequently, the presence of unpredictable frictional forces does not influence the degree of reliability with which the applied normal load can be selected. From the point of view of repeatability and sensitivity, however, every consideration was given to reducing all possible sources of friction in the system to a minimum.

ii) RESPONSE OF THE SYSTEM TO A SUDDEN CHANGE IN OPERATING CONDITIONS

If there is a sudden change in conditions at the wheel - test piece interface, e.g., a rapid increase in the rate of metal removal, the system must respond in a manner that will maintain the concept of a continuous controlled force operation. The response will in fact depend on the inertia of the system (and to a lesser extent the frictional characteristics), and

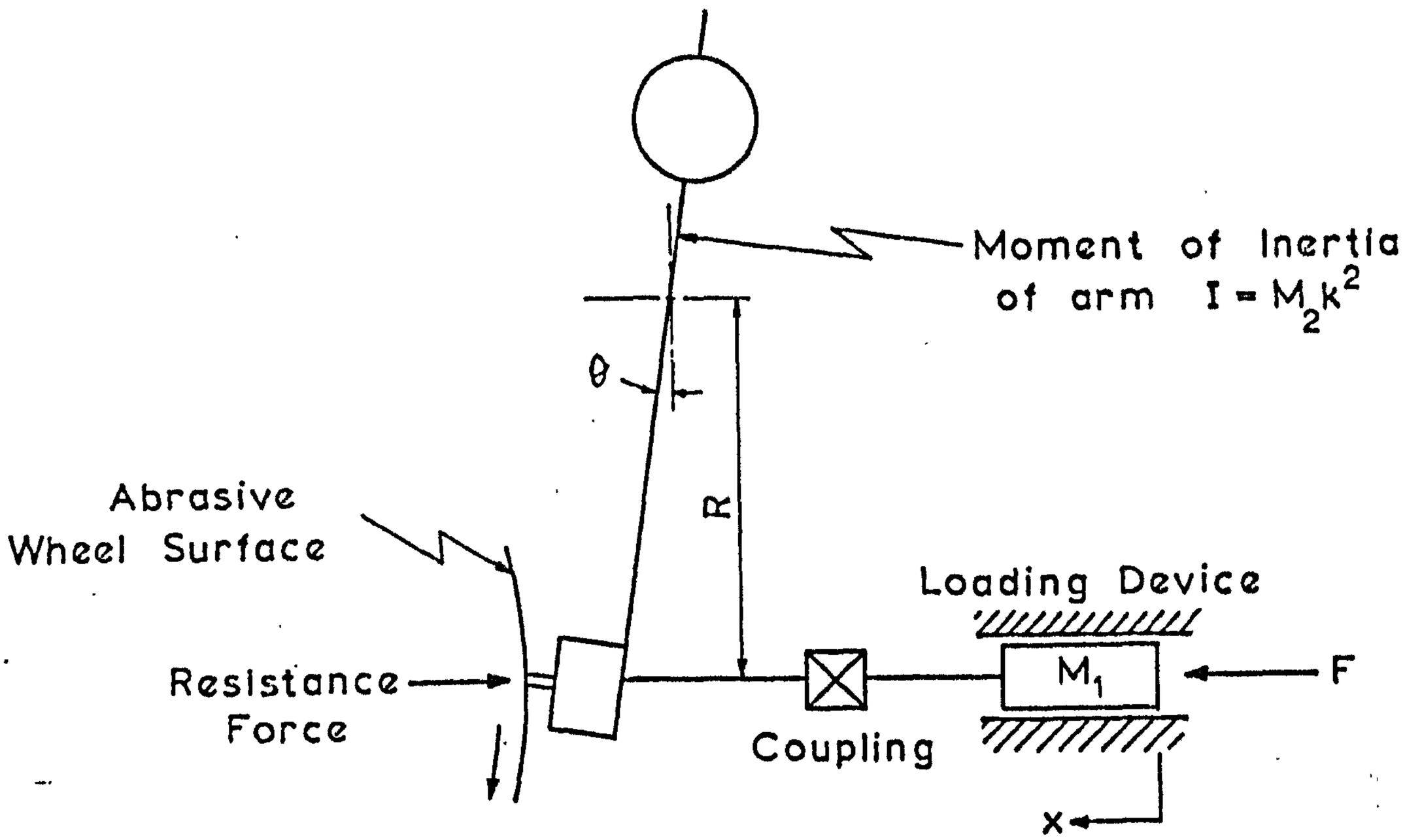

Fig. 1b Ideal Arrangement of Rig

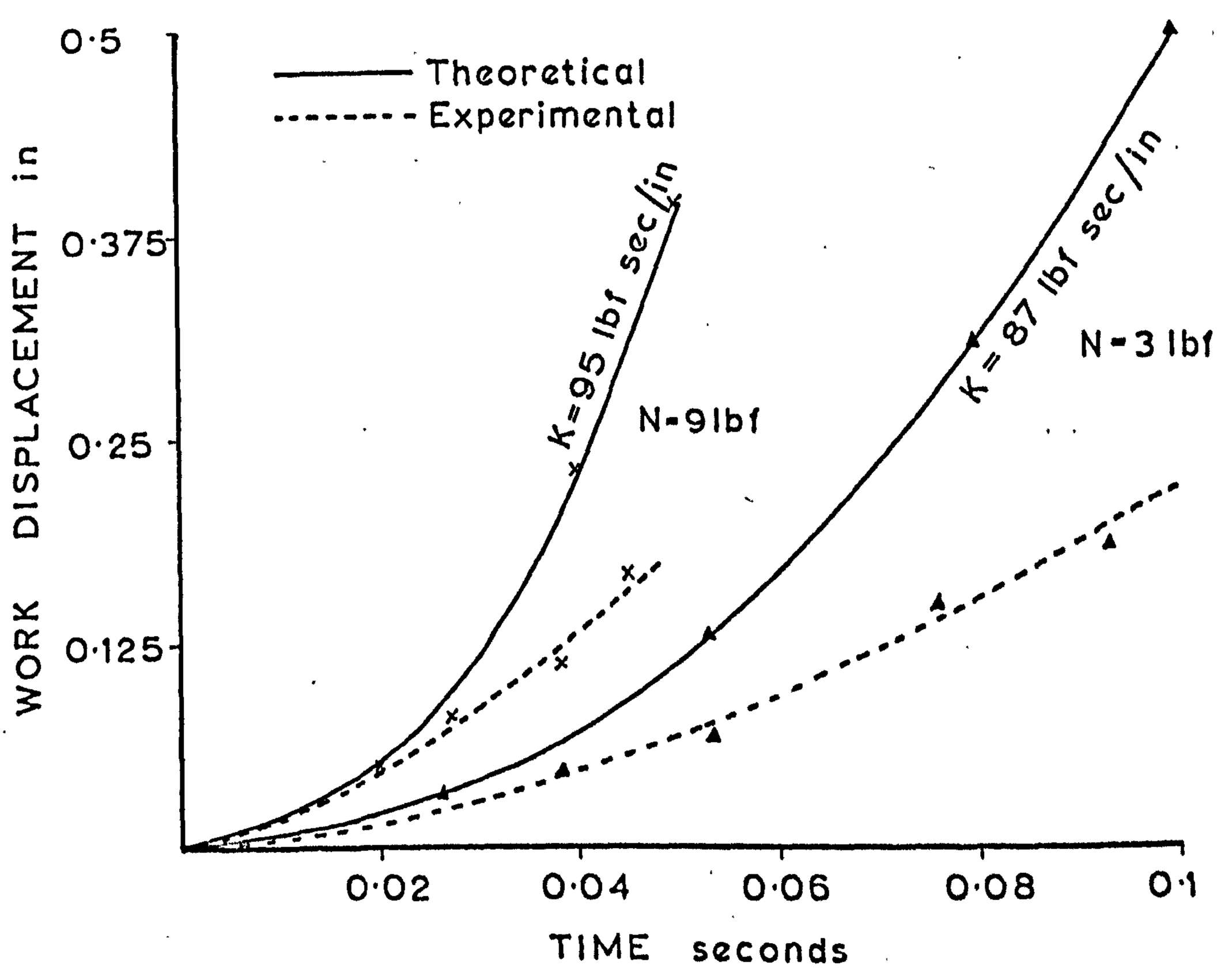

Fig. 2b Response of System to a Sudden Change in Operating Conditions

in order to investigate these further, the effect of applying a step load was considered. In practice, this was obtained by loading the test piece against a mechanical stop which was then suddenly removed. The experimental time displacement curve was then recorded and compared with the theoretical curve derived in the following manner:-

The equation of motion can be written:-

$$PA - K_2\dot{x} = M_1\ddot{x} + \frac{I}{R}\ddot{\theta}$$

For small values of θ, $x = \theta/R$ and putting $I = M_2k^2$,

$$PA = \left[\frac{M_1R^2 + M_2k^2}{R^2}\right]\ddot{x} + K_2\dot{x}$$

$$\text{Let } M_3 = \frac{M_1R^2 + M_2k^2}{R^2}$$

$$\text{Then } PA = M_3\ddot{x} + K_2\dot{x}$$

Applying the known boundary conditions this can be solved to give

$$x = \frac{PA}{K_2}\left[t + \frac{M_3}{K_2}e^{-\frac{K_2}{M_3}\cdot t} - \frac{M_3}{K_2}\right]$$

i.e. the displacement depends on the oil pressure, the effective area of the piston, the combined moment of inertia of arm and piston, and the constant of proportionality K_2.

Now $K_2 = \frac{PA}{V_T}$ (V_T = terminal velocity)

and was determined experimentally by varying P and measuring the resultant terminal velocity. In practice, the magnitude of K_2 was seen to increase slightly with increasing pressure,

suggesting the presence of coulcomb friction between the piston and supporting bushes.

The radius of gyration of the arm was determined by pivoting the arm about a point 8 in. from the centre of gravity. The period of oscillation was found to be 1.46 seconds and by using the concept of an equivalent simple pendulum, and knowing M_2, a value of $M_2k^2 = 1400\ \text{lb in}^2$ was obtained.

Knowing M_1 and R, M_3 can be determined and the displacement is given by

$$x = \frac{170P}{K_2}\left[t + \frac{10.6}{K_2}\, e^{-\frac{K_2}{10.6}\cdot t} - \frac{10.6}{K_2}\right]$$

Fig. 2b shows the experimental and theoretical displacements for values of P giving an approximate applied load of 3 and 9 lbf. Agreement between the two curves is quite reasonable for this type of comparison, the discrepancy possibly being due to indeterminate coulomb frictional effects not considered in the theoretical derivation.

By comparing the time displacement curves with the later metal removal rates from equal values of N, it was concluded that the response of the system was rapid enough to maintain a controlled force concept over the entire operating range.

iii) THE DYNAMIC RESPONSE OF THE SYSTEM

Since during a grinding test, the system will be subjected to a periodic excitation resulting from the wheel out-of-roundness, it is necessary to consider the dynamic response. This was achieved by subjecting the test piece to a periodic force in a

direction corresponding to the line of action of the applied load, N. The force was generated using a Goodman 390A Vibrator capable of giving a peak force of 30 lbf, linear within the range 0 - 4k Hz. The amplitude of vibration of the test piece was measured by an accelerometer attached to the main support arm, used in conjunction with a Dawe Vibration meter.

The response of the system to a periodic force of peak value 7.5 lbf is given in Fig. 3b, for different values of the load cylinder oil pressure, P. (P is expressed in terms of the equivalent applied load, N). The curves indicate that the system possesses reasonable damping properties and provide a means of estimating the natural frequency, f_n, for different values of N.

In general, with a newly dressed wheel the out-of-roundness is unilobal, further lobes developing as grinding proceeds. For the short duration tests conducted in this investigation, the out-of-roundness was assumed to remain unilobal, resulting in an excitation frequency of 25 c/s. For a minimum applied load of 2 lbf the corresponding system natural frequency is 85 c/s (Fig. 3b), which is well above the expected frequency of vibration.

NOTE: If the rig had been designed to give high stiffness in the infeed direction regardless of the magnitude of the applied load, any wheel out-of-roundness would have induced large normal load fluctuations thus destroying the concept of a controlled force operation.

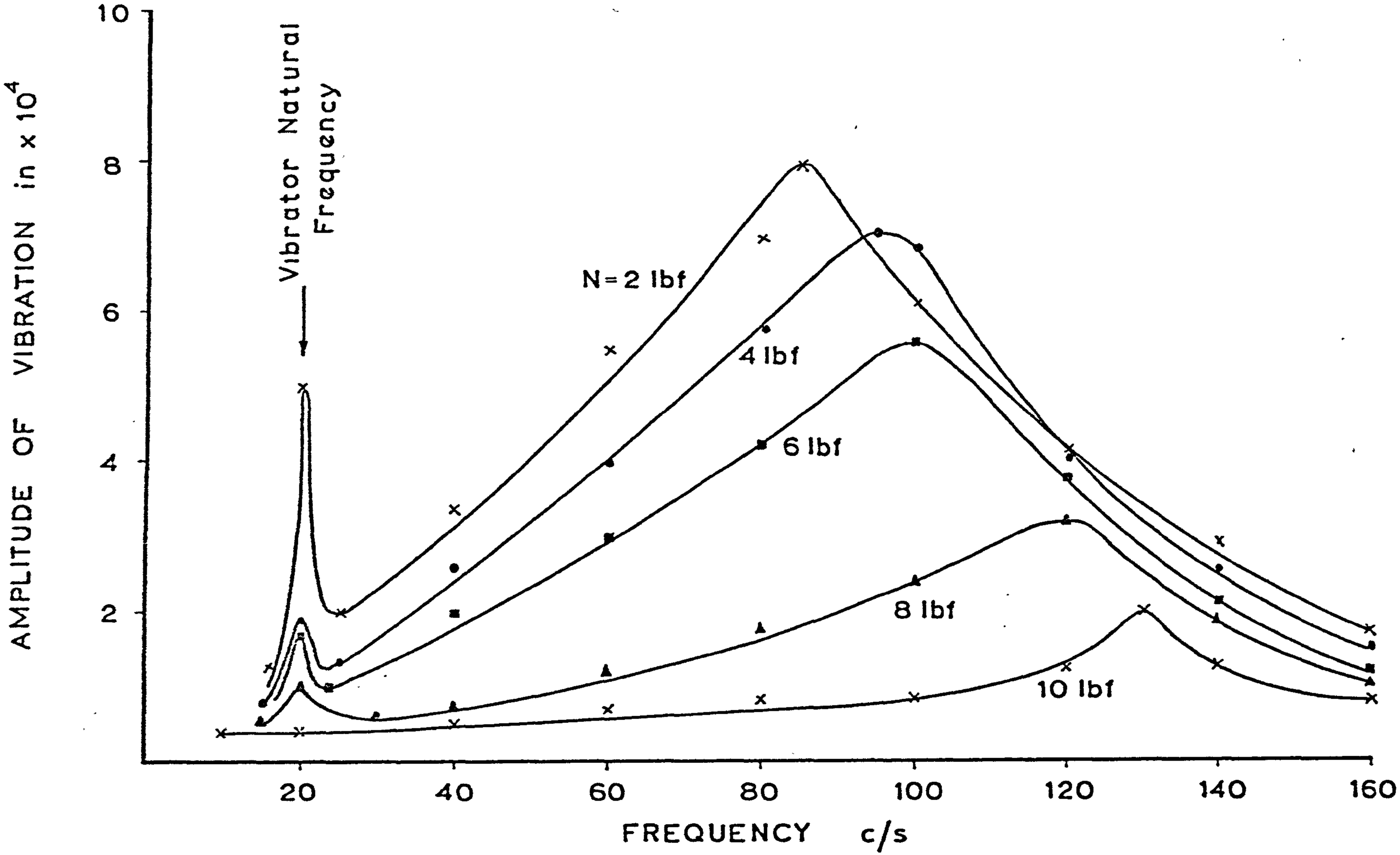

Fig. 3b Dynamic Response

APPENDIX C

C1 COMPUTER GENERATION OF RANDOM VARIABLES

1) Generation of a discrete random variable (due to Marsaglia[75]

Let Y be a discrete random variable with point probabilities p_i.

Let p_i for i = 1, 2, . . . n be expressed by k decimal digits:-

i.e. $p_i = \delta_{1i}, \delta_{2i}, \ldots \delta_{ki}$

Define $P_o = 0$, $P_r = 10^{-r} \sum_{i=1}^{n} \delta_{ri}$ for r = 1, 2, . . . k

and $\pi_s = \sum_{r=0}^{s} 10^r P_r$ for s = 1, 2 . . . k

Number the computer memory locations by 0, 1, 2 . . . π_{k-1}

The memory locations are divided into k mutually exclusive sets such that the s^{th} set consists of locations $\pi_{s-1}, \pi_{s-1} + 1 \ldots$

The information stored in the memory locations of the s^{th} set consists of y_1 in δ_{s1} locations, y_2 in δ_{s2} locations . . . y_n in δ_{sn} locations.

Denote the decimal expansion of the uniform deviates generated by the computer by

$$u = .d_1 d_2 d_3$$

and finally, let a $[m]$ be the contents of memory location m.

Then if

$$\sum_{i=0}^{s-1} P_i \leqslant U < \sum_{i=0}^{s} P_i$$

put

$$y = a\left[d_1 d_2 \ldots d_s + \pi_{s-1} - 10^s \sum_{i=1}^{s-1} P_i\right]$$

Example

Value of Variable	Point Probability
0	0.3277
1	0.4096
2	0.2048
3	0.0512
4	0.0064
5	0.0003

By definition,

$$P_o = 0, \quad P_1 = \frac{1}{10}(3 + 4 + 2) = 0.9$$

and similarly $P_2 = 0.07$, $P_3 = 0.027$, and $P_4 = 0.0030$

$$\pi_o = 0 \quad \pi_1 = 10 \times 0.9 = 9$$

and $\pi_2 = 16$, $\pi_3 = 43$, and $\pi_4 = 73$

The 73 memory locations are divided into 4 mutually exclusive sets such that

Set	Memory Location
1	0, 1, . . . 8
2	9, 10, . . . 15
3	16, 17, . . . 42
4	43, 44, . . . 72

Among the nine memory locations of Set 1, zero is stored $\delta_{10} = 3$ times, 1 is stored $\delta_{11} = 4$ times, 2 is stored $\delta_{12} = 2$ times, etc.

The seven locations of Set 2 store zero $\delta_{20} = 2$ times, store 3 $\delta_{23} = 5$ times, etc.

The locations can be summarised:-

		Value of Random Variable					
		0	1	2	3	4	5
Frequency	Set 1	3	4	2	0	0	0
	Set 2	2	0	0	5	0	0
	Set 3	7	9	4	1	6	0
	Set 4	7	6	8	2	4	3

Then to generate the random variables if

$0 \leqslant u < 0.9$ put $y = a[d_1]$

$0.9 \leqslant u < 0.97$ $y = a[d_1 d_2 - 81]$

$0.97 \leqslant u < 0.997$ $y = a[d_1 d_2 d_3 - 954]$

$0.997 \leqslant u < 1.000$ $y = a[d_1 d_2 d_3 d_4 - 9927]$

ii) Generation of a continuous random variable

The above method can be adapted to random variables having a continuous distribution. Let F(y) be the cumulative distribution function and assume that the domain of the random variable is (a, b) where the interval is finite. Divide the interval (b - a) into n sub intervals of lenth Δ such that $n\Delta = b - a$ and the boundary of the i^{th} interval is (y_{i-1}, y_i) where $y_i = a + i\Delta$ for $i = 0, 1, \ldots n$

Define a distribution having domain:-

$$\left\{ z_i = \frac{y_i + y_{i-1}}{2} \right\}$$

with point probabilities $p_i = F(y_i) - F(y_{i-1})$

Finally let N be a random variable having a uniform distribution within the interval $-\Delta/2, \Delta/2$. This can be done by setting $W = \Delta(U - \frac{1}{2})$. Then random deviates having a distribution F(y), can be generated approximately be setting $y = z + W$

$= z + \Delta(u - \frac{1}{2})$

This is simply an approximate decomposition of the continuous random variable into the sum of a discrete and continuous random variable. The discrete variable can be generated quickly by the method described previously. The smaller the value of Δ, the better will be the approximation.

Each number can be generated by using the leading digits of U to generate the discrete random variable Z, the remaining digits forming a uniformly distributed deviate having (0, 1) domain.

C2 METAL STRIP GRINDING SIMULATION

Nomenclature

alpha	=	class interval of experimental height ordinate distribution
b	=	equilibrium level (Fig. 103)
beta [1:m]	=	height distribution probability array
cff	=	critical form factor
co	=	number of contacting grits
contact [1:co]	=	array containing individual penetration depths of contacting grits
de	=	dressing depth, in.
depth [1:n]	=	array containing individual penetration depths (including non-contacting grits)
f	=	dressing feed in/min.
force	=	tangential force, T lbf
form [co]	=	array containing the individual groove form factors
h	=	metal strip thickness (0.125 in.)

This is simply an approximate decomposition of the continuous random variable into the sum of a discrete and continuous random variable. The discrete variable can be generated quickly by the method described previously. The smaller the value of Δ, the better will be the approximation.

Each number can be generated by using the leading digits of U to generate the discrete random variable Z, the remaining digits forming a uniformly distributed deviate having (0, 1) domain.

C2 METAL STRIP GRINDING SIMULATION

Nomenclature

alpha	=	class interval of experimental height ordinate distribution
b	=	equilibrium level (Fig. 103)
beta [1:m]	=	height distribution probability array
cff	=	critical form factor
co	=	number of contacting grits
contact [1:co]	=	array containing individual penetration depths of contacting grits
de	=	dressing depth, in.
depth [1:n]	=	array containing individual penetration depths (including non-contacting grits)
f	=	dressing feed in/min.
force	=	tangential force, T lbf
form [co]	=	array containing the individual groove form factors
h	=	metal strip thickness (0.125 in.)

infeed	=	infeed velocity in./sec.
load	=	normal applied load, N, lbf
m	=	no. of height distribution intervals + 1
n	=	size of roughness array
p	=	effective material flow pressure (0.75×10^6 lb/in^2)
pen	=	scanning depth of the profile measurement, in.
percent	=	percentage accuracy in determining the equilibrium indentation position
R	=	nominal grain radius, in.
rough [1:n]	=	height ordinates of the simulated surface, in.
space 1	=	percentage spacing, S, in fine dressing condition
space 2	=	percentage spacing in a coarse condition
total	=	number of consecutive wheel engagements (5)
w	=	metal strip width, (0.5 in.)
wh	=	wheel grain size (mesh number)
width/co	=	average form factor
x	=	random number generator starter (4376)

EBMDGG133APU-M/36/02 12/11/70
STR 15 1857HRS

```
begin
comment This program presents a mathematical model
of a simplified controlled force plunge grinding
operation viz. the grinding of metal strip. The influence
of dressing conditions, grain size, and normal applied
load upon the specific energy of metal removal is
predicted. In determining the specific energy values,
the likely mode of metal deformation associated with
the individual grit-workpiece interactions is an
important consideration.;
libraryA0,A6,A12;
integer i,j,z,int,pia,pib,pic,pid,m,for,x,xb,xd,rana,
total,wh,f,p,na,nc,n,load,fa,c,con,scan,co,add;
real force, alpha, pa,pb,pc,xa,dom,xc,ran,ranb,w,r,b,an,
suma,h,step,infeed,de,dist,cff,percent,space1,space2,pen,
y,q,width;
boolean bool;
open(20); open(30);
percent:=read(20);
w:=read(20);
h:=read(20);
wh:=read(20);
r:=read(20);
f:=read(20);
de:=read(20);
p:=read(20);
cff:=read(20);
load:=read(20);
pen:=read(20);
alpha:=read(20);
m:=read(20);
total:=read(20);
x:=read(20);
scan:=0;
space1:=read(20);
space2:=read(20);
for:=format([sss-d.ddddw-ndc]);
fa:=format([sss-d.ddddw-nd]);
write text(30,[grain*size*is]);
write(30,for,wh);
write text(30,[nominal*grain*radius*is]);
write(30,for,r);
write text(30,[feed*in*ins*per*min*is]);
write(30,for,f);
write text(30,[depth*in*ins*is]);
write(30,for,de);
write text(30,[applied*load*is]);
write(30,for,load);
if f=1 then
begin
na:=entier(w/(2xr));
nc:=entier(h/(2xr));
n :=naxnc;
end
else
```

```
begin
y:=r-sqrt((2xr-pen)xpen);
q:=space2/space1xy;
na:=entier(w/(2xr+2x(q-y)));
nc:=entier(h/(2xr+2x(q-y)));
n:=naxnc;
end;
write text(30,[size*of*roughness*array*is]);
write(30,for,n);
new line(30,3);
begin
integer array beta[1:m],gamma[1:m,1:3];
real array theta,omega,omegb,omegc,omegd[1:m],
rough,depth[1:n];
for i:=1 step 1 until m do
begin
beta[1]:=read(20);
scan:=scan+beta[i];
end;
close(20);
c:=add:=1;
for i:=1 step 1 until m do
begin
omega[1]:=beta[1]/scan;
theta[1]:=(i-1)xalpha;
end;

for i:=1 step 1 until m do
begin
omega[1]:=10.0xomega[1];
gamma[1,1]:=entier(omega[1]);
omegb[1]:=10.0x(omega[1]-gamma[1,1]);
gamma[1,2]:=entier(omegb[1]);
omegc[1]:=10.0x(omegb[1]-gamma[1,2]);
gamma[1,3]:=entier(omegc[1]);
omegd[1]:=omegc[1]-gamma[1,3];
if omegd[1]>0.5then gamma[1,3]:=gamma[1,3]+1;
end;
pa:=pb:=pc:=0;
for i:=1 step 1 until m do
begin
 pa:=pa+gamma[1,1]/10;
pb:=pb+gamma[1,2]/100;
pc:=pc+gamma[1,3]/1000;
end;
pia:=pax10; pib:=pia+100xpb;  pic:=pib+1000xpc;
j:=0; z:=0;
pid:=pic-1;
begin
array sigma[0:pid];
for int:=1 step 1 until 3 do
fori:=1 step 1 until m do
begin
loop:
if gamma[1,int]=0then goto another;
sigma[j]:=theta[1];
if j+1<gamma[1,int]+z then
begin
j:=j+1; goto loop;
end;
j:=j+1;
another:
```

```
z:=z+gamma[1,int];
end;
begin
real procedure  sud(x);
integer x;
KDF9  5/1/0/1;
V0=455 470 314;
V1=2 147 483 647;
[x]; V0; XD; SHAD+16; SHA+16;
ZERO; REV; ZERO; +D; REV;
SHA-16; +; DUP; =[x]; V1;
+; SET 0; FLOAT;
EXIT;ALGOL;
marker:
xa:=sud(x)x1000;
xb:=entier(xa);
dom:=xb/1000;
xc:=(xa-xb)x1000;
xd:=entier(xc);
ran:=xd/1000;
if 0.0000≤ ran and ran≤ pa then
begin
ran:=ranx10;
rana:=entier(ran);
ranb:=sigma[rana];
end
else  ifpa ≤ ranand ran ≤ pa+pb then
begin
ran:=ranx100;
rana:=entier(ran);
ranb:=sigma[rana+pia-100xpa];
end
else if pa+pb≤ran and ran≤1.0000 then
begin
ran:=ranx1000;
con:= ran+pib-1000x(pa+pb);
if con>pid then goto label;
ranb:=sigma[con];
end;
If ranb=0 then dist:=0 else dist:=ranb+alphax(dom-0.500);
rough[c]:=dist;
c:=c+1;
if c≤n then goto marker;
an:=load/p;
label:
infeed:=width:=force:=0;  co:=0;
b:=alpha;
bool:=false;
step:=alpha;
tab:
suma:=0.0000;
for i :=1 step 1 until n do depth[i]:=0.0000;
for i:=1 step 1 until n do
begin
If rough[i]>b then depth[i]:=rough[i]-b;
suma:=suma+(3.142xrxdepth[i]);
end;
If abs((an-suma)/an)≤percent then goto mark;
if suma>an then
begin
If bool then step:=step/100;
b:=b+step;
```

```
bool:=false;
end
else
begin
b:=b-step/10;
bool:=true;
end;
goto tab;
mark:
for1:=1 step 1 until n do
if depth[1]>0 then co:=co+1;
begin
real array  contact,form[1:co];
co:=0;
for i:=1 step 1 until n do
if depth[1]>0 then
begin
co:=co+1;
contact[co]:=depth[1];
form[co]:=2xsqrt(2xrxdepth[1])/depth[1];
end;
for i:=1 step 1 until co do
begin
if form[1]<cff then infeed:=infeed+contact[1]↑1.5;
force:=force+contact[1]↑1.5;
width:=width+form[1];
end;
infeed:=(1.87xsqrt(r)xinfeed)/(wx1.33b-4);
force:=1.87xsqrt(r)xpxforce;
write text(30,[infeed*vel.*in*ins*per*sec*is]);
write(30,for,infeed);
write text(30,[cutting*force*in*lbs*is]);
write(30,for,force);
write text(30,[s.e.*in*in.lb.*per*cubic*inch*is]);
if infeed=0 then write(30,for,1b10) else
write(30,for,17600xforce/infeed);
write text(30,[number*of*contacts*is]);
write(30,for,co);
write text(30,[average*form*factor*is]);
write(30,for,width/co);
new line(30,2);
if add=1 then
begin
write text(30,[****penetration**form*factor]);
new line(30,1);
for i:=1 step 1 until co do
begin
write(30,fa,contact[1]);
write(30,for,form[1]);
end;
end;
add:=add+1;
if add≤total then
begin
c:=1;
new line(30,2);
goto marker;
end;
end;
end;
close(30);
end;
end;
end↑
```

TYPICAL OUTPUT

```
GRAIN SIZE IS     4.6000     1
NOMINAL GRAIN RADIUS IS     7.5000     -3
FEED IN INS PER MIN IS     5.0000     1
DEPTH IN INS IS     5.0000     -4
APPLIED LOAD IS     2.5000     1
SIZE OF ROUGHNESS ARRAY IS     1.5600     2

INFEED VEL. IN INS PER SEC IS     2.9994     -2
CUTTING FORCE IN LBS IS     1.7005     0
S.E. IN IN.LB. PER CUBIC INCH IS     9.9785     5
NUMBER OF CONTACTS IS     1.8000     1
AVERAGE FORM FACTOR IS     3.3119     1

PENETRATION     FORM FACTOR
1.2860     -4     2.1600     1
9.0700     -5     2.5720     1
3.8300     -5     3.9580     1
9.3500     -5     2.5332     1
8.9900     -5     2.5834     1
2.2100     -5     5.2105     1
1.5300     -5     6.2622     1
5.0800     -5     3.4367     1
3.0300     -5     4.4499     1
3.1500     -5     4.3644     1
6.1100     -5     3.1337     1
1.5050     -4     1.9967     1
1.4640     -4     2.0244     1
1.0570     -4     2.3825     1
2.1600     -5     5.2705     1
6.7400     -5     2.9836     1
1.3560     -4     2.1035     1
1.2520     -4     2.1891     1

INFEED VEL. IN INS PER SEC IS     2.9061     -2
CUTTING FORCE IN LBS IS     1.7079     0
S.E. IN IN.LB. PER CUBIC INCH IS     1.0343     6
NUMBER OF CONTACTS IS     2.000     1
AVERAGE FORM FACTOR IS     3.3910     1

INFEED VEL. IN INS PER SEC IS     2.1915     -2
CUTTING FORCE IN LBS IS     1.5272     0
S.E. IN IN.LB. PER CUBIC INCH IS     1.2265     6
NUMBER OF CONTACTS IS     2.2000     1
AVERAGE FORM FACTOR IS     4.8354     1

INFEED VEL. IN INS PER SEC IS     3.0708     -2
CUTTING FORCE IN LBS IS     1.7744     0
S.E. IN IN.LB. PER CUBIC INCH IS     1.0170     6
NUMBER OF CONTACTS IS     1.6000     1
AVERAGE FORM FACTOR IS     3.8164     1

INFEED VEL. IN INS PER SEC IS     3.0749     -2
CUTTING FORCE IN LBS IS     1.8258     0
S.E. IN IN.LB. PER CUBIC INCH IS     1.0451     6
NUMBER OF CONTACTS IS     1.8000     1
AVERAGE FORM FACTOR IS     3.1328     1
```

C3 DETERMINATION OF THE SPECTRAL DENSITY

Nomenclature

cal	=	calibration factor inch/volt
cov [0:max m]	=	array of autocorrelation values
delta	=	sampling time, seconds
f	=	resolution bandwidth c/s
m [j]	=	array of 'nt' number of lags
maxm	=	maximum number of correlation points
n	=	sample size
nf	=	number of frequency points required in the spectrum
nt	=	number of spectra required, each computed with 'm' correlation points
period	=	equivalent period of the abrasive surface, in
run	=	experimental reference number
spec	=	power spectrum (divided by $[\mathrm{cov}(0)]^2$ to give density)
speed	=	ratio of tape recorder speed to the original scanning speed

```
begin
comment A program to determine the spectral density
estimate of an abrasive profile from the raw
autocorrelation measurements;
library A30,A6,A12;
real delta,c,v0,v1,v2,spec,logspec,speed,f,period,cal;
integer run,n,maxm,nf,nt,j,k,b,i,fa,fb;
open(20); open(30);
run:=read(20);
cal:=read(20);
n:=read(20);
maxm:=read(20);
delta:=read(20);
nf:=read(20);
nt:=read(20);
speed:=read(20);
begin
integer array m[1:nt];
real array cov[0:maxm],w[0:maxm];
for j:=1 step 1 until nt do m[j]:=read(20);
for k:=0 step 1 until maxm do
begin
cov[k]:=read(20);
cov[k]:=cov[k]xcal;
end;
close(20);
fa:=format([2s-nd.dddd]);
fb:=format([2s-d.dddb-nd]);
for j:=1 step 1 until nt do
begin
b:=m[j];
write text(30,[[4c]run]);
write(30,format([2sndd]),run);
write text(30,[[c]sample*size]);
write(30,format([2sndddd]),n);
write text(30,[[c]truncation*pt*(lags)]);
write(30,format([2sndd]),b);
write text(30,[[c]bandwidth(hz)]);
write(30,fb,4/(3xbxdelta));
write text(30,[[2cs]frequ(hz)[5s]spec[7s]logspec[6s]period]);
for k:=1 step 1 until b-1 do
w[k]:=0.5x(1+cos(3.14159xk/b));
for i:=0 step 1 until nf do
begin
c:=cos(3.14159xi/nf);
v0:=v1:=0;
for k:=b-1 step -1 until 1 do
begin
v2:=2xcxv1-v0+w[k]xcov[k];
v0:=v1;
v1:=v2;
end;
```

```
spec:=2×deltax(cov[0]+2×(v1×c-v0));
if spec<10↑-10 then logspec:=-100
else logspec:=ln(spec)/ln(10);
f:=1/(nf×2×delta);
write text(30,[[c]]);
write(30,fa,f);
write(30,fb,spec/cov[0]↑2);
write(30,fb,logspec);
if f=0 then period:=1↑6 else period:=speed/(60×f);
write(30,fb,period);
end;
jump:
end;
end;
close(30);
end↑
→
```

ACKNOWLEDGEMENTS

I should like to express my gratitude to Dr. R.M. Baul for his advice and encouragement which were generously given throughout the project.

I am indebted to the technical staff of the Mechanical Engineering Department and would like to thank in particular Mr. J. Mosedale, Mr. J. McNicol and Mr. H. Jones.

I should also like to thank Professor B.N. Cole for the opportunity to carry out this research, and the Science Research Council for their financial support.

REFERENCES

1. GREENWOOD, J.A. "Surface Measurement" Symposium on Experimental Methods in Tribology. London March 1968

2. WILLIAMSON, J.B.P. "Microtopography of Surfaces" Paper 1 Conf. on Properties and Metrology of Surfaces. Oxford April 1968

3. PEKLENIK, J. "New Developments in Surface Characterisation and Measurements by Means of Random Process Analysis" Paper 24 Conf. on Properties and Metrology of Surfaces. Oxford April 1968

4. ABBOTT, E.J. FIRESTONE, F.A. "Specifying Surface Quality" Mechanical Engineering 1933 (Sept.)

5. REASON, R.E. "The Bearing Parameters of Surface Topography" Proc. 5th M.T.D.R. Conf. Sept. 1964

6. GRIEVE, D.J. KALISZER, H. ROWE, G.W. "The Effect of Cutting Conditions on Bearing Area Parameters" Proc. 9th M.T.D.R. Sept. 1968

7. MYERS, N.O. "Characterisation of Surface Roughness" Wear 1962, 5, 182

8. KUBO, M. "Instrument for the Measurement of Slope and Height Distribution of Surface Roughness" Rev. Sci. Inst. 1965, 36, 236

9. PEKLENIK, J.
KUBO, M.
"A Basic Study of 3-D Assessment of the Surface Generated in a Manufacturing Process"
17th CIRP Assembly, Ann Arbour, U.S.A.
Sept. 1967

10. PEKLENIK, J.
KUBO, M.
"An Analysis of Microgeometrical Isotropy for Random Surface Structures"
17th CIRP Assembly, Ann Arbour, U.S.A.
Sept. 1967

11. PEKLENIK, J.
"Contribution to the Theory of Surface Characterisation"
CIRP Meeting Annalen BD XII

12. BACKER, W.R.
MARSHALL, E.R.
SHAW, M.C.
"Size Effect in Metal Cutting"
Trans. A.S.M.E. Jan. 1952

13. REDKO, S.G.
"The Maximum Thickness of the Metal Removed by a Single Abrasive Grit in the Course of Grinding"
Collection of Scientific Reports No. 9
Saratov Motor Road Institute, U.S.S.R. 1957

14. REDKO, S.G.
"The Hardness of Abrasive Tools"
ZhTF Vol. 27 1957

15. PATTINSON, E.
CHISHOLM, A.
"The Effect of Dressing Techniques on Grinding Wheel Wear"
Proc. 8th M.T.D.R Manchester 1967

17. SUTO, T.
WAIDA, T.
SATA, T.
"In-Process Measurement of Wheel Surface in Grinding Operations"
M.T.D.R. Manchester Sept. 1969

18. PEKLENIK, J. "Contribution to the Correlation Theory for the Grinding Process" Prod. Eng. Conf. A.S.M.E. Cincinnati May 1963

19. BRÜCKNER, K. "Der Schleifvorgang und Seine Betwortung Durch die Autretenden" Schnittlkraft Thesis T.H. Aachen 1962

20. PEKLENIK, J. "Versuchsergebnisse zur Ausbildung der Schneidelemente an Schleifwerkzeugen" Industrie Anzeiger Vol. 83 1961

21. BRÜCKNER, K. "Betrachtungen zum Verschleifvorgang Beim Schleifen" Industrie Anzeiger Vol. 82 1960

22. McAdams, H.T. "The Role of Topography in the Cutting Performance of Abrasive Tools" A.S.M.E. Journal Eng. for Ind. Feb. 1964

23. PAHLITZSCH, G. "Influence of Dressing Conditions on Grinding and Cylindrical Grinding Results" Extract from a lecture in Delft Oct. 1953 Microtecnic Vol. 8 No. 5

24. PAHLITZSCH, G. THOEING, R. "New Research into the Truing Process in Grinding" Ind. Diamond Rev. 19 June 1959

25. HAHN, R.S. LINDSAY, R.P. "The Influence of Process Variables on Material Removal, Surface Integrity, Surface Finish, and Vibration in Grinding" M.T.D.R. Manchester Sept. 1969

26. KRAGELSKII, I.V. "Friction and Wear"
A translation by L. Ronson and
J.K. Lancaster Butterworths Scient. Pub.
1965

27. GRISBROOK, H. "Metal Removal by a Single Abrasive Grit"
MORAN, H. Conf. on Machinibility London 1965
SHEPERD, D. Iron and Steel Institute

28. BACKER, W.R. "On the Basic Mechanics of the Grinding
MERCHANT, M.E. Process"
Trans. A.S.M.E. May 1956

29. ARMAREGO, E.J. "On the Size Effect in Metal Cutting"
BROWN, R.H. Int. Journ. Prod. Research 1961

30. HAHN, R.S. "On the Nature of the Grinding Process"
Paper to 2nd M.T.D.R. 1962

31. HAHN, R.S. "On the Mechanics of the Grinding Process
under Plunge Cut Conditions"
A.S.M.E. Journ. Eng. for Ind. Paper 65
Prod. 7

32. SEDRIKS, A.J. "Mechanics of Cutting and Rubbing in
MULHEARN, T.O. Simulated Abrasive Processes"
Wear Vol. 6 1963 457-466

33. BOWDEN, F.P. "The Friction and Lubrication of Solids"
TABOR, D. Clarendon Press, Oxford 1950 p.90-100

34. MERCHANT, M.E. "Mechanics of the Metal Cutting Process"
Journ. of App. Phys. Vol. 16 No. 5
May 1945

35. SEDRIKS, A.J.
MULHEARN, T.O.
"The Effect of Work-Hardening on the Mechanics of Cutting in Simulated Abrasive Processes"
Wear Vol. 7 1964 451-459

36. RUBENSTEIN, C.
GROSZMAN, F.K.
KOENIGSBERGER, F.
"Force Measurements During Cutting Tests with Single Point Tools Simulating the Action of a Single Abrasive Grit.
Proc. Int. Ind. Diamond Conf. Oxford 1966

37. ROWE, G.W.
WHETTON, A.G.
"Theoretical Considerations in the Grinding of Metals"
Journ. Inst. of Metals July, 1969

38. TANAKA, Y.
TSUWA, H.
KAWAMURA, S.
"Rubbing of Abrasive Grains in Grinding Process"
Bull. Jap. Soc. Precision Eng. Vol.1 No.3

39. SHONOZAKI, T.
SHIGEMATU, H.
"Mechanism of Rubbing and Biting of Cutting Edges on Work Surface in the Grinding Process"
Bull. Jap. Soc. Prec. Eng. Vol.2 No.1
1966

40. CRISP, J.
SEIDEL, J.R.
STOKEY, W.F.
"Measurement of Forces during Cutting with a Single Abrasive Grain"
Int. Journ. of Prod. Research Vol.7 No.2

41. ALDEN, G.I.
"Operations of the Grinding Wheel in Machine Grinding"
Trans. A.S.M.E. 1914 36, 451

42. GUEST, J.J. "Theory of Grinding with reference to the Selection of Speeds in Plain and Internal Work" Proc. Inst. Mech. Eng. 1915

43. HUTCHINSON, R.V. S.A.E. Journ. 1938

44. HEINZ, W.B. "Metal Cutting with Abrasive Wheels" Trans. A.S.M.E. 1943

45. REICHENBACH, G.S.
MAYER, J.E.
KALPAKCIOGLU, S. "The Role of Chip Thickness in Grinding" Trans. A.S.M.E. May 1956

46. MARSHALL, E.R.
SHAW, M.C. "Forces in Dry Surface Grinding" A.S.M.E. Trans. 1952

47. GRISBROOK, H. "Precision Grinding Research" Prod. Engineer 1960 (May)

48. KUMAGAI, N.
KOBAYASHI, A.
HAN, T. General Meeting of CIRP Cinicinnati, U.S.A. 1963

49. STORY, R.W. "Forces and Force Ratios in Grinding with Coated Abrasives" A.S.M.E. Journ. Eng. for Ind. May 1968

50. PEKLENIK, J. "Untersuchurgen über das Verchleisskriterium Beim Schleifer" Industrie - Anzeiger Vol. 80 No. 27 1958

51. TSUWA, H. "Evaluation of Grinding Wheel by Behaviour of Cutting Edges" Science of Machine Tokyo, Japan Vol. 13 1961

52. GOEPFERT, G.J.
WILLIAMS, J.L.
"The Wear of Abrasives in Grinding"
Mech. Eng. Vol. 81 April 1959

53. HAHN, R.S.
"Some Observations on the Wear and Lubrication of Grinding Wheels"
Symp. on Friction and Lubrication in Metal Processing New Orleans, Louisiana June 1966. Proceedings published by ASME

54. KUMAGAYA, N.
"Spontaneity of Cutting Edges of Abrasive Grains in Grinding Wheel"
Bull. Jap. Soc. Prec. Eng. 1961 1

55. TAKENO, N.
NAGAOKA, S.
"Electron Microscope Observations of Abrasive Grain in Precision Grinding Operations"
Bull. Jap. Soc. Prec. Eng. 1965
Vol. 1 No. 3

56. YOSHIKAWA, H.
SATA, T.
"Study on Wear of Grinding Wheels"
A.S.M.E. Journ. Eng for Ind. Feb. 1963

57. MAKINO, H.
"Roughness of Finished Surface in Grinding Operation of Hardened Steel"
Bull. Jap. Soc. Prec. Eng. Vol. 1 No. 4

58. HARADA, M.
SHINOZAKI, N.
"Effect of Grinding Fluids on Grinding"
Rod. Eng. Research Conf. Sept. 1963

59. DUWELL, E.J.
HONG, I.S.
M^{c}DONALD, W.J.
"The Effect of Oxygen and Water on the Dynamics of Chip Formation During Grinding"
A.S.L.E. Trans. 12, 86-93 (1969)

60. DUWELL, E.J.
HONG, I.S.
M^CDONALD, W.J.
"The Role of Chemical Reactions in the Preparation of Metal Surfaces by Abrasion"
Wear 1966

61. CHALKEY, J.R.
"Grinding and Lubrication"
Tribology Vol. 4 Nov. 1968

62. FURUICHI, R.
NAKAYAMA, M.
DOI, T.
"Influence of Dressing Conditions of Grinding Wheel on Grinding Fluid Performance in Free Infeed Plunge Grinding"
Bull. J.S.M.E. Vol. 10 No. 38

63. SLUHAN, C.
"Obtaining the Best Results from Grinding Fluids"
Machinery and Prod. Eng. July 1969

64. ARCHARD, J.F.
"Wear"
N.A.S.A. Symposium on Friction and Wear 1968

65. WETTON, A.G.
"A Review of Theories of Metal Removal in Grinding"
Journ. Mech. Eng. Science Vol. 11 No. 4 1969

66. BLACKMAN, R.B.
TUKEY, J.W.
"The Measurement of Power Spectra"
Dover Public Inc. New York

67. BENDAT, J.S.
PIERSOL, A.G.
"Measurement and Analysis of Random Data"
Pub. by John Wiley & Sons 1966

68. JENKINS, G.M.
WATTS, D.G.
"Spectral Analysis and its Applications"
Published by Holden Day 1968

69. BAUL, R.M. "Basic Mechanics of a Controlled Force Cylindrical Grinding System with Continuous Infeed" Ph.D. Thesis University of Leeds Nov. 1966

70. WHITEHOUSE, D.J. ARCHARD, J.F. "The Properties of Random Surfaces of Significance in their Contact" Proc. Roy. Soc. Lond A 316, 97-121 (1970)

71. DALL, A.H. "A Review of the Grinding Theories" Modern Machine Shop Nov. 1939

72. RICHARDSON, H.H. "Static and Dynamic Characteristics of Compensated Gas Bearings" Trans. A.S.M.E. 1958

73. YANG, C.T. "Design of Surface Grinding Dynamometer" A.S.M.E. Journ. Eng. for Ind. Feb. 1968

74. BAUL, R.M. PALMER-LEWIS, I. "Coolant Supply for High Speed Grinding" Metal Working Production 18/25 Dec. 1968

75. MARSAGLIA, G. "Random Variables and Computors" Proc. 3rd Prague Conf. in Probability Theory 1962
Refer "Handbook of Mathematical Functions" Dover Publications
Page 950